ISSN: 2067-3809

Universitatea Politehnica Timișoara

ACTA TECHNICA CORVINIENSIS – Bulletin of Engineering

Fascicule 3

[July–September]

Tome XVI [2023]

Editura POLITEHNICA

ACTA TECHNICA CORVINIENSIS

Bulletin of Engineering

Edited by:

UNIVERSITY POLITEHNICA TIMISOARA

Universitatea Politehnica Timişoara

Editor / Technical preparation / Cover design:

Assoc. Prof. Eng. KISS Imre, PhD.
UNIVERSITY POLITEHNICA TIMISOARA,
FACULTY OF ENGINEERING HUNEDOARA

Commenced publication year:
2008

ACTA TECHNICA CORVINIENSIS

Bulletin of Engineering

ASSOCIATE EDITORS and REGIONAL COLLABORATORS

The Editor and editorial board members do not receive any remuneration. These positions are voluntary. The members of the Editorial Board may serve as scientific reviewers.

We are very pleased to inform that our journal **ACTA TECHNICA CORVINIENSIS – Bulletin of Engineering** is going to complete its ten years of publication successfully. In a very short period it has acquired global presence and scholars from all over the world have taken it with great enthusiasm. We are extremely grateful and heartily acknowledge the kind of support and encouragement from you.

ACTA TECHNICA CORVINIENSIS – Bulletin of Engineering seeking qualified researchers as members of the editorial team. Like our other journals, **ACTA TECHNICA CORVINIENSIS – Bulletin of Engineering** will serve as a great resource for researchers and students across the globe. We ask you to support this initiative by joining our editorial team. If you are interested in serving as a member of the editorial team, kindly send us your resume to redactie@fih.upt.ro.

ISSN: 2067-3809

INTERNATIONAL SCIENTIFIC COMMITTEE MEMBERS and SCIENTIFIC REVIEWERS

MANAGER & CHAIRMAN

ROMANIA 

Imre KISS, University Politehnica TIMISOARA, Faculty of Engineering HUNEDOARA

INTERNATIONAL SCIENTIFIC COMMITTEE MEMBERS & SCIENTIFIC REVIEWERS from:

ROMANIA 

Viorel–Aurel ȘERBAN, University Politehnica TIMIŞOARA – TIMIŞOARA
Teodor HEPUȚ, University Politehnica TIMIŞOARA – HUNEDOARA
Ilare BORDEAȘU, University Politehnica TIMIŞOARA – TIMIŞOARA
Liviu MARȘAVIA, University Politehnica TIMIŞOARA – TIMIŞOARA
Ioan VIDA–SIMITI, Technical University of CLUJ–NAPOCA – CLUJ–NAPOCA
Sorin VLASE, "Transilvania" University of BRAŞOV – BRAŞOV
Horatiu TEODORESCU DRĂGHICESCU, "Transilvania" University of BRAŞOV – BRAŞOV
Maria Luminița SCUTARU, "Transilvania" University of BRASOV – BRASOV
Carmen ALIC, University Politehnica TIMIŞOARA – HUNEDOARA
Sorin DEACONU, University Politehnica TIMIŞOARA – HUNEDOARA
Liviu MIHON, University Politehnica TIMIŞOARA – TIMIŞOARA
Valeriu RUCAI, University Politehnica BUCUREŞTI – BUCUREŞTI

SLOVAKIA 

Ervin LUMNITZER, Technical University of KOŠICE – KOŠICE
Miroslav BADIDA, Technical University of KOŠICE – KOŠICE
Karol VELIŠEK, Slovak University of Technology BRATISLAVA – TRNAVA
Imrich KISS, Institute of Economic & Environmental Security – KOŠICE
Vladimir MODRAK, Technical University of KOSICE – PRESOV

CROATIA 

Drazan KOZAK, Josip Juraj Strossmayer University of OSIJEK – SLAVONKI BROD
Predrag COSIC, University of ZAGREB – ZAGREB
Milan KLJAJIN, Josip Juraj Strossmayer University of OSIJEK – SLAVONKI BROD
Antun STOIĆ, Josip Juraj Strossmayer University of OSIJEK – SLAVONKI BROD
Ivo ALFIREVIĆ, University of ZAGREB – ZAGREB

HUNGARY 

Imre DEKÁNY, University of SZEGED – SZEGED
Cecilia HODÚR, University of SZEGED – SZEGED
Béla ILLÉS, University of MISKOLC – MISKOLC
Imre RUDAS, Óbuda University of BUDAPEST – BUDAPEST
István BIRÓ, University of SZEGED – SZEGED
Tamás KISS, University of SZEGED – SZEGED
Imre TIMÁR, University of Pannonia – VESZPRÉM
Károly JÁRMAI, University of MISKOLC – MISKOLC
Ádám DÖBRÖCZÖNI, University of MISKOLC – MISKOLC
György SZEIDL, University of MISKOLC – MISKOLC
Miklós TISZA, University of MISKOLC – MISKOLC
József GÁL, University of SZEGED – SZEGED
Ferenc FARKAS, University of SZEGED – SZEGED
Géza HUSI, University of DEBRECEN – DEBRECEN

SERBIA 

Sinisa KUZMANOVIC, University of NOVI SAD – NOVI SAD
Mirjana VOJINOVIĆ MILORADOV, University of NOVI SAD – NOVI SAD
Miroslav PLANČAK, University of NOVI SAD – NOVI SAD

MACEDONIA 

Valentina GECEVSKA, University "St. Cyril and Methodius" SKOPJE – SKOPJE
Zoran PANDILOV, University "St. Cyril and Methodius" SKOPJE – SKOPJE

The SCIENTIFIC COMMITTEE MEMBERS AND REVIEWERS do not receive any remuneration. These positions are voluntary.

We are extremely grateful and heartily acknowledge the kind of support and encouragement from all contributors and all collaborators!

ACTA TECHNICA CORVINIENSIS – Bulletin of Engineering is dedicated to publishing material of the highest engineering interest, and to this end we have assembled a distinguished Editorial Board and Scientific Committee of academics, professors and researchers.

ACTA TECHNICA CORVINIENSIS – Bulletin of Engineering publishes invited review papers covering the full spectrum of engineering. The reviews, both experimental and theoretical, provide general background information as well as a critical assessment on topics in a state of flux. We are primarily interested in those contributions which bring new insights, and papers will be selected on the basis of the importance of the new knowledge they provide.

ACTA TECHNICA CORVINIENSIS – Bulletin of Engineering encourages the submission of comments on papers published particularly in our journal. The journal publishes articles focused on topics of current interest within the scope of the journal and coordinated by invited guest editors. Interested authors are invited to contact one of the Editors for further details.

ACTA TECHNICA CORVINIENSIS – Bulletin of Engineering accept for publication unpublished manuscripts on the understanding that the same manuscript is not under simultaneous consideration of other journals. Publication of a part of the data as the abstract of conference proceedings is exempted.

Manuscripts submitted (original articles, technical notes, brief communications and case studies) will be subject to peer review by the members of the Editorial Board or by qualified outside reviewers. Only papers of high scientific quality will be accepted for publication. Manuscripts are accepted for review only when they report unpublished work that is not being considered for publication elsewhere.

The evaluated paper may be recommended for:

- **Acceptance without any changes** – in that case the authors will be asked to send the paper electronically in the required .doc format according to authors' instructions;
- **Acceptance with minor changes** – if the authors follow the conditions imposed by referees the paper will be sent in the required .doc format;
- **Acceptance with major changes** – if the authors follow completely the conditions imposed by referees the paper will be sent in the required .doc format;
- **Rejection** – in that case the reasons for rejection will be transmitted to authors along with some suggestions for future improvements (if that will be considered necessary).

The manuscript accepted for publication will be published in the next issue of **ACTA TECHNICA CORVINIENSIS – Bulletin of Engineering** after the acceptance date.

All the authors and the corresponding author in particular take the responsibility to ensure that the text of the article does not contain portions copied from any other published material which amounts to plagiarism. We also request the authors to familiarize themselves with the good publication ethics principles before finalizing their manuscripts.

ISSN: 2067–3809

Fascicule 3

[July – September]

tome [2023] XVI

ACTA Technica CORVINIENSIS
BULLETIN OF ENGINEERING

ISSN: 2067-3809

TABLE of CONTENTS

ACTA TECHNICA CORVINIENSIS – Bulletin of Engineering

Tome XVI [2023],

Fascicule 3 [July – September]

The ACTA TECHNICA CORVINIENSIS – Bulletin of Engineering, Tome XVI [2023], Fascicule 3 [July–September] includes original papers submitted to the Editorial Board, directly by authors or by the regional collaborators of the Journal.

Also, the ACTA TECHNICA CORVINIENSIS – Bulletin of Engineering, Tome XVI [2023], Fascicule 3 [July–September], includes scientific papers presented in the sections of:

- ISB–INMA TEH' 2022 – International Symposium (Agricultural and Mechanical Engineering), organized by Politehnica University of Bucharest – Faculty of Biotechnical Systems Engineering (ISB), National Institute of Research–Development for Machines and Installations Designed to Agriculture and Food Industry (INMA Bucharest), Romanian Agricultural Mechanical Engineers Society (SIMAR), National Research & Development Institute for Food Bioresources (IBA Bucharest), National Institute for Research and Development in Environmental Protection (INCDPM), Research–Development Institute for Plant Protection (ICDPP), Research and Development Institute for Processing and Marketing of the Horticultural Products (HORTING), Hydraulics and Pneumatics Research Institute (INOE 2000 IHP) and "Food for Life Technological Platform", in Bucharest, ROMANIA, between 06–07 October, 2022. The current identification numbers of the selected papers are the #10–12, #15–17 and #19–20, according to the present contents list.

ACTA TECHNICA CORVINIENSIS – Bulletin of Engineering is a good opportunity for the researchers to exchange information and to present the results of their research activity. Scientists and engineers with an interest in the respective interfaces of engineering fields, technology and materials, information processes, research in various industrial applications are the target and audience of ACTA TECHNICA CORVINIENSIS – Bulletin of Engineering. It publishes articles of interest to researchers and engineers and to other scientists involved with materials phenomena and computational modeling.

The journal's coverage will reflect the increasingly interdisciplinary nature of engineering, recognizing wide–ranging contributions to the development of methods, tools and evaluation strategies relevant to the field. Numerical modeling or simulation, as well as theoretical and experimental approaches to engineering will form the core of ACTA TECHNICA CORVINIENSIS – Bulletin of Engineering's content, however approaches from a range of environmental science and economics are strongly encouraged.

Publishing in ACTA TECHNICA CORVINIENSIS – Bulletin of Engineering is free of charge. There are no author fees. All services including peer review, copy editing, typesetting, production of web pages and reproduction of color images are included. The journal is free of charge to access, read and download. All costs associated with publishing and hosting this journal are funded by ACTA TECHNICA CORVINIENSIS – Bulletin of Engineering as part of its investment in global research and development.

ISSN: 2067–3809

Fascicule 3

[July – September]

tome [2023] XVI

ACTA Technica CORVINIENSIS
BULLETIN OF ENGINEERING

ISSN: 2067-3809

[1.]Babatope Abimbola OLUFEMI, [1.]Habeeb Olabisi ALABI

OPTIMUM ADSORPTION OF LEAD FROM WASTE WATER USING BEANS HUSK

[1.]Chemical and Petroleum Engineering Department, University of Lagos, Akoka, Yaba, Lagos, NIGERIA

Abstract: This study is aimed at determining the optimum adsorption of lead from waste water onto activated carbon prepared from bean husk. The optimization was designed using response surface methodology. Box–Behnken design was employed to generate a matrix and the factors considered were pH (2–10), temperature (25–65 °C) and contact time (20–120 minutes). It generated 12 experimental runs and the selected responses were adsorption capacity and removal efficiency. Run nine (9) gives the highest adsorption capacity (19.8 mg/g) and removal efficiency (99%) while run five (5) gives the lowest adsorption capacity (7 mg/g) and remover efficiency (33%). The result indicates that the Optimum condition for the adsorption Pb (II) from waste water were pH (10), temperature (65^{0}C) and Contact time (120 minutes). This gave Adsorption Capacity of 19.940mg/g and 99.698% Removal Efficiency of Pb from waste water. There was good agreement between experimental value and predicted value. The study also showed that activated carbon from beans husk is an effective adsorbent for the removal of Pb (II) from waste water.
Keywords: Beans husk, Optimum, Adsorption capacity, Removal efficiency

INTRODUCTION

Discharge of pollutants containing heavy metals into water systems is one of the most serious environmental problems globally (Das et al., 2007; Ibrahim et al., 2010). With the rapid industrialization in developing and developed countries, large volumes of wastes containing heavy metals are generated and directly or indirectly discharged into water ecosystems thus posing significant danger to human health.

Pollutants enter aquatic systems via numerous pathways, including metal finishing, electroplating, painting, dying, photography, surface treatment and printed circuit board manufacture (Papageorgiou et al., 2006). Heavy metals can also enter water bodies via mining activities, agricultural run–off and domestic effluent which lead to increase in metallic species released into the environment (Churong et al., 2013). The presence of toxic and polluting heavy metals in wastewaters from industrial effluents, water supplies and mine waters and their removal has received much attention in recent years. The number of heavy metals that industrial wastewaters often contain is considerable and would endanger public health and the environment if discharged without adequate treatment.

Among all the water pollutants, heavy metal contaminations are posing a serious threat for human society. Heavy metal is a general collective term applying to the group of metals and metalloids with an atomic density higher than 6 g cm^{-3}. However, it is only a loosely defined term, which is widely recognized and usually applied to the metal elements associated with pollution and toxicity problems. Three categories of heavy metals viz. toxic metals, precious metals and radionuclides are of environmental concern. Substantial amount of various toxic metals is released into water system by many types of industries, such as mining and smelting of minerals, the surface finishing industry, energy and fuel production, fertilizer and pesticide industry and subsequent application, metallurgy, iron and steel, electroplating, electrolysis, electro–osmosis, leatherworking, electric appliance manufacturing, photography, aerospace and atomic energy installation etc. For example, mining industries release heavy metal ions such as lead (Pb (II)), mercury (Hg (II)), silver (Ag(I)), chromium (Cr (III)), arsenic (As (V)), cadmium (Cd (II)), palladium (Pd (II)), zinc (Zn (II)) and aluminum (Al (III)) to the environment.

Water pollution by heavy metals has been a major concern for chemists and environmental engineers (Ekpete, 2017). Heavy metals are of concern because of their toxicity, bio–accumulating tendency, threat to human life and the environment (Dorris et al., 2000).

Throughout history, human progress has depended on access to clean water and on the ability of societies to harness the potential of water as a productive resource (HDR, 2006). Water for life in the household and water for livelihoods through production are two of the foundations for human. Therefore, there is a growing concern that the world is facing a crisis of shortage of clean water that if left unchecked, will derail progress towards the Millennium Development Goals and hold back human development.

In cooperation with the U.S. Environmental Protection Agency, the Agency for Toxic Substances and Disease Registry (ATSDR) has compiled a Priority List for 2011 called the ATSDR 2011 Substance Priority List. Based on the list, lead is ranked as second hazardous heavy metals among the substances after arsenic (ATSDR, 2011).

Lead is of concern because once it gets into the environment, it bio–accumulate and bio–magnify as it go through the tropic levels of the food chain. Furthermore, metals being inorganic, they are non–biodegradable. It is

therefore important that they are excluded from circulation in the ecosystem due to various neurological, reproductive and systemic impacts on humans and negative impacts on other animals especially the aquatic species.

Conventional physicochemical methods for metals remediation include chemical precipitation, filtration, coagulation, evaporation, ion exchange, membrane separation and solvent extraction. However, application of such processes is always expensive and ineffective in terms of energy and chemical products consumption, especially at low metal concentrations of 1–100 mg/L (Bian et al., 2015). Therefore, there is a great need for an alternative technique, which is both economical and efficient. Adsorption has been shown as the most appealing as an economic and environmentally friendly procedure to remove heavy metals in wastewater (Ahmad et al., 2009). Activated carbon is the most popular material used as an adsorbent. However, it is quite expensive. The search for alternative adsorbents to replace the costly activated carbon is highly encouraged. Adsorption, based on live or dead adsorbent, has been regarded as a cost–effective biotechnology for the treatment of complex wastewater containing heavy metals at high volume and low concentration (Amboga et al., 2014).

In addition, converting beans husk into value added products such as adsorbents would serve as a way to mitigate the disposal challenges posed by this waste materials to the environment. Also, the industries involved in conversion of this waste materials would serve as an indirect way of revenue generation and simultaneously for job creation. This research is part of that process of developing an alternative technology for utilizing cheap effective and available adsorbent for the adsorptive removal of lead from wastewater.

Optimization using response surface methodology can be used to determine the optimum conditions involved in a process (Onu et al., 2014 and Ositadinma et al., 2019). It is different from the method of one factor at a time (OFAT) which involves keeping all other parameters constant while varying one factor. OFAT method uses a large number of experiments in determining the optimum condition. It is time consuming and does not show the interactive effects of the independent factors unlike optimization using response surface methodology (RSM). Design of experiment using RSM is an enhanced systematic experimentation that takes into consideration all the process parameters involved simultaneously (Onu et al., 2014 and Ositadinma et al., 2019).

Hence the aim of this work is to use response surface methodology to optimize the process parameters for the optimum adsorption of lead from waste water onto activated carbon prepared from bean husk.

MATERIALS & METHOD

Materials

The beans husk was collected from the local market in Oyingbo, Lagos, Nigeria.

Apparatus and Reagents used

The following apparatus and reagents were used: analytical grade hydrochloric acid (Epoxy Oilserv, 30% w/w purity); analytical grade sodium hydroxide (Epoxy Oilserv, 98% purity); analytical grade Lead (II) nitrate (Indian Platinum, 98% purity); distilled water; Rotary shaker (Bioevopeak SHK–O0310111, China); Weighing balance (AL Mettler Toledo GmbH); Furnace (Bioevopeak FNC–TB1700, China); Oven (Gallenkamp, England); pH meter (HANNA Instrument pHep®); Beaker (Pyrex, England); Conical flask (Pyrex, England); Measuring cylinder (Pyrex, England); Atomic absorption Spectrophotometer (Perkin Elmer Analyst 200); Scanning electron Microscope (Model Jeol–JXA 840 A, Japan); Water bath shaker (Grant OLS 200); Filter paper (Whatman)'Stop watch (Electronic Timer,TIME–Q118, China); Sieve (B.S.S. 200–100); FTIR Spectrometer (Nicolet Avator 330, England).

Adsorbent Preparation

The beans husk was prepared by adopting the method of Ositadinma et al., (2019). It was washed thoroughly with distilled water to remove dust and soil, dried in sunlight for 2 days and kept in an oven at 70°C for 24hours.

Carbonization

The carbonization process was done by the procedure adopted by Sandip et al., (2017). The beans husk was heated in the Muffle Furnace at 450°C for 30min then permitted to cool. The beans husk was then crushed with blender and sieved to a size smaller than 850 µm. The yield of carbon is defined as the ratio of final weight of the obtained product after carbonization to the weight of dried precursor initially used was calculated using:

$$\text{Yield}(\%) = \frac{\text{product}}{\text{reactant}} \times 100 \quad (1)$$

Activation

The activation process was done by the procedure adopted by Hanum et al., (2017). The carbonized beans husk was impregnated with 1M HCL at carbon to acid ratio of 1:3(w/v) for 24 hours. Afterwards it was placed in a furnace and heated at 650°C for 30minutes. The resulting sample was allowed to cool and watched with distilled water until neutral pH was reached.

Moisture Content

1 g of activated carbon was placed oven and heated at 105–110°C for 1.5 hr (Hanum et al., 2017). Then, sample was cooled in and the weight of dried sample was measured. Moisture content was calculated as follow:

$$\text{M} = \frac{\text{weight of dried sample}}{\text{weight of original sample}} \times 100 \quad (2)$$

Ash Content

1 g of activated carbon was heated in a muffle furnace at 750°C for 1.5 hr hr (Hanum et al., 2017).

The sample was cooled and the weight of the ash was measured

$$A = \frac{\text{weight of ash sample}}{\text{weight of sample}} \times 100 \quad (3)$$

Scanning Electron Microscope (SEM)

To determine the surface morphological composition of the prepared adsorbent. The SEM analysis was carried out at the magnifications X–900, and X–10,000.

Adsorbate

Lead (II) nitrate (Indian Platinum, 98% purity) was used as the adsorbate and was obtained from luth Lagos. It was prepared by dissolving 1 g of Pb(NO3)2 in 1 litres of distilled water.

Design of Experiment

Design Expert 13 was used to design the experiment. It was employed to check for the interdependence of more than one factor by identifying their overall effect (Olufemi et al.,2018). Box–Behnken design was employed.

Box–Behnken design

The main factors (pH, temperature and contact time) were selected, as well as their factor levels, coded as –1 (low) and +1 (high), as seen in Table 3.2 Box–Behnken design was employed and a matrix generated. It generated 12 experimental runs. The selected responses were adsorption capacity and removal efficiency.

Table 1. Input factors with their code levels using Box–Behnken design

Factors	Units	Low	High
Ph	–	2	10
Time	Min	20	120
Temperature	°C	25	65

Batch adsorption Process

2 g of beans husk derived activated and 40ml of 1000 mg/L lead solution was fixed in all the batch sorption experiment on a water bath shaker (Grant OLS 200) at 120rpm. Process optimization was done by altering the pH (2–10), contact time (20–120 minutes) and temperature (25–65°C). The final concentration of lead was determined through the use atomic absorption Spectrophotometer (Perkin Elmer Analyst 200). The % removal of Lead (II) ion and the adsorption capacity of the beans husk was calculated using the following equation,

$$q_e = \frac{C_0 - C_t}{M} \times V \quad (4)$$

$$\text{Removal (\%)} = \frac{C_0 - C_t}{C_0} \times 100 \quad (5)$$

M = mass of activated carbon in gram
V = volume of test solution in liter
C_o = initial concentration of lead
C_t = final concentration of lead
q_e is the amount of solute removed or adsorbed

RESULTS & DISCUSSION

Physical Properties of the Adsorbent

Table 2 presents the physical properties of the adsorbent with values of the ash content, moisture content and pH.

Table 2. Physical Properties Beans Husk Adsorbent

Properties	Bean Husk
Ash Content (%)	3.5
Moisture Content (%)	8.8
pH	6.8

Scanning Electron Microscopy (SEM)

Scanning electron microscopy has been extensively used to study the surface morphology of the Activated carbons.

The SEM images of the HCL impregnated activated carbon before and after adsorption are shown in the figures below. The SEM analysis was carried out at a magnification of 9,000X Before adsorption and 8,000X after adsorption, the surface morphology of activated carbon has uneven cavities and fine open pores which indicate its ability to absorbed metal ions from wastewater.

The large pores observed is due to the fact the activating agents promote the contact area between the carbon and the activating agent. The HCL activated carbon clearly showed partially developed honey comb like highly defined pores and cavities in its surface. However, the pores are not–uniform.

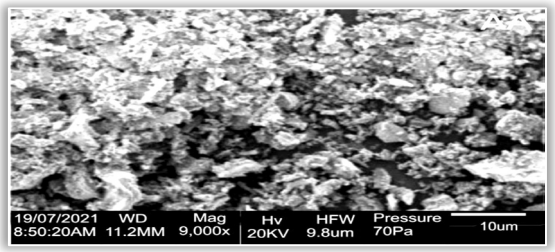

Figure 1. SEM of beans husk before Adsorption

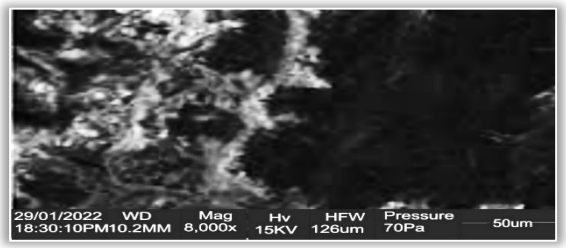

Figure 2. SEM of beans husk after Adsorption

During carbonization process, pores are developed in the carbon and promote the diffusion of HCL molecules into these pores and thereby increase the HCL–carbon reactions which would then create more pores in the activated carbon. This would enhance the surface area and pore volume of the activated carbon so prepared. The SEM image after adsorption shows smaller pores as a result of adsorption Pb on the beans husk.

Optimization Process

The result of the experimental runs in the optimization process indicated that the best adsorption conditions are at pH of 6, contact time of 120 minutes and temperature of 65°C. This gave the highest adsorption capacity of 19.8(mg/g) and removal efficiency lead. The result

equally revealed that the three factors optimized have great effect on the adsorption of lead from waste water.

The model summary values suggested that a linear model best fitted the optimization process. The R–squared values for the quadratic and 2FI models is slightly greater than of linear. But we focus on the model maximizing the adjusted R^2 predicted R^2. The quadratic model was aliased and aliases are false signals of any sort present hence the linear model was suggested.

Table 3. Experimental Design Matrix for the Optimization Studies

Std	Run	pH	Time (Min)	Temperature (°C)	Adsorption Capacity (mg/g)	Removal Efficiency (%)
4	1	10	120	45	18.2	91
6	2	10	70	25	18.5	92.5
10	3	6	120	25	17.6	88
3	4	2	120	45	12	60
7	5	2	70	65	7	35
11	6	6	20	65	13.6	68
1	7	2	20	45	12.4	62
2	8	10	20	45	16	80
12	9	6	120	65	19.8	99
8	10	10	70	65	16.8	84
5	11	2	70	25	10	50
9	12	6	20	25	9.6	48

Table 4. Model Summary Statistics for adsorption capacity

Source	Std. Dev.	R^2	Adjusted R^2	Predicted R^2	
Linear	2.63	0.7027	0.5913	0.3312	Suggested
2FI	3.24	0.7184	0.3805	–0.6219	Not Suggested
Quadratic	3.79	0.7687	0.1521	–2.7000	Aliased

Table 5. Model Summary Statistics for removal efficiency

Source	Std. Dev.	R^2	Adjusted R^2	Predicted R^2	
Linear	13.16	0.7027	0.5913	0.3312	Suggested
2FI	16.20	0.7184	0.3805	–0.6219	
Quadratic	18.95	0.7687	0.1521	–2.7000	Aliased

Analysis of Variance (ANOVA) for Adsorption Capacity and Removal Efficiency

The ANOVA in Table 5 and 6 was used to analysis the result and validate the adsorption model.

Table 6. ANOVA for Adsorption Capacity

Source	Sum of Squares	Df	Mean Square	F–value	p–value	
Model	130.98	3	43.66	6.30	0.0168	significant
A–pH	98.70	1	98.70	14.25	0.0054	
B–Contact time	32.00	1	32.00	4.62	0.0638	
C–Temperature	0.2813	1	0.2813	0.0406	0.8453	
Residual	55.41	8	6.93			
Cor Total	186.39	11				

Table 7. ANOVA for Removal Efficiency

Source	Sum of Squares	Df	Mean Square	F–value	p–value	
Model	3274.56	3	1091.52	6.30	0.0168	significant
A–pH	2467.53	1	2467.53	14.25	0.0054	
B–Contact time	800.00	1	800.00	4.62	0.0638	
C–Temperature	7.03	1	7.03	0.0406	0.8453	
Residual	1385.17	8	173.15			
Cor Total	4659.73	11				

The lack of fit test and the adequacy of the regression models were equally performed. A significance level of 5% was used hence P–values greater than 0.05 are considered insignificant while those at 0.05 or less are significant. Hence, only the interactions of A, B and C are significant. The model F–value of 6 implies that the model is significant agreeing with the P–value being less than 0.05. There is only a 1.68% chance that an F–value this large could occur due to noise. There is only a 1.68% chance that an F–value this large could occur due to noise. The P values check the significance of the factors and equally help to understand the pattern of the mutual interactions between the test variables (Shrivastava, 2008).

Optimum Model Equations

The generated model equations for the adsorption process in terms of coded factors are:

$$\text{Adsorption Capacity (mg/g)} = 4.29+3.51A+2B+0.1875C \quad (6)$$

$$\text{Removal Efficiency (\%)} = 71.46+17.56A+10B+0.9375C \quad (7)$$

The equation in terms of coded factors can be used to make predictions about the response for given levels of each factor. By default, the high levels of the factors are coded as +1 and the low levels are coded as –1. The coded equation is useful for identifying the relative impact of the factors by comparing the factor coefficients. The positive sign of a factor indicates that there will be increase in the response when there is an increase in the factor while negative sign will lead to decrease in the response (Kumar, 2008). The generated model equations for the adsorption process in terms of actual factors are:

$$\text{Adsorption Capacity (mg/g)} = 5.80104+0.878125A+0.040B+0.009375C \quad (8)$$

$$\text{Removal Efficiency (\%)} = 29.00521+4.39063A+0.2000B+0.046875C \quad (9)$$

The equation in terms of actual factors can be used to make predictions about the response for given levels of each factor. Here, the levels should be specified in the original units for each factor. This equation should not be used to determine the relative impact of each factor because the coefficients are scaled to accommodate the units of each factor and the intercept is not at the center of the design space.

Diagnostics Case study

Table 7 shows the diagnostic case study of adsorption capacity and removal efficiency of Pb.

Table 8. Diagnostic case study of adsorption capacity and removal efficiency of Pb

Run Order	Adsorption Capacity			Removal Efficiency		
	Actual Value	Predicted Value	Residual	Actual Value	Predicted Value	Residual
1	18.20	19.80	–1.60	91.00	99.02	–8.02
2	18.50	17.62	0.8833	92.50	88.08	4.42
3	17.60	16.10	1.50	88.00	80.52	7.48
4	12.00	12.78	–0.7792	60.00	63.90	–3.90
5	7.00	10.97	–3.97	35.00	54.83	–19.83
6	13.60	12.48	1.12	68.00	62.40	5.60
7	12.40	8.78	3.62	62.00	43.90	18.10
8	16.00	15.80	0.1958	80.00	79.02	0.9792
9	19.80	16.48	3.32	99.00	82.40	16.60
10	16.80	17.99	–1.19	84.00	89.96	–5.96
11	10.00	10.59	–0.5917	50.00	52.96	–2.96
12	9.60	12.10	–2.50	48.00	60.52	–12.52

The residual values represent the closeness of actual to the predicted value. When the predicted value is greater than the actual, there will be a negative residual but when the value of actual is greater than the predicted, we have a positive residual.

Error Graph

The Predicted vs Actual plot in Fig. 3 and the Normal plot of Residuals in Fig. 4 were used to determine if the residuals follow a normal distribution.

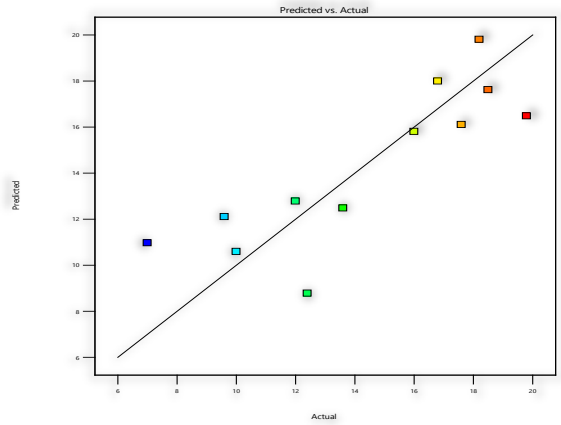

Figure 3. Predicted vs Actual plot

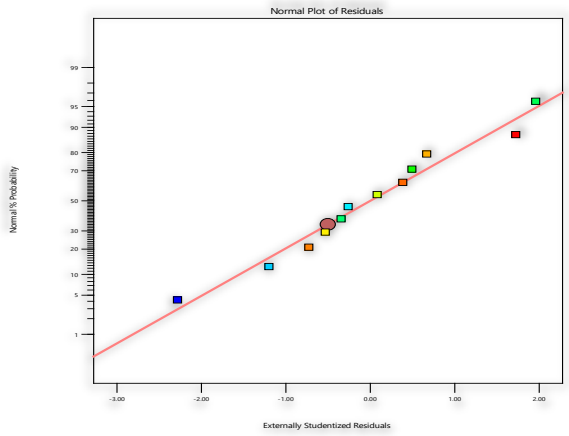

Figure 4. Normal plot of Residuals

It is assumed to have followed a normal distribution as the points closely aligned to the straight line of the plot thereby confirming the good relationship between the experimental values and the predicted values of the response and the adequacy of the suggested model in predicting the response variables in the experimental values (Ositadinma, et al., 2019). From the plot of predicted versus actual, the closer the points to the normal line, the greater the R–squared and vice–versa

Model Graph

The 3–D response surface plots are graphical representation of the interactive effects of any two variables factors. Response surface estimation serves as a function of two factors at a time, maintaining other factors at fixed levels. This is more helpful in understanding both the main and the interaction effects of those two factors. These plots can be easily obtained by calculating from the model, the values taken by one factor where the second varies with constraint of a given response value. The response surface curves were plotted to understand the interaction of the variables and to determine the optimum levels of each variable for maximum response. The nature of the response surface curves shows the interaction between the variables. The elliptical shape of the curve indicates good interaction of the two variables and circular shape indicates no interaction between the variables (Ositadinma et al., 2019). There was a relative significant interaction between every two variables, and there was a maximum predicted efficiency as indicated by the surface confined in the smallest ellipse in the contour diagrams. It was also observed from contour and 3D representation that increase in contact time, temperature and pH increases adsorptio capacity and removal efficiency.

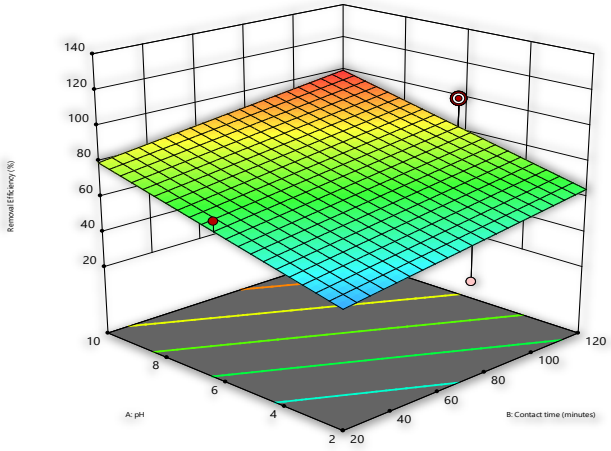

Figure 4. Interactive effect of pH and contact time

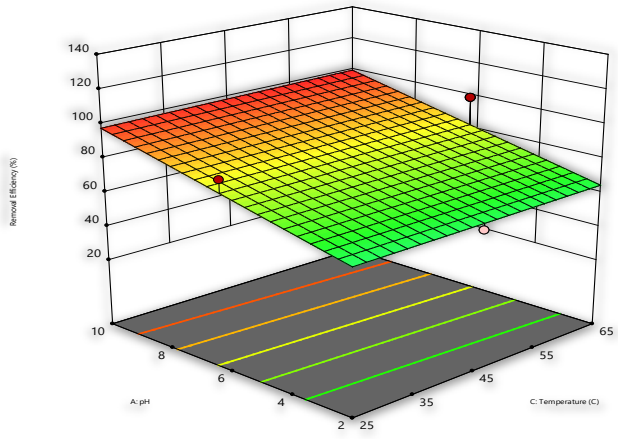

Figure 5. Interactive effect of pH and temperature

Numerical Operation Studies on Adsorption Capacity and Removal Efficiency

The optimization study for adsorption capacity and removal efficiency was obtained from Design expert software (13). The three selected factors which are pH, Temperature, and Contact time were all set to "maximize" with their respective upper and lower limit as shown in table 8. Optimum value suggested for pH was

10, temperature value was 65°C and Contact time was 120 minutes. There was agreement between actual and predicted value.

Table 9. Selected factors used for optimization showing their respective ranges

Name	Goal	Lower Limit	Upper Limit	Lower Weight	Upper Weight	Importance
A: pH	maximize	2	10	1	1	3
B: Contact time	maximize	20	120	1	1	3
C: Temperature	maximize	25	65	1	1	3
Adsorption Capacity	maximize	7	19.8	1	1	3
Removal Efficiency	maximize	35	99	1	1	3

CONCLUSIONS

Optimization of factors for the adsorption Pb (II) was successfully carried out using the Box–Behnken design in the design of expert. 12 experimental runs were generated. run nine (9) with experimental condition of (65°C, 120 mins and pH 6) gives the highest adsorption capacity and removal efficiency of 19.8(mg/g) and 99% respectively while run five (5) with experimental condition of (65°C, 70mins and pH 6) gives the lowest adsorption capacity and remover efficiency of 7(mg/g) and 33% respectively. A linear model with a high correlation coefficient was suggested in describing the interactive effects of the process parameters The numerical values for the optimum adsorption of Pb (II) from waste water was optimized to be pH (10), temperature (65°C) and Contact time (120 minutes). There was agreement between actual and predicted optimization value. The Activated carbon was prepared from beans husk via the chemical method using HCL as activating agent and was also characterized to determine the basic properties and surface morphology of activated carbon. The ash content, moisture content and pH value of the beans activated carbon are 3.5%, 8.8% and 6.8 respectively. It can be concluded that a waste material like beans husk is an effective and suitable adsorbent for removing Pb (II) ion from aqueous solution, and a probable cost–effective adsorbent for treating Pb (II) contaminated water.

References

[1] Agency for Toxic Substance and Disease Registry. Toxicological profile for lead. Atlanta: U.S. Department of Health and Humans Services, Public Health Service, Centres for Diseases Control,2011.

[2] Ahmad, A., Rafatullah, M., Sulaiman, O., Ibrahim, M. H., Chii, Y. Y., & Siddique, B. M., Removal of Cu (II) and Pb (II) ions from aqueous solutions by adsorption on sawdust of Meranti wood. Desalination, 247(1–3), 636–646,2009.

[3] Amboga, M., Shah, J. A., Ashfaq, T., Gardazi, S. M. H., Tahir, A. A., Pervez, A., Haroon, H. & Mahmood, Q., Waste biomass adsorbents for copper removal from industrial wastewater—a review. Journal of hazardous materials, 263, 322–333,2014

[4] Bian, Y., Bian, Z., Zhang, J., Ding, A., Liu, S., Zheng, L. & Wang, H., Adsorption of cadmium ions from aqueous solutions by activated carbon with oxygen–containing functional groups. Chinese Journal of Chemical Engineering, 23, 1705–1711,2015.

[5] Churong, N. & Gradwohl, R., Estimation of Cd, Pb, and Zn bioavailability in smelter–contaminated soils by a sequential extraction procedure. Journal of Soil Contamination, 9, 149–164,2013.

[6] Das, N., Vimala, R., & Karthika, P., Biosorption of heavy metals, an overview. Indian journal of Biotechnology,7(2), 159–169,2008.

[7] Dorris, P. H., The use of extractants in studies on trace metals in soils, sewage sludges, and sludge–treated soils. Advances in soil science. Springer,2000.

[8] Ekpete, O. A., Marcus, A. C., & Osi, V., Preparation and characterization of activated carbon obtained from plantain (Musa paradisiaca) fruit stem. Journal of Chemistry,2017.

[9] Hanum, F., O. Bani, and L.I. Wirani. Characterization of Activated Carbon from Rice Husk by HCl Activation and Its Application for Lead (Pb) Removal in Car Battery Wastewater. Applied Science and Engineering Conference,2017.

[10] Human Development Report. Beyond scarcity: Power, poverty and the global water crisis,2006.

[11] Ibrahim M. A., New trends in removing heavy metals from industrial wastewater. Review Article. Arabian Journal of Chemistry, 4: 361–377, 2010.

[12] Kumar, N., Application of Response Surface Methodology for Multiple Responses in Turning AISI 1045 Steel. Arab J Sci Eng,2008.

[13] Olufemi, B. A. and O. Eniodunmo. Adsorption of Nickel (II) Ions from Aqueous Solution using Banana Peel and Coconut Shell. International Journal of Technology, vol. 9, no.3, 434 –445, 2018.

[14] Onu C.E., Nwabanne JT. Application of Response Surface Methodology in Malachite green adsorption using Nteje clay. Open Journal of Chemical Engineering and Science.1(2):19–33, 2014.

[15] Ositadinma, I.C., Tagbor, N.J. and Elijah, O.C., Optimum Process Parameters for Activated Carbon Production from Rice Husk for Phenol Adsorption. Current Journal of Applied Science and Technology, 36(6): 1–11, 2019

[16] Papageorgiou C. A., Somasundaram, M., Kannadasan, T. & Lee, C. W., Heavy metals removal from copper smelting effluent using electrochemical filter press cells. Chemical Engineering Journal, 171, 563–571, 2006.

[17] Sandip M., Kaustav A., and Gopinath H: Biosorptive uptake of arsenic(V) by steam activated carbon from mung bean husk: equilibrium, kinetics, thermodynamics and modelling. Appl Water Sci,2017.

[18] Srivastava, N.K., & Balomajumder, C., Novel biofiltration methods from industrial wastewater. Journal of Hazardous Materials,151(1):1–8, 2008.

ISSN: 2067-3809

[1.] Alexandru–Polifron CHIRIȚĂ, [1.]Andrei–Alexandru BENESCU, [1.]Adriana Mariana BORȘ,
[1.]Ștefan–Mihai ȘEFU, [1.]Robert BLEJAN

THE IMPORTANCE OF REVERSE ENGINEERING AND 3D SCANNING IN REMANUFACTURING HYDRAULIC DRIVE SYSTEM COMPONENTS IN THE CIRCULAR ECONOMY CONTEXT

[1.] National Institute of Research & Development for Optoelectronics/INOE 2000, Subsidiary Hydraulics and Pneumatics Research Institute/IHP, Bucharest, ROMANIA

Abstract: Reverse engineering and 3D scanning are critical tools for remanufacturing components in the context of the circular economy. By disassembling and measuring existing components, companies can design and develop new parts replacing the old ones, parts that are compatible with the original equipment, either to repair faulty subassemblies, or to improve efficiency or functionality. 3D scanning captures all information needed to reproduce components, allowing them to be created using additive manufacturing processes. Combining these technologies reduces waste by maximizing the use of existing products, and it reduces the amount of new raw materials and energy required for remanufacturing as well. The circular economy encourages companies to embrace a sustainable approach by considering the entire product lifecycle. Adopting these principles leads to a more environmentally friendly business model, avoids waste, reduces material consumption, and creates new revenue streams for remanufactured products. The current paper shows a way of adapting the principle of reverse engineering and a particular way of involving 3D scanning and 3D printing for the remanufacturing of hydraulic system components by using additive manufacturing. The use of 3D scanning is necessary in the reverse engineering process especially for components with complex geometry; in the present paper, the geometry of such a component is created.
Keywords: reverse engineering, 3D scanning, 3D printing, MSLA, remanufacturing, circular economy

INTRODUCTION

In today's rapidly evolving industrial landscape, sustainability and resource efficiency have emerged as critical concerns. As the world faces challenges associated with limited natural resources and increasing waste, the circular economy has gained momentum as a promising solution to foster sustainable practices. Central to the circular economy is the concept of remanufacturing, a process that aims to extend the lifespan of products and reduce waste generation (Turner *et al.*, 2019). In this context, reverse engineering and 3D scanning play indispensable roles, providing innovative and efficient approaches to remanufacturing hydraulic drive system components.

The imperative to enhance sustainability practices in manufacturing has never been more pressing. Traditional linear manufacturing processes follow a "take, make, dispose" model – Figure 1 (Perr, 2020), which inevitably results in the depletion of resources and the accumulation of waste. In stark contrast, the circular economy represents a paradigm shift, envisioning a regenerative system where products are designed to be reused, repaired, and remanufactured (Sun *et al.*, 2022). This approach fosters a closed–loop system, wherein products' end–of–life becomes the beginning of a new production cycle, minimizing the environmental impact (Karimova *et al.*, 2022).

Remanufacturing, as a core pillar of the circular economy, aims to recover value from used products by restoring them to their original condition or better. One of the key challenges in remanufacturing is the need to recreate components that may have become obsolete or damaged over time. This is where reverse engineering steps in as a pivotal technique (Tian *et al.*, 2022).

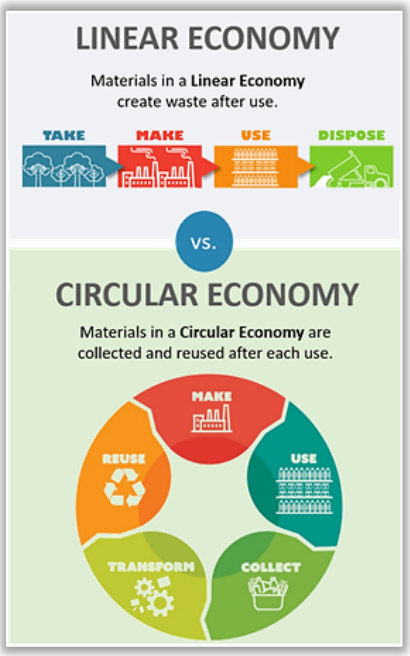

Figure 1. Linear vs circular economy

Reverse engineering involves the disassembly, analysis, and measurement of existing components to understand their design, materials, and functionality. By deconstructing a product, manufacturers gain valuable

insights into its intricacies, facilitating the development of replacement parts that are both compatible and efficient (Atta, 2023). Consequently, this process not only extends the life of the product but also reduces the overall demand for new raw materials, thus contributing to resource conservation (European Commission, n.d.).

In conjunction with reverse engineering, 3D scanning emerges as a cutting–edge technology that revolutionizes the remanufacturing landscape. 3D scanning enables the precise capture of a component's geometrical data, creating a digital replica of the object with remarkable accuracy (Kataev *et al.*, 2023). This digital representation serves as the foundation for employing additive manufacturing processes, commonly known as 3D printing, to recreate the component.

The integration of 3D scanning with additive manufacturing holds immense potential, particularly for components with complex geometry that may be challenging to reproduce using traditional manufacturing methods. By translating digital data into tangible components, manufacturers can effectively remanufacture hydraulic drive system parts with an unparalleled level of precision, reliability, and cost–effectiveness.

Through the convergence of reverse engineering and 3D scanning, remanufacturing processes become more streamlined and environmentally friendly. The reuse of existing components minimizes waste generation, while the incorporation of 3D scanning and additive manufacturing reduces the need for virgin raw materials, thereby lowering the ecological footprint of the remanufacturing process. As a result, companies embracing these innovative techniques position themselves as pioneers in adopting sustainable practices, while also unlocking new revenue streams through the sale of remanufactured products (Ma *et al.*, 2020).

In conclusion, the synergistic use of reverse engineering and 3D scanning represents a transformative approach in remanufacturing hydraulic drive system components within the context of the circular economy. By embracing these advanced technologies, companies can enhance their environmental stewardship (Stuart Chapin III *et al.*, 2010), optimize resource utilization, and ultimately foster a more sustainable and prosperous future for all.

In the following, part of the remanufacturing methodology for a flowmeter is presented, namely the production procedure for the damaged rotor of the flowmeter.

MATERIALS AND METHODS

In the initial stage of the remanufacturing process, the first crucial step towards creating a 3D model of the component involves the application of a matte spray onto the entire surface of the piece (Figure 2). This matte spray plays a pivotal role in enabling successful 3D scanning, as it effectively addresses the challenge posed by glossy surfaces that are difficult for the 3D scanner (with structured light) to capture accurately.

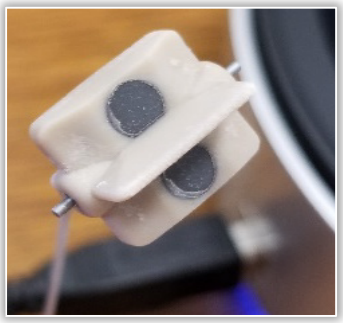

Figure 2. Part sprayed with matte spray

By applying the matte spray, all surfaces of the part become amenable to scanning, ensuring a comprehensive and precise digital representation of the component. The use of the matte spray not only streamlines the 3D scanning process but also enhances the overall remanufacturing endeavor in the circular economy context. By enabling accurate and comprehensive scans of existing components, manufacturers can effectively optimize their resources, minimize waste generation, and contribute to a more sustainable and environmentally responsible approach to manufacturing. The application of a matte spray on the scanned part plays a critical role in facilitating successful 3D scanning for remanufacturing purposes. This technique allows the 3D scanner to capture the entire geometry of the component, overcoming the limitations posed by glossy surfaces.

The process began by placing the part meticulously on the EinScan–SP V2 scanner table, ensuring it was stable and appropriately positioned for scanning. To ensure a comprehensive representation of the part's geometry, two distinct groups of scans were carried out with precision.

In the first scan, the piece was thoughtfully positioned horizontally on the scanning surface. This meticulous arrangement allowed the scanner to capture the intricate details of the part from one vantage point. As the scanning process unfolded, a multitude of data points were gathered, ultimately forming a dense and detailed cloud of 92,000 points. These points served as a digital footprint of the part's surface, effectively mapping its contours and features.

Moving on to the second scan, a deliberate shift of 180 degrees from the part's initial placement was executed. This strategic alteration in positioning ensured a comprehensive view of the part's surfaces from an entirely different perspective. As the scanning commenced once again, a second cloud of points materialized, recording the part's geometry from this new orientation.

With both sets of scans completed, the next crucial step was to merge the two point clouds. By superimposing and aligning the data points obtained from the first and second scans, a cohesive and unified representation of the entire part was achieved. This overlapping process aimed to fill any gaps or discrepancies present in either scan, resulting in a seamless and complete point cloud of the entire part's surface. Figure 3 highlights this process. Finally, leveraging the comprehensive point cloud data, the process culminated in the creation of an STL model of the part. The STL format is widely used for 3D printing and computer–aided design applications. The model accurately mirrored the physical part's geometry, making it a versatile and valuable digital representation for various engineering, manufacturing, and design endeavors. Overall, this meticulous and well–choreographed process of 3D scanning and STL model creation ensured a precise and detailed digital representation of the physical part, opening up a realm of possibilities for its utilization across diverse industries and applications.

Figure 3. The process of 3D scanning of the part and the cloud of points obtained

After generating the STL model through the 3D scanning process, the next step involved importing the model into the SolidWorks software, a powerful computer–assisted modeling (CAD) software widely used in engineering and design industries. SolidWorks offers a robust set of tools and features, enabling the creation and manipulation of complex 3D models with precision. Within SolidWorks, specific measurements and analyses were performed on the 3D model of the piece. By defining three points on two surfaces of the part, multiple planes were obtained. These planes served as references for various geometric analyses and measurements, especially in determining angles between surfaces that could be challenging to obtain using other conventional methods. CAD modeling technology within SolidWorks allowed the team to accurately measure the angles between different surfaces of the 3D model. This was particularly valuable for intricate and complex parts, where manual measurements might have been error–prone or time–consuming. With the aid of the software's advanced features, the team could efficiently analyze the model and ensure that the angles between surfaces conformed precisely to those of the physical part.

Once all the necessary measurements and analyses were completed, the 3D model of the part was now fully realized, including all visible surfaces with their accurate angles. This comprehensive model was then used as the basis for creating a new STL file, ensuring that the digital representation perfectly mirrored the physical part's geometry.

Figures 4 and 5 properly depicted and highlighted the key steps and processes involved in SolidWorks, including importing the STL model, defining reference points and planes, and measuring the angles between surfaces. These visual representations served as essential guides, aiding in understanding and documenting the intricate steps taken to ensure the accurate replication of the physical part through the 3D printing process.

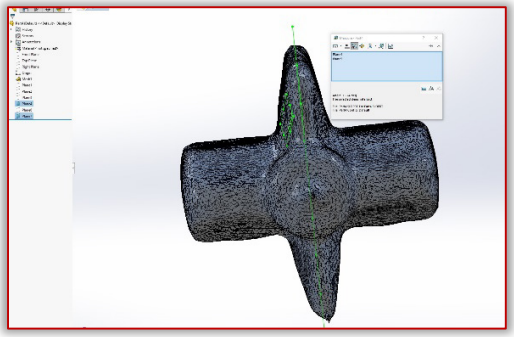

Figure 4. Determination of angles between the surfaces of the part

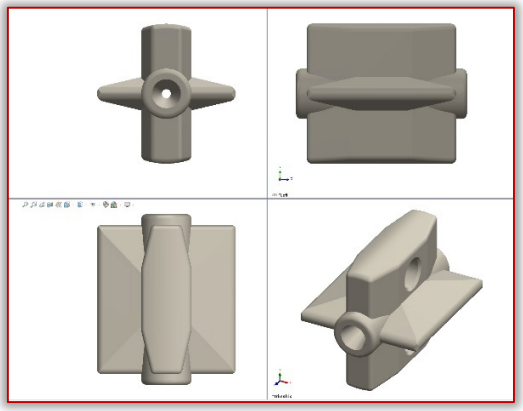

Figure 5. 3D model of the piece, from different angles, in the SolidWorks software

In Figure 6 one can see how the STL model fully reproduces the geometry of the part, made in the SolidWorks software.

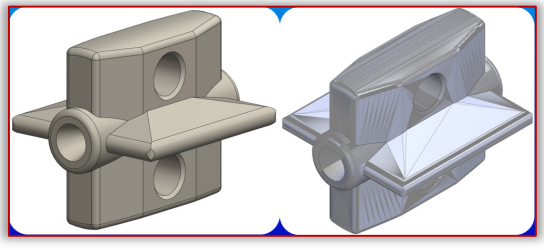

Figure 6. The model made in the SolidWorks software, on the left, and the STL model of the piece, on the right

The newly generated STL model, now aligned with the precise angles measured using SolidWorks, was ready to be further processed for 3D printing with PRUSA SL1S. It was imported into the PrusaSlice slicing software, a crucial component in the 3D printing workflow that converts the 3D model into a series of instructions for the printer to follow layer by layer.

Figure 7 provides a visual representation of the final stages of the post–processing of the 3D model of the piece. After generating the 3D model of the part using SolidWorks and converting it into an STL file, the model was imported into the slicer software. The slicer software plays a crucial role in translating the 3D model into a format that the 3D printer can understand and execute.

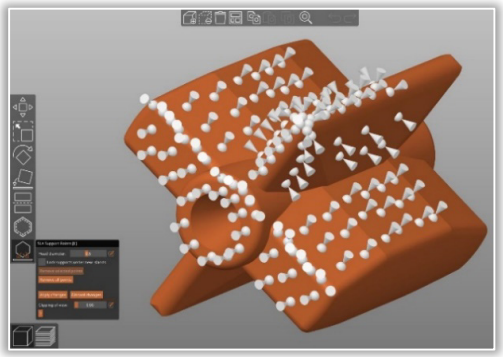

Figure 7. Manual application of the support layers

Within the slicer, the 3D model was processed, and various printing parameters were set, such as layer height (0.05 mm), print speed (2 seconds / layer), and infill density (100%). The slicer divided the 3D model into numerous horizontal layers, generating a set of instructions that the 3D printer would follow to create the physical object layer by layer.

In preparation for printing, additional support structures were applied to the 3D model. These support structures are temporary elements added to the design to provide stability and prevent overhangs or unsupported sections from collapsing during the printing process. (Figure 8)

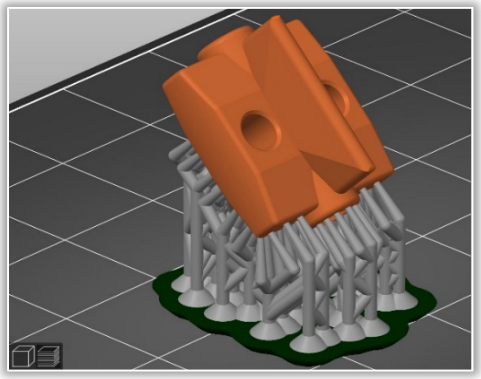

Figure 8. The support of the piece (in gray colour)

Typically, the slicer software automatically generates support structures based on the part's geometry and the chosen printing settings. However, in some cases, manual intervention is required to optimize the support structures so that the first layers of the piece are successful or add custom supports to specific areas of the part.

Figure 9 shows how the first layer of the piece is printed on the support. By carefully adding supports, the part's stability during printing was greatly enhanced, ensuring that it retained its intended shape and accuracy throughout the printing process. The support structures could be removed easily after printing was complete, leaving the final 3D printed part in its desired shape without any residual supporting material.

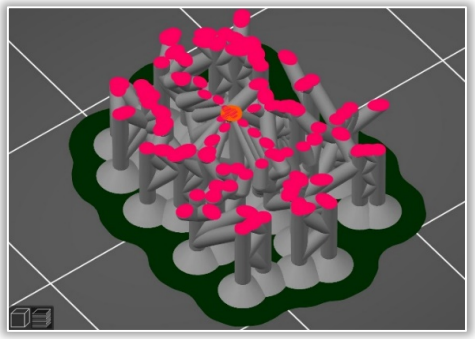

Figure 9. The first layer of the piece

Figure 10 highlights the print parameters of the piece. The piece contains 517 layers, each layer having a thickness of 0.05 mm. These layers represent the total layers, which also include the layers of the part support. The entire printing time is 40 minutes, the piece having a height of 25.85 mm. In all additive manufacturing technologies, proper setting of the initial parameters is critical for the success of the fabrication process; similar work was accomplished by the main author in a previous research (Chirita *et al.*, 2021).

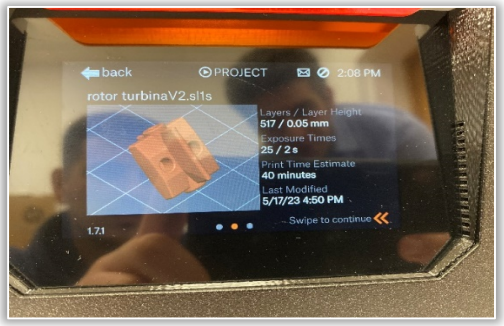

Figure 10. 3D printing parameters of the part

Figure 11 depicts the latter stages of post–processing for the 3D printed part. The 3D printer used in the laboratory utilizes MSLA technology, a form of resin–based 3D printing that employs ultraviolet (UV) light to cure the resin layer by layer, resulting in high precision and detailed prints.

Once the printing process is complete, the part remains coated in uncured resin, which needs to be removed to reveal the final, fully cured part. To accomplish this, the printed piece is placed in a container filled with isopropyl alcohol (IPA). The IPA works as a solvent to dissolve and wash away the excess uncured resin from the surface of

the part. To further ensure the thorough removal of any remaining uncured resin the part undergoes additional cleaning using an ultrasonic cleaner (Figure 12). The ultrasonic cleaner utilizes high–frequency sound waves to create tiny, rapid bubbles in the IPA. As these bubbles collapse near the surface of the 3D printed part, they agitate and dislodge any remaining resin, leaving the part clean and free of unwanted residue.

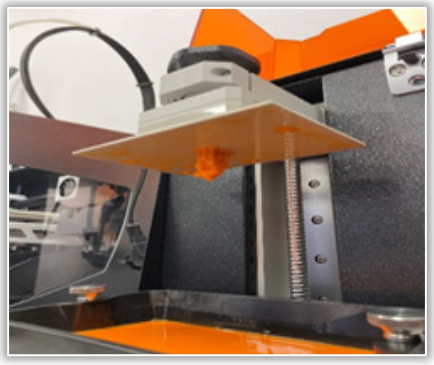

Figure 11. The piece at the end of the 3D printing process

Figure 12. Cleaning of the part in ultrasonic bath with IPA

Once the cleaning process is completed, the 3D printed part is removed from the ultrasonic cleaner, now fully cleaned. At this stage, the part may still exhibit some level of flexibility or brittleness. To enhance its mechanical strength, the part is inserted into a curing device (Prusa Curing and Washing Machine (CW1S)). This device, which is a post–processing station with UV chamber, exposes the part to additional UV light for a specific period. The UV light further cures the resin and ensures its complete hardening, resulting in a final part with improved mechanical properties and durability (Figure 13).

Figure 13. The part at the end of the curing process

RESULTS AND DISCUSSIONS

The culmination of the 3D scanning, 3D modeling, and 3D printing processes, as well as the meticulous post–processing steps, is the functional part presented in Figure 14. This final result showcases a high–quality 3D printed part, free from defects and accurately representing the original physical piece.

The successful completion of these intricate processes ensures that the 3D printed part possesses the necessary geometrical precision and mechanical integrity to seamlessly fit into the intended device. The part's dimensions, angles, and intricate details have been faithfully reproduced, guaranteeing its proper functionality and optimal performance within specified parameters.

The absence of defects in the final 3D printed part indicates the effectiveness of the entire workflow, from the initial scanning to the post–processing procedures. The meticulous alignment of multiple scans, proper support generation, and thorough cleaning of the part during post–processing have all contributed to achieving a flawless and reliable end product.

By adhering to these comprehensive procedures, the 3D printed part fulfills its designated functions entirely. Its accuracy and structural integrity enable smooth interaction with other components within the device, ensuring seamless operation and reliable performance in real–world applications.

The successful completion of this project highlights the potential and versatility of 3D scanning, modeling, and printing technologies. The ability to accurately reproduce complex parts using advanced CAD modeling techniques and 3D printing with MSLA technology showcases the power of additive manufacturing in various industries, such as engineering, medicine, and design.

Figure 14 serves as a visual representation of the triumph of the entire process, depicting the functional 3D printed part in all its detail and complexity. This result stands as a testament to the team's dedication, expertise, and the effectiveness of integrating cutting–edge technologies to create functional parts with outstanding precision and reliability.

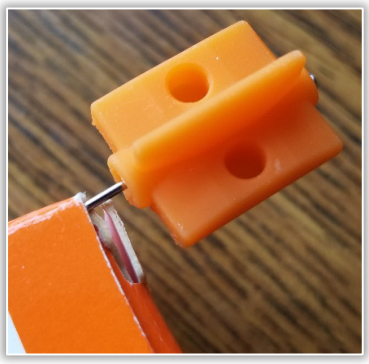

Figure 14. The final result of the entire process – the fully functional flowmeter rotor

CONCLUSION

The presented remanufacturing methodology for flowmeter rotor production showcases the effectiveness of integrating reverse engineering, 3D scanning, and additive manufacturing in the circular economy context. By adopting these advanced techniques, companies can prolong the lifespan of critical components, reduce waste, and contribute to a more sustainable industrial ecosystem. Remanufacturing not only conserves resources but also presents a cost–effective and environmentally responsible solution for ensuring the continued efficiency and reliability of flowmeters in various industrial processes.

The dimensions of the 3D printed part are the same as those of the initial part. Using 3D scanning, additive manufacturing and adapting the principle of reverse engineering, the rotor of a flowmeter was remanufactured. Without these technologies, the flowmeter would have been considered a waste, and would have been thrown in the trash. By remanufacturing its rotor, the flowmeter was returned to nominal operating parameters, reusing the other components of the flowmeter, according to the principle of the circular economy.

Acknowledgements

This work was carried out through the Core Program within the National Research Development and Innovation Plan 2022–2027, carried out with the support of the Romanian Ministry of Research, Innovation and Digitalization (MCID), project no. PN 23 05. The research was financially supported by a project funded by MCID through Programme 1 – Development of the national research & development system, Sub–programme 1.2–Institutional performance–Projects financing the R&D&I excellence, Financial Agreement no. 18PFE/30.12.2021.

References

[1] Atta, N.: Remanufacturing Towards Circularity in the Construction Sector: The Role of Digital Technologies, 493–503. In: Arbizzani, E., et al.: Technological Imagination in the Green and Digital Transition. CONF.ITECH 2022. The Urban Book Series, Cham, Springer, 2023.

[2] Chirita, A.–P.; Sovaiala, G.; Barbu, V.; Blejan, M. and Pavel, I.: Determining the optimal printing conditions for the production of a Fertigation Pump Prototype with FDM Technology, Materiale Plastice, 58(2), 140–149, 2021.

[3] European Commission: Internal Market, Industry, Entrepreneurship and SMEs. Critical Raw Materials Act. https://single–market–economy.ec.europa.eu/sectors/raw–materials/areas–specific–interest/critical–raw–materials/critical–raw–materials–act_en, n.d.

[4] Karimova, G.–S. and LeMay, S. A.: Consumer Social Responsibility (CnSR) in the Circular Economy of Global Value Chains: What Does It Mean, and Why Does It Matter?, International Journal of Circular Economy and Waste Management, 2(1), 1–19, 2022.

[5] Kataev, Yu.V.; Goncharova, Yu.A.; Sviridov, A.S. and Tuzhilin, S.P.: Application of 3D Printing and 3D Scanning Technologies in the Manufacture and Repair of Agricultural Machinery, Machinery and Equipment for Rural Area, 34–38, 2023.

[6] Ma, P.; Gong, Y. and Mirchandani, P.: Trade–in for remanufactured products: Pricing with double reference effects, International Journal of Production Economics, 230, 107800, 2020.

[7] Perr, J.: Hi–Cone. Consumption, sustainability, and the circular economy: Hi–cone, August 13, 2020. https://hi–cone.com/2020/08/the–total–cost–of–consumption/.

[8] Stuart Chapin III, F.; Carpenter, S.; Kofinas, G.; Folke, C.; Abel, N.; Clark, W.; Olsson, P.; Stafford Smith, M.; Walker, B.; Young, O.; Berkes, F.; Biggs, R.; Grove, M.; Naylor, R.; Pinkerton, E.; Steffen, W. and Swanson, F.: Ecosystem Stewardship: Sustainability Strategies for a Rapidly Changing Planet, Trends in Ecology & Evolution, 25(4), 241–249, 2010.

[9] Sun, H.; Zheng, H.; Sun, X. and Li, W.: Customized Investment Decisions for New and Remanufactured Products Supply Chain Based on 3D Printing Technology, Sustainability, 14(5), 2502, 2022.

[10] Tian, Y.; Wang, X.; Li, J.; Yang, J. and Liu, Y.: Rapid Manufacturing of Turbine Blades Based on Reverse Engineering and 3D Printing Technology, CISC 2022: Proceedings of 2022 Chinese Intelligent Systems Conference, 540–553, 2022.

[11] Turner, C.; Moreno, M.; Mondini, L.; Salonitis, K.; Charnley, F.; Tiwari, A. and Hutabarat, W.: Sustainable Production in a Circular Economy: A Business Model for Re–Distributed Manufacturing, Sustainability, 11(16), 4291, 2019.

ISSN: 2067-3809

[1.] Joseph ABUTU, [1.] F. KOJENG, [2.] K. MEDUPE, [3.] Sunday Albert LAWAL

DEVELOPMENT OF BOX–TYPE SOLAR COOKER FROM LOCALLY SOURCED MATERIALS

[1.]Department of Mechanical Engineering, Taraba State University, Jalingo, NIGERIA
[2.]Department of Mechanical Engineering, Federal University of Technology, Owerri, NIGERIA
[3.]Department of Mechanical Engineering, Federal University of Technology, Minna, NIGERIA

Abstract: In this study, a solar box–type cooker was developed using locally available materials with the aim of investigating the thermal performance of the constructed solar cooker using standard test procedure. Several tests were conducted on the constructed cookers under Jalingo (Nigeria) prevailing weather conditions during December 2021. The thermal performance of the solar cooker revealed that it attained a maximum average temperature of 77.1 °C for boiling test and 67.7°C for cooking test. Also, the results of the thermal efficiency for the constructed cooker during boiling test and cooking test were maximum at 9.00 hour (73.01%) and 15.30 hour (95.54%) respectively while cooking power during boiling test and cooking test were maximum at 13.30 hour with values of 0.472 and 0.83J respectively. However, it can be concluded that the use of solar energy in cooking is capable of protecting the environment and reducing health risks

Keywords: Solar cooker; temperature; time; cooking power; thermal efficiency

INTRODUCTION

Cooking plays a very essential role in human life because of the very existence of humans who depend on the food for survival. This food can be cooked in different ways (Yuksel et al., 2012). Lim and Seow (2012) have revealed that approximately 2.4 billion people depend on wood, dung charcoal and other biomass fuels for cooking and most of this population cook on open fires, which burn incompletely thereby leading to low fuel efficiency and high pollution missions. Zenebe et al. (2018) have also reported that approximately 4 million people die annually through cooking with traditional cook stoves and fuels, which mainly consist of firewood and charcoal.

The authors also revealed that most of these victims are women and children. Hence, the World Health Organization (WHO) suggested that indoor air pollution resulting from indoor burning solid fuels in poorly ventilated conditions causes diseases such as asthma, cancer, heart disease, chronic bronchitis and tuberculosis (WHO, 2009). Also, Ajibola et al. (2020) have also observed that conventional traditional methods of cooking poses a lot of hazards such as the alarming rate of climate changed, increased number of deaths and health hazards and deforestation.

Therefore, there is need to find an alternative source for fuel for indoor cooking. Solar cooker is a device which uses energy of direct sunlight for cooking (Tiba et al, 2010). This cooker allows Ultra–violet (UV) light rays in and thereafter converting them to longer infrared light rays that cannot escape (Uhuegbu, 2011). Solar Cookers currently in use are relatively expensive and considered as low–tech devices. However, some are powerful and expensive as traditional stoves, and advanced. Though, large–scale solar cookers can cook for hundreds of people. Moreover, fossil resources have dominated the energy market for a long period of time and the pressure on global energy resources is on the increase (Adegbola et al., 2012).

Solar energy technology is not conceptually new and many efforts have been made over the years to developed different solar cookers which have been tested by researchers at several geographic locations and under unique climate and physical conditions (Klemens and Maria, 2008). Uhuegbu (2011) have reported three different types of solar cooker, which include; box type solar cooker, parabolic solar cooker and panel solar cooker.

The box–type cooker is an insulated container with a single or multiple glass cover and relies on the greenhouse effect in which passage of shorter wavelength solar radiation is permitted by transparent glazing. However, it is opaque to longer wavelength radiation coming from moderately small temperature heated objects. Hence, mirrors are sometimes used for reflecting additional solar radiation into the cooking chamber.

Also, the parabolic solar cookers consist of a dish–type reflector which direct intercepted solar radiation to focus point. This type of cooker must be frequently oriented towards the sun, as a result, it is also referred to as direct concentrating cookers consisting of dish–type concentrators which needs direct sun light to perform optimally (Elamin and Abdalla, 2015). In addition, the

panel solar cookers incorporate the features of both parabolic cookers and box–type (Muthusivagami et al., 2010). However, the box–type solar cooker is the most inexpensive and common of the three solar cooker types as it very easy to construct and are made of low cost materials (Klemens and Maria, 2008). Solar energy has gained high importance in the current global discussions on energy and environment. Hence, several attempts have been made to introduce and popularize the use of solar cookers in Nigeria (Uhuegbu, 2011). Therefore, in this study, a box–type solar cooker is been developed using locally sourced material. The performance of the developed cooker was evaluated through cooking test (using Yam) and boiling test (using water) by determining the cooking power and thermal efficiencies at constant time interval.

MATERIALS & METHODS

This study was conducted at the Faculty of Engineering, Taraba State University, Jalingo–Nigeria, lies between latitudes, 8.90° North and longitudes, 11.32° East.

Materials

The material utilized for this study include; 2cm plywood, glass lid (0.3mm) mild steel (0.4mm), screw and hinges (metal) mirror (0.3mm), rollers (plastic), paint (black). These materials were sourced locally from commercial shops in Jalingo – Nigeria. Also, the performance of the developed cooker was evaluated using water, slices of yam a thermometer and a silver painted pot weighing 20.80grams. In addition, the solar radiation intensity for the test period was measured using a Pyrheliometer (DR03, sensitivity: 10 x 10–6V/{W/m^2}, operating temperature: –40 – 80^{o}C, Response time: 2sec)

Methods

Solar cooker construction

The box–type solar cooker constructed comprised of five components, this includes; wooden box which serves as container, heat insulator, glass cover, absorber plate (heat collector) and reflector. The isometric, sectional and orthographic view of the box–type solar cooker are shown in Figure 1, 2 and 3 respectively. A box container (1.15m height) with outer box, 0.45 x 0.45 x 0.3 m and inner box 0.35 x 0.35 x 0. 295 m. The entire inner and outer surface of the box were painted black for better absorption of solar energy. In addition, the absorber plate with 0.4m × 0.4 m made of metal sheet was also installed and was painted black (upper surface) so as to absorb the sun rays. A plane mirror 3mm thick (0.76 x 0.25m) was placed trapezoidal on to the wooden frame at an angle of 30^{o} to ensure that maximum irradiation falls on it and was used as reflector. However, inner sides of the box were covered with aluminium foil in order to also serves as reflector. In addition, a transparent adjustable glass sheet 5mm thick (0.48m x 0.48m) was fitted at the top of the constructed box between the reflector and the absorber to serve as transparent cover and to ensure that greenhouse effect which is the basis of operation of the solar device is created. The developed box–type solar cooker is presented in Figure 4

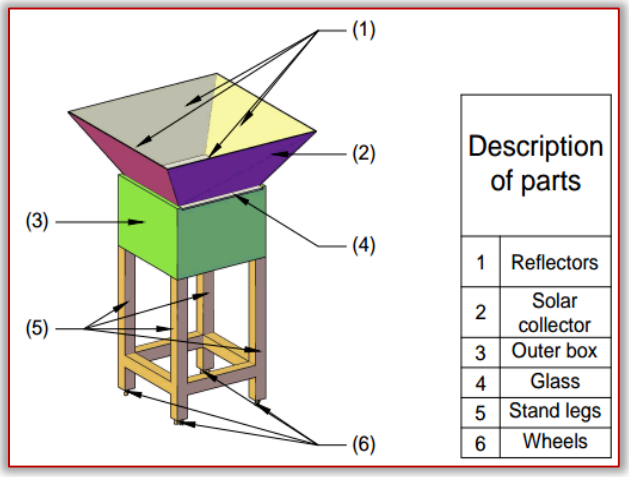

Figure 1: Isometric view of the developed solar cooker

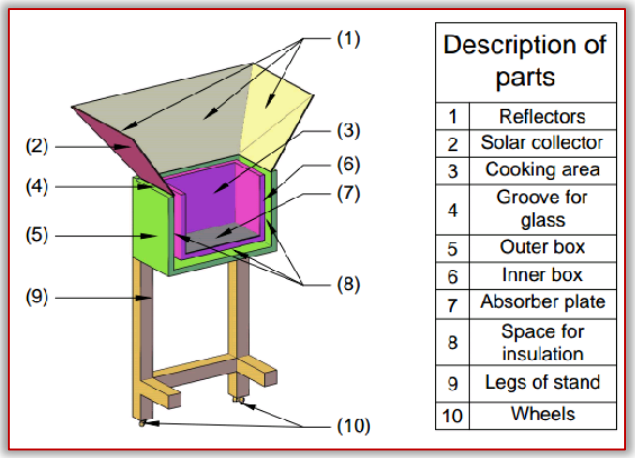

Figure 2: Sectional view of the developed solar cooker

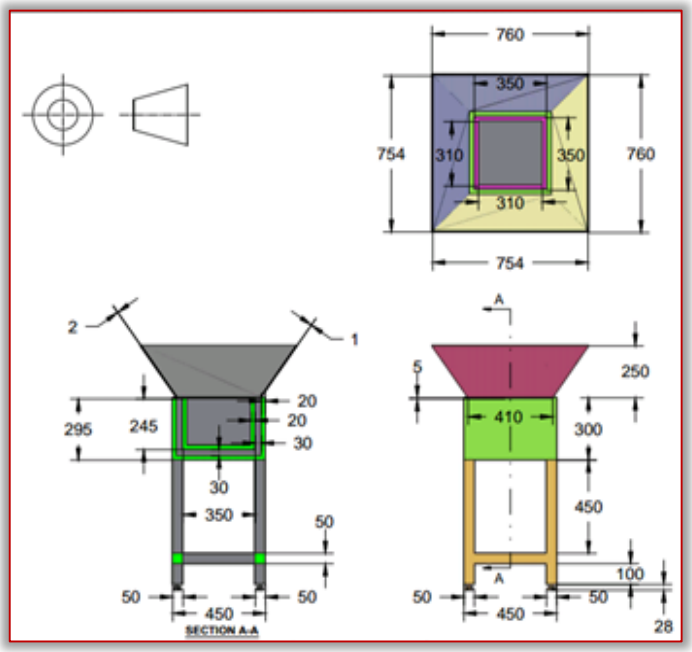

Figure 3: Orthographic view of the developed solar cooker

(a)

(b)

Figure 4: Developed box–type solar cooker: (a) Complete view, (b) Top view

Performance Evaluation

a. Boiling and cooking tests

The performance of the constructed solar cooker was evaluated through boiling test (using water) and cooking test (using water and yam). These tests were conducted in accordance with procedure outlined by (Elamin and Abdalla, 2015).

However, tests were conducted for five days between 1st December, 2021 and 5th December, 2021 from 9:00 to 16:00 hours daily for boiling test and five days between 6st December, 2021 and 10th December, 2021 from 9:00 to 16:00 hours daily at the premises of the Faculty of Engineering, Taraba State University, Jalingo (Annex) using digital thermometers (Temp. range: 0–300°C), slices of yam and silver–painted cooking pot. During the experiment, the ambient temperature and the temperature at the different parts of the cookers (the test sample, reflector and the absorber plate) was measured and recorded at 30 minutes intervals.

Also, a digital weighing balance (TAPSONS™, Accuracy: 0.001) was used to measure the mass of water, pot and yam slices. However, the measured variables were: ambient temperature, the temperature of the water in cooking pot, the reflector and the absorber plate temperature. The recorded data was used to determine the thermal efficiency and cooking power of the constructed solar cooker.

b. Thermal Efficiency

The overall thermal efficiency (η) of the cooker was calculated using Eqn. 1 (Saxena and Karakilcik, 2017). The maximum projected area of a solar collector represent the aperture area through which the unconcentrated solar radiant energy is admitted.

$$\eta = \frac{m_w \, x \, C_w \, x \, \Delta T_w}{I_{av} \, x \, A \, x \, \Delta t} \quad (1)$$

where;

m_w = mass of water (kg)

C_w = specific heat of water (4.168 kJ/kg K)

ΔT_w = Temperature difference between the maximum and ambient air

I_{av} = average solar intensity (W/m²) during the time interval.

A_c = is the aperture area (m²) of the cooker (0.1035m²)

Δt = time required to achieve the maximum temperature of the water (s).

c. Cooking Power

The cooking power (P) of the solar cooker was calculated using Eqn. 2 (Elamin and Abdalla, 2015).

$$P = \frac{T_{w_2} - T_{w_1}}{t} \, x \, m_w \, x \, C_w \quad (2)$$

where;

T_{w2} = final temperature of water in °C

T_{w1} = initial temperature of water in °C

m_w = mass of water in kg

t = time in seconds

C_w = heat capacity of water (4.168 kJ/kg K)

RESULTS &DISCUSSION

Boiling & cooking tests

The average experimental results obtained from water boiling and yam cooking test is shown in Table 1 and 2 respectively.

These results are represented in Figure 5 and 6 respectively. The experimental results revealed that the more heat was generated at the absorber plate during the water boiling and cooking test. The results also indicates that the radiation of the sun affects the heat and cooking performance of the solar system.

The ambient temperature and the temperature at the different parts of the cooker increases with time of the day. However, there was a gradual drop at the different part of the cooker from 14.30 hour to 16.00 of the day.

- Volume of water = 30.90ml
- Weight of yam = 26.90 grams
- Average solar radiation intensity for boiling test = 6.06 kWh/m²
- Average solar radiation intensity for cooking test = 6.11 kWh/m²

Table 1: Experimental results for water boiling test

Run	Time (sec)	Time of the day (hr)	Ambient temp. (°C)	Temp. of reflector (°C)	Temp. of test sample (°C)	Temp. of absorber plate (°C)	Thermal efficiency (%)	Cooking power (W)
1	0	9.00	28.2	35.3	34.6	37.2	73.01	–
2	1800	9.30	30.1	37.2	36.2	39.2	69.59	0.114
3	1800	10.00	36.5	39.2	38.6	42.7	23.96	0.172
4	1800	10.30	40.2	43.1	41.1	45.4	10.27	0.179
5	1800	11.00	43.2	46.6	44.5	48.2	14.83	0.243
6	1800	11.30	45.9	48.8	47.4	51.7	17.11	0.207
7	1800	12.00	48.1	52.0	51.3	55.4	36.50	0.279
8	1800	12.30	54.8	57.5	57.5	61.8	30.80	0.444
9	1800	13.00	59.3	62.3	63.8	67.7	51.33	0.451
10	1800	13.30	66.5	51.4	70.4	75.8	44.49	0.472
11	1800	14.00	68.1	53.1	72.2	77.1	46.77	0.129
12	1800	14.30	66.7	51.2	70.7	75.7	45.63	0.107
13	1800	15.00	65.3	50.7	69.5	73.8	47.91	0.086
14	1800	15.30	64.6	49.2	68.8	72.2	47.91	0.050
15	1800	16.00	63.9	47.9	68.3	71.6	50.19	0.036

Table 2: Experimental results for cooking test

Run	Time (sec)	Time of the day (hr)	Ambient temp. (°C)	Temp. of reflector (°C)	Temp. of test sample (°C)	Temp. of absorber plate (°C)	Thermal efficiency (%)	Cooking power (J)
1	0	9.00	28.8	32.5	31.3	32.9	24.62	–
2	1800	9.30	29.6	33.2	32.2	34.2	25.61	0.064
3	1800	10.00	35.9	39.2	38.6	39.7	26.59	0.458
4	1800	10:30	39.4	43.1	42.1	43.4	26.59	0.250
5	1800	11.00	42.4	46.6	45.5	40.2	30.53	0.243
6	1800	11.30	44.9	48.8	47.4	42.7	24.61	0.136
7	1800	12.00	47.3	51.4	50.3	45.4	29.55	0.207
8	1800	12.30	53.3	57.5	56.5	51.8	31.52	0.444
9	1800	13.00	58.7	62.3	62.8	57.7	40.38	0.451
10	1800	13.30	65.1	69.4	74.4	63.8	91.60	0.830
11	1800	14.00	68.4	72.1	77.2	66.1	86.68	0.200
12	1800	14.30	66.8	70.2	75.7	67.7	87.66	0.108
13	1800	15.00	64.9	69.7	73.5	65.8	84.71	0.157
14	1800	15.30	62.1	67.2	71.8	63.2	95.54	0.122
15	1800	16.00	60.9	65.9	70.3	62.6	92.59	0.107

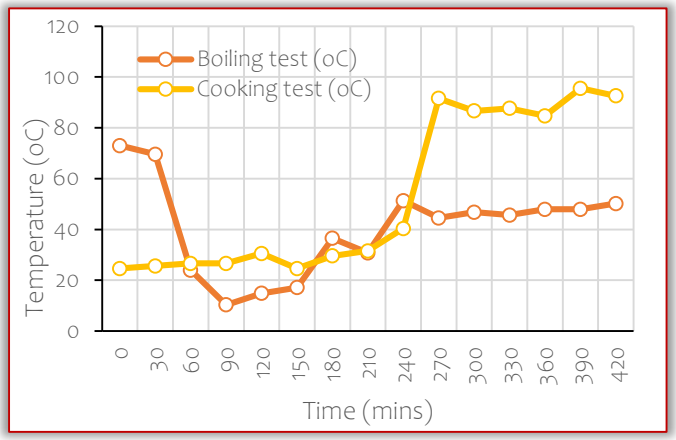

Figure 5: Temperature variation for water boiling test

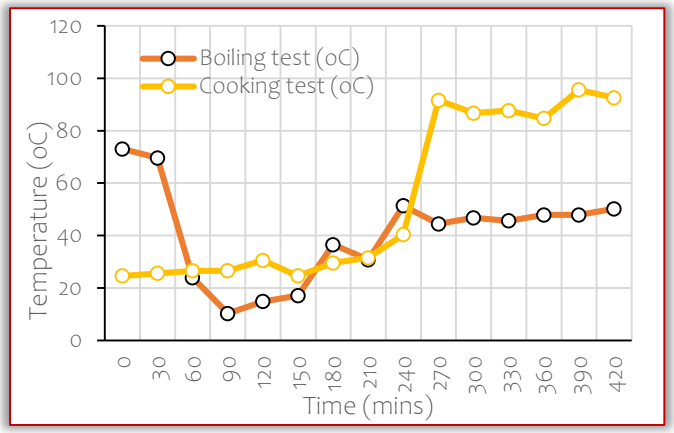

Figure 6: Temperature variation for cooking test

Thermal efficiency and cooking power

The thermal efficiency and cooking power calculated using Eqn. 1 and 2 are presented in Figure 7 and 8 respectively. The results presented in Figure 7 revealed that during the water boiling test, the developed box–type solar cooker attained the highest thermal efficiency (73.01%) at 9.00am and lowest thermal efficiency (10.27%) at 10.30am while the highest thermal efficiency (95.54%) was attained during the cooking test at 15.30hour and the lowest thermal efficiency (24.61%) was achieved at 11.30am.

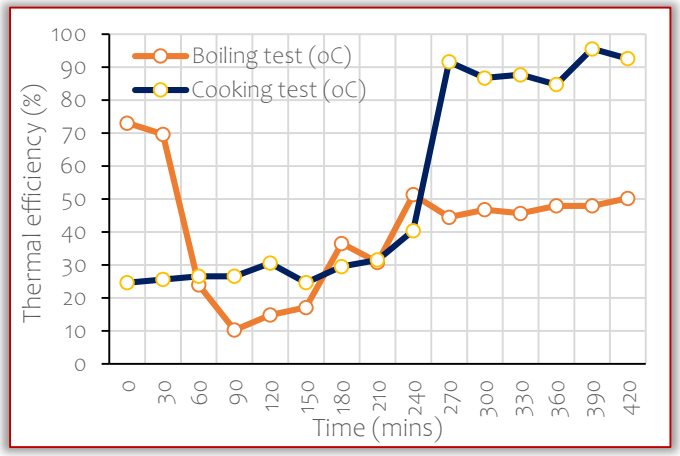

Figure 8: Thermal efficiency for water boiling and cooking test

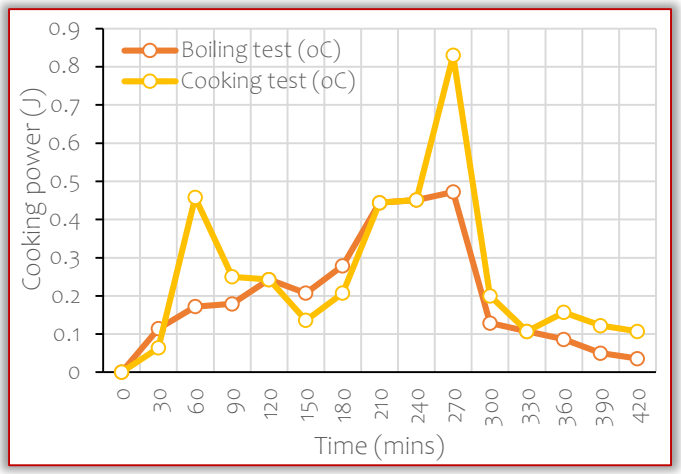

Figure 9: Cooking power for water boiling and cooking test

The differences in the thermal efficiencies could be attributed to heat losses to the surrounding as a result of the high temperature gradient (Elamin and Abdalla, 2015). Also, the high thermal efficiency of 95.54% obtained during the cooking test was attributed to the fact that the solar box cooker have retains sufficient heat inside the box for the cooking process. In addition, the calculated results of the cooking power of the constructed solar cooker presented in Figure 8 showed that of the cooking power is highest at 13.30 hour and lowest at 16.00 hour for both water boiling and cooking test. This explains that the solar collecting ability of the cooker increases with increasing solar radiation therefore, converted heat will be larger at higher solar radiation.

Table 1: Experimental results for Cooking power and thermal efficiencies

Run	Time (sec)	Time of the day (hr)	Water boiling test		Cooking test	
			Thermal efficiency (%)	Cooking power (W)	Thermal efficiency (%)	Cooking power (W)
1	0	9.00	73.01	–	24.62	–
2	1800	9.30	69.59	0.114	25.61	0.064
3	1800	10.00	23.96	0.172	26.59	0.458
4	1800	10.30	10.27	0.179	26.59	0.250
5	1800	11.00	14.83	0.243	30.53	0.243
6	1800	11.30	17.11	0.207	24.61	0.136
7	1800	12.00	36.50	0.279	29.55	0.207
8	1800	12.30	30.80	0.444	31.52	0.444
9	1800	13.00	51.33	0.451	40.38	0.451
10	1800	13.30	44.49	0.472	91.60	0.830
11	1800	14.00	46.77	0.129	86.68	0.200
12	1800	14.30	45.63	0.107	87.66	0.108
13	1800	15.00	47.91	0.086	84.71	0.157
14	1800	15.30	47.91	0.050	95.54	0.122
15	1800	16.00	50.19	0.036	92.59	0.107

CONCLUSIONS

Cooking plays a very essential role in human life as a result of the existence of humans who solely depend on the food for survival. A box–type solar cooker has been developed using locally sourced material and the performances were evaluated by investigating the thermal efficiencies and cooking power. Based on the results obtained, the following conclusion can be drawn;

- The constructed solar cooker was satisfactorily used to boil water. However, the cooking of slices of yam could not be completed on the first day but the yam completely cook on the second day.
- The ambient temperature and the temperature at the different parts of the cooker increases with time and there was a gradual drop at the different part of the cooker between 14.30 and 16.00 hour of the day.
- The developed box–type solar cooker attained the highest thermal efficiency (73.01%) at 9.00 hour and lowest thermal efficiency (10.27%) at 10.30 hour while the highest thermal efficiency (95.54%) was attained during the cooking test at 15.30 hour and the lowest thermal efficiency (24.61%) was achieved at 11.30 hour.
- Also, the cooking power of the constructed solar cooker power is maximum at 13.30 hour and minimum at 16.00 hour for both water boiling and cooking test
- The use of solar energy in cooking is capable of protecting the environment and reducing health risks.

References

[1] Adegbola, A.A., Adogbeji, O.V, Abiodun, O. and Olaoluwa S. (2012), Design construction and performance evaluation of low cost electric baking oven, Innovative Systems Design and Engineering, 11(3), 2222–2217.
[2] Ajibola, A. F., Raimi, M. O., Steve–Awogbami, O. C., Adeniji, A. O. and Adekunle, P. A. (2020). Policy Responses to Addressing the Issues of Environmental Health Impacts of Charcoal Factory in Nigeria: Necessity Today; Essentiality Tomorrow, 3(3)
[3] Elamin O. M. A. and Abdalla I. A. A. (2015). Design, Construction and Performance Evaluation of Solar Cookers, Journal of Agricultural Science and Engineering, 1(2), 75–82.
[4] Ilenikhena, P A; Ezemonye, L I.N. (2010). Solar energy applications in Nigeria. WEC: N. p. https://www.osti.gov/etdeweb/biblio/21390205.
[5] Klemens, S. and Maria, E. V. S. (2008). Characterization and design methods of solar cookers, Solar Energy, 82(2), 157–163.
[6] Lim, W. and Seow, A. (2012). Biomass fuels and lung cancer, Journal of the Asian Pacific Society of Respirology, 17(1), 20–31.
[7] Muthusivagami, R.M., Velraj, R. and Sethumadhavan, R. (2010). Solar cookers with and without thermal storage––A review," Renewable and Sustainable Energy Reviews, Elsevier, 14(2), 691–701,
[8] Muthusivagami, R.M; Velraj, R. and Sethumadhavan R. (2010). Solar cookers with and without thermal storage–a review. Renewable and sustainable energy reviews, Elsevier, 14:691–701.
[9] Saxena, A. and Karakilcik, M. (2017). Performance Evaluation of a Solar Cooker with Low Cost Heat Storage Material, International Journal of Sustainable and Green Energy, 6(4): 57–63.
[10] Tiba, C., Candeias, A.L.B., Fraidenraicha, de S.Barbosa, N.E.M., de Carvalho, P.B.N., de Melo, F. J.B. (2010). A GIS–based decision support tool for renewable energy management and planning in semi–arid rural environments of northeast of Brazil, Renewable Energy, 35(12), 2921–2932
[11] Uhuegbu, C. C. (2011). Design and Construction of a Wooden Solar Box Cooker with performance and efficiency test, Journal of basic and applied scientific research, 1(7), 533–538.
[12] Yuksel, N.,Arabacigil, B., and Avci, A.(2012). Thermal analysis of paraffin wax in box type solar cooker. Renewable and sustainable Energy, 4(6), 63126
[13] Zenebe, G., Abebe, D. B, Randall, B., Peter, M., Alemu, M. and Michael, A.T. (2018). Fuel savings, cooking time and user satisfaction with improved biomass cook stoves: Evidence from controlled cooking tests in Ethiopia, Resource and Energy Economics, 52, 173–185

ISSN: 2067-3809

Fascicule 3

[July – September]

tome [2023] XVI

ACTA Technica CORVINIENSIS
BULLETIN OF ENGINEERING

ISSN: 2067-3809

[1.]Abderrazek MESSAOUDI, [1.]László Péter KISS

IN–PLANE AND OUT–OF–PLANE STABILITY OF CURVED BEAMS – AN OVERVIEW

[1.] Institute of Applied Mechanics, University of Miskolc, 3515 Miskolc–Egyetemváros, HUNGARY

Abstract: The current review paper summarizes a wide variety of research articles that focus on different stability issues of curved beams. It delves into various theories and solutions that got in the spotlight on curved beam stability during the last few decades. This brief review article brings together the major findings of in–plane and out–plane curved beam stability from several scientific perspectives, including analytical, numerical and experimental investigations of either homogenous or nonhomogeneous materials under multiple load cases and different support conditions.

Keywords: review, curved beam, arch, stability, buckling

INTRODUCTION

Euler, the pioneer of beam buckling, presented his famous formula for the critical (buckling) load of straight columns under compression in 1757 [1]. Since then, his finding has ignited interest in this field and a large number of new models have emerged in the literature. Because of the initial curvature, curved beams act in a different way under mechanical loads in comparison with straight beams which led to garnering considerable interest from researchers. The usage of curved beams is continuously growing in popularity for a variety of reasons, including their beneficial mechanical behaviour, particularly when the dominant load results in compression, and the appreciated aesthetics of curved elements in contemporary architecture is also a factor to be considered. In the aerospace, civil, and marine engineering sectors, the curved beams are a widely used structural element [2,3]. Many infrastructure systems, such as long–span roofs, utilize the arch as a structural shape and as a result, in engineering design, a thorough knowledge of its stability behaviour under various loading conditions is crucial.

Many researchers have studied numerous kinds of curved beam behaviour to understand the complexity and give engineers practical knowledge and adequate information on the stability. To mention some classical findings, Simitses [4] and Timoshenko and Gere [5] studied the classical theory extensively to predict elastic buckling loads and they came up with an approximation for the classical buckling load for sinusoidal shallow arches under evenly distributed load. Many researchers expanded the above mechanical approach, resulting in closed–form solutions. There were several attempts to deal with the nonlinear arch stability problem using the finite element method under a variety of assumptions [6,7]. In order to avoid arch buckling, it is essential to be able to accurately predict the buckling load required for the resistance design [8].

The current article aims to give an insight to the most popular research findings about the stability of curved beams. It is divided into two major parts, as the results are gathered and distinguished as in–plane and out –of plane stability issues.

IN–PLANE STABILITY OF CURVED BEAMS

The examination of a curved beam's in–plane stability is a classical topic in applied mechanics. Curved beams may buckle in a snap–through mode or bifurcation mode. Study [9] focused on pin–ended and fixed uniform circular arches with any arbitrary symmetric cross–section subjected to a radial force distributed uniformly around the arch axis. Both non–linear equilibrium equations and buckling equations for shallow and non–shallow arches were established using a variational principle. Both analytical and approximate solutions were obtained and proposed, verified by finite element computations. Additionally, the characteristics that distinguish between shallow and non–shallow arches were also mentioned. It was discovered that since the classical linear buckling theory does not take into consideration the pre–buckling deformations, it couldn't be utilized to predict the in–plane buckling of shallow arches accurately. The buckling load of non–shallow arches might, however, be predicted by the linear theory since their pre–buckling deformations are not that relevant. The stability of a uniform half–sine shallow arch was examined under static loading in a thermal environment in study [10]. The arch had pinned supports and the material was linearly elastic, isotropic. The kinematical model was based on a modified Euler–Bernoulli theory, assuming large transverse displacements. Furthermore, the axial force was assumed

to be constant throughout the arch. The effect of three mechanical loading types (concentrated, uniform distributed and asymmetrical distributed) were examined by tracking the equilibrium paths of the arches. The findings revealed that shallow arches behaved similarly under concentrated loading at the midpoint and uniformly distributed loading. Rubin [11] used the Cosserat theory, a special continuum theory with its own balance rules (conservation of mass, balances of linear and angular momentum, and balance of director momentum), to estimate the buckling loads and deformed shapes of elastic clamped circular arches. Those predictions were in a very good agreement with the experiments across the entire range of arch geometries tested by Gjelsvik and Bodner [12]. In the experiments, the arches were made of 2024–T4 aluminum plate that was sliced into strips of constant width and then formed into circular arches of various radius under displacement control. The arch was split into N equal elements so that the experiment might be modeled using the theory of a Cosserat point. It was demonstrated, in particular, that the theory of a Cosserat point gave predictions of the buckling loads and buckled shapes by utilizing a modified thickness that was within the range of manufacturing tolerances of the plates. The results showed that the buckling force was sensitive to the thickness of the plate used to build the arches.

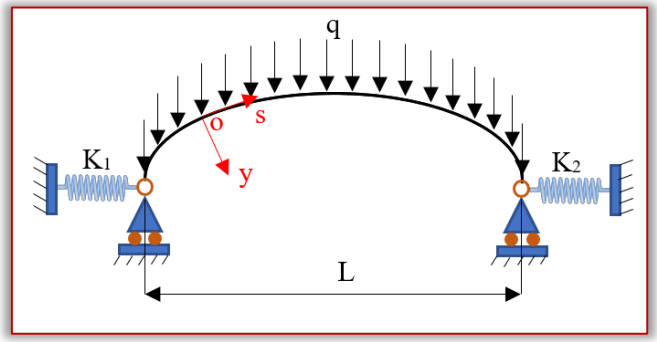

Figure 1. A shallow parabolic arch with horizontal spring supports [13]

In paper [13], the authors developed an analytical model using the virtual work principle for the in–plane elastic stability of a shallow parabolic arch supported by horizontal springs. The arch was subjected to a uniformly distributed load as depicted in Figure 1. They specifically looked at the impact of the stiffness of the horizontal springs on the buckling behavior. It was assumed that (a) the vertical displacements at the ends were completely prevented by roller supports, but rotations at the ends might happen freely, (b) the stiffness of both horizontal springs was equal with each other so the arch flexes symmetrically before buckling, and (c) the arch material was linear elastic. The stiffness of the horizontal springs were discovered to have a significant impact on the buckling load.

Cai and Feng [14] examined the nonlinear in–plane stability of parabolic shallow arches with elastic supports under a central concentrated force. The nonlinear equilibrium equation and the buckled equilibrium equation were established using the virtual work principle. It was assumed that k is the stiffness of the rotational elastic spring which is defined by $k=(\alpha+\eta^2\beta)\ EI_z/L$. Here η denoted the stiffness change of the structural supports with respect to the axial force; α and β are the initial stiffness coefficient and the stiffening rate, while I_zE is the bending stiffness and L is the initial arch length. The critical loads were determined for both symmetric snap–through buckling and antisymmetric bifurcation buckling. The critical load increased when either the initial stiffness of the elastic supports or its stiffening rate increased. It was found that the rotational stiffness has a more severe impact on antisymmetric buckling than on symmetric buckling. With pinned ends, the critical load for any stiffening rate is lower, while with clamped ends, it is greater.

Researches on the stability of arches made of functionally graded materials (FGM) can also be found in the open literature. A non–linear stability study of FGM (constituted of metal and ceramic phases) circular shallow arches under central concentrated force was presented in [15]. The boundary conditions of simple support and clamped–clamped end was assumed, and material characteristics changed according to a power–law distribution across the arch thickness. To approximate the displacement field over the arch, the conventional single layer theory was applied as per the Donnell shallow shell theory together with von–Karman type geometrical nonlinearities. Small strains and moderately large rotations were assumed. All the stretching, coupled stretching–bending and bending stiffnesses were accounted in the model. The governing static equilibrium equation yielded the classical finding that the axial force is constant along the centerline. The impact of material dispersion, geometrical parameters, and boundary conditions on the stability of shallow arches subjected to a central concentrated force was investigated. A change in the power–law index in the Voigt rule of mixture could significantly affect the stability behavior of the arches. Furthermore, the results showed that the elasticity modulus ratio of the constituents also had an impact on the findings. Under a central point force, the authors of paper [16] examined the instability of functionally graded multilayer composite shallow arches reinforced with a low amount of graphene platelets (FG–GPLRC in short). The nonlinear equilibrium equations for the FG–GPLRC arch, fixed or pinned at both ends, were established using the virtual work concept and then solved analytically. GPL nanofillers were discovered to have a significant reinforcing impact on the buckling and post–buckling performances of nanocomposite shallow arches. The buckling and post–buckling behaviors were analyzed in relation to the distribution pattern,

weight percentage, and size of GPL nanofillers as well as the geometrical parameters of the arch. No matter how GPLs were distributed, all FG–GPLRC arches loaded by a central point force had a considerably greater limit point buckling load than a pure epoxy arch, demonstrating the strong reinforcing impact of GPL nanofillers. Limit point buckling load and bifurcation load increased as GPL weight fraction increased and pattern X had a greater reinforcing effect among the three GPL distribution patterns evaluated (U, X, and O).

Guo et al. [17] examined the nonlinear behaviour of fixed parabolic shallow arches under a vertical uniform load to determine the in–plane buckling behaviour. The non–linear equilibrium and buckling equations were developed using the virtual work principle. For the non–linear in–plane symmetric snap–through and antisymmetric bifurcation buckling loads, analytical solutions were found. The finite element package ANSYS was used in the numerical analysis where I– and circular sections were considered. Investigations were done on the connection between the slenderness and dimensionless buckling loads. It was demonstrated that the results of the model agreed well to the numerical outcomes. The authors suggested to use cables in order to enhance the in–plane performance of the parabolic shallow arches and it was concluded from the finite element results that although the cable's impact on the symmetric buckling was minor, it was more noticeable as the modified slenderness of the arch increased.

The in–plane elastic static stability of circular beams with cross–sectional inhomogeneity when exposed to a vertical load at the crown point, was investigated by Kiss [18]. He developed a novel non–linear model for shallow curved beams based on the principle of virtual work to determine the critical loads both for symmetric snap–through and antisymmetric bifurcation buckling for pinned–pinned, fixed–fixed and rotationally restrained supports. The buckling ranges and its ends points, which were dependent on the supports and the geometry parameter, were investigated. The results were compared with those in the literature and with the use of commercial FE software to confirm that the new model was more accurate to predict the critical loads for the above–mentioned beams. The coupling effects of intrinsic geometric non–linearity and extra complexity, such as temperature variations have gotten scientific attention. The in–plane stability of rotationally restrained shallow arches subjected to temperature variations and a vertical uniform mechanical load was investigated by Cai et al [19]. The nonlinear equilibrium and buckling equations were established using the virtual work principle, and analytical solution for the nonlinear in–plane symmetric and asymmetric bifurcation critical loads were found. Temperature variations had a considerable impact on the critical loads for both the symmetric snap–through and asymmetric bifurcation modes. For arches under uniform temperature field and mechanical load, the limit points and bifurcation points appeared at higher load levels than for only externally loaded members. An increase in rotational stiffness of supports resulted an increase in the impact of the uniform temperature field, but it resulted a decrease in the effects of the temperature gradient. Hu and Huang [20] proposed an analytical method for the in–plane nonlinear elastic buckling and post–buckling of pin–ended parabolic multi–span continuous arches. On the basis of the virtual work principle and the non–linear strain expression, the in–plane nonlinear equilibrium differential equations of were developed. The deformed buckled symmetric or asymmetric shape of pin–ended parabolic multi–span continuous arches varies notably from single arches – see Figure 2. The results of the buckling load were in good agreement with the finite element results. Their research can be extended by taking into account the lateral torsional deformations and the inhomogeneous material to study the out of– plane stability of multi –span arches.

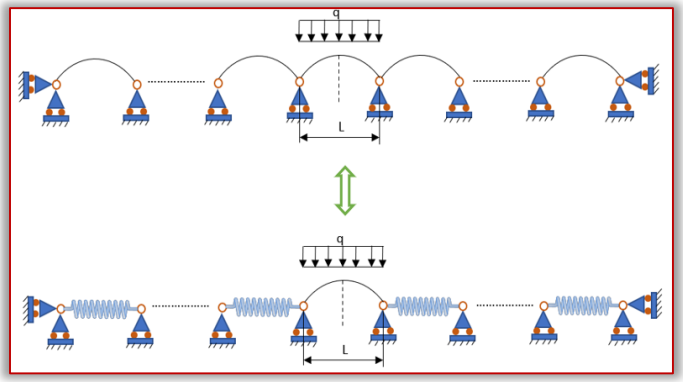

Figure 2. Nonlinearity effect of multi–span continuous arch [20]

A theoretical investigation of the linear and nonlinear elastic in–plane behavior of pinned–fixed circular arches subjected to a radial load distributed uniformly around the arch axis was reported in paper [21]. It was presumed that the arch's deformations adhere to the Euler–Bernoulli hypothesis and the cross–section's height was much smaller than the circular arch's original radius. It was discovered that a pinned–fixed arch could buckle in a limit point mode but not in a bifurcation mode when applied to a uniform radial load. That was quite different to pinned–pinned or fixed–fixed arches subjected to a uniform radial load, which might buckle in a bifurcation and limit point mode. Analytical solutions accurately described the shallow pinned–fixed arches' nonlinear buckling and post–buckling behavior, according to comparisons with finite element findings. In paper [22], the nonlinear elastic in–plane dynamic buckling of a fixed shallow circular arch was investigated when it was subjected to an arbitrarily located step radial point load. Analytical solutions for the

nonlinear dynamic buckling load of the arch were derived using the principle of the conservation of energy. It was discovered that the load position's asymmetric effects on the dynamic buckling load were considerable. It turned out that as the load application point moved further away from the crown, the dynamic buckling load initially dropped and subsequently increased. Additionally, the effects of the modified slenderness on dynamic buckling were examined, and it was shown that as the modified slenderness increased, the dynamic buckling load also increased.

Novel functionally graded porous (FGP) materials have been suggested and developed by many researchers to combine the benefits of functionally graded materials and porous materials in the production of lightweight structures [23]. Under a time–varying uniform radial pressure, the dynamic instability behavior of FGP pinned arch reinforced with uniformly distributed graphene platelets (GPLs) was investigated in the study [24] using Euler–Bernoulli theory, Hamilton's principle, the Galerkin technique, and Bolotin's approach. The symmetric, asymmetric, and uniform porosity distributions of GPLs reinforced arches were examined. The effect of GPL weight fraction and dimensions, porosity distribution, pore size, and arch geometry on the dynamic stability characteristics of the arch were studied. The arch with a symmetric porosity distribution was shown to be more stable than the other two porosity distributions. A bigger unstable region was associated with a higher porosity coefficient. The inclusion of minor numbers of GPLs improved the arch's stability performance considerably, according to numerical findings. The impacts of GPL shape and size were shown to be far less important.

OUT–OF–PLANE STABILITY OF CURVED BEAMS

The usage of single freestanding arches has risen in recent decades. Because these arches lack lateral bracing, they are susceptible to out–of–plane buckling movements and failure. Out–of–plane buckling is one of the buckling modes that can take place when an arch is subjected to a combination of bending and compression [25]. A number of analytical and numerical studies on elastic and inelastic out–of– plane buckling has been published in the literature. In paper [26], the authors investigated the out–of–plane elastic and inelastic stability of concrete–filled steel tubular (CFST) circular arches as shown in Figure 3. The effect of uniformly distributed radial loading or central concentrated loads and elevated temperature fields was investigated. An elastic pre–buckling and out–of–plane buckling analysis was carried out using energy techniques, providing numerical systems to determine the buckling loads for pinned /fixed–ended shallow arches. It was discovered that, in contrast to steel arches, the elastic buckling loads of CFST arches were sensitive to temperature. For the uniformly distributed radial loading case, the effects of thermal loads increased with arch slenderness. However, this thermal load on the buckling strength was unaffected by the arch slenderness in the case of central concentrated loads. Using FE analysis, it was determined how temperature changes affected the out–of–plane buckling loads of CFST arches and the numerical system developed for the calculation of elastic buckling loads was used to validate the FE model. The author can extend his research based on this paper's findings to study the out–plane stability of CFST arches for other support circumstances like elastic supports and take into account that the temperature field varies through the length of the arch.

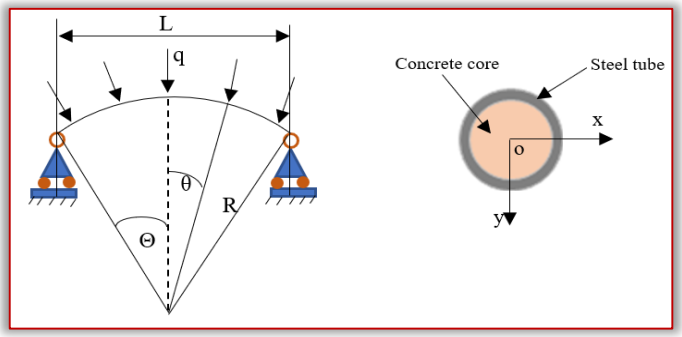

Figure 3. Geometrical and loading conditions for a pin–ended shallow CFST arch [26]

Study [27] examined a fixed CFST parabolic arch under uniformly distributed loads. Using a test–verified FE approach, authors analyzed the out–of–plane buckling behavior of CFST arches with various rise–to–span ratios while taking material and geometric non–linearities into account. It was pointed out that the axial force, out–of–plane bending moment, and torque all increased when the rise–to–span ratio increased.

The stability of CFST arches for long–span arch bridges may be impacted by the time–dependent behavior of the core concrete. Using the finite element technique, Geng et al. [28] looked at how pre–buckling deformations driven by time effects impact the out–of–plane stability of single parabolic arches with fixed ends and uniformly distributed loads were applied throughout the span. It was assumed that plane sections would stay plane and that there would be no slipping or separation of the steel tube from the concrete core. Timoshenko beam elements were used to model the concrete core and the steel tubes in ABAQUS. It turned out that the pre–buckling deformations induced by time effects can reduce the arch's ultimate capacity by up to 18%. On the basis of the findings from the finite element analysis, designing equations were suggested to estimate the ultimate loads while taking time effects into consideration. In study [29], an experimental investigation was reported on the inelastic buckling behavior of fixed circular steel I–cross–section arches under symmetric three–point loading and non–symmetric two–point loading as depicted in Figure 4.

The out–of–plane inelastic buckling strength of fixed steel arches was found to be significantly influenced by the geometric imperfections, the out–of–plane elastic buckling modes and in–plane loading patterns, according to the experimental results and commercial FE investigations. It was discovered that the FE findings of the buckling strength, with relative errors of less than 8%, correlate quite well with the test results. Fixed arches under non–symmetric two–point load had lower out–of–plane buckling strengths than that under symmetric three–point loading.

A fixed steel arch may fail under in–plane stress in an out–of–plane inelastic buckling if it lacks sufficient lateral bracings. In this case, their research can be extended to examine the impact of bracing factors, such as bracing stiffness, brace types, the number and longitudinal position of bracing points, on the arches' out–of–plane stability.

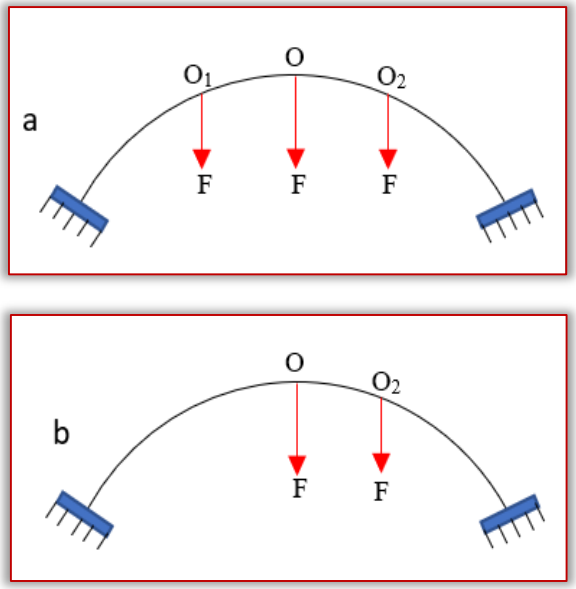

Figure 4. (a) Symmetric three–point loading;
(b) non–symmetric two–point loading [29]

Pi and Trahair [30] presented a nonlinear inelastic approach for studying circular arches' out–of–plane inelastic flexural–torsional behavior. Subtended angle, in–plane curvature, initial crookedness, and material inelasticity were all taken into consideration to examine the strength of steel arches in uniform compression and in uniform bending.

By including material inelasticity into a nonlinear elastic finite–element model for arches [31], a nonlinear finite–element model for the three–dimensional large deformation analysis of circular arches was created. It was discovered that the in–plane curvature and subtended angle had a substantial impact on the inelastic buckling and strength of arches. It was shown that when the subtended angle and in–plane curvature increased, the strength of the arches also dropped. When the subtended angles or in–plane curvatures are unchanged, the reduced slenderness of arches caused a decrease in their out–of–plane strengths in uniform compression and in uniform bending. Both in uniform compression and bending, the effects of initial crookedness on the out–of–plane strengths were considerable for arches.

The AS4100 design guidelines [32] for steel beams do not immediately apply to the design of steel arches under uniform compression and uniform bending since they do not take the effects of in–plane curvature into account. So the specified equations to their model could cover this gap. In many circumstances, circular arches that are loaded in–plane are constrained with discrete lateral bracings to increase their out–of–plane stability. If the effective length of the arch segment between two consecutive bracings is sufficiently great, the arch section may bend out of plane. Adjacent arch segments can act as elastic end restraints for the ends of the arch segment during the out–of–plane buckling of an arch segment.

Out–of–plane elastic buckling of circular arch segments with elastic end restraints that were subjected to a uniform radial force, as shown in Figure 5, was the subject of paper [33]. Authors developed an approximate solution for the out–of–plane elastic buckling forces by utilizing the energy method in combination with the Rayleigh–Ritz method. It was assumed that the cross sections were doubly symmetrical and the shear deformation of the cross–section was ignored. The approximate solutions were compared to the FE findings and were found to be accurate enough. It was found that out–of–plane buckling loads increased significantly with an increase in the rotational restraint's coefficient.

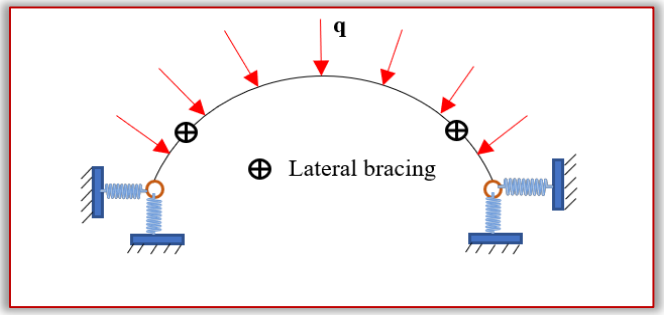

Figure 5. Circular arch with discrete lateral bracings [33]

CONCLUSIONS

This study overviewed certain analytical, numerical and experimental solutions from the open literature of recent decades in the in– plane/out –of– plane stability issues of curved beams. Lot of researches on the stability problems of curved beams have been investigated, each with its unique set of boundary conditions and methods. As shown in the reviewed articles, there is still a lot of interest in the stability of arches and their applications in real–world problems. Some of the proposed methodologies and equations in the reviewed papers can be extended to investigate the dynamic in– or out–of–

plane stability problem of various arches with different cross–sectional shapes, with different profiles (catenary, parabola) under different types of instantaneous loadings.

References

[1] Euler, L.: Sûr la force des colonnes. Memoires de V Academie de Barlin, 1759.
[2] Liu, A.R., Yang, Z.C., Bradford, M.A. and Pi, Y–L.: Nonlinear dynamic buckling of fixed shallow arches under an arbitrary step radial point load. Journal of Engineering Mechanics, 144(4), 04018012, 2018.
[3] Liu, A. R., Huang, Y. H., Fu, J. Y., Yu, Q.C. and Rao, R.: Experimental research on stable ultimate bearing capacity of leaning–type arch rib systems. Journal of Constructional Steel Research, 114, 281–292, 2015.
[4] Timoshenko, S. P. and Gere, J. M.: Theory of elastic stability, 2nd Ed., McGraw Hill, New York, 1961.
[5] Simitses, G. J.: An introduction to the elastic stability of structures, Prentice Hall, Englewood Cliffs, NJ, 1976.
[6] Calboun, P. R. and DaDeppo, D. A.: Nonlinear finite element analysis of clamped arches, Journal of Structural Engineering, ASCE, 109(3), 599–612, 1983.
[7] Elias, Z. M. and Chen, K. L.: Nonlinear shallow curved beam finite element, Journal of Engineering Mechanics, ASCE, 114(6), 1076–1087, 1988.
[8] Pi, Y–L. and Bradford, M. A.: In–plane strength and design of fixed steel I–section arches, Engineering Structures, 26(3), 291–301, 2004.
[9] Pi, Y–L., Bradford, M. A. and Brian, Uy.: In–plane stability arches. International Journal of Solids and Structures, 39(1), 105–125, 2002.
[10] Moghaddasie, B. and Stanciulescu, I.: Equilibria and stability boundaries of shallow arches under static loading in a thermal environment, Latin American Journal of Solids and Structures, 51, 132–144, 2013.
[11] Rubin, M. B.: Buckling of elastic shallow arches using the theory of a Cosserat point, Journal of Engineering Mechanics, 130(2), 216–224, 2004.
[12] Gjelsvik, A. and Bodner, S. R.: The energy criterion and snap buckling of arches, Journal of the Engineering Mechanics Division, 88(5), 87–134, 1962.
[13] Bradford, M. A., Wang, T., Pi, Y.–L. and Gilbert, R. I.: In–plane stability of parabolic arches with horizontal spring supports, I. Theory, Journal of Structure and Engineering, 133(8), 1130–1137, 2007.
[14] Cai, J., and Feng, J.: Effect on support stiffness on stability of shallow arches. International Journal of Structural Stability and Dynamics, 10(5), 1099–1110, 2010.
[15] Bateni, M., Eslami, M.R.: Non–linear in–plane stability analysis of FGM circular shallow arches under central concentrated force, International Journal of Non–Linear Mechanic, 60, 58–69, 2014.
[16] Yanga, Z., Yang, J., Liua, A. and Fu, J.: Nonlinear in–plane instability of functionally graded multilayer graphene reinforced composite shallow arches, Composite Structures, 204, 301–312, 2018.
[17] Cai, J., Feng, J., Chen, Y. and Huang, L.: In–plane elastic stability of fixed parabolic shallow arches, Science in China Series E: Technological Sciences, 52(3) 596–602, 2009.
[18] Kiss, L.P.: Vibrations and Stability of Heterogeneous Curved Beams, PhD Thesis, Department of Mechanics, University of Miskolc, Hungary, 2015.
[19] Cai, J., Yixiang, X., Feng, J and Zhang, J.: In–plane elastic buckling of shallow parabolic arches under an external load and temperature changes, Journal of Structure Engineering, 138(11), 1300–1309, 2012.
[20] Hu, C–F. and Huang, Y–M.: In–plane nonlinear elastic stability of pin–ended parabolic multi–span continuous arches, Engineering Structures, 90, 435–446, 2019.
[21] Pi, Y–L. and Bradford, M. A.: Nonlinear elastic analysis and buckling of pinned–fixed arches, International Journal of Mechanical Sciences, 68, 212–223,2013.
[22] Liu, A., Yang, Z., Bradford, M. A. and Pi, Y–L.: Nonlinear dynamic buckling of fixed shallow arches under an arbitrary step radial point load, Journal of Engineering Mechanics, 144(4), 04018012, 2018.
[23] Lefebvre, L.P., Banhart, J. and Dunand, D. C.: Porous metals and metallic foams: current status and recent developments, Advanced Engineering Materials, 10(9), 775–787, 2008.
[24] Zhao, S., Yang, Z., Kitipornchai, S. and Yang, J.: Dynamic instability of functionally graded porous arches reinforced by graphene platelets, Thin–Walled Structures, 147, 106491, 2020.
[25] La Poutre, D. B., Spoorenberg, R. C., Snijder, H. H. and Hoenderkamp, J. C. D.: Out–of–plane stability of roller bent steel arches – an experimental investigation. Journal of Constructional Steel Research, 81, 20 34, 2013.
[26] Bouras, Y. and Vrcelj, Z. Out–of–plane stability of concrete–filled steel tubular arches at elevated temperatures, International Journal of Mechanical Sciences, 187, 105916, 2020.
[27] Yuan, C., Hu, Q., Wang, Y. and Liu, C.: Out–of–plane stability of fixed concrete–filled steel tubular arches under uniformly distributed loads, Magazine of Concrete Research, 73(18), 945–957, 2021.
[28] Geng, Y., Ranzi,G., Wang, Y–T., Wang ,Y–Y.: Out–of–plane creep buckling analysis on slender concrete–filled steel tubular arches, Journal of Constructional Steel Research, 140, 174–190, 2018.
[29] Guo, Y.–L., Zhao, S.–Y., Pi, Y.–L., Bradford, M. A. and Dou, C.: An experimental study on out–of–plane inelastic buckling strength of fixed steel arches. Engineering Structures, 98, 118–127, 2015.
[30] Pi, Y–L and Trahair, N. S.: Out–of–plane inelastic buckling and strength of steel arches, Journal of Structural Engineering, 124(2), 174–183, 1998.
[31] Pi, Y.–L., and Trahair, N. S.: Three–dimensional nonlinear analysis of elastic arches. Engineering Structures, 18(1), 49–63, 1996.
[32] AS4100, Steel Structures, Standards Australia, Sydney, Australia, 1990.
[33] Guo, Y.–L., Zhao, S–Y. Dou, C and Pi, Y.–L.: Out–of–plane elastic buckling of circular arches with elastic end restraints, Journal of Structural Engineering, 140(10), 04014071, 2014.

ISSN: 2067–3809

[1.] Cătălin-Ioan ICHIM-BURLACU, [1.] Cezara-Liliana RAT

MODELLING THE HYDROKINETIC TURBINE

[1.] Politehnica University of Timisoara, Faculty of Engineering, Hunedoara, ROMANIA

Abstract: Hydrokinetic turbines are an emerging type of hydroenergy converters used for small rivers and streams usually in run-of-the-river installations. Run-of-the-river installations are micro-hydropower plants built without significantly altering the natural flow of the river (no dams, no reservoir). They represents one of the most environment friendly hydropower plants available today. In order for these turbines to be deemed a cost effective solution, extensive research is required. To this end, a mathematical model of the hydrokinetic turbine is required. The aim of this paper is to determine a model of a hydrokinetic turbine using polynomial regression. A model is necessary for simulating the energy conversion system which is, in turn, necessary for designing the control of the system, the protection, etc. The power coefficient on which the model is based describes the efficiency of the turbine in extracting power from the water. It is highly dependent on the characteristics of the turbine: its type, shape, dimensions, material, etc. However, the power coefficient is seldom provided by literature. Therefore, being able to obtain an estimative relationship based on experimental data is a necessity. Since hydrokinetic turbines have a very different, less controllable installation compared cu conventional hydropower plants (zero head with no reservoir), they are modelled in a completely different fashion.

Keywords: regression, hydrokinetic turbine, power coefficient

INTRODUCTION

The current global energy crisis has forced researchers to find new and innovative ways of generating energy, pushing the boundaries of science and technology. The main challenge is not only extracting more energy, but doing it in a more environmentally friendly way. This is a serious problem for large power plants, which can potentially generate more power, but at the cost of a very high carbon footprint. One solution could be the use of small-scale renewable energy sources, such as micro-hydropower plants. These small sized installations, generating between 5 and 100 kW, which can be installed to power remote areas or standalone loads, harnessing energy from nearby rivers or streams. Compared to other renewable energy sources, micro-hydropower plants have certain advantages such as higher efficiency and slower change rates. One such hydropower source is the hydrokinetic turbine [1,2].

Hydrokinetic turbines are an emerging type of hydroenergy converters used for small rivers and streams usually in run-of-the-river installations. Run-of-the-river installations are micro-hydropower plants built without significantly altering the natural flow of the river (no dams, no reservoir). They represents one of the most environment friendly hydropower plants available today [1,3].

Their advantages compared to conventional hydropower plants are lower costs, scalability, simpler mechanical structure and the ability to generate energy near the place of consumption as well as a much smaller effect on the ecosystem. Their disadvantages are the frequent presence of floating and submerged debris, reduced adaptability to consumer variations and possible damaging during flash floods [1,3].

In order for these turbines to be deemed a cost effective solution, extensive research is required. To this end, a mathematical model of the hydrokinetic turbine is required.

WATER TURBINE MODELING

Since hydrokinetic turbines have a very different, less controllable installation compared cu conventional hydropower plants (zero head with no reservoir), they are modelled in a completely different fashion [4]. Given that their structure and functioning are similar to those of wind turbines, they are modelled based on the same principles. Wind turbines utilize the power of the wind, transforming it into rotational power. This is then changed into electrical power with the help of a generator and, usually, a gearbox. Electrical power is used to supply a load, but there may be other components between the generator and the load that ensure that its particular requirements (voltage level, frequency, etc.) are being met [5]. The models of the individual components of the system as well as the model for the interaction between the components are determined based on the transformation of the power. Therefore the bare minimum models required to simulate a wind turbine system are [6]:

- the aerodynamic model which represents the transformation from wind power to rotational power and pertains to the turbine itself;

- the mechanical model which represents the interaction between the turbine and the generator with/without a gearbox;
- and the generator model which represents the transformation from rotational power to electrical power and pertains to the generator.

In this paper, the authors are only concerned with modeling the turbine, hence the only model discussed here will be the aerodynamic model which, considering the fact that the turbine is a water turbine, will be called the hydrodynamic model. The aim of this paper is to provide a relatively low complexity hydrodynamic model for a constant-pitch hydrokinetic turbine.

THE HYDRODYNAMIC MODEL

Hydropower depends on the speed and flow rate of the water flowing through the turbine. The theoretical maximum power available from such a turbine is equal to the kinetic energy ($^1/_2\, mv^2$) of the water passing through the turbine, which can be expressed as [1, 7]:

$$P_h=0.5\rho Q v^2 \quad (1)$$

where: ρ is the density of water and v is the speed of water. Q is the flow rate of water, being described by the following relationship [1, 7]:

$$Q = Av \quad (2)$$

where A is the cross-sectional area of the turbine.

The hydraulic power can be derived from relationships 1 and 2 as:

$$P_h=0.5\rho A v^3 \quad (3)$$

The power that can be extracted by a hydrokinetic turbine depends on the efficiency of the turbine, as described by its power coefficient C_P [8, 9]. C_P is defined as the ratio of the actual power delivered by the turbine (P_{ht}) to the theoretically available power of the water (P_h) [1,7]:

$$C_p=\frac{P_{ht}}{P_h} \quad (4)$$

Based on relationships (3, 4), the output power of the turbine can be expressed as:

$$P_{ht}=0.5 C_p \rho A v^3 \quad (5)$$

Since the river speed varies slowly over time, the most commonly used hydrokinetic turbines are fixed-pitch: $C_P(\lambda)$, where λ is the speed ratio defined as [1, 7]:

$$\lambda=\omega_r R/v \quad (6)$$

where ω_r is the rotational speed.

THE POWER COEFFICIENT C_P

Relationships for $C_P(\lambda)$ are seldom found in literature and the given ones [4, 5, 7] are highly dependent on the type of turbine used (Figure 1), as well as its shape, dimensions, material, etc. One solution is to find the relationship using data from an existing turbine through polynomial regression. This method will lead to finding a polynomial function $\mathbf{C_{Px}(\lambda)}$, where x is the order of the polynomial, using a set of discrete experimentally determined values. This method is demonstrated using data provided by [1].

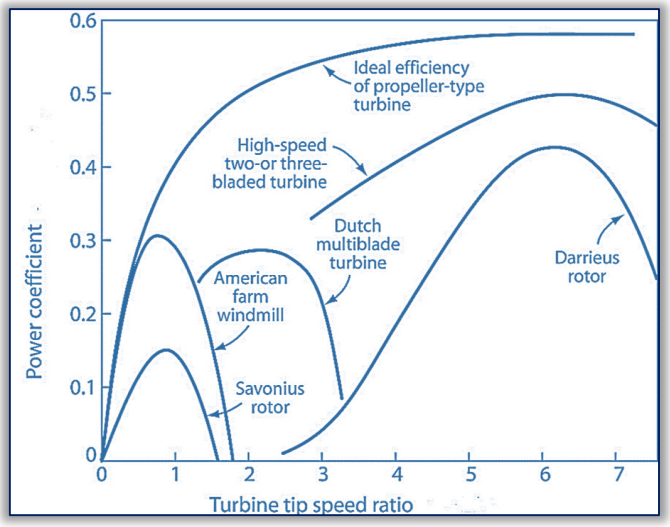

Figure 1. Power coefficient for different types of turbines [10]

Multiple polynomial expressions with orders between 5 and 10 have been thus obtained. Relationships of lower orders were not given due to low precision. These relationships can all be used to simulate the turbine depending on the accuracy required by the simulation. In order to find the best fit for the data given, the values of the standard deviation and the Pearson correlation coefficient for each expression must be taken into consideration. These quality indicators, along with the coefficients of the polynomial expressions are given in Table 1.

The most accurate approximation (minimal standard deviation and a correlation coefficient very close to one) is that obtained by a polynomial expression of the tenth order of the form:

$$C_{P10}(\lambda)=c_{10}\lambda^{10}+c_9\lambda^9+c_8\lambda^8+c_7\lambda^7+c_6\lambda^6+c_5\lambda^5 +c_4\lambda^4+c_3\lambda^3+c_2\lambda^2+c_1\lambda+c_0 \quad (7)$$

The graphical representation of the variation of the power coefficient C_p based on the experimental data, as well as of the estimated power coefficient C_{P10} according to the tip-speed-ratio λ are shown in Figure 2.

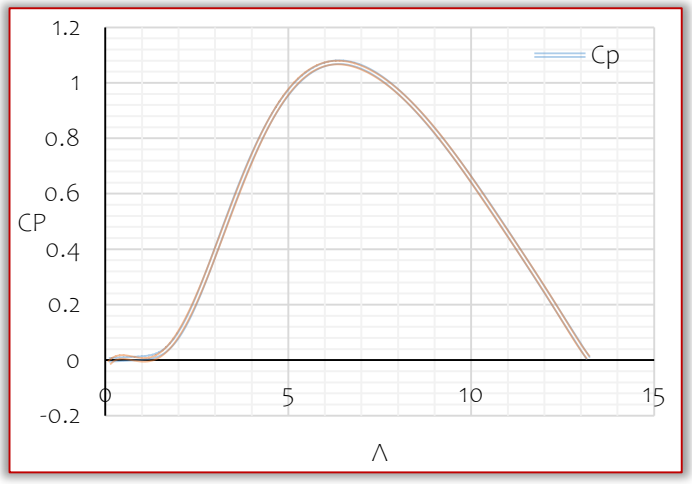

Figure 2. Experimental data and tenth order polynomial regression C_{P10} as a function of λ

Table 1. The values of the coefficients and of the quality indicators

Order	Coefficients	Quality indicators
5	c_5=-8.54215 ·10^{-5}, c_4=0.00349077, c_3=-0.051324348, c_2=0.296784331, c_1=-0.420405312, c_0=0.127342352	RMSE: 0.162156199 Correlation coefficient: 0.998637
6	c_6=-2.52329 · 10^{-6}, c_5=1.52576 ·10^{-5}, c_4=0.001966774, c_3=-0.040467936, c_2=0.260337255, c_1=-0.370811775, c_0=0.11044871.	RMSE: 0.158873265 Correlation coefficient: 0.998691666
7	c_7=3.04083 · 10^{-6}, c_6=-0.000144074, c_5=0.002625396, c_4=-0.022223132, c_3=0.077351441, c_2=-0.025770853, c_1=-0.079832401, c_0=0.034260413	RMSE: 0.092381068 Correlation coefficient: 0.999557824
8	c_8=-6.07676 ·10^{-7}, c_7=3.53692 ·10^{-5}, c_6=-0.000847159, c_5=0.010663518, c_4=-0.073908635, c_3=0.262562848, c_2=-0.368330677, c_1=0.191720015, c_0=-0.022581018	RMSE: 0.03559426 Correlation coefficient: 0.999934369
9	c_9=4.77701 · 10^{-8}, c_8=-3.46672 · 10^{-6}, c_7=0.000107019, c_6=-0.001822371, c_5=0.018481979, c_4=-0.111348347, c_3=0.366152862, c_2=-0.519797748, c_1=0.288354707, c_0=-0.039258557	RMSE: 0.02790428 Correlation coefficient: 0.999959665
10	c_{10}=8.45877 ·10^{-9}, c_9=-5.14738 ·10^{-7}, c_8=1.24952 ·10^{-5}, c_7=-0.000145141, c_6=0.000603993, c_5=0.003862527, c_4=-0.05674158, c_3=0.245383463, c_2=-0.376175568, c_1=0.212710609, c_0=-0.028223172	RMSE: 0.024747898 Correlation coefficient: 0.999968274

CONCLUSIONS

This paper provides a simple yet accurate method of determining the model of a hydrokinetic turbine. The model can be used to simulate the turbine as well as to improve its features. It can also be used to design the energy conversion system centered on the turbine to ensure compatibility between the components. It can also be used to design the control system that ensures the maximization of the power obtained from the water by the turbine.

The functions obtained in this paper are polynomial functions, but other types of functions such as power, exponential, moving average, or even custom functions can be used according to the level of complexity/simplicity and performance required.

References

[1] Rat, C. L.; Prostean, O.; Filip, I.: Hardware-in-the-Loop emulator for a hydrokinetic turbine, IOP Conference Series: Materials Science and Engineering, 294(1), IOP Publishing, 2018.

[2] Paish, O.: Micro-hydropower: status and prospects, Proceedings of the Institution of Mechanical Engineers, Part A: Journal of Power and Energy, 216(1), 31-40, 2002.

[3] Rat, C.; Prostean, O.; Filip, I: Power Control of a Variable-Pitch Hydrokinetic Turbine, 13th International Symposium on Applied Computational Intelligence and Informatics (SACI), pp. 167-172, IEEE, 2019.

[4] Chica, E.; Perez, F.; Rubio-Clemente, A.; Agudelo, S.: Design of a hydrokinetic turbine, WIT Transactions on Ecology and the Environment, 195, 137-148, 2015.

[5] Guney, M. S.: Evaluation and measures to increase performance coefficient of hydrokinetic turbines, Renewable and Sustainable Energy Reviews, 15(8), 3669-3675, 2011.

[6] Vasar, C.; Rat, C. L.; Prostean, O.: Experimental model of a wind energy conversion system, IOP Conference Series: Materials Science and Engineering, IOP Publishing, 294(1), 012081, 2018.

[7] Talukdar, P. K.; Sardar, A.; Kulkarni, V.; Saha, U. K.: Parametric analysis of model Savonius hydrokinetic turbines through experimental and computational investigations, Energy Conversion and Management, 158, 36-49, 2018.

[8] Mangold, E.: Hydrokinetic Power: An Analysis of Its Performance and Potential in the Roza and Kittitas Canals, The Evergreen State College, 2012.

[9] Lago, L. I.; Ponta, F. L.; Chen, L.: Advances and trends in hydrokinetic turbine systems." Energy for Sustainable Development, 14(4), 287-296, 2010.

[10] Kumara, E. A. D.; Hettiarachchi, N.; Jayathilake, R.: Overview of the vertical axis wind turbines, Int. J. Sci. Res. Innov. Technol, 4, 56-67, 2017.

ISSN: 2067-3809

Fascicule 3

[July – September]

tome [2023] XVI

ACTA Technica CORVINIENSIS
BULLETIN OF ENGINEERING

ISSN: 2067-3809

[1.]Agung CHANDRA, [2.]Christine NATALIA

THE EFFECT OF TERTIARY PACKAGING ON DISTRIBUTION

[1.] Universitas Mercu Buana, Jl. Raya Meruya Selatan no.1, Jakarta Barat 11650, INDONESIA
[2.] Universitas Katolik Indonesia Atma Jaya, Jl. Jenderal Sudirman no.51, Jakarta Selatan 12930, INDONESIA

Abstract: Packaging as an outbound process in warehouse plays important roles in product safety such as avoiding lost and damaged product or inner packaging. In this study, there were 1.11% customer complains in average each month that relates to damaged and lost product. This complains happened because there was no tertiary packaging during the shipment: land, water and air transports. The properties of tertiary packaging must be water resistant, lightweight and cheap, then polymer material matched these requirements, specifically was woven plastic sack that made of polypropylene (PP). After tertiary packaging implementation, the customer complains decreased to 0%. Other considerations by using this material are benefit-cost and time. Costs incurred are investment cost and operational costs and benefit are risks minimization such as lost and damaged products. There will also be packing process time around six minutes but tertiary packaging will shorten loading and unloading time. The objective of research is to minimize customer complain which is mostly caused by poor packaging. This research specifically studies tertiary packaging effect on distribution.

Keywords: Tertiary packaging, costs, time, shipment

INTRODUCTION

The packaging industry is one of the fastest growing sector in the world economy and expected to grow around 3% per year. Asia is the largest market and accounts for 40.6% of global packaging consumption in 2018 [1]. Packaging is defined as a product promotion or product protection that relates to logistics [2] and as a part of logistical systems [3], it means delivery must be safe to the final customer in good condition, and without packaging, materials handling would be a messy, inefficient and costly exercise, and modern consumer marketing would be virtually impossible [4].

There are many categories of packaging which are based on raw materials such as paperboard, flexible and rigid plastic, metal, glass and other [5], but plastic packaging has become popular in the industrial sector because of their special properties such as flexibility to shape according to needs; lightweight and easy to transport; durability; safe from chemical contamination and its impacts; sealability; weather and temperature resistance; water resist; and more importantly, it is cheap [6]. When the goods combined with packaging is known as a packing process.

According to [7], there are two physical processes in warehouse:

- inbound (receiving and putaway), and
- outbound (order picking and checking, packing and shipping)

which outbound process is more labor intensive. In packing process, each product is handled and checked in order to produce high accuracy and to minimize complain and return from the customer.

Packing contributes 23.2% in distribution of costs and 28.8% in distribution of working time in distribution centers where storage and picking contribute 45.9% and 34.7% [8], it means almost 70% of cost is resulted from outbound process and of course it is important for companies to reduce this cost. In this paper, we focus at the organization that is running its business in fashion and apparel of baby and kids cloths, and now, it has a packaging problem.

Every month, there were some complains from customers about damaged packaging that could possibly cause lost product, torn primary packaging, and dusty product. All complains happened when the products were shipped to out of town, it can be different islands or different towns, in other words, when the product was sent by third party logistics (3PL).

The objective of research is to minimize customer complain which is mostly caused by poor packaging. This research specifically studies tertiary packaging effect on distribution.

MATERIALS AND METHODS

Types and Function of Packaging

There are three types of packaging: primary, secondary and tertiary.

- Primary packaging can protect the product inside and is removed from the product by the user at the time of its usage.

- Secondary packaging helps in transportation of goods and should be easily removed so that primary packaging is not harmed when opening the product.
- Tertiary packaging sometimes described as transport packaging is necessary for producers as it helps in handling, storage and transportation of goods [9, 10]

Materials and Components of Packaging

Materials packaging that commonly used are plastics, paper, paperboard, metal, glass and wood. Plastic is the most common packaging option because it is light, easy to shape, durable, chemical resistance, suitable for coloring and labeling, and cost effectiveness option of packaging material [11].

Based on the type of material, the plastics/polymers segment is valued for profitable growth.

Regular plastic polymers that commonly used in packaging are as follows:

- Polyethylene (PE) is available in low density (LDPE) and has a low melting point and does not provide moisture blockade.
- High Density (HDPE) is generally used for bottles and tubs. It has a high melting point although it cannot take oven heat. It has high chemical resistance but cannot be used for aerated drinks.
- Linear Low Density (LLDPE) plastics are mainly used as seals in bottles and pouches.

Polypropylene (PP) has a high melting point and is durable for making lids, dispensers, bottles, jars, cartons, trays, etc. Polypropylene typically have higher melting point than PE yet they are not 'oven-able' and are better suited to hot fill products. Most food packaged and water bottles are made using this plastic, and this plastic. This kind of plastic is considered safe and can be easily recycle. The recycling code is 5.

Woven Plastic Sack - Polypropylene

PP is the lightest weight polymer and has a good rigidity and surface hardness. PP is better than PE in chemical resistance and grease resistance [12]. PP has an excellent physical, mechanical, and thermal properties when used in room temperature, relatively good resistance to impacts, high temperature resistance which is better than PE [13]. Woven plastic sacks can be made from PP. The strength and durability of woven plastic sacks produce reliability for containing and carrying a wide range of materials. Its waste was collected, cleaned and recycled by a complicated process [14].

RESEARCH METHODOLOGY

The first step is to formulate the problem currently exist at the company. In this stage, we investigate the main problem that cause the box damaged. After finding the main problem, we have to know the root cause and give the best solution from potential solutions. The framework of research is in figure 1 below:

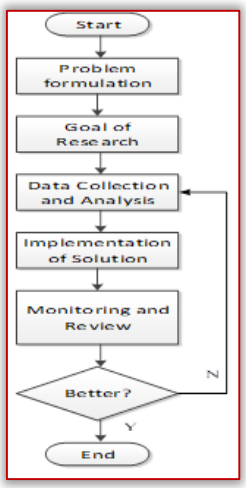

Figure 1. Framework of Research

RESULTS AND DISCUSSIONS

Finding the root cause of the problem

From January 2022 to November 2022, there were two to three complains per month. All complains were about damaged packaging and lost products. Figure 2 showed damaged packaging that received by one of the customers.

As a one of the top five branded fashion for baby and kids, of course this company must do finding the root cause of the damaged packaging problem.

Figure 2. Damaged secondary packaging

Table 1. Data of complains

Month	Number of item complained	Item qty shipped	Pct complain
Jan	9	206	4.37%
Feb	1	302	0.33%
Mar	2	384	0.52%
Apr	2	204	0.96%
May	2	250	0.80%
Jun	3	382	0.79%
Jul	2	442	0.45%
Aug	4	411	0.97%
Sep	2	364	0.55%
Oct	3	305	0.98%
Nov	4	274	1.46%
Average	3.09	320.36	1.11%

Although, the percentage of complain was under 1% per month in average, the company needed to know why and to solve the problem.

The existing conditions of product were:

- The product – baby or kids cloths were packaged by primary and secondary packaging. Primary packaging used was transparent plastics and secondary packaging used was one layer - carton box.
- The shipment of product was transported by truck or container. There were four to seven piles in a box. When the shipment was moved by water mode transportation, the humidy was higher and affected secondary packaging
- There was no tertiary packaging so that the carton box was easily scratched, torn and potentially damaged. If the carton box was torn then, the product was easily lost.
- Each carton box was moved manually when loading and it frequenty happened from seller to buyer.

From these conditions, we concluded that primary and secondary packaging were not enough, then the tertiary packaging was needed to avoid this damage. The properties of tertiary packaging must be water resistance in order to avoid humidity, lightweight in order to minimize the transportation cost, and good resistance to impact in order to avoid shock. From these properties, the most suitable material was polymer or plastics and we choose to use the woven plastic sack as a tertiary packaging.

Cost considerations

It is very important for organization to analyze cost that arised from tertiary packaging. Costs that possibly arised are:

- investment cost: sewing machine
- operational costs: sewing thread, plastic sack, label, and wage for operator

These costs will minimize some risks during the journey from warehouse to customer such as damaged product, lost product, and returned product from customer

Time considerations

When tertiary packaging is used, there will be additional time for outbound process, it is packing time. The details are as follow:

- To insert a carton box into plastic sack = 30 seconds. Maximum capacity is 8 carton boxes. Time estimation per plastic sack = 4 minutes
- To sew a plastic sack = 1 minute
- To attach a label to a plastic sack = 18 seconds

Normal time = (inserting time+sewing time+attaching label time) x rating

Normal time = (4 minute + 1 minute + 0.3 mi-nute) x 1.1 = 5.83 minutes

Standard time = normal time x allowances

Standard time = 5.83 x 1.1 = 6.41 minutes

Allowances is intended to worker for recovery from fatique and relaxation.

From this, we know that standard time for packing one plastic sack is 6.41 minutes. Although there is an additional packing time but this tertiary packaging – plastic sack will shorten loading time in warehouse and unloading time at the destination, because one plastic sack consists of 8 boxes, on the other hand, without tertiary packaging, loading and unloading time will be longer because the operators will input the boxes into the truck one by one.

Implementation stage: Implementing the usage of tertiary packaging

There are some steps for packing the secondary packaging. The steps are:

- Several carton boxes are put into plastic sack, the dimension is 110 cm x 150 cm. The amount of carton boxes that can be inserted into the plastic sack depends on dimension of carton box. Generally, there are 4 to 8 boxes per plastic sack.

Figure 3. Carton box in plastic sack

- The plastic sack is sewn

To avoid undesirable things and to guarantee the customers receive what they order, the plastic sack is sewn by an opera-tor that shown in figure 4.

Figure 4. Tertiary packaging is sewn

- Label is attached on plastic sack. Label consists of name of customer, destination and name of product. This package is sent by 3PL whether water transport, land transport, and air transport.

Post Implementation Stage

After doing the research, now the idea would be implemented for all shipment in December 2022. There were 220 items that shipped to the customers. There was no complain about damaged packaging. From this data, Tertiary packaging effectively prevents loss and avoids carton box from getting dirty.

Table 2. Number of complains per month

Month	Number of item complained	Item qty shipped	Pct complain
Jan	9	206	4.37%
Feb	1	302	0.33%
Mar	2	384	0.52%
Apr	2	204	0.96%
May	2	250	0.80%
Jun	3	382	0.79%
Jul	2	442	0.45%
Aug	4	411	0.97%
Sep	2	364	0.55%
Oct	3	305	0.98%
Nov	4	274	1.46%
Dec	0	220	0.00%
Average	3.09	312.00	1.02%

Figure 5. Complains from Jan to Dec 2022

The results of tertiary packaging implementation will be monitored every month and become one of the warehouse's key performance indicator (KPI).

Further research can be extended from this topic and will explore other tertiary packaging and its effect.

CONCLUSION

Decreasing customer complain about damaged packaging can be done by giving an additional packaging - tertiary packaging and it is plastic sack that made from polypropylene (PP). PP plays important roles for preventing damaged packaging, product loss, and dirtiness because it has properties that matches requirements such as water resistance, lightweight, good resistance to impact, and cheap. After implementing the tertiary packaging, the customer complain on damaged packaging was decreasing to zero.

Acknowledgement

This research was funded by Universitas Mercu Buana and Universitas Katolik Indonesia Atma Jaya

References

[1.] Marinova, V. "Trends in Packaging Sector," Izvestia Journal of the Union of Scientists, Economic Sciences Series. Varna: Union of Scientists - Varna. volume 10, issue 1, 2021.
[2.] Otava, A.P. "The Effects of Packaging in the Supply Chain," Thesis. Tampere University of Applied Science, Finlandia, 2012.
[3.] Pfohl, H.C, Logistiksysteme: Betriewbswirtschaftl. Grundlagen, 4th edn. Springer-Verlag, Berlin, 1990.
[4.] Cardenas, M.A.S. "Research Systems and Waste: Packaging Systems and Waste," Introduction to Circular Economy, Harvard University, 2018.
[5.] Pongrácz, E, "The Environmental Impacts of Packaging," In M. Kutz (Ed.): Environmentally Conscious Materials and Chemicals Processing, pp.237-278, 2007.
[6.] Pramiati, S.K., Soesilo, T.E.B., Agustina, H., "Post-Consumer Plastic Packaging Waste Management in Indonesia: A Producer Resposibility Approach," E3S Web of Conferences 325.03005, ICST, 2021.
[7.] Bartholdi III, J.J. and Hackman, S.T. Warehouse and Distribution Science R.0.96. Atlanta, USA: The Supply Chain and Logistics Institute, School of Industrial and Systems Engineering, Georgia Institute of Technology, 2014, pp.23-28.
[8.] Weiblen, J. "Determining Cycle Times for Packing in Distribution Centers,". Dissertation, Karlsruhe Institute of Technology (KIT), Karlsruhe, Germany, 2014.
[9.] Sharma, A, "Packing and Packaging Management," Logistics Management paper, Alagappa University, India, 2017.
[10.] Regattieri, A. and Santarelli, G. "The Important Role of Packaging in Operations Management," Intech, 2015
[11.] Atagan, G. and Yukcu, S. Effect of Packing Cost on the Sales and Contribution Margin, Ege Academic Review, 2013.
[12.] Wessling, C, Interaction between polymeric packaging materials, fatty foods and food or polymer additives – Literature Review. Lund Institute of Technology, Lund, Sweden: SIK Rapport no.626, 1996.
[13.] Maddah, H.A. "Polypropylene as a Promising Plastics: A Review," American Journal of Polymer Science, Vol.6(1), p.1-11, 2016
[14.] Bui, N.K. , T. Satomi, T., Takahashi, H., "Recycling Woven Plastic Sack Waste and PET Bottle Waste as Fiber Recycled Aggregate Concrete: An Experimental Study," Waste Management, Vol.78, p.79-93, 2018

ISSN: 2067-3809

[1.]Mladen DUMANOVIĆ, [2.]Saša ČEKRLIJA, [2.]Mirko SAJIĆ, [3.]Dušanka BUNDALO,
[4.]Zlatko BUNDALO, [2.]Radmila BOJANIĆ, [5.]Željko VIDOVIĆ

APPLICATION OF ARTIFICIAL INTELLIGENCE IN HUMAN RESOURCES SECTOR PROCESSES

[1.]Faculty of Technical Sciences, University of Novi Sad, Trg Dositeja Obradovića 6, 21000 Novi Sad, SERBIA
[2.]Indenpendent University of Banja Luka, Veljka Mladjenovića 12e, 78000 Banja Luka, BOSNIA & HERZEGOVINA
[3.]Faculty of Philosophy, University of Banja Luka, Bulevar Petra Bojovića 1A, 78000 Banja Luka, BOSNIA & HERZEGOVINA
[4.]Faculty of Electrical Engineering, University of Banja Luka, Patre 5, 78000 Banja Luka, BOSNIA & HERZEGOVINA
[5.]University of East Sarajevo, Faculty of Transport and Traffic Engineering Doboj, Živojina Mišića 52, 74000 Doboj, BOSNIA & HERZEGOVINA

Abstract: This paper deals with the possibility of adequate use of artificial intelligence (AI) in the sphere of human resources (HR) sector activities. All positive aspects of such use are considered, the advantages offered by the application of artificial intelligence in practice in the part of jobs covered by human resources are explained. All the reasons why the use of AI would be significant are highlighted and explained. All those reasons and dilemmas that entail the application of AI are mentioned, both in jobs covered by human resources, and the dilemmas that the use of AI brings as a whole. Logical organization of AI application in HR sector activities is proposed. It is also shown through a couple of imaginary examples how that use would look concretely in applied in practice. Some of the currently most commonly used AI algorithms, which are already used in practical applications, are mentioned.
Keywords: AI – Artificial Intelligence, HR – Human Resources, AI algorithm, AI software

INTRODUCTION

The development of artificial intelligence (AI) and its application opens up many opportunities for research and discussion, including the advantages and challenges of applying AI in general, but also in the field of human resources (HR) sector activities in many enterprises and institutions. Some of the challenges, dilemmas and issues are: ethical issues, issues of defining adequate algorithms and decision-making software, as well as the impact on traditional recruitment processes and the role of HR professionals.

There are a lot of different definitions for AI and HR, which can be found in books and the Internet. Definitions presented here are the ones that can be found most often. Intelligence can be defined as the ability to learn and perform appropriate techniques to solve problems and achieve goals. Artificial intelligence (AI) is a term coined by Stanford Professor John McCarthy in 1955. He defined it as "the science and engineering of making intelligent machines". [1]

Human Resources Management (HR) is the process of recruiting, selecting, introducing employees, providing orientation, providing training and development, evaluating employee performance, deciding on compensation and benefits, motivating employees, maintaining fair relations with employees and their trade unions, ensuring employee safety, welfare and health measures in accordance with the labour laws of the country. [2]

The application of AI technology can prove to be very useful when using it as a Human Resource sector aid. This enables more efficient filtering and evaluation of candidates, as well as the identification of the best profiles for specific jobs. In particular, AI algorithms can automatically review and analyse the CVs of all candidates, while recognizing their key skills and qualifications, and based on that, rank candidates according to certain criteria.

If used in practice, and properly trained and used, the application of AI technologies in the field of human resources processes could bring a number of advantages, such as greater objectivity in the selection process, more efficient linking of candidates with appropriate workplaces, reducing the time required to process applications and reducing human error. But in addition to these listed advantages, certain challenges and issues that necessarily arise regarding the use of AI in HR should be considered, such as data privacy issues, the possible bias of algorithms, and the need for human surveillance and intervention.

USAGE OF AI

In general, there are reasons for and against the use of artificial intelligence. The use of artificial intelligence brings with it advantages and challenges.

Some of the key advantages of using artificial intelligence over the classical way of working, using human labour could be: [3,4,5]

- Faster decision-making capability: AI algorithms can quickly analyse large amounts of data and make faster and more accurate decisions based on that information.
- Modelling at an analytical and predictively advanced level: AI can use complex models and algorithms to analyse data and predict future events and trends.
- Demonstrated greater efficiency and a higher degree of automation: AI can automate routine tasks and processes, leading to greater efficiency, fewer errors and higher productivity.
- Making good decisions in a very short period of time: AI algorithms can analyse large amounts of data and make quick and accurate decisions in a very short time.
- Customer experience is enhanced: AI can personalize and improve the user experience by providing relevant recommendations, support, and interaction.
- Discovering patterns and trends: AI can reveal hidden patterns and trends in large datasets, providing useful insights for strategic decision-making.
- However, as with all new technologies, there are also dilemmas here, and some new questions and fears are being raised, primarily from the misuse of AI:
- Social problems caused by job losses: The introduction of AI can lead to job automation and potential job losses for people employed in those areas.
- Prejudices and ethical dilemmas: AI algorithms can be susceptible to prejudice and dishonesty, which can lead to unfair decisions and discrimination.
- Data protection and privacy protection: The use of AI involves processing large amounts of data, which may raise user concerns about privacy and data protection.
- Lack of necessary human interaction: In some cases, the use of AI can lead to less human interaction, which can affect the quality of relationships and experiences.
- Technical challenges and errors: AI systems are complex and can be susceptible to technical faults, requiring additional resources and support for maintenance and troubleshooting.

It is necessary to carefully consider all these advantages and challenges when applying AI and make informed decisions that strike a balance between the usefulness of using AI and the risks of using AI. It is also very important to, carefully and with measure, align the application of AI with ethical standards, legislation and regulations in order to ensure the responsible and purposeful use of this technology.

The usage of AI technologies in the field of human resources sector could give a number of advantages. Some of the advantages in HR sector are: greater objectivity in the selection processes, more efficient linking of candidates with appropriate workplaces, reducing the time required to process applications and reducing human error. In addition to the advantages, certain problems arise regarding the use of AI in HR sector, as data privacy issues, the used algorithm, the possible bias of algorithms, the need for human surveillance and intervention. Proper use of AI in HR sector activities required appropriate organization of implementation of AI application in the HR tasks and jobs. It could be used the different types of algorithms that can be applied in data analysis and decision-making. The algorithms use artificial intelligence and machine learning to process large amounts of data and extract useful information. There are a few specific AI algorithms and AI software that can be applied in HR processes. Proposed way of logical organization of use of AI application for activities in HR sector is shown in Figure 1.

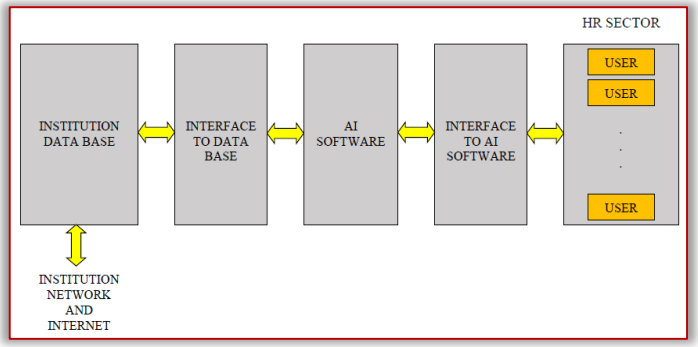

Figure 1. Logical organization of AI application in HR sector

HYPOTHETICAL EXAMPLES OF USING AI IN HR

It will be described three possible examples of application AI in HR activities.

- First example: A company called "NoName1" wants to hire a system engineer of a specific profile and the knowledge of a specific operating system. There is a lot of interest and HR sector has received a very large number of applications. The fact that an HR team has to review each CV individually can be very time-consuming and susceptible to human error. If the company decides to use AI technologies, it can use AI algorithms and software to automatically view CVs. The AI system and software can select and analyse key information such as skills, education, qualifications and work experience of each candidate. Then, the collected data can be compared by the AI software with data on previously successful candidates for similar positions, in order to establish a success template. After completing the analysis, the AI system can rank candidates according to their professional eligibility for that position, according to the defined criteria by the employer. A well-designed and properly used AI algorithm and AI software can identify candidates with appropriate skills and experience, as well as those who have achieved good results in similar

roles. This helps the HR team to focus only on the best qualified candidates and speed up the selection process. However, it is important to note that this use of AI in recruiting new employees is not a substitute for the human knowledge and experience of HR team. HR professionals continue to play an important role in making the final decision and assessing candidates' soft skills that AI may not be able to adequately assess, such as teamwork or communication skills.

- Example 2: Some company "NoName2", which deals with software development, has a need to fill a position for a programmer – senior developer. Instead of the traditional process of manually reviewing hundreds of applications, the company decides to apply AI in the selection process of candidates. Using AI software specializing in application processing, HR team sets criteria such as relevant education, experience in software testing, knowledge of certain programming languages, and skills in automated testing. AI software automatically analyses candidates' CVs and evaluates them according to the set criteria. For example, the algorithm recognizes words such as "software testing", "manual testing", "automatic testing", "Python", "Java", etc. Also, the algorithm can provide a relevance rating of each candidate based on the matching of keywords from their work experience and CVs. After analysis, the AI software generates a ranked list of candidates according to how much they are suitable for the position. The company HR team can then access and assess this list, review AI scores, and focus on top-rated candidates. It is clear that this achieves savings of time and resources of the HR team, all those who participate in the evaluation, focusing attention on the most qualified candidates for the process of further evaluation. Probably the next stage is an interview with these candidates.
- Example 3: Some company "NoName3" has a large team of developers and wants to improve its teamwork process. They decide to use AI to analyse and evaluate team performance to identify the strengths and weaknesses of each team member. Using AI software, the company collects each team member activity data from a variety of sources, such as project management tools, communication channels, and code versioning system. The AI software analyses this data and provides insight into team efficiency, collaboration, communication, and each member's contribution. For example, AI can identify team members who often solve complex problems, suggest innovative solutions, or communicate effectively with other team members. Also, AI can recognize team members who have low productivity or are often late in delivering their tasks. Based on AI analysis, the company HR team can identify areas where the team has exceptional results and support that dynamic. They can also identify weaknesses and provide additional training or support to team members facing challenges. Using AI to analyse team performance allows a company to make informed decisions about resource allocation, training, and team development. It also helps identify highly performing individuals and supports the company's human resource management strategy.

Adequate application of artificial intelligence (AI) in HR can result in the following basic advantages: [6,7]

- Evident process acceleration and efficiency: AI can automate a number of tasks that otherwise require time and resources, such as reviewing and analysing a large number of candidates applications. This allows the HR team to focus on key activities, such as interviewing candidates and making final decisions.
- Reducing the risk of human error: Using AI in HR can reduce the possibility of human error in processes such as filtering applications, data analysis, and decision making. AI algorithms work based on preset criteria and have greater precision in data processing compared to manual processes.
- Better pairing of candidates and jobs: AI can quickly analyse data on candidates' qualifications, skills and experience to find the best matching profiles for a specific job. This helps reduce the time and resources required to manually search for applications and increases the likelihood of finding highly qualified candidates for specific positions.
- Performance and productivity increase: Through the application of AI in team performance analysis, HR can identify areas where teams are achieving high scores and support that dynamic. They can also identify weaknesses and provide support or training to team members facing challenges. This leads to increased productivity and performance of teams.
- Decrease in bias/increase objectivity: AI relies on preset criteria and algorithms, which reduces the impact of human prejudices or subjective decisions. This can lead to fairer decisions, if the AI criteria are well set.
- The quality of human resource management strategy is improving: Through the use of AI, the HR team can collect and analyse extensive data on employees, performance, trainings and other aspects of work. This enables a better understanding of trends, identification of areas for improvement and making informed decisions about human resource management strategy.
- Improving customer experience: Candidates and employees can have a better experience through the application of AI in HR. Efficiency in processes such as application, grade and training can reduce waiting time and improve the overall experience of candidates.

Also, AI can provide personalized career development and training recommendations to employees based on an analysis of their skills and interests.

- Focus on strategic initiatives: Using AI in the operational aspects of HR can free up the time and resources of HR professionals, enabling them to focus on strategic initiatives. Instead of spending time on administrative tasks, the HR team can be more engaged in hiring strategies, talent development, and shaping corporate culture

This example shows how AI can be applied in HR. People are essential for interpreting AI results, making final decisions, evaluating certain skills, and establishing human connections with candidates and employees.

NEGATIVE SIDES OF AI USAGE IN HR

Despite the listed some of the basic, so far recorded, advantages of the application of artificial intelligence (AI) in HR, it is necessary to point out the potential problems that can be expected with this application: [6,7]

- Human interaction is missing or underutilized: Using AI systems in HR can lead to a lack of human interaction and personalization. Candidates and employees may feel a lack of empathy or the ability to ask questions or express their specific needs. It is important to maintain a balance between process automation and human factor maintenance in HR to ensure employee satisfaction and engagement.
- Human skills and knowledge are slowly being lost: As AI is increasingly used in HR, there is a possibility of losing certain human knowledge and skills. Process automation can lead to less engagement of HR professionals in certain tasks and a decrease in the need for certain skills. It is important that the HR team continuously develops its skills in order to adapt to changes in technology and maintain its relevance.
- Choosing the wrong algorithms that reinforce the possibility of prejudice and discrimination: AI systems work on the basis of preset algorithms based on existing data. If this data contains prejudice or discrimination, the AI system can convey and reinforce those prejudices when making decisions. AI algorithms need to be carefully designed and monitored to ensure fairness and avoid discriminatory decision-making.
- Privacy breach and insufficient data protection: When AI systems are used to analyse data on candidates and employees, there is a risk of privacy breaches and inadequate data protection. It is important to carefully manage data, comply with relevant privacy regulations and implement appropriate data security measures to minimize the risk of data misuse or leakage.
- Overdependence on technology and technical errors: When we rely on AI systems, there is a risk of technical errors or failures. Errors in algorithms or technical problems can lead to inaccurate or unfair decisions. It is important to have precautions, such as regular testing and monitoring of AI systems, to minimize the risk of technical errors and ensure proper functionality.

However, the mentioned negatives should not in any way discourage the use of AI in HR sector activities. The goal is to point out the importance of carefully selecting criteria that guide AI algorithms, planning, monitoring and management in order to take advantage of the benefits of AI, while at the same time working to reduce potential risks and disadvantages.

When AI algorithms are mentioned in the context of HR systems, we mean the different types of algorithms that can be applied in data analysis and decision-making. These algorithms use artificial intelligence and machine learning to process large amounts of data and extract useful information. A few specific AI algorithms and AI software that can be applied in HR are:

- Application filtering algorithms: These algorithms can analyse CV or application data and automatically select candidates based on predefined criteria, such as relevant experience, skills, or education. Some of the most famous such algorithms are:

— Random Forest (Scikit-learn library [8] in Python): An algorithm that combines multiple decision trees to classify candidates based on different attributes. [9, 11] (Figure 1).

— Support Vector Machines (SVM) (Scikit-learn): An algorithm used to classify candidates based on defined criteria. [10]

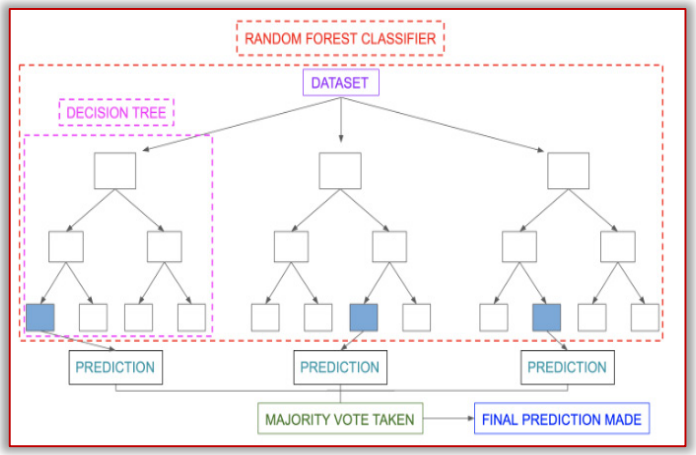

Figure 1. Random Forest Classifier View [11]

- Employee data analysis algorithms: These algorithms can analyse employee data, such as ratings, work performance, feedback, and hiring history, to identify patterns and trends. Based on this data, algorithms can provide insight into the efficiency of employees, identify potential talent, or identify risks of employee departure. Some of the most famous such algorithms are:

— K-means clustering (Scikit-learn): An algorithm that groups employees based on similarities in their

attributes, such as performance and ratings. [12, 13] (Figure 2).

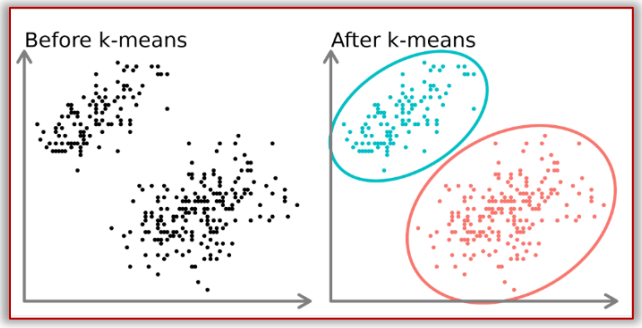

Figure 2. Use of K-means clustering [13]

— Naive Bayes (Scikit-learn): An algorithm that uses probability and Bayes' theorem to classify employees based on their attributes. [14, 15] (Figure 3).

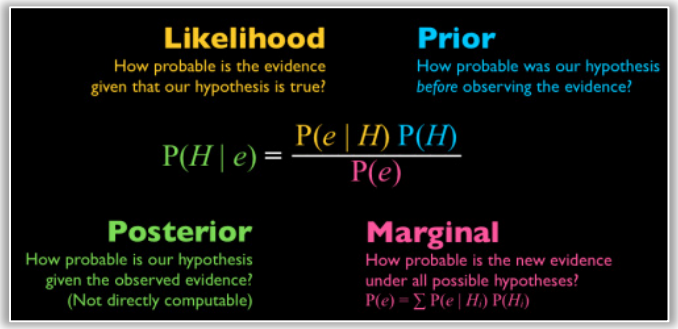

Figure 3. Bayes' theorem [15]

Training and development recommendation algorithms

These algorithms can analyse data on employees' skills, interests, and career goals to recommend relevant training, courses, or mentoring programs that could help them develop further. Some of the most significant such algorithms are:

— Collaborative Filtering (Python Surprise Library) [16]: An algorithm that recommends training based on similarities between the interests and preferences of employees. [17, 19] (Figure 4).

— Content-Based Filtering (Python Surprise): An algorithm that recommends training based on content analysis, such as previous training, experience, and employee skills. [18, 19] (Figure 4).

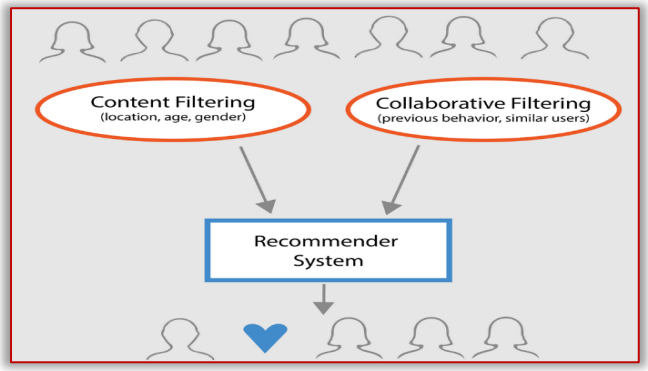

Figure 4. Content and collaborative filtering [19]

These algorithms can analyse employee data, such as work performance, job satisfaction, engagement, and other relevant factors, to predict the likelihood of employees leaving an organization. This allows the HR team to take preventive measures, such as improving engagement or offering development opportunities, to retain key talent. Some of the more commonly used such algorithms are:

— Logistic regression (Scikit-learn): An algorithm used to predict the likelihood of employees leaving based on various factors, such as performance, job satisfaction, and engagement. [20] (Figure 5).

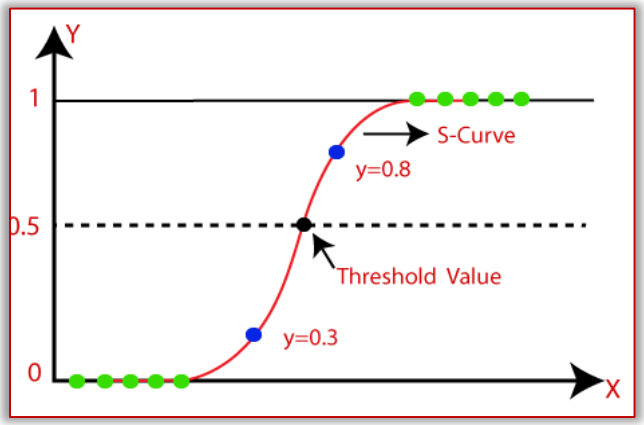

Figure 5. Logistic regression [20]

— Gradient Boosting (XGBoost library in Python): An algorithm used to predict employee departures based on multiple factors and attributes. [21, 22] (Figure 6).

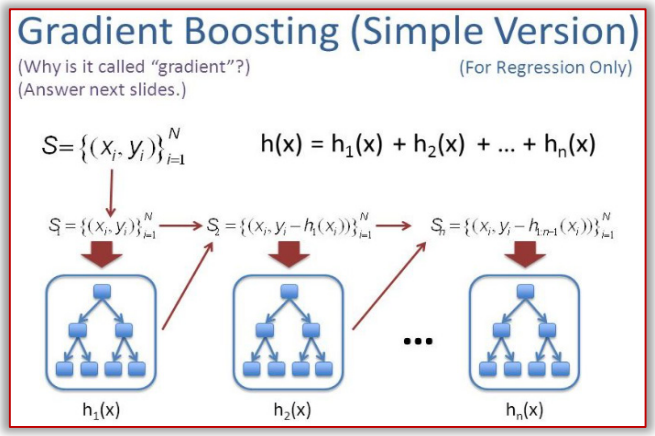

Figure 6. Gradient Boosting [22]

These algorithms can be found in popular programming languages such as Python and libraries such as Scikit-learn, XGBoost and Surprise. These libraries provide implementations of various machine learning and artificial intelligence algorithms that can be used in HR projects. These are just some examples of AI algorithms and AI software that can be applied in the field of HR sector tasks and jobs. Different algorithms can be used depending on the specific needs of the organization and the objectives of the HR process, artificial intelligence and work transformation.

CONCLUSIONS

The application of artificial intelligence (AI) in the human resources (HR) sector can bring a number of advantages. The main advantages include:

- better pairing of candidates,
- efficiency of the complete process,
- objectivity in decision-making,
- increased productivity,
- improvement of human resource management strategy, and
- improvement of user experience.

However, it is also important to be aware of potential negative aspects, such as lack of human interaction, technical errors, loss of human knowledge, privacy and data protection, the possibility of prejudice.

That is why it is crucial to carefully select AI algorithms, the criteria by which they are guided, plan, implement and monitor the implementation of AI in HR sector. It should be implemented respecting relevant privacy and data protection regulations, ensuring fairness and eliminating prejudices in algorithms, maintaining a balance between automation and human interaction, conducting regular testing and supervision of AI systems, and constantly improving the skills of HR professionals.

Implementing AI in HR tasks requires careful planning, proper data management, proper employee selection and training, and transparency in processes. All these measures should be directed towards creating a fair, inclusive and efficient environment for all parties involved.

HR professionals need to follow information technology trends, be open to innovation and constantly improve in order to keep up to date with changes and take advantage of all the opportunities that technology provides. With the right approach and careful management, the application of information technology in HR can contribute to achieving better results, more efficient human resource management and creating value for an organization.

Based on the advantages and disadvantages presented, the general conclusion would be that the best results can be achieved by an adequate combination of AI technology and human resources, enabling HR teams to achieve their goals, improve efficiency and provide value to both candidates, employees and the organization as a whole. The integration of information technologies, such as artificial intelligence, into the field of HR has the potential to transform the way human resources are managed. However, it is important to keep in mind that technology should serve as a support for people, not as a substitute for them. The human factor, empathy and soft skills assessment continue to play a key role in HR sector.

References

[1] https://hai.stanford.edu/sites/default/files/2020-09/AI-Definitions-HAI.pdf,
[2] https://www.whatishumanresource.com/human-resource-management,
[3] Davenport Thomas H., "The AI Advantage: How to Put the Artificial Intelligence Revolution to Work", The MIT Press; (2018),
[4] Lee, Kai-Fu, "AI Superpowers: China, Silicon Valley, and the New World Order", Harper Business; (2018),
[5] Darrell M. West, "The Future of Work: Robots, AI, and Automation", Brookings Institution Press (2018),
[6] Strohmeier Stefan, " Handbook of Research on Artificial Intelligence in Human Resource Management", Edward Elgar Publishing (2022),
[7] Bauer Talya, Erdogan Berrin, Caughlin David, Truxillo
[8] Donald, "Human Resource Management: People, Data, and Analytics", SAGE Publications, Inc; (2019), https://scikit-learn.org/stable/,
[9] https://scikit-learn.org/stable/modules/generated/sklearn.ensemble,
[10] https://scikit-learn.org/stable/modules/svm.html
[11] https://miro.medium.com/v2/
[12] https://scikit-learn.org/stable/modules/generated/,
[13] https://www.datacamp.com/tutorial/k-means-clustering-python,
[14] https://scikit-learn.org/stable/modules/naive_bayes.html,
[15] https://deeppatel23.medium.com/
[16] https://pypi.org/project/scikit-surprise/1.0.2/,
[17] https://developers.google.com/machine-learning/,
[18] https://developers.google.com/machine-learning/recommendation/content-based/basics,
[19] https://www.datacamp.com/tutorial/recommender-systems-python,
[20] https://www.javatpoint.com/logistic-regression-in-machine-learning,
[21] https://xgboost.ai/,
[22] https://dimensionless.in/gradient-boosting/.

ISSN: 2067-3809

[1.]Ioana FĂRCEAN, [1.]Gabriela PROȘTEAN, [2.]Erika ARDELEAN, [2.]Ana SOCALICI

MANAGEMENT AND CHARACTERISATION OF INDUSTRIAL WASTE CONTAINING IRON

[1.]Politehnica University Timisoara, Faculty of Management in Production and Transportation, ROMANIA
[2.]Politehnica University Timisoara, Faculty of Engineering Hunedoara, ROMANIA

Abstract: In the steel industry, a significant amount of waste is frequently generated, the vast majority having a high content of iron and other useful elements; for this reason, it is necessary and recommended that small and powdery industrial waste containing iron be recovered and not stored, within the same manufacturing flows where it was generated following the principles of the circular economy or, where it is not possible (due to limiting factors related to chemical composition, granulation, technological limitations, etc.), recycling is carried out in other industries (e.g. nonferrous, building materials, etc.). Their capitalization and return in the form of by–products in the steel industry or other industrial sectors produces economic and ecological effects. The work presents the possibilities of managing and characterizing some industrial waste with iron content, historically stored, and results on manufacturing flows.
Keywords: steel industry, industrial waste containing iron, management, long storage

INTRODUCTION

A significant amount of iron–containing industrial waste is generated annually in Romania, especially by the steel industry. Approximately 45–50% of the generated waste is currently reintroduced into manufacturing streams, while 55–50% of the waste is deposited, accumulating in storage ponds or other types of sites (dumps), leading to a major negative impact on the environment [1].

For these reasons, the situation of the sites where the storage of iron–containing industrial waste was carried out, on the territory of Romania, is being investigated.

Within the work, the objective is to carry out an analysis of inventory and identification of the main industrial wastes with iron content predominantly from the steel industry that are historically deposited on the territory of our country and for which it is necessary to take recovery measures (following the principles of the circular economy and introducing the waste with iron content in the processes in which they were generated, basically in the steelmaking process).

METHODOLOGY

In this paper, the authors sought to identify iron–containing waste that has historically been stored and to present a detailed description of their situation, on the territory of Romania, supported by current data.

TYPOLOGY & SOURCES OF IRON–CONTAINING WASTE HISTORICALLY STORED

Steel industry

≡ Slag

At the national level, the storage of slag in dumps has been uncontrolled, which is why there is no record of the quantity and quality of this type of waste. These sites are in fact undeveloped areas, exposed to the action of chemical and physical agents, which makes it difficult to efficiently capitalise on the heaps [2,3]. The theoretical concept of a "zero dump" is a goal that is tended towards; from a realistic point of view, the purpose of this concept is to continuously minimise the existing heaps by finding and applying modern technologies to harness the slags [2,4].

In Romania, at the moment, there are dumps where a large amount of steelworks are stored; these dumps are presented in Table 1, specifying the years related to the start of the storage activity, respectively, of the recovery activity. It should be noted that some of the sites are still in the recovery phase [2].

Table 1. Slag dumps in Romania [2–6]

Location of the dump	The beginning year of the dump	The beginning year of the capitalisation processes of the dump
Reșița	1771	2002
Oțelul Roșu	1857	1999
Hunedoara	1965	2007
Călan	1871	2000
Câmpia Turzii	1920	2002
Galați	1968	2003
Târgoviște	1971	1998

Capitalisation of the slag dumps is carried out by specialised companies. The slag dumps located in Târgoviște, Câmpia Turzii, and Reșița began to be capitalised by companies such as Alexander Mills Service and Slag Recycling Enterprise (Reșița). To capitalise on the slag dump from Galați, DSU Duisburg was contracted in the first phase. For the capitalisation of the Hunedoara dump, companies such as Slag Processing Service and S.C Grampet S.A. were contracted [2,3,7].

And in terms of the slag dump in Călan, this was also concessioned; On the ruins of the former Victoria Călan complex, greening activities were carried out that led to the opening of an industrial park.

The old slag dump of the Hunedoara plant was arranged in 1965, occupying an area of 40 hectares on which about 21 million tons of slag were stored [8]. At the beginning of 1978, the area was extended by another 40ha, due to the increase in the company's production capacity and implicitly, the increase in the amounts of slag generated in flows (furnaces, steelworks) [9].

Currently, the slag stored in the Buituri landfill is being processed. Since 2018, the company that deals with the activity of slag exploitation stored on the dump site is S.C. Grand Smithy Works International S.R.L., which has the responsibility of processing the slag (12200t/day) to obtain the ferrous fraction, sorted by three categories of dimensions, respectively, of the non–ferrous fraction [8].

A part of the processed slag in the pile in Buituri–Hunedoara (the non–ferrous fraction) was used for the construction of roads/ highways and as levelling material for parking spaces (for example, rehabilitation works of the county road section Sântuhalm–Hunedoara, parking spaces in Deva, parking spaces Kaufland Hunedoara) [3].

On the site of the slag dump initially generated by the Steel Plant in Galați, accelerated slag processing activities are currently being carried out, the activity being subcontracted by the current management of Liberty Galați S.A., to two companies, namely Phoenix Slag Services Galati and GSWI Galați [10]. To reduce the operating period of the slag dump, the amount of slag processed annually has increased according to the data presented in Table 2.

Table 2. Quantities proposed and processed at the Liberty Galati S.A. [10]

Year	Amount of slag proposed for mill.t/year processing	Amount of slag processed mil.t/year
9 months 2013	4,170	5,678
2014	5	7,638
2016	5	7,972
2017	5	8,308
2018	5	9,744
2019	5	9,446
2020	5	9,840
2021	9	–
2022	6	–
2023	Greening activities	

According to the analyses carried out in the framework of the study project "Closing the nonhazardous waste deposit Slag Dump from Liberty Galați S.A" on the stored waste, it was found that in the various areas of the dump there is steel slag, furnace slag and mixed slag.

The slag dump in Resita was organised in 1771 when the blast furnaces of the Reșița Steel Plant [5], which became TMK Reșița and now Artrom Steel Tubes, were put into operation, forming as a result of the storage of residues from the technological flows of the production of cast iron and steel.

In 2005, slag storage activities were stopped at the dump site and as a result a warehouse was designed and arranged for temporary storage of the fresh slag generated by current flows of steel elaboration [5]. Starting in 2018, the TMK Reșița plant slag was under the concession of the Swiss Swiss Trade S.R.L. company, which is the only operator responsible for the processing and maximisation of fresh slag in the warehouse and old slag in the slag dump [5]. For 7 years (the dump concession), Swiss Trade S.R.L took the risk of processing a minimum amount of old slag of about 620000 tons [5], the proposed quantities are presented in Table 3.

Table 3. Total amounts of slag expected to be processed from TMK Resita dump [5,11]

Year	Total processed slag, fresh slag + old slag, [tonnes]
2019	106 000
2020	124 000
2021	154 000
2022	154 000
2023	154 000
2024	154 000
2025	154 000

In the case of this dump, some of the processed slag amounts were used to build roads and highways.

The need for pile exploitation activities is justified by the negative impact that these sites generate on environmental factors (air, water, soil).

In these dumping's where steel slag is stored, there is a significant amount of iron, the recovery of which is carried out by magnetic separation, and this processing process can represent an important source of savings, by reducing the import of raw materials [4].

Concerns regarding the capitalisation of the slag have generated a lot of research in recent years, according to which, depending on the elaboration process within which it was generated, the ferrous fraction of the slag can be reintroduced in the steel elaboration process and the nonferrous fraction has uses in different sectors of activity (road constructions, railway constructions, hydrotechnical constructions, civil, in agriculture, cement industry, etc.) [2–4].

In conclusion, slag is waste that, if properly exploited, can be used in various fields without significantly influencing the production processes, respectively, the finished products.

≡ Dust & sludge agglomeration furnaces

In the process of drawing cast iron, through the preliminary operations that are carried out to optimise the metal load, a fine, powdery ferrous fraction is obtained, which should not be introduced into the blast furnace. In addition, a quantity of blast furnace dust is obtained from the treatment of the blast furnace gases resulting from the elaboration of the first fusion cast iron.

The amounts of blast furnace dust that results in the casting iron process are directly influenced by the quality of the load, the operating regime of the blast furnace, etc. [2,4,12,13].

In the case of the agglomeration plant, the same situation is encountered, in which the gases captured in the

vacuum chambers are purified, resulting in waste such as dust and agglomeration sludge.

Within the technological process, the main areas where the largest amount of dust is generated are the area near the agglomeration belt, the agglomerate classification area, and transport areas [2,12,13].

Agglomeration dust is the result of the purification of gases collected in the agglomeration installation, and blast furnace dust and slurry are generated as a result of the blast furnace gas treatment processes that resulted in the cast iron elaboration processes.

Furnace charge preparation and agglomeration facilities are important sources of dust and sludge generation, these wastes contain around 30–40% Fe, an aspect that recommends their reintroduction into the steel circuit [2].

If recycling of the entire amount of waste cannot be achieved, it is recommended to store the waste in permanently covered ponds with water, which must be avoided because it has the potential to pollute water and soil [12].

Historical sludge deposits from agglomeration furnaces generated due to the activities of the former steel plants in Hunedoara and Călan are located on the territory of Romania. From studies carried out in the specialised literature, on the chemical composition of sludge waste stored on the territory of Hunedoara county [2–4,12], an average iron content of approximately 27% resulted, which makes it possible to recycle it in the steel industry (but in processed form, if we consider the average diameter of the blast furnace sludge particles, which is 24,721µm). If the concentration of non–ferrous elements (Cu, Pb, Cd, Zn) is above the permitted limits, the waste cannot be recovered in the steel industry, so it is recommended that it be processed in non–ferrous metallurgy [3].

At the Galați steel plant in Galați, since the first month of 2022, the project on the installation of blast furnace slurry treatment facilities was approved. The project envisages replacement of the filtration system for suspended solids in water from the treatment of blast furnace gas, to increase the capitalisation of the blast furnace slurry [14].

Currently, in Romania, slurry and blast furnace dust is still generated only in Galați, where the installations for the recovery of these types of waste are modernised to increase the speed of processing and recovery.

≡ Converter dust and sludge

The source of the generation of these types of waste is the steelmaking process in the aggregate known as the converter.

Dust from the converter is generated in the process of making steel in the converter, driven by exhaust gases. The gases discharged during the preparation process are captured and subjected to primary treatment operations which are performed predominantly wet and rarely in dry systems [3,4,15].

Wet cleaning is usually carried out in stages. In the first stage, the gas is cooled, and the coarse dust is recovered. In the second stage, fine dust fractions are captured from exhaust gases, resulting in coarse sludge with particle sizes below 90µm and fine sludge with particle sizes below 50µm [3,4,15]. After exhaust gas treatment operation, the dust content is reduced to below 15mg/Nm3, the dust obtained containing approximately 60% Fe [12].

In Romania, the converter sludge was and is generated within the Liberty Galati company, where it is stored mixed with the agglomeration furnace sludge (quantity estimated at more than 8 million tons) [2,15]. The annual quantities generated from this type of waste are approximately 50–70 thousand tons [2,4,15,16].

The high iron content of converter dust and sludge, the average values of SiO2 and CaO compounds, and the low Zn content reflect the positive aspects according to which these wastes are suitable for recycling in the steel industry [2,3,4,12,15].

According to some studies [2,4,12,15] the recycling process of converter dust and sludge in the agglomeration process is hampered by the high degree of fineness of the waste, more than 70% of the particles having dimensions below 50 µm. Of the two types of sludge, only fine sludge presents problems for recycling.

Since 1992, the Galati steel plant has used approximately 0.4% of the sludge produced in the agglomeration process [3]. Currently, Liberty Galati has modernised its steel mill slurry processing facilities by opening a new recovery station [17].

▩ Mining industry: Sideritic waste

This type of waste was generated as a result of the preparation activities of the siderite iron ore that was exploited intensively in the area of the Hunedoara County area. The process to which the siderite iron ore was subjected involved roasting it to remove carbon dioxide, and then it was subjected to magnetic concentration, with the aim of increasing the iron content in the roasted ore, which initially had a content between 25–40% Fe [2,4 12,15].

The magnetic concentration operation results in two components: the steel iron concentrate, which according to the research and studies carried out [2,4,12,15], has values between 49–53%Fe, and the mining tailings, which is actually the part of an ore deposit or a mining product that no longer has any utility. In the case of siderite–type iron ores, this mine waste is called siderite waste and can be stored in settling ponds.

On the territory of Hunedoara County, more precisely in the Teliuc commune, three tailings' dams are located for sideritic waste resulting from the preparation of the siderite ore used in the former Hunedoara Steel Plant — Figure 1.

Figure 1. The tailings dams where the mining tailings (sideritic waste) were stored at Teliuc [2,4,12,15]

Within a research contract carried out by a part of the team by the teaching staff of the Faculty of Engineering Hunedoara, the occupied areas and the amounts of waste deposited in the siderite sterile tailings dams from Teliuc were determined. After analysing and processing the measurements, the following were determined [12,15]:

- The area of pond no.1 is 25ha and the amount of sidereal waste stored is 7 million tons;
- The area of pond no.2 is 18ha and the amount of waste stored is 5 million tons;
- The area of pond no.3 is 32ha and the amount of waste stored is 9 million tons.

Regarding the chemical composition of the sideritic waste historically deposited in the three tailings dams, it goes without saying that it is inevitable to change it over time. Currently, tailings dams are not adequately greened and pose a substantial risk of pollution.

Due to the iron content, the steel waste deposited in Teliuc ponds has the possibility of being recovered from the steel industry only if combined with other waste rich in iron (steel mill dust, slag, mill scale) [15]. According to some studies [4,18,19], minimal amounts of precious metals (gold, silver) can be extracted from the waste deposited in the three ponds, and sideritic waste can also be used in the construction industry in addition to road construction.

At the international level, the greening of the areas occupied by the tailing's dams with mining tailings, through the full capitalisation of the stored quantities, is successfully applied in countries such as the USA, Great Britain, India, China, and Japan, etc. In this chapter, Romania is quite far behind, the research presented in the specialised literature [4,18] on these wastes aims only to recover useful minerals (in this case iron), the vast majority of the material reaching again the tailings dam.

Teliuc tailings dams are still in the conservation phase, because ecological development and rehabilitation works are very expensive. For the Teliuc ponds, the company S.C Eco Invest S.R.L Deva was contracted, with a deadline for the completion of the works set for March 2025 [20].

In Romania, at the moment, no complete method of greening the areas occupied by tailings dams has been developed and there are no known installations or projects aimed at the full recovery of the deposited waste. A method was tried to green Bălan, located in Harghita County, but the method did not involve the valorisation of the tailings, but only its introduction into the mine for final storage [18].

Energy industry: Ash from the thermal power plant ash

The processes carried out in coal power plants result in a large amount of ash that contains significant amounts of iron and carbon [2]. The amount of ash generated is represented by the amount of impurities in the coal, directly influenced by the type and method of coal exploitation [2,4].

The ashes of the thermal power plant are frequently stored in landfills, causing soil and atmosphere, due to the wind that drives the dust particles (dry ash) from the surface of the warehouse and transports them to the air [21].

On the territory of Hunedoara County as a result of the operation of the Mintia thermal power plant, one of the largest thermal power plants in the region (it was stopped at the beginning of 2022 [22]), there are deposits of slag and ash resulting from the activity of the thermal power plant — Figure 2.

Figure 2. One of the ash deposits of the Mintia thermal power plant, Source: Google maps

The amounts of slag and ash generated annually by the thermal power plant reach a value of about 1 million tons. They are stored in two warehouses, the first located near the Mureș River on the right bank, which occupies an area of approximately 70ha and the second about 4km from the thermal power plant, an area of approximately 130ha [21,23,24].

According to the literature [2,4,21], from the chemical analysis of the ash of the thermal power plant stored in Mintia it is found that it is silicoaluminal and has the highest values for SiO_2 and Al_2O_3 and an iron content that exceeds the value of 25%.

From the research present in the specialised literature, it has been found that, in terms of chemical composition, the concentrations of thermal power plant ashes resemble powdery waste (steel dust) and due to the fact

that they do not contain elements harmful to the quality of cast iron or steel and can be processed together with other steel waste with a high iron content, which are subsequently used in the elaboration processes. In the processing of small and powdered waste with an iron content, the ashes from the thermal power plant are used as a binder [2,4].

The ashes of the thermal power plant can be recovered in the cement industry, representing an alternative source of raw materials that can present technical and economic advantages to producers interested in implementing new technologies to capitalise on this waste [25].

In Romania, the use of ash from power plants has been successfully demonstrated in the production of cement and concrete [26], in the manufacture of bricks [25], in road construction, in the manufacture of pavements [27], and in agriculture to correct the soil.

Chemical industry: Pyritic ash

This type of waste is the result of the sulfuric acid manufacturing process, an activity that also took place on the territory of Romania in Baia Mare (Phonix factory), the Măgurele Tower (chemical plant), Valea Călugărească (Romfosfochim plant), Năvodari (superphosphate and sulfuric acid plant), Făgăraș (Victoria chemical plant). Currently, none of these plants are functional anymore, but as a result of their activities, quantities of pyritic ash have been generated, which were deposited in landfills (Figure 3), still present today and whose quantity is estimated at almost 4.5 million tons [2,4,15].

Figure 3. Storage of pyritc ash in landfills [2]

Pyritc ash is interesting to harness in the steel industry due to its high iron content of more than 50%. This finding was made as a result of studies in the specialised literature [2,4,15] carried out on the chemical composition of pyritic ashes stored in Valea Călugărească, Turnu Măgurele, Baia Mare, Năvodari, and Făgăraș.

In Romania, pyritc ashes have been exploited using the Kowa Swiko technology developed by the Japanese company Toyo Engineering Corporation. This technology was implemented in the pyrite ash valorisation plant established at Turnul Măgurele. Through technology, pyrite ash was converted to metallized pellets and metals such as Cu and Zn were extracted from its composition [28].

The Kowa–Seiko technology involved the separation of non–ferrous metals by roasting. Metal pellets made of pyritic ash and additions such as lime, calcium chloride, etc., were transported to Hunedoara and Galați plants to be used in the manufacture of cast iron in the blast furnace [2,28].

Currently, the pyrite ash utilisation plant in Turnul Măgurele is completely decommissioned, and the existing pyrite ash deposits cause serious environmental problems.

In conclusion, the pyrite ash obtained in the sulfuric acid manufacturing process can be processed and subsequently recovered in the steel industry due to its iron content, but there are also situations in which its use in the steel industry is practically impossible due to the heavy metal content that can affect the quality of cast iron and steel. According to studies in the literature [2,4,15], the cause that makes it difficult to use pyrite ashes in steelworks is the arsenic content, an undesirable element in ferrous metal alloys.

Aluminium industry: Sludge and red mud

The process of manufacturing alumina using the Bayer process from bauxite ore results in significant amounts of waste, such as slurry and red sludge.

The alumina factory slurry is actually a sludge with a very fine particle size fraction, which together with the red sludge (Figure 4) is usually stored in the ponds. It is recommended to always keep the surface of the ponds moist, because otherwise the air currents will scatter this dry powdery material, causing a much higher degree of pollution [2].

(a)   (b)

Figure 4. Red sludge generated in the alumina manufacturing process [2]
a – red sludge; b –red sludge tailings pond

Studies in the literature [4,29,30] show that red sludge and slurry have a high content of iron oxides (35–60% Fe2O3).

It should be mentioned that on the territory of Romania, plants for the extraction of alumina from bauxite are in Tulcea, Oradea, and in Slatina the production and processing capacities of aluminum are located. Currently, the Oradea plant, the only one to use bauxite ore mined on the territory of our country, is no longer functional, having been completely decommissioned since 2006. However, in its wake, the landfills were used as dumping

grounds for the sludge and red mud resulting from the alumina manufacturing activity.

At the ALRO–owned Tulcea plant, red sludge is stored in two waterproof warehouses with capacities of 23 and 7,5 million tons, respectively. Now, there is no integrated recovery solution for the deposited red sludge [4,15].

Because slurry and red sludge–type waste are deposited at sites that occupy large areas of land, studies and research have been carried out to find chemical composition and recovery solutions. According to studies carried out [2,4] on the chemical composition of red sludge, the predominant elements of the composition are iron and alumina.

Regarding the valorisation activity of the valorisation activity of the valorisation activity of the red mud valorisation activity, it was found that by its processing an iron alloy (pellets) can be obtained that can be used in the activity of steel mills in the charge of steelmaking furnaces [15].

CONCLUSIONS

From the data presented, it is found that most of the slag dumps on Romanian territory were and are leased to specialised companies to better capitalise the different fractions of the slag. But, nevertheless, sites still exist, the works for the greening of the occupied lands are non–existent, or, at best, they were only planned (the case of the Galați dump). The processing speed of the slag in landfills is still low and does not generate a significant reduction in the amount of waste; these types of sites continue to endure. Another factor with a negative impact on the low level of slag recovery in landfills is also the frequent change of companies specialised in the recovery of waste from the steel industry (the case of the landfill in Hunedoara, in Reșița).

It is necessary to find efficient solutions for the complete elimination, through recycling, of the blast furnace slurry and agglomeration dust historically stored in the Hunedoara and Călan areas. Finding or developing an optimal recycling solution for blast furnace sludge and dust will lead to the total elimination of this type of waste from the area, as the streams in which it was generated are completely decommissioned. For industrial waste with iron content historically deposited on the territory of Romania, it is necessary to find optimal solutions for the valorisation and greening of the land to return the environmental spaces.

References/Bibliography

[1] Matei, E., Predescu, A.M., Săulean, A.A., Râpă, M., Sohaciu, M.G., Coman, G., Berbecaru, A.C., Predescu, C., Vâju, D., Vlad, G., Ferrous Industrial Wastes—Valuable Resources for Water and Wastewater Decontamination, International Journal of Environmental. Research and Public Health, 19, 13951, (2022)
[2] Popescu, D., Research on the recovery of small and powdered waste in the metallurgical industry, Ph.D. thesis, Politehnica University Timisoara, Faculty of Engineering Hunedoara, 2018.
[3] Miloștean, D., Technologies for Industrial Waste Recovery II, Course, 2014
[4] Hepuț, T., Socalici, A., Ardelean, E., Ardelean, M., Constantin, N., Buzduga, M., Recovery of small and powdery ferrous waste, Politehnica Timişoara Publishing House, 2011
[5] Site report on Slag Heap Țerova – Reșița, Beneficiary: SWIISS TRADE SRL, 2018 http://www.anpm.ro/
[6] Borza, M., Research on the valorization of coke oven muds from the Victoria Călan steel plant and the greening of the area, PhD thesis, University of Petroșani, 2015.
[7] Hunedoara City Hall – Local Committee for Emergency Situations, The Plan for Analysis and Coverage of Risks of the Municipality of Hunedoara, 2014
[8] National Environmental Protection Agency, Environmental Protection Agency, Hunedoara, Integrated Environmental Permit no.1 of 02.05.2018
[9] Guță, D., The gray colossus. What hides the mountain of clay, one of the largest dumps in Romania, 2022
[10] Presentation memoir Slag dump – Mal Stabilisation as a Malina Watercourse, 2020
[11]Application form for integrated environmental authorisation for Reșița slag dump, SWISS TRADE SRL, 2019, http://www.anpm.ro/
[12] Păcurar, C.D., Research on the influence of the structure of the metal load on the reduction of specific consumption and the degree of pollution in electric steelworks, Ph.D. thesis, Politehnica University Timisoara, 2019.
[13] Lupu, O., Research Report — Procedures and technologies for the recovery of small waste resulting from the steel elaboration and processing process, related to the Doctoral Thesis, Politehnica University Timisoara, Faculty of Engineering Hunedoara, 2019.
[14] Ministry of Environment, Water and Forests, National Environmental Protection Agency, Environmental Protection Agency, Galați, Decision of the framework phase no.130 of 31.01.2022, http://www.anpm.ro/
[15] Socalici, A., Miloștean, D., The base of energy and raw materials in the materials industry, Politehnica Publishing House Timişoara, 2014.
[16] Socalici, A., Contributions on improving steel quality, Skill thesis, Politehnica University Timișoara, Faculty of Engineering Hunedoara, Romania, 2016.
[17] Liberty Galati member of the GFG Alliance, Welcome to the tabs of our history, 2019
[18] Project 31–011/2007 (CNMP) – Romanians, Ecotechnologies for the rehabilitation and ecological reconstruction of mining perimeters affected by the pollution of tailings dams, Contracting Authority: National Centre for Programme Management, Contractor: National Institute of Research and Development for Metals and Radioactive Resources – Bucharest
[19] Chindriș, L.C., Geotechnical research on the possibility of using sterile material left over from mining operations – Deva mine – in the field of construction, Ph.D. thesis, University of Petroșani, 2019.
[20] Ministry of Economy, Department of Mineral Resources, Information Note of the City Hall of Teliucul Inferior commune, 2022
[21] Inișconi, I., Study of environmental risks generated by ash and slag deposits in S.C. Electrocentrale Deva S.A. and measures to prevent them, Ph.D. thesis, University of Petroșani, 2015.
[22] Fati, S., Mintia Thermal Power Plant: how it died and why salvation is secret, 2022
[23]The energy complex Hunedoara S.A. Mintia Power Plant, http://www.termodeva.ro/index.php/despre–noi/
[24]Draft Western Region Environmental Report, 2014, https://www.adrvest.ro/
[25] Croitoru (married Anghelescu), L, Possibilities of using waste from the energy industry (slag and ash from burning coal) to reduce their impact on the environment, Ph.D. thesis, University of Petroșani, 2015.
[26] "Constantin Brâncuși" University of Târgu Jiu, CHARPHITE Project Progress Report 2018
[27] Badea, C., Contributions regarding the use of reusable waste for the production of new types of building materials, Ph.D. thesis, Politehnica University Timisoara, Faculty of Constructions, 2004.
[28] National Environmental Protection Agency, Integral Environmental Permit, 2006
[29] Moșneguțu, E.F., Industrial waste management – A theoretical course for students' use, Bacau, 2007.
[30] Project No. 31–098/2007: "Preventing and combating pollution in the steel, energy, and mining industry by recycling small waste and powder waste", responsible: Prof. Ph.D. Eng. Teodor Hepuț, beneficiary: CNMP, Romania.

[1.]Hyginus Emeka OPARA, [2.]Uchechi George EZIEFULA

EXPERIMENTAL OPTIMISATION OF AGGREGATE GRADING AND WATER–CEMENT RATIO FOR SANDCRETE PRODUCTION

[1.]Department of Civil Engineering, Faculty of Engineering, Imo State University, Owerri, NIGERIA
[2.] Department of Civil Engineering, Faculty of Engineering, University of Agriculture and Environmental Sciences, Umuagwo, NIGERIA

Abstract: The aim of this study is to experimentally optimise the aggregate grading and water–cement ratio of sandcrete. River sand was sieved and separated into fine sand (particle sizes less than 1 mm), medium sand (1–2 mm particle size), and coarse sand (2–4 mm particle size). These particle size groups were blended in different proportions by weight to produce six combinations of sand particle sizes. For different water–cement ratios, simple mix proportions (by weight) were adopted for the different sand size combinations. Fresh sandcrete mixtures were cast in 150 mm × 150 mm × 150 mm moulds and adequately compacted. The 7– and 28–day density and compressive strength values of the sandcrete specimens were determined. It was found that a high coarse sand content tended to increase the bulk density of sandcrete. The compressive strength of the sandcrete specimens increased with an increasing proportion of coarse–grained sand. Specimens fabricated with lower water–cement ratio exhibited a significant compressive strength increase from 7 to 28 days than specimens produced with higher water–cement ratios. The optimum sand combination is 25% fine sand, 25% medium sand, and 50% coarse sand for all the evaluated water–cement ratios.

Keywords: aggregate grading, compressive strength, density, experimental optimisation, sandcrete

INTRODUCTION

In Nigeria and other West African countries, sandcrete is used for fabricating blocks used in building construction (Ettu et al., 2013). In these regions, sandcrete has become more widely used than traditional construction materials, such as laterite and mudcrete, for constructing walls in buildings. Wall units constructed with sandcrete may be designed as load–bearing or non–load–bearing elements, but sandcrete blocks are mainly used as partition members rather than load–bearing elements.

Sandcrete blocks may be hollow or solid, and different standard sizes of sandcrete are used, depending on the intended application. Sandcrete contains the conventional constituent materials used in concrete, except coarse aggregate. Sandcrete has a zero slump and typically contains coarser sand and a lower cement content than mortar. The zero slump of sandcrete makes it possible for the moulds to be removed immediately after mixing, compacting, and placing sandcrete blocks on a flat, horizontal surface. Hence, freshly manufactured sandcrete blocks are self–supporting.

Compressive strength and density are critical mechanical properties of sandcrete. Compressive strength is widely regarded as a reliable parameter for predicting other mechanical properties, while density directly correlates with the dead load in structural design.

Cement sandcrete blocks should have minimum compressive strength values of 1.85–3.45 MPa (NIS, 2007), depending on the block size and load application. Worryingly, commercially manufactured sandcrete blocks produced in different states of Nigeria suggest that the compressive strength of blocks generally fails to satisfy the NIS 87 (2007) strength requirements (Odeyemi et al., 2018; Ambrose et al., 2019; Tiough and Nande, 2019; Agbi et al., 2020; Anosike, 2021). In some cases, blocks fail under their self–weight, even when transported (Omoregie, 2013).

Although sandcrete blocks are mainly used as partition members rather than load–bearing members, it is still necessary to manufacture them according to standard specifications. In laboratory experiments, the strength of sandcrete can be determined using standard 100 or 150 mm cubes instead of blocks to save material costs. For example, the volume of a 450 mm × 100 mm × 225 mm solid block is three times greater than that of a 150 mm × 150 mm × 150 mm cube.

Sandcrete cubes tend to have a higher compressive strength than sandcrete specimens cast in block moulds; nevertheless, the strength of sandcrete cubes is related to that of sandcrete blocks. The strength and density of cement–based materials are influenced by several parameters, including aggregate size, aggregate grading, cement–aggregate proportion, and water–cement ratio. Some cases of building collapse recently observed in different regions of the country have been linked to low–quality construction materials and inadequate cement–

based mixtures (for example, attributed to poor aggregate grading and inappropriate mix ratios) (Odeyemi et al., 2019).

The influence of aggregate size and grading on the mechanical properties of sandcrete has been investigated in previous studies. Omoregie and Alutu (2006) assessed the strength of sandcrete blocks produced with sands obtained from different parts of Benin, Nigeria. They found that when higher silty sand is blended with lower silty sand, the compressive strength of the higher silty sand significantly increases with minimal cost effects. Oyekan (2008) observed that the compressive strengths of sandcrete blocks increased when coarse aggregate was used as a partial replacement for sand, and the optimum coarse aggregate content ranged from 25% for 5 mm aggregate to 35% for 15 mm aggregate. Ibearugbulem *et al.* (2018) investigated the physicomechanical behaviour of sandcrete produced with different sand grain size proportions and cement–sand mix ratios. They found that the grain size combination yielding the optimum sandcrete compressive strength contained 50% fine sand, 10% medium sand, and 40% coarse sand. Rimintsiwa *et al.* (2019) found that the higher the silt content of fine aggregate, the lower the compressive strength of the sandcrete block, as the silt tended to influence the cement properties.

The water–cement ratio for sandcrete should be selected such that it facilitates adequate cement hydration and enables the sandcrete blocks to stand unsupported after de–moulding. Some previous studies on sandcrete did not specify the water–cement ratio applied in mixing the sandcrete cubes or blocks (Ibearugbulem *et al.*, 2018; Anya and Osadebe, 2015). In such studies, water was gradually added to the cement–aggregate mixture with continuous mixing until a fresh homogenous mixture with a uniform colour was obtained. However, this procedure may lead to adding an excess amount of water during mixing, decreasing the sandcrete strength during the hardening process. Such an approach does not promote the replication of experimental studies. In addition, different sets of fine aggregates may have the same maximum particle size and material composition but exhibit different grading behaviour. Thus, there is a need to optimise the aggregate grading and water–cement ratio of sandcrete to save costs and improve material properties, such as strength and durability.

The aim of this study is to experimentally optimise the aggregate grading and water–cement ratio of sandcrete. This study seeks to determine the optimum sand size proportion that yields the maximum compressive strength of sandcrete. The compressive strength and density values of sandcrete specimens produced with different water–cement ratios and fine–aggregate size proportions were obtained.

MATERIALS

Binder

Grade 42.5 Portland–limestone cement manufactured to Nigerian Industrial Standards (NIS 444–1, 2003) was used as the binder. The cement was stored in bags and protected from dampness.

Water

Water obtained from a borehole in Imo State University, Nigeria, was used for preparing and curing the specimens. The water satisfied BS EN 1008 (2002) requirements.

Fine aggregate

River sand obtained from Otammiri River in Ihiagwa, Imo State, Nigeria, was used as the fine aggregate. The sand was white, well–graded, and coarse.

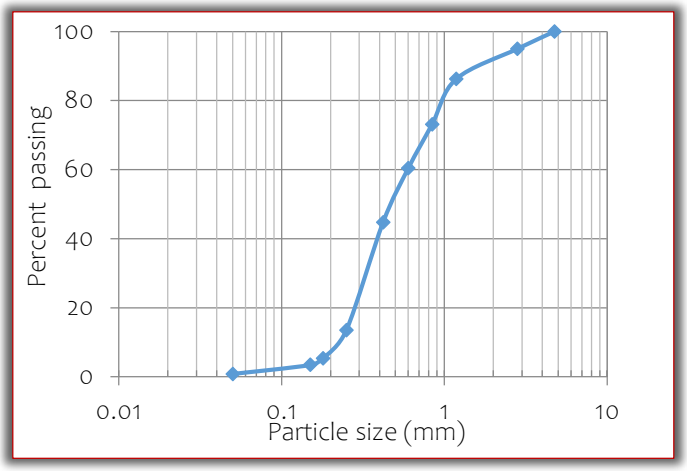

Figure 1. Particle size distribution of river sand

Figure 1 shows the particle size distribution of the river sand before sieving. The physical properties of the non–sieved sand are fineness modulus = 2.93, bulk density = 1490 kg/m^3, specific gravity = 2.65, and water absorption = 1.7%.

METHODS

Mix proportioning

The sand was first sieved and separated into different particle sizes (Table 1). A maximum grain size of 4 mm was adopted as the fine aggregate based on the specifications of BS EN 12620 (2002), and grains with sizes exceeding 4 mm were discarded. X_1, X_2, and X_3 represent fine, medium, and coarse sands, respectively. These three sets of particle sizes were blended in different proportions by weight to produce six combinations of sand particle sizes (Table 2). The combinations of the sand size were designed such that each sand proportion combination yielded a total sum of X_1, X_2, and X_3 equal to 100%. No single size range exceeded 50% of the total weight combination.

The constituent materials of the sandcrete were batched by weight. A cement–sand mix ratio of 1:6 was selected, as recommended by NIS 87 (2007) for sandcrete production. Three water–cement ratios (0.4, 0.5, and 0.6) were adopted in the experimental programme. For each water–cement

ratio, simple mix proportions (by weight) were adopted for the different sets of sand particle sizes (Table 3).

Table 1. Particle sizes of sieved sand

Set no.	Particle size	Designation
1	$X_1 \leq 1$ mm	Fine sand
2	1 mm $\leq X_2 \leq$ 2 mm	Medium sand
3	2 mm $\leq X_3 \leq$ 4 mm	Coarse sand

Table 2. Percentages (by weight) for different sets of sand particle sizes

Proportion no.	X_1	X_2	X_3
P1	50%	50%	0%
P2	50%	25%	25%
P3	50%	0%	50%
P4	25%	50%	25%
P5	25%	25%	50%
P6	0%	50%	50%

Table 3. Mix proportioning of constituents of sandcrete specimens

w/c	Prop. no.	Water (kg)	Cement (kg)	Sand (kg)		
				X_1	X_2	X_3
0.4	P1	0.4	1	2	2	0
	P2	0.4	1	2	1.6	0.4
	P3	0.4	1	2	1.2	0.8
	P4	0.4	1	2	1	1
	P5	0.4	1	2	0.8	1.2
	P6	0.4	1	2	0.4	1.6
0.5	P1	0.5	1	2.5	2.5	0
	P2	0.5	1	2.5	2	0.5
	P3	0.5	1	2.5	1.5	1
	P4	0.5	1	2.5	1.25	1.25
	P5	0.5	1	2.5	1	1.5
	P6	0.5	1	2.5	0.5	2
0.6	P1	0.6	1	3	3	0
	P2	0.6	1	3	2.4	0.6
	P3	0.6	1	3	1.8	1.2
	P4	0.6	1	3	1.5	1.5
	P5	0.6	1	3	1.2	1.8
	P6	0.6	1	3	0.6	2.4

Preparation of sandcrete specimens

The cement and sand were first uniformly mixed in a dry state. The calculated amount of water, based on the selected water–cement ratio, was added was mixing was continued until a homogenous mixture of constant colour was obtained. The fresh sandcrete mixtures were cast in 150 mm × 150 mm × 150 mm moulds and compacted.

The moulds were initially oiled to minimise friction and reduce the difficulty of removing the moulds after the sandcrete set. Compaction was performed using a standard 16 mm tamping rod. Each side received 30 blows, resulting in 90 blows per cube. Six specimens were produced for each selected sand mix proportion and water–cement ratio, and 108 sandcrete cubes were fabricated.

The concrete specimens were retained in the moulds for 24 h, after which the moulds were removed. The de–moulded cube specimens were cured by sprinkling water twice a day (at 0900 and 1700 hours each day) for 7 and 28 days.

Tests

The 7– and 28–day density and compressive strength values of the sandcrete specimens were determined. On the day of testing, three specimens were subjected to tests for each particle size proportion and water–cement ratio. The density of each air–dried sandcrete cube was determined by dividing its mass by the volume. Tests to determine the compressive strength of the hardened cubes were performed according to BS EN 12390–3 (2009) specifications.

RESULTS AND DISCUSSION

Density

The density values of the 7– and 28–day sandcrete are listed in Tables 4 and 5, respectively. The densities of the 7–day sandcrete specimens ranged from 1700 to 2120 kg/m^3. The densities did not show a specific trend with variation in the water–cement ratio at 7 and 28 days.

The densities of the 28–day sandcrete cubes were slightly higher than those of the corresponding 7–day sandcrete cubes for a specific water–cement ratio and sand mix proportion. All the 28–day densities exceeded 2000 kg/m^3 and ranged between 2000 and 2300 kg/m^3. The densities obtained for the sandcrete specimens at 28 days are comparable to the sandcrete density values reported by Ibearugbulem *et al.* (2013). For the 28–day density, P5 and P6 specimens had higher density values than others; this increase could be attributed to the higher coarse sand contents of P5 and P6.

Table 4. Density values of sandcrete cubes at 7 days

Prop. no.	Density (kg/m^3)		
	w/c = 0.4	w/c = 0.5	w/c = 0.6
P1	1913	1802	1703
P2	1890	2002	1819
P3	2170	1903	1993
P4	2026	2066	1876
P5	2209	2108	2093
P6	2071	2064	2117

Table 5. Density values of sandcrete cubes at 28 days

Prop. no.	Density (kg/m^3)		
	w/c = 0.4	w/c = 0.5	w/c = 0.6
P1	2060	2179	2128
P2	2193	2083	2072
P3	2171	2063	2042
P4	2232	2133	2073
P5	2318	2219	2109
P6	2311	2210	2183

Compressive strength

The compressive strengths of the sandcrete specimens are listed in Tables 6 and 7. The 7–day compressive strength values for the different sand blends were 5.4–13.4, 6.1–13.03, and 6.3–13.0 MPa for the 0.4, 0.5, and 0.6 water–cement ratios, respectively (Table 6). For all the water–cement ratios, P5 had the highest compressive strength values, followed by P6, whereas P1 had the lowest compressive strength. For some sand mix proportions, the variation in the

7–day compressive strength was irregular. For P1 and P4, the 0.6 water–cement ratio yielded the maximum compressive strength; for P2 and P6, the 0.5 water–cement ratio resulted in the maximum strength; for P3 and P5, the water–cement ratio of 0.4 yielded the maximum strength.

Table 6. Compressive strength values of sandcrete cubes at 7 days

Prop. no.	Compressive strength (MPa)		
	w/c = 0.4	w/c = 0.5	w/c = 0.6
P1	5.91	6.05	6.16
P2	6.74	6.86	6.79
P3	7.25	7.38	7.68
P4	6.65	6.90	6.99
P5	13.32	13.03	12.96
P6	9.85	10.69	9.80

Table 7. Compressive strength values of sandcrete cubes at 28 days

Prop. no.	Compressive strength (MPa)		
	w/c = 0.4	w/c = 0.5	w/c = 0.6
P1	7.41	7.35	7.27
P2	8.56	8.26	8.09
P3	9.23	8.93	8.76
P4	8.11	8.01	7.89
P5	18.23	16.05	15.84
P6	16.50	13.69	11.96

The compressive strength values of the sandcrete specimens on the 28th day of curing were 7.4–18.3, 7.3–16.1, and 7.27–15.9 MPa for the 0.4, 0.5, and 0.6 water–cement ratios, respectively (Table 7).

Similar to the 7–day compressive strength results, P5 had the highest 28–day compressive strength for all water–cement ratios, followed by P6. P5 had higher compressive strength than P6 because the fine sand filled the voids formed by the medium and coarse sands in the sandcrete matrix. P1 had the lowest 28–day compressive strength. The increasing ranks of the sandcrete specimens based on their 28–day compressive strengths are as follows:

$$P1 < P4 < P2 < P3 < P6 < P5.$$

The ranking indicated that the specimens with increased coarse sand contents (50%) had higher compressive strengths than specimens with low (25%) and no (0%) coarse sand contents. Moreover, the variation in the water–cement ratio with the 28–day compressive strength was consistent; an increase in the water–cement ratio decreased the 28–day compressive strength of sandcrete specimens for all the sand mix proportions.

The 7–day compressive strength of cement–based materials can be expressed as a ratio or percentage of its corresponding 28–day compressive strength.

Figure 2 shows the percentage of the 7–day compressive strength of sandcrete compared to the corresponding 28–day compressive strength. The 7–day compressive strength of sandcrete was 60–90% of the corresponding 28–day compressive strength for all aggregate grades and water–cement ratios. The relatively high values might be attributed to the absence of coarse aggregate, which accelerated the fine aggregate–cement paste bond. The values of the 7–to–28–day strength ratio tended to increase with the water–cement ratio; this increase was higher for sandcrete specimens with higher proportions of coarse sand (P5 and P6). Thus, mixtures produced with lower water–cement ratios gained more strength from 7 to 28 days than mixtures produced with higher water–cement ratios.

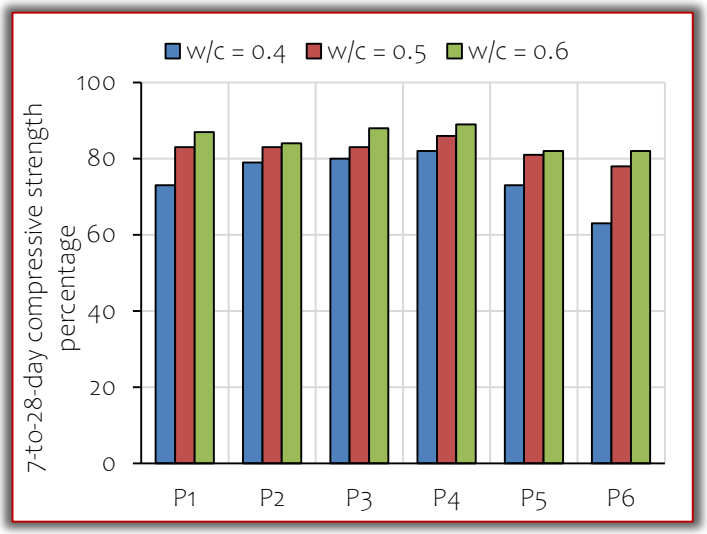

Figure 2. Percentage of 7–day compressive strength to 28–day compressive strength

CONCLUSIONS

In this study, the experimental optimisation of aggregate grading and water–cement ratio of sandcrete was investigated. The compressive strengths and densities of sandcrete specimens produced with different water–cement ratios and fine–aggregate size proportions were obtained. The following conclusions were drawn.

- A high coarse sand content tended to increase the bulk density of sandcrete, and the 28–day densities of all the sandcrete specimens exceeded 2000 kg/m^3.
- The compressive strength of the sandcrete specimens increased with an increasing proportion of coarse–grained sand.
- Specimens fabricated with lower water–cement ratio exhibited a significant compressive strength increase from 7 to 28 days than specimens produced with higher water–cement ratios.
- Based on the density and compressive strength values obtained in this study, the optimum sand combination is 25% fine sand (particle sizes less than 1 mm), 25% medium sand (1–2 mm particle size), and 50% coarse sand (2–4 mm particle size).

Sands used for cement sandcrete construction should be well–graded to optimise the physical and mechanical properties of sandcrete. The long–term mechanical properties of sandcrete, such as compressive strength, splitting tensile strength, and flexural strength, should be investigated in future studies. In addition, the use of

industrial and agricultural by–products as pozzolana and supplementary cementitious materials, such as rice husk ash and fly ash, in sandcrete, should be assessed.

References

[1] Agbi, G. G., Akpokodje, O. I., and Uguru, H. (2020). Compressive strength of commercially produced sandcrete blocks within Isoko metropolis of Delta State, Nigeria. Turkish Journal of Agricultural Engineering Research, 1(1):91–103.

[2] Ambrose, E. E., Etim, R. K., and Koffi, N. E. (2019) Quality assessment of commercially produced sandcrete blocks in part of Akwa Ibom State, Nigeria. Nigerian Journal of Technology, 38(3):586–593.

[3] Anosike, N. M. (2021). Assessment of sandcrete blocks quality in Owerri, Imo State, Nigeria. Journal of Engineering Research and Reports, 21(1):15–24.

[4] Anya, C. U., and Osadebe, N. N. (2015). Effect of partial replacement of sand with quarry dust on the structural characteristics of sandcrete blocks. Nigerian Journal of Technology, 34(4):679–684.

[5] BS EN 1008 (2002). Mixing water for concrete — Specification for sampling, testing and assessing the suitability of water, including water recovered from processes in the concrete industry, as mixing water for concrete. British Standards Institution, London.

[6] BS EN 12390–3 (2009). Testing hardened concrete — Compressive strength of test specimens. British Standards Institution, London.

[7] BS EN 12620 (2002). Aggregates for concrete. British Standards Institution, London.

[8] Ettu, L. O., Arimanwa, J. I., Njoku, F. C., Amanze, A. P. C., and Eziefula, U. G. (2013). Strength of blended cement sandcrete and soilcrete blocks containing sawdust ash and pawpaw leaf ash. International Journal of Engineering Inventions, 2(8):35–40.

[9] Ibearugbulem, O. M., Eziefula, U. G., and Opara, H. E., Physico–mechanical behaviour of sandcrete produced with different proportions of sand grain sizes. Engineering and Applied Science Research, 45(2):83–88.

[10] NIS 444–1 (2003). Quality standard for ordinary Portland cement — Part 1: Composition, specification and conformity criteria for common cements. Standards Organisation of Nigeria, Lagos.

[11] NIS 87 (2007) Standards for sandcrete blocks. Standards Organisation of Nigeria, Lagos.

[12] Odeyemi, S. O., Akinpelu, M. A., Atoyebi, O. D., and Orire, K. J. (2018). Quality assessment of sandcrete blocks produced in Adeta, Kwara State, Nigeria. Nigerian Journal of Technology, 37(1):53–59.

[13] Odeyemi, S. O., Giwa, Z. T., and Abdulwahab, R. (2019). Building collapse in Nigeria (2009–2019), causes and remedies – A review. USEP: Journal of Science and Engineering Production, 1(1):122–135.

[14] Omoregie, A. (2013). Optimum compressive strength of hardened sandcrete building blocks with steel chips. Buildings, 3:205–219.

[15] Omoregie, A., and Alutu, O. E. (2006). The influence of fine aggregate combinations on particle size distribution, grading parameters, and compressive strength of sandcrete blocks. Canadian Journal of Civil Engineering, 33(10):12–17.

[16] Oyekan, G. L. (2008). Single and mixed size coarse aggregates in sandcrete block production. 33rd Conference on Our World in Concrete and Structures, Singapore, August 25–27, 2008. [Online]

[17] Rimintsiwa, N. S., Muhammed, A., and Aminu, A. (2019). Effect of sand grading on the compressive strength of sandcrete block. The International Journal of Science and Technoledge, 7(2):105–121.

[18] Tiough, D. M., and Nande, V. M. (2019). An evaluation of the strength properties of commercially produced sandcrete blocks in Makurdi metropolis. International Journal of Education Development, 24(1):1–10.

ISSN: 2067-3809

Fascicule 3

[July – September]

tome [2023] XVI

ACTA Technica CORVINIENSIS
BULLETIN OF ENGINEERING

ISSN: 2067-3809

[1.]Costin MIRCEA, [1.]Florin NENCIU, [2.]Constantin STAN, [3.]Lavinia BERCA

CONSIDERATIONS REGARDING THE IMPORTANCE OF USING OPTICAL SEED SORTING MACHINES

[1.]INMA Bucharest – National Institute for Research–Development of Machines and Installations designed for Agriculture and Food Industry, ROMANIA
[2.]Politehnica University of Bucharest, Faculty of Energy, Bucharest, ROMANIA
[3.]National Research and Development Institute for Food Bioresources – IBA Bucharest, ROMANIA

Abstract: In the preparation and storage of grains, seed cleaning is a highly important phase. There has been extensive research regarding the cleaning and classifying grains. The grain seeds are usually contaminated right from the harvest with the seeds from other plants, with other materials (soil, plant residues, etc.) or even with their own degraded seeds. Since they are the same size and weight, they are difficult to be sorted mechanically. The degree of seed purity may be significantly increased by optical sorting after dedusting and mechanical sorting. The separation of seed mixtures by colour is achieved by using photoelectric devices, which, being sensitive to differences in the intensity of the reflected light beam, emit pulses that are used to carry out orders to separate the seeds of the wrong color. This article emphasizes the importance of introducing new or innovative methods in the seed separation process, especially optical systems. Various ways of sorting were discussed, the design of super interesting sorting systems.

Keywords: separation efficiency; optical sorting

INTRODUCTION

One of the most significant subsectors of the agricultural processing sector is food production. The goals of contemporary agriculture include obtaining higher yields and better crop quality (*Nenciu, F et al. 2022*). The agri–food industry has likewise seen similar developments for many years. In the preparation and storage of grains, seed cleaning is a highly important phase. There has been extensive research regarding the cleaning and classifying grains (*Mircea et al. 2014, Yuan J. et al., 2018, and Krzysiak Z. et al., 2020*). Effective seed mixture separation must be based on the characteristics of mixture components that lend themselves to separation, which have been studied by several authors.

Recently, colour sorters have begun to be installed in both wheat flour mills and durum grain mills. Ergot wheat, black tip, fusarium, charred, other discoloured grains, and other internal impurities are removed from wheat using colour sorters during the cleaning process (Inamdar, A., et al. 2014). (*Kunhimohammed C.K. et al. 2015*) proposed an automatic machine that sorted color using a special color sensor that was TCS230 and PIC microcontroller.

Under these conditions, a colour sensor was used for detection and identification, and the complete procedure was managed by a PIC16F628A microcontroller. Furthermore, the product was evaluated and divided into sections as needed with the use of two conveyor belts. The results showed a precise quality and a higher rate of production in the area of automation.

Kex Technology et al. [12] represented food processing solutions through digital sorting. Various ways of sorting were discussed, the design of super interesting sorting systems. Supplier, receiver, testing, announcing, and globally performed. Selin Macwan et al. [2] introduced a machine using IOT which sorted color.

As per different analyses of objects or pieces such as color, weight, size, and shape, they formulated a way of color sorting of objects using the TCS3200 sensor along with motors and Arduino. Meanwhile, the GSM technique was also performed. Keeping average time consumption before and after contact, a maximum and minimum speed of conveyor belt, blow distances of flow through nozzles productivity, precision, and accuracy of object color sorting was tested.

Other research studies are oriented towards upgrading optic equipment using IOT (*Macwan, S., et al. 2018*). As per different analyses of objects or seeds such as colour, weight, size, and shape, they formulated a methodology of colour sorting of objects using the TCS3200 sensor. Dumanay, A.B., et al. (2016) represented a newly designed equipment which processed coloured image of olive fruits using an optic sorting technique, while Inamdar A., et al. (2014) proposed the application of optic sorting into wheat milling. Wheat cleaning was performed by removing egret wheat, fusarium, black tip. (*Halder, S., et al. 2014*) proposed a sorting machine using two ladders development on belt conveyor.

Colour sensor, microcontroller, servo motors, programming helps in the accumulation of data and commands further to operate accurately. (*Sheth, S.M., et al. 2010*) proposed

automatic sorting system using machine vision. Microcontroller and sorters are used for colour inspection and finally performed using machine vision. Algorithm are calculated using MATLAB software.

(Sachdeva, A., et al. 2017) introduced counting and color sorting machine to developed industrial automation using a nano microcontroller and color sensor of type TCS3200. Various techniques such as optical sensors, sets of inductive, and capacitive are going on nowadays resulted in saving money and time (Chatte, U.A., et al. 2018). (Shen, L.J., et al. 2015) introduced the development and designing of the robot which sorted colors. With the advancement in technology, applications are started widening using the new approach. (Jaisingpure, P.S., et al.2017) introduced automated object sorting based on colour detection in which USB camera is used for detection purpose and raspbian operating system (Raspberry Pi 2) functioned as automated sorter. Saurin Mukundbhai Sheth et al. [16] proposed automatic sorting system using machine vision. Microcontroller and sorters are used for color inspection and finally performed using machine vision. Algorithm are calculated using MATLAB software.

Saurin Mukundbhai Sheth et al. [16] proposed automatic sorting system using machine vision. Microcontroller and sorters are used for color inspection and finally performed using machine vision. Algorithm are calculated using MATLAB software.

Saurin Mukundbhai Sheth et al. [16] proposed automatic sorting system using machine vision. Microcontroller and sorters are used for color inspection and finally performed using machine vision. Algorithm are calculated using MATLAB software.

MATERIALS AND METHODS

The separation of seed mixtures by colour is achieved by using photoelectric devices, which, being sensitive to differences in the intensity of the reflected light beam, emit pulses that are used to carry out orders to separate the seeds of the wrong color. When a seed passes between the photoelectric cell and the screen, it intercepts the light rays reflected by the screen.

If the seed has the same color as the screen, the light reflected by the seed in the direction of the photoelectric cell has the same intensity, and the current emitted by the photocell remains the same. If the seed has a different color than the screen, then the photocell is impressed differently and emits an electric current of a different intensity. In this way, the color differences are transformed into electrical impulses of different intensity that act on the separation device which, usually through a jet of compressed air, diverts the seeds of different color from the path of the seed row.

In order for the separation to be of quality, it is necessary for the seeds to pass one by one through the space between the screen and the photocell. For this purpose, the machines that work on this principle have organs for ordering the seeds in a row.

Usually, seed color detection cameras are equipped with several channels working in parallel. In these conditions, the seeds are observed on all sides. The organs that execute the separation

RESULTS

The sorting machines produced by SEA (figure 1) are equipped with both front and rear cameras, so that both sides of the seed are examined. Seeds or impurities that have a different color than normal are deflected from their normal fall path with the help of a jet of air. Along with the elimination of unhealthy elements, good grains can also be eliminated, which can be recovered to a good extent by a new pass.

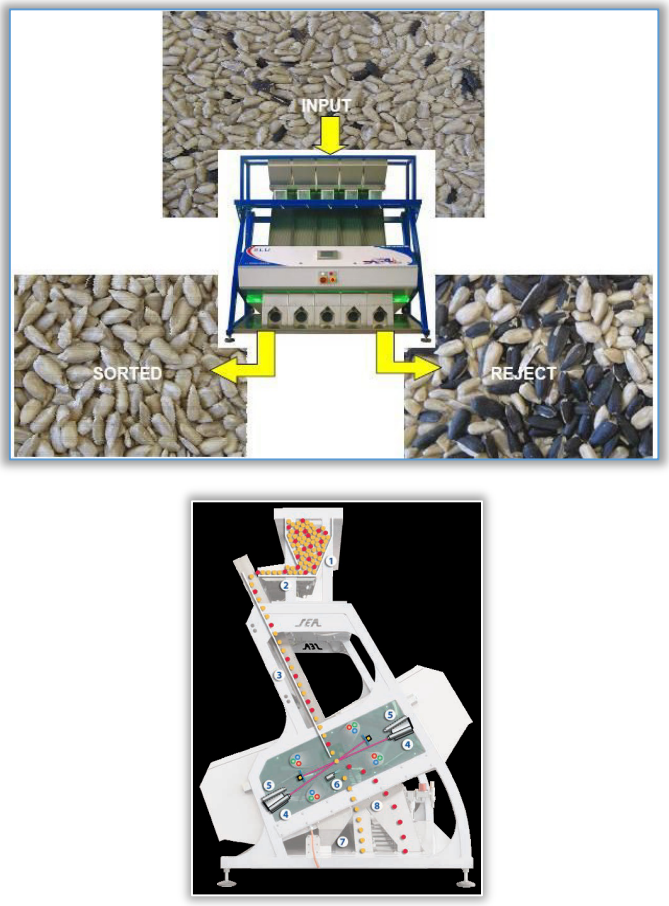

Figure 1 – The principle of operation of the optical seed sorting equipment, SEA (www.geangu.ro; www.cimbria.ro)

The machines are modular, they can have from one to five channels. In the case of machines with more than one channel, an automatic passage of the material rejected by the first channels can be designed through the channel or channels prepared for this purpose. In the course of time, the machines were always perfected.

To eliminate, for example, black sclerotia from black sunflower seeds, the machines were equipped with an infrared ray system. For a better examination, the resolution has been increased and the lighting with

fluorescent tubes has been replaced with lighting produced by red, green and blue LEDs. Through the different combination of the three colors, various other intermediate colors can be obtained to be used for each individual case. This new version is called Pixel NEXT, it can have up to 7 channels and can sort 35 tons/hour of wheat. For each individual material the productivity is different.

The operating principle of a sorting equipment: 1 Input product is loaded into the in–feed hopper, 2 it moves along the vibrating plate 3 until it flows on to a sloping chute where it is individually checked and sorted by state–of–the–art cameras 4 (CCD cameras for standard version and 5 additional cameras for bichromatic, NIR and InGaAs versions) situated in the front and rear of the flow. 6 Depending on the signals received by the optical device, the sorter software controls the pneumatic device, 7 which physically separates the unwanted products out of the conforming ones which naturally reach their discharging hopper. 8 The rejected products are instead deviated by a jet of compressed air produced by the relevant ejector and discharged in the front side hopper. In automatic re–pass versions, the sorted or rejected product is automatically conveyed to another section of the machine for undergoing an identical process.

Table 1. Possible configurations

Model	Next 1	Next 1,5	Next 2	Next 3	Next 4	Next 5	Next 6	Next 7
Vibrator	1	2	2	3	4	5	6	7
Chute	1	2	2	3	4	5	6	7
CCD cameras	2 to 4	2 to 4	4 to 8	6 to 12	8 to 16	10 to 20	12 to 24	14 to 28
Ejectors	54	77	108	162	216	270	324	378
Width	1560	920	1560	1560	1950	1950	2540	2540
Depth	1550	1715	1550	1550	1550	1550	1550	1550
Height	2100	2100	2100	2100	2100	2100	2100	2100
Weight	600	650	700	800	850	950	1.100	1.200
Power cons.	1,5	1,5	1,5	1,5	2,5	2,5	3,5	3,5
Air cons at 4 bar	8,4	12,6	16,8	25,2	33,6	42,0	50,4	58,8

GROTECH manufactures high–end optical seed sorting machines of the ZF series (figure 2), capable of well sorting different products, such as rice and wheat.

Figure 2 – ZF series multi–function colour sorting machine (www.grotechcolorsorter.com)

Table 2. Parameter Table

Model	ZF700
Optimized Carryover (Bad : Good)	30:1
Product output(t/h)	3.0–8.0
Heating of tray	YES
Camera	CCD
Type of selection	Per size/color
Remote Access&Control (connectivity)	YES
Channel split	N/A
Net Weight (kg)	1665
Europe Certification	Type of illumination
Power consumption(kw)	3.5
Dimension L×W×H(mm)	3030*1658*1850
Power supply(V/HZ)	220V±10% 50/60HZ

Multifunction color sorting advantage:

- high reliability – excellent anti–interference ability;
- high precision – support high–end processing algorithms such as artificial intelligence and neural network;
- high consistency – using the most advanced assembly technology and calibration technology on the market to ensure the consistency of the whole machine and channels.

Multifunction color sorting application: the high level ZF series multi–function color sorter machine able to sorting different products well with one machine.

CONCLUSIONS

The main purpose of seed conditioning is to improve seed quality by removing impurities (broken seeds, chaff, weed seeds, plant debris, etc.).

Optical seed sorting machines have the ability to check each seed and identify possible defects that may affect the germination or vigor of future plants and automatically eliminate those with defects.

Optical sorters can recognize the color, size, shape, structural properties and chemical composition of objects. Compared to manual sorting, which is subjective and inconsistent, optical sorting helps improve product quality, maximize yield and increase yields while reducing labor costs.

Note: This paper was presented at ISB–INMA TEH' 2022 – International Symposium on Technologies and Technical Systems in Agriculture, Food Industry and Environment, organized by University "POLITEHNICA" of Bucuresti, Faculty of Biotechnical Systems Engineering, National Institute for Research–Development of Machines and Installations designed for Agriculture and Food Industry (INMA Bucuresti), National Research & Development Institute for Food Bioresources (IBA Bucuresti), University of Agronomic Sciences and Veterinary Medicine of Bucuresti (UASVMB), Research–Development Institute for Plant Protection – (ICDPP Bucuresti), Research and Development Institute for Processing and Marketing of the Horticultural Products (HORTING), Hydraulics and Pneumatics Research Institute (INOE 2000 IHP) and Romanian Agricultural Mechanical Engineers Society (SIMAR), in Bucuresti, ROMANIA, in 6–7 October, 2022.

References

[1] Ciobotaru, I.E., Nenciu, F., Vaireanu, D.I. (2013). The Electrochemical Generation of Ozone using an Autonomous Photovoltaic System. Rev. Chim., 64, 1339–1342.

[2] Chatte, U.A., Kadam, U., Khupase, V., Mane, S., Kharat, P., (2018). Arduino based object sorting. International Journal of Innovations in Engineering Research and Technology (IJIERT), ISSN: 2394–3696.

[3] Dumanay, A.B., Sakin, R., Istanbullu, A. (2016) A New Design of Olive Fruit Sorting Machine Using Color Image Processing. IOSR Journal of Agriculture and Veterinary Science (IOSR–JAVS) Volume 9, Issue 11 Ver. 1, PP 41–47T.

[4] Halder, S., Islam, M.K., Chowdhury, M.S. and Banik. S.C. (2014). Development of an automatic color sorting machine on belt conveyer. International Conference of Mechanical Engineering and Renewable Energy, Chittagong, Bangladesh.

[5] Inamdar, A., and Sakhare, S.D. (2014). Application of color sorter in wheat milling. International Food Research Journal 21(6):2083–2089.

[6] Jaisingpure, P.S., Kulkarni, A.B., (2017). Automated Object Sorting Based On Colour Detection. Conference Proceeding of 2nd International conference on Science, Technology & Management (ICSTM–2017) at The Institution of Electronics and Telecommunication Engineers, Osmania University Campus, Hyderabad, India

[7] Jianbo, Y., Chongyou, W., Hua, L., Xindan Q., Xingxing, X., Xinxin, S., (2018), Movement rules and screening characteristics of rice–threshed mixture separation through a cylinder sieve. Computers and Electronics in Agriculture, 154, pp. 320–329

[8] Krzysiak Z., Samociuk W., Zarajczyk J., Beer–Lech K., Bartnik G., Kaliniewicz Z., Dziki D., (2020), Effect of Sieve Unit Inclination Angle in a Rotary Cleaning Device for Barley Grain. Transactions of the ASABE. 63(3), pp. 609–618;

[9] Kunhimohammed C.K, Muhammed, S.K.K., Sahna, S., Gokul, M.S., Shaeez, U.A. (2015). Automatic Color Sorting Machine Using TCS230 Color Sensor And PIC Microcontroller. International Journal of Research and Innovations in Science and Technology Volume2, pp:2394–3866.

[10] Macwan, S., Hardik, M., (2018). IOT Color Based Object Sorting Machine. International Journal of Applied Engineering Research ISSN 0973–4562 Volume 13, Number 10, pp. 7383–7387.

[11] Mircea, C., Nenciu, F., Vlăduț ,V., Voicu, G., Cujbescu, D., Gageanu I., Voicea, (2020) I. Increasing the performance of cylindrical separators for cereal cleaning, by using an inner helical coil, INMATEH Agricultural Engineering 2020, 62 (3), 249–258

[12] Nenciu, F., Paraschiv, M., Kuncser, R., Stan, C., Cocarta, D., Vladut, V.N. (2022) High–Grade Chemicals and Biofuels Produced from Marginal Lands Using an Integrated Approach of Alcoholic Fermentation and Pyrolysis of Sweet Sorghum Biomass Residues. Sustainability 2022, 14, 402

[13] Nenciu, F., Stanciulescu, I.; Vlad, H., Gabur, A., Turcu, O.L., Apostol, T., Vladut, V.N., Cocarta, D.M.; Stan, C. (2022). Decentralized Processing Performance of Fruit and Vegetable Waste Discarded from Retail, Using an Automated Thermophilic Composting Technology. Sustainability 2022, 14, 2835

[14] Nenciu, F., Vladut, V. (2020) Studies on the perspectives of replacing the classic energy plants with Jerusalem artichoke and Sweet Sorghum, analyzing the impact on the conservation of ecosystems. IOP Conf. Ser. Earth Environ. Sci. 2020, 635, 012002

[15] Sachdeva, A., Gupta, M., Pandey, M., Khandelwal, P. (2017). Development of industrial automatic multicolor sorting and counting machine using Arduino NANO Microcontroller and TCS3200 color sensor. The International Journal of Engineering and Science (IJES) Volume 6, Issue 4, pp56–59.

[16] Sheth, S.M., Kher, R.K., (2010). Automatic Sorting System Using Machine vision. Multi–Disciplinary International Symposium on Control, Automation & Robotics At: DDIT, Nadiad Volume: 1

[17] Ștefănescu, I.I., (2003). Utilaje pentru prelucrarea primară a materiilor prime din industria alimentară, Editura Tehnică–Info Chișinău.

[18] Yuan J., Wu C., Li H., Qi X., Xiao X., Shi X., (2018), Movement rules and screening characteristics of rice–threshed mixture separation through a cylinder sieve, Computers and Electronics in Agriculture, 154 pp. 320–329;

[19] ***www.geangu.ro/echipamente–agricole/masini–de–sortare–optica–a–semintelor/

[20] ***www.cimbria.ro

[21] ***www.grotechcolorsorter.com/multifunction–color–sorter_c14

ISSN: 2067-3809

[1.]Iulia Andreea GRIGORE, [1.]Laurențiu VLĂDUȚOIU, [1.]Cristian SORICĂ, [1.]Mario CRISTEA, [1.]Elena SORICĂ

STUDY ON THE EFFICIENCY OF BIOFERTILIZERS IN THE CONTEXT OF SUSTAINABLE DEVELOPMENT

[1.] National Institute of Research & Development for Machinery and Installations for Agriculture & Food Industry – INMA Bucharest, ROMANIA

Abstract: Sustainable agriculture is an action with a long–term aim that seeks to overcome the problems and restrictions faced by conventional agriculture, society in general, in order to ensure economic viability, the good state of the environment, the acceptance by society of agricultural production systems. This system of sustainable agriculture requires economically viable technologies over a long period of time, with high harvests, obtained at lower costs. Sustainable development combines the demands of the present without compromising the ability of future generations to meet their own needs. Among the materials used in agriculture, fertilizer is the most widely used. Each type of fertilizer, chemical or organic, has its advantages and disadvantages. These advantages must be integrated in order to achieve optimal performance by each type of fertilizer and to achieve a balanced nutrient management for crop growth. Biofertilizers differ from chemical and organic fertilizers in that they do not directly supply nutrients to crops, and they are crops of special bacteria and fungi. The production technology for biofertilizers is simple, and the cost of use is low compared with chemical fertilizers for plants.

Keywords: durable agriculture, agrochemical, biofertilizers, soil fertility

INTRODUCTION

Sustainable agriculture involves healthy food for consumers at balanced prices, respect for the environment, attention to animals, viable economic methods, a contribution to the beautification of landscapes, protection of precious ecosystems and biodiversity *(Vanghele N. et al., 2019)*. Sustainable agriculture has as exact objectives the production of food in sufficient quantities and quality, the conservation of natural resources (products obtained from nature must return in different forms to nature), landscape management, etc *(Anghel M.G. et al., 2017)*.

This system of sustainable agriculture requires economically viable technologies over a long period of time, with high harvests, obtained at lower costs. In order to be sustainable and viable a system must meet the following conditions:

- maintenance and improvement of the physical environment and resistance to external pressures or strong disturbances;
- satisfying the society's requirements in food products;
- ensuring the economic and social well–being of agricultural producers

Sustainable agriculture, with all the substantial contributions to social progress, is still far from what means a sustainable development, which means not only a fixed state in harmony with nature but, rather, a development in a dynamic process, in accordance with modern ecological principles, by which the use of resources, the direction of investments, the orientation of the development of technologies and institutional changes are made taking into account the requirements, both current and future of society's progress *(Ahlem Z. and Hammas M. A., 2017)*.

This type of agriculture, sustainable, is an integrated system of plant and animal production practices with a specific local application which, in the long term, achieves:

- meeting the requirements of food and fiber;
- improving the quality of the environment and the resource base;
- maximum efficient use of non–renewable resources;
- improving the quality of life and the whole of society.

In the modern ecological concept, alternative agriculture is the strategy, and sustainable agriculture is the goal, while soil quality is the role and position of the link, constituting the key to agricultural sustainability *(Chand S. et el., 2006)*.

Sustainable agriculture is an action with a long–term aim that seeks to overcome the problems and restrictions faced by conventional agriculture, society in general, in order to ensure economic viability, the good state of the environment, the acceptance by society of agricultural production systems *(Ramakrishnan B. et al., 2021)*.

The concept of sustainable agriculture is based on achieving optimal yields of inclusive economic efficiency and ensuring ecological balance. Hence the need to integrate agricultural policy into environmental policy *(Petre A. et al., 2019)*.

In order to achieve the objective of harmonising the development of agriculture with the environment, an

integrated approach is needed both to considerations relating to the development of agriculture and to ensuring environmental protection *(Willer H. and Sahota A., 2020)*.

Among the materials used in agriculture, fertilizer is the most widely used. Each type of fertilizer, chemical or organic, has its advantages and disadvantages. These advantages must be integrated in order to achieve optimal performance by each type of fertilizer and to achieve a balanced nutrient management for crop growth *(Micu A. et al., 2017)*. Based on the production process, it can be roughly classified into three types: chemical, organic and biofertilizing.

ORGANIC FERTILIZERS. ADVANTAGES AND DISADVANTAGES OF USING ORGANIC FERTILIZERS

Advantages of using organic fertilizers:

- Nutrient intake is more balanced, which helps maintain plant health;
- They increase the biological activity of the soil, which improves the mobilization of nutrients from organic and chemical sources and the decomposition of toxic substances;
- They increase the colonization of mycorrhizae, which improves the supply of P;
- They increase the growth of roots due to a better structure of soil;

Disadvantages of using organic fertilizers:

- They are relatively low in nutrient content, so a larger volume is needed to provide enough nutrients for crop growth;
- The rate of release of nutrients is too slow to meet the requirements of crops in a short time, therefore, a certain nutrient deficiency may occur;

CHEMICAL FERTILIZERS. ADVANTAGES AND DISADVANTAGES OF USING CHEMICAL FERTILIZERS

Advantages of using chemical fertilizers:

- Nutrients are soluble and immediately available to plants; therefore, the effect is usually direct and fast;
- The price is lower and more competitive than organic fertilizer, which makes it more acceptable and often applied by users;
- They are quite high in nutrient content; only relatively small amounts are needed for growing crops;

Disadvantages of using chemical fertilizers:

- Over–application can have negative effects, such as leaching, pollution water resources, the destruction of microorganisms and friendly insects, the susceptibility of crops to the attack of diseases, acidification or alkalization of the soil or the reduction of soil fertility – thus causing irreparable damage to the general system;
- Overeating N leads to softening of plant tissue, resulting in plants that are more susceptible to diseases and pests (Bokhtiar S.M. and Sakurai K., 2005).

THE ROLE OF BIOFERTILIZERS IN CROP PRODUCTION

Soil microorganisms play a significant role in regulating the dynamics of the decomposition of organic matter and the availability of plant nutrients such as N, P and S. It is well recognized that microbial inoculants are an important component of the integrated nutrient management that lead to sustainable agriculture. In addition, microbial inoculants can be used as an economic factor to increase crop productivity; doses of fertilizers can be reduced and more nutrients can be harvested from the soil (*Laza E. A. et al., 2021*).

The biofertilizer is defined as a substance containing live microorganisms and is known to help expand the root system and better seed germination. A healthy plant usually has a healthy rhizosphere, which should be dominated by beneficial microbes *(Chen J. H., 2006)*.

Inoculation of biofertilizers

Biofertilizers are generally applied to soil, seeds or seedlings, with or without a specific carrier for microorganisms, for example, peat, compost or stickers. Regardless of the methods, the number of cells reaching the soil from commercial products is less than the existing number of microorganisms in the soil or rhizosphere; it is unlikely that these added cells will have a beneficial impact on the plant, unless there is a lot of application. In addition, the population of the introduced microorganisms will decrease and be eliminated in a very short time, often days or weeks. The formulation of inoculums, the method of application and storage of the product are all essential for the success of a biological product. Short shelf life, lack of adequate transport materials, susceptibility to high temperatures, transport and storage problems are biofertilyzing blockages that still need to be solved in order to obtain effective inoculated ions *(Young C.C. et al., 2004)*.

Inoculation of seeds

Seed inoculation uses a specific microbe strain that can grow in association with plant roots; soil conditions must be favorable for the inoculants to work well. Selected strains of N–fixing Rhizobium bacteria have proven to be effective as seed inoculants for legumes *(Kaur K. et al., 2005)*.

Seed treatment can be done with any of two or more bacteria without antagonistic effect. In the case of seed treatment with Rhizobium, Azotobacter, Azospirillum together with PSB, the seeds must first be covered with Rhizobium or Azotobacter or Azospirillum. Where each seed has a layer of the abovementioned bacteria, the PSB inoculant must be treated on the outer layer of the seed. This method will provide a maximum population of each bacterium to generate better results *(Young C.C. et al., 2003)*.

MATERIALS AND METHODS

Examples of microorganisms used as biofertilizers and their roles:

- Azotobacters and azospirillum. These are free living bacteria that fix atmospheric nitrogen in grain crops without symbiosis and do not need a specific host plant. They can fix 15– 20 kg/ha N per year. Azotobacter sp. can also produce antifungal compounds to fight many plant pathogens (Kunda B. S. and Gaur A. C., 1984). They also increase germination and vigor in young plants, which leads to improved crop stands (Joergensen R. G. et al., 2019).
- Solubilizing bacteria in phosphate (PSB). In conditions of acidic or calcareous soil, large amounts of phosphorus are fixed in the soil, but are not available for plants. Phosphobacterins, mainly bacteria and fungi, can make insoluble phosphorus available to the plant. The solubilization effect of phosphobacterins is generally due to the production of organic acacids that lower the pH of the soil and cause the dissolution of phosphate–related forms. It is reported that the PSB culture has increased the yield to 200–500 kg/ha and thus can save 30 to 50 kg of superphosphate (Sundara B. et al., 2002).
- Plant growth that promotes rhizosis (PGPR). PGPR is a wide variety of bacteria in the soil that, when grown in combination with a host plant, lead to stimulation of host growth. PGPR modes include fixing N2, increasing the availability of nutrients in the rhizosphere, positively influencing root growth and morphology, and promoting other beneficial plant symbiosis – the microbe (Dutta S. et al., 2003). Some researches have indicated that PGPR will often have several modes of action. Some researchers found that a combination of the mycorrhizal shrub mushroom Glomus aggregatum, PGPR Bacillus polymyxa and Azospirillum brasilense maximized biomass and the P content of palmarosa aromatic grass (Cymbopogon martinii) when grown with an insoluble inorganic phosphate *(Young C.C. et al., 2003)*.

In this research, we applied two biofertilizers to cultures located within experimental lots, which can be found at the National Institute of Research and Development for Machinery and Installations For Agriculture and Food Industry – INMA Bucharest, in 2021.

The products used in this research were *Cystium–k* and *Ficosagro,* biofertilizers obtained in Spain from algae. *Cystium–k* is a liquid bio stimulant made from Macrocystis pyrifera seaweed, with high polysaccharides content. Its main functions are: Contribution of alginates and polysaccharides and fertilization support.

We apply foliar, in vegetative growth periods by spraying. Some benefits:

- Prompts the natural defences of the crop into action;
- Improves crop yields;
- Increases cell multiplication and differentiation in the early stages of growth;

FICOSAGRO

This product aids the development and strength of plants by enriching the biological potential of the soil. Its application areas including agriculture, horticulture, and turf fields for sports use.

Is it composed from Lactic acid bacteria (Lactobacilus plantarum) and Fungus and yeasts (Saccharomyces c.). We applied this product foliar.

- Crops of strawberries, tomatoes and cucumbers are placed in protected areas, cherries and blueberries are placed in unprotected areas. The first application of biofertilizers was on April, foliar. It was foreseen a control lot for each crop, with an area of 1/2 of the surface on which the biofertilizers were applied. The crops to which they have been applied, the areas on which they have been applied and the doses of biofertilizers used are listed below:
- Strawberries 50 sqm: Cystium–k, 15ml; Ficosagro, 75 ml
- Tomatoes 100 sqm: Cystium–k, 30ml; Ficosagro, 100 ml
- Cucumbers 50 sqm: Cystium–k, 15 ml; Ficosagro, 50 ml
- Cherries 25 sqm: Cystium–k, 5 ml; Ficosagro, 50 ml
- Blueberries 25 sqm: Cystium–k, 10 ml; Ficosagro, 25 ml

Below are some images from the application time.

Figure 1 – Application on blueberries;

Figure 2 – Application on cucumber

- At an interval of about 30 days, in May, we still used Cystium–k and Ficosagro products, we applied them foliar. The control lots for crops were observed, in the area of 1/2 of the areas on which we applied. The crops to which they have been applied, the areas on which they have been applied and the doses of biofertilizers used have been the same as in the first case of application. Below are some images from the application time (Figure 3 and 4).
- In June, at an interval of about 30 days, using Cystium–k and Ficosagro products, we applied them foliar. The control lots for crops were observed, in the area of 1/2 of the areas on which we applied. The crops to which they have been applied, the areas on which they have been applied and the doses of biofertilizers used have been

the same as in the first and second application. Below are some images from the application time (Figures 5 and 6).

Figure 3 – Application on cherries;

Figure 4 – Application on blueberries

Figure 5 – Application on blueberries;

Figure 6 – Application on cherries;

RESULTS

We left a control lot for each crop. Please note that strawberries, tomatoes and cucumbers are placed in protected areas, cherries and blueberries are placed in non–protected areas.

In this research, we found an increase in the size of the fruits in the plants where we used the biofertilizing products mentioned between 5 – 10% compared to the control groups, an increase in the foliar mass and more vigorous roots, at the same time the plants being less attacked by diseases and pests. We found that Ficosagro aids the development and strength of plants by enriching the biological potential of the soil. Is it composed from Lactic acid bacteria (Lactobacilus plantarum) and Fungus and yeasts (Saccharomyces c.). It speeds up the decomposition of organic matter, it is rich in microorganisms that aid the recovery of microflora and microfauna in the soil, helping in their regeneration.

We use also Cystium–k, foliar, a liquid bio stimulant made from Macrocystis pyrifera seaweed, with high polysaccharides content. We found the development of axillary branching, foliar mass and photosynthetic capacity, and increases root hairiness.

For optimal plant growth, nutrients must be available in sufficient and balanced quantities. Soils contain natural reserves of plant nutrients, but these reserves are mostly in forms unavailable to plants and only a small part has been released each year through biological activity or chemical processes. This release is too slow to compensate for the elimination of nutrients through agricultural production and meet crop requirements. Therefore, fertilizers are designed to supplement the nutrients present in the soil. The use of chemical fertilizers, organic fertilizers or biofertilizer has its advantages and disadvantages in the context of nutrient supply, crop growth and the quality of the environment. The advantages must be integrated into the sauna in order to make the optimal use of each type of fertilizer and to achieve a balanced nutrient management for crop growth. Below are some images from the application time.

Figure 7 – Application on strawberries; Figure 8 – Application on cherries;

CONCLUSIONS

The intensive system of modern agriculture requires an intense energy flow, it has also put into circulation the solar energy previously accumulated in the form of fossil fuel, has generalized the use of mechanical energy in the processing of soil and chemical energy (fertilizers, pesticides) to increase fertility and productivity. In this way, the plant–soil system came out of the sub influence of natural regularity and became dependent on the energy intake from outside. As a consequence, it is not possible to ensure the maintenance of the physico–chemical balance in a long time, which leads to degradation *(Chand S. et el., 2006)*.

As a result of exaggerated chemistry, involutional processes occur, the microbial life of the soil disappears, structural destabilization occurs, the decomposition of organomineral complexes occurs. In order to be able to occur, in order to maintain the fertility of the soil, it is necessary to continue to apply chemical fertilizers, which brings the soil to intoxication, and the degradation can only be avoided.

Sustainable agriculture requires economically viable technologies over a long period of time, with high harvests, obtained with lower costs. Any agricultural

system must have long–term and high productivity, which is conditioned not only by the quality of the resource base, but also by the social and economic framework. Therefore, the sustainability of agricultural production systems, has a physical and a socio–economic dimension. More specifically, in order to be sustainable and viable, a system must meet the following conditions:

- maintenance and improvement of the physical environment and resistance to external pressures or strong disturbances;
- satisfying the society's requirements in food products;
- ensuring the economic and social well–being of agricultural producers (*Chandran, S. et al., 2018*).

In this research of using biofertilizers Cistium–k and Ficosagro, made in Spain, from algae.

We found that Ficosagro aids the development and strength of plants by enriching the biological potential of the soil. Its application areas including agriculture, horticulture, and turf fields for sports use.

Is it composed from Lactic acid bacteria (Lactobacilus plantarum) and Fungus and yeasts (Saccharomyces c.) The most important benefits are: speeds up the decomposition of organic matter, it is rich in microorganisms that aid the recovery of microflora and microfauna in the soil, helping in their regeneration; improves the absorption of nutrients through the crops root system, helps unblock and absorb nutrients such as nitrogen and phosphorus, improves crop yields. We applied this product foliar.

Cystium–k is a liquid bio stimulant made from Macrocystis pyrifera seaweed, with high polysaccharides content. Its main functions are:

- contribution of alginates and polysaccharides and
- fertilization support

The most important benefits are: prompts the natural defences of the crop into action, improves crop yields, increases cell multiplication and differentiation in the early stages of growth, promotes the development of axillary branching, foliar mass and photosynthetic capacity, and increases root hairiness.

Methods of application was foliar: apply in vegetative growth periods by spraying.

During this research, we found an increase in the size of the fruits in the plants where we used the biofertilizing products mentioned between 5–10% compared to the control groups, an increase in the foliar mass and more vigorous roots, at the same time the plants being less attacked by diseases and pests. We recommend continuing the study.

Effective management of plant nutrition should ensure improved and sustainable agricultural production and protect the environment. Chemical, organic or microbial fertilizer has its advantages and disadvantages in terms of nutrient supply, soil quality and crop growth. Developing an appropriate nutrient management system that integrates the use of these three types of fertilizers can be a challenge to achieve the objective of sustainable agriculture; however, much research is still needed.

Acknowledgement

This work was supported by a grant of the Romanian Education and Research Ministry, through Sectoral Plan, contract no. 1 PS / 2019 and through Programme 1 – Development of the national research–development system, subprogramme 1.2 – Institutional performance – Projects for financing excellence in RDI, contract no. 16 PFE.

Note: This paper was presented at ISB–INMA TEH' 2022 – International Symposium on Technologies and Technical Systems in Agriculture, Food Industry and Environment, organized by University "POLITEHNICA" of Bucuresti, Faculty of Biotechnical Systems Engineering, National Institute for Research–Development of Machines and Installations designed for Agriculture and Food Industry (INMA Bucuresti), National Research & Development Institute for Food Bioresources (IBA Bucuresti), University of Agronomic Sciences and Veterinary Medicine of Bucuresti (UASVMB), Research–Development Institute for Plant Protection – (ICDPP Bucuresti), Research and Development Institute for Processing and Marketing of the Horticultural Products (HORTING), Hydraulics and Pneumatics Research Institute (INOE 2000 IHP) and Romanian Agricultural Mechanical Engineers Society (SIMAR), in Bucuresti, ROMANIA, in 6–7 October, 2022.

References

[1] Ahlem, Z., & Hammas, M. A. (2017). Organic farming: A path of sustainable development. International Journal of Economics & Management Sciences, 6(5), 1–7.

[2] Anghel, M.G., Anghelache, C. and Panait, M. (2017). Evolution of agricultural activity in the European Union. Romanian Statistical Review, Supplement, 6, 63–74.

[3] Bokhtiar, S.M. & Sakurai, K. (2005). Effects of organic manure and chemical fertilizers on soil fertility and crop productivity and sugar cane ratoon. Archives of Agronomy and Soil Science, 51, 325–334.

[4] Chand, S., Anwar, M. & Patra, D.D. (2006). Influence of long–term application of organic and inorganic fertilizers to build soil fertility and absorption of nutrients in the cultivation sequence of peppermint mustard. Communications in Soil Science and Plant Analysis, 37, 63–76.

[5] Chandran, S., Unni, M. R., & Thomas, S. (2018). Organic farming: Global perspectives and methods. Woodhead Publishing, 1, 10–15.

[6] Chen, J. H. (2006). The combined use of chemical and organic fertilizers and/or biofertilizer for crop growth and soil fertility. International Workshop on sustained management of the soil–rhizosphere system for efficient crop production and fertilizer use, Thailand, 16 (20), 1–11.

[7] Dutta, S., Pal, R., Chakeraborty, A. & Chakrabarti, K. (2003). The influence of the integrated system of supply of vegetal nutrients on the restoration of soil quality in a red and laterite soil. Archives of Agronomy and Soil Science, 49, 631–637.

[8] Joergensen, R. G., Toncea, I., Boner, M., & Heß, J. (2019). Evaluation of organic sunflower fertilization using δ15N values. Organic Agriculture, 9, 365–372.

[9] Kaur, K., Kapoor, K.K. & Gupta, A. P. (2005). Impact of organic manure with and without mineral fertilizers on the chemical and biological properties of the soil under tropical conditions. Journal of Plant Nutrition and Soil Science, 168, 117–122.

[10] Kunda, B. S., & Gaur, A. C. (1984). Rice responses to inoculation with nitrogen fixing and P–solubilizing micro–organics. Plant and Soil, 79, 227–234.

[11] Laza, E. A., & Caba, I. L. (2021). The production of biohumus for a healthy and organic agriculture. Acta Technica Corviniensis–Bulletin of Engineering, 14(2), 27–30.
[12] Micu, A., Dumitru, E., Tudor, V., Alecu, I., Micu, M. (2017). The Factors that influence the development of rural villages – Case Study Semlac Commune, Arad County. Proceedings of the 29th International Business Information Management Association Conference, Austria, Education Excellence and Innovation Management through Vision 2020: From Regional Development Sustainability to Global Economic Growth, 1, 748–756.
[13] Petre, A., Voicea, I., Vlăduț, V., Vlăduțoiu, L., (2019). Considerations on monitoring the state of soil and vegetation pollution in the affected areas. International Conference on Hydraulics, Pneumatics, Sealing Systems, Precision Mechanics, Tools, Specific Electronic Devices & Mechatronics, HERVEX, România, 25, 301–307.
[14] Ramakrishnan, B., Maddela, N. R., Venkateswarlu, K., & Megharaj, M. (2021). Organic farming: Does it contribute to contaminant–free produce and ensure food safety. Science of The Total Environment, 769, 145079, 11–13
[15] Vanghele, N., Vlăduț, V., Voicea, I., & Pruteanu, A. (2019). Research on methods of de–pollution soils contaminated with heavy metals. International Conference on Hydraulics, Pneumatics, Sealing Systems, Precision Mechanics, Tools, Specific Electronic Devices & Mechatronics, HERVEX, România, 25, 283–290.
[16] Willer, H., & Sahota, A. (2020). The world of organic agriculture, statistics and emerging trends 2020. BIOFACH Congres 2020, France, 1, 11–17.
[17] Young, C.C., Lai, W.A., Shen, F.T., Hung, M.H., Hung, W.S. & Arun, A.B. (2003). Exploring microbial potential to enhance soil fertility in Taiwan. In Proceedings of the 6th ESAFS International Conference: Soil Management Technology on Low Productivity and Degraded Soils, Taiwan, 25–27.
[18] Young C.C., Lai W.A., Shen, F.T., Huang, W.S. & Arun, A.B. (2004). Characterization of multifunctional biofertilizer in Taiwan and biosecurity considerations. International symposium on the future development of the agricultural biotechnology park. The symposium esteeries for celebrating the establishment of the Agricultural Biotechnology Park, the Agriculture Council, Executive Yuan, and the 80th anniversary of the Pingtung National University of Science and Technology, Taiwan, 373–388.

ISSN: 2067-3809

[1.]Nicoleta UNGUREANU, [2.]Valentin VLĂDUȚ, [1.]Sorin-Ștefan BIRIȘ,
[1.]Mădălina IVANCIU (POPA), [1.]Mariana IONESCU

VALORIZATION OF MICROALGAE IN WASTEWATER TREATMENT AND BIODIESEL PRODUCTION

[1.]University Politehnica of Bucharest, Faculty of Biotechnical Systems Engineering, ROMANIA;
[2.]INMA Bucharest, ROMANIA

Abstract: Micro and macroalgae are renewable and carbon-neutral sources of energy that can grow naturally or can be cultivated in nutrient-rich wastewater, without compromising the production of food crops. Microalgae use nutrients, accumulate heavy metals and reduce coliform bacteria from wastewater, thus contributing to their phytoremediation. Furthermore, the conversion of algae biomass into biofuels contributes to reducing the dependence on fossil fuels and greenhouse gas emissions in the atmosphere. Depending on the species and cultivation method, microalgae have a very fast growth rate (12 days) and their potential to produce biodiesel is 15 to 300 times higher than that of agricultural and energy crops conventionally used for biofuels. Lipid content in microalgae can reach 75–80% by weight of dry biomass. To produce 39 billion liters of biodiesel, 15 million tons of nitrogen and 2 million tons of phosphorus are required during the growth process of microalgae. From algae cultivated in 500 billion m^3 of industrial wastewater, approximately 37 million tons of oil can be extracted that can be transformed into biodiesel. However, there are also challenges in large-scale utilization of microalgae, due to the high energy input, technical difficulties encountered in harvesting unicellular microalgae, and the need for subsequent pretreatment operations to improve lipid extraction. This paper reviews the potential of microalgae species to thrive in wastewater and the technological achievements in converting microalgae biomass for the sustainable biodiesel production.

Keywords: algae, wastewater, phytoremediation, biomass, biofuels

INTRODUCTION

Energy is essential for generating industrial, commercial and social well-being, as well as ensuring personal comfort and mobility. However, its predominant production from non-renewable sources (coal, natural gas, oil, tar sands, oil shale and nuclear sources) put considerable pressure on the environment: emissions of greenhouse gases and other polluting gases, land use, waste generation and oil spills. These pressures contribute to climate change, damage the natural ecosystems and the human environment, and have adverse effects on human health.

About 80% of the total amount of energy used globally each year comes from fossil fuels. It is estimated that by 2030, the total consumption of fossil fuels will decrease by 16% compared to current levels, and these fuels will represent 62% of the primary energy supply. Thus, the share of fossil fuels in the European Union's energy supply could be further reduced, to represent only 55% of the region's primary energy supply by 2030. The transition from imported fossil fuels to renewable energy is one of the key objectives of the European Union to achieve sustainability and climate neutrality. Over the last two decades, the European Union's share of renewable energy has increased mainly due to climate and energy policies, and to the technological progress. In the European market, France, Italy, Germany, Spain, Denmark, and the Czech Republic are also permitting full tax exemption for a specific volume of biodiesel production. Recently, Brazil, Germany, and the U.S. have initiated tax incentives to increase the production of biofuels and reduce the price of biodiesel at pumps (*Grand View Research*).

Although biofuels (including biodiesel, bioethanol, biohydrogen, biogas, biohytane) produced from biomass waste and the biodegradable portion of industrial waste, are still more expensive than fossil fuels, their production and use are increasing worldwide. In 2017, the gross inland energy consumption of biofuels in European countries was estimated at approximately 16500 ktoe for biodiesel, 4000 ktoe for bioethanol and 1000 ktoe for other biofuels. Biofuels are the prime source of renewable energy (89%) used by the transport sector (*Calderon and Colla, 2019*). In addition to being used in vehicle transportation, algae oil can be used to blend aviation fuel as it has a positive impact on aircraft performance by lowering operating expenditures (*Grand View Research*).

Biomass has become one of the most frequently used sources of renewable energy in the last two decades and the second form of energy, after hydropower, in the generation of electricity. However, problems have arisen because conventional biomass crops for biofuel production require large areas of arable land and high water supply to grow, thus competing with food crops and endangering food security. For this reason, in recent

years, attention has turned to biomass sources whose cultivation is not in conflict with food security.

Algae are a diverse group of highly productive organisms that include microalgae, macroalgae (seaweed), and cyanobacteria (formerly called "blue-green algae"). Major taxonometric orders are *Bacillariophyta* (diatoms), *Chlorophyta* (green algae), *Chrysophyta* (golden algae) and *Rhodophyta* (red algae) (*Udaiyappan et al., 2017*). Many of these groups of aquatic microorganisms use sunlight, CO_2 and nutrients to create biomass, which contains key components, including lipids, proteins, and carbohydrates, that can be turned into a variety of biofuels and products.

Caulerpa prolifera (green algae)

Sargassum (brown algae)

Laminaria (brown algae)

Figure 1 - Some algae species (*Ungureanu et al., 2019*)

Microalgae biomass results mainly from photosynthesis; they consume atmospheric CO_2 as carbon source during photosynthesis and they can capture more than 40% of global carbon; hence they are carbon-neutral biomass and reduce the greenhouse gas emissions. It was estimated that 100 tons of algal biomass can capture 183 tons of CO_2 from the atmosphere, along with soluble carbonates and heavy industry gases (*Qari et al., 2017*).

Biosynthesis of algal biomass ($C_{106}H_{263}O_{110}N_{16}$) is described by the following chemical reactions, where ammonium and nitrate serve as nitrogen sources (*Dalrymple et al., 2013*):

$$16NH_4^+ + 92CO_2 + 92H_2O + 14HCO_3^- + HPO_4^{2-} \rightarrow C_{106}H_{263}O_{110}N_{16}P + 106O_2$$

$$16NO_3^- + 124CO_2 + 140H_2O + HPO_4^{2-} \rightarrow C_{106}H_{263}O_{110}N_{16}P + 138O_2 + 18HCO_3^-$$

Microalgae have developed morphological, behavioral and chemical mechanisms to defend themselves from bacteria, fungus, protozoans, aquatic invertebrates, other algae and even viruses (*Hannon et al., 2010*). An undeniable advantage of algae is their tremendous ability to grow easily in areas that are not suitable for other crops, such as arid or desert areas using seawater, brackish water, wastewater, seashores, and lakes and even on systems placed on top of buildings.

Algae thrive in nutrient-rich wastewater (from domestic, agricultural, swine farms, cattle farms, agro-industrial and industrial sources etc.) consuming the nutrients (nitrogen, phosphorous and potassium) and converting them into useful biomass (*Komolafe et al., 2014*). Their small size offers a large surface area, which increases the rate of nutrient uptake in the wastewater (*Udaiyappan et al., 2017*).

Nutrient removal is an important step in wastewater treatment because the discharge of nutrient-rich effluents into natural water bodies leads to eutrophication. In wastewater treatment, algae could be integrated into the secondary stage or added as a tertiary (polishing) stage, because, apart from consuming nutrients, they are efficient in removing biochemical oxygen demand, chemical oxygen demand, and suspended solids (*Chamberlin J.F., 2016*). Algae improve the quality of final effluent through natural disinfection and incorporation of contaminants like heavy metals, pharmaceuticals, endocrine disrupters and coliform bacteria *Salmonella*, *Shigella*, viruses and protozoa (*Ungureanu et al., 2019*). A study conducted by *Zainal et al. (2022)* reported that *Spirulina platensis* removed heavy metals from palm oil mill effluent with good efficiencies: Fe by 45.1%, Cu by 52.8%, Zn by 55%, Ni by 61.9%, As by 71.4%, Cr by 83.8% and Mn by 84.9%. Growing of microalgae in wastewater reduces the need of chemical fertilizers and their related burden on life cycle (*Unpaprom et al., 2015*). Thus, microalgae-based wastewater treatment is a sustainable process and the treated effluents can be safely discharged into natural water courses, or they can be recovered for irrigation of agricultural and energy crops or for landscape purposes.

MATERIALS AND METHODS

Wastewater treatment by algae coupled with biofuels production emerged as a promising strategy to decrease the economic and environmental costs of energy (*Cheah et al., 2016*). Micro and macroalgae earned global attention as feedstock for the production of third

generation biofuels. Microalgae-derived biofuels are renewable, highly biodegradable, nontoxic and eco-friendly in comparison to fossil fuels.

Initial testing of microalgae as potential sources for biofuel production began in 1970, but it was temporarily stopped due to economic and technical problems. Studies resumed from 1980 onwards showed that there is high potential in biofuel production from microalgae (*Medipally et al., 2015*).

Microalgae biomass can be converted into different biofuels by means of biochemical and thermochemical processes, chemical reactions and direct combustion (Figure 2).

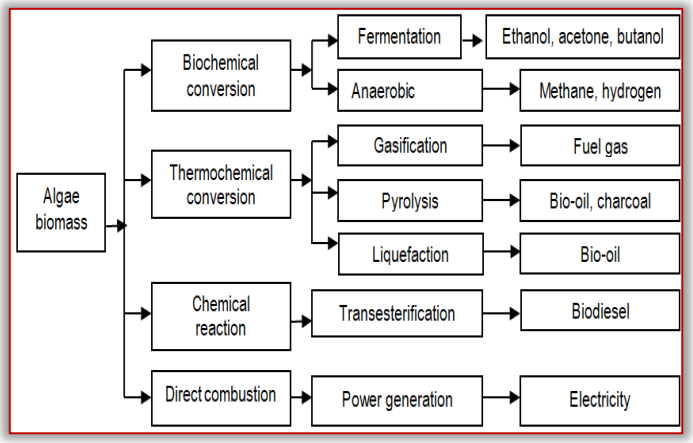

Figure 2 - Possibilities of converting the algae biomass into biofuels *(Medipally et al., 2015)*

The technology for producing biodiesel from conventional oily crops has been known for more than 60 years. The production of methyl esters or biodiesel from microalgae oil uses the same processes (Figure 3). Microalgae grow easier and faster and contain more oil than macroalgae, the latter being less used in biodiesel production.

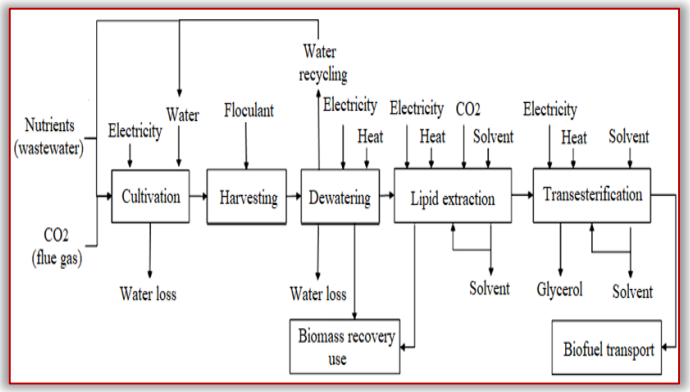

Figure 3 - Generalized processes for the production of biodiesel from microalgae *(Collotta et al., 2018)*

However, there are some drawbacks in large-scale commercial production of microalgae for biofuels industry. Industrial production of algae biomass can be more expensive than growing conventional crops; it is an energy intensive process that requires large amounts of energy and water, and the use of off-site generated CO_2. Harvesting of algal biomass can account for 20–30% of the total cost of production (*Guttierez et al., 2016*). To minimize expenses, biodiesel production must rely on freely available sunlight, regardless of the daily and seasonal variations in light levels (*Chisti Y., 2007*). Biodiesel production from microalgae would be more easily implemented at large scale if viable advances would be achieved in designing advanced photobioreactors, low cost technologies for biomass harvesting, drying and oil extraction.

Selection of adequate microalgae species has an important role in obtaining the desired product and the maximum microalgae productivity (Figure 4). Fast growing and high lipid producing microalgae strains should be carefully chosen for cultivation in order to increase the feasibility of biodiesel production.

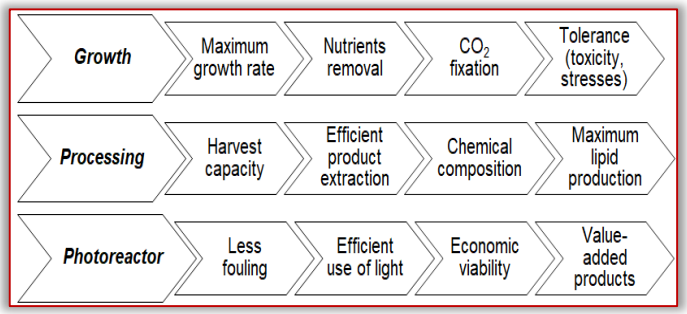

Figure 4 - Important criteria in the selection of microalgae for biodiesel production *(adapted from SundarRajan et al., 2019)*

Cultivation methods, from lab scale to industrial facilities, include man-made algae cultivation systems, like open pond systems such as high-rate algal ponds or raceway ponds, and closed systems such as different types of photobioreactors exposed to sunlight or artificial UV light and independent of seasons.

Open systems are preferred in most existing large scale microalgae cultivation plants because they provide easy operation, low costs of investments and maintenance (*Bilad et al., 2014*), are more durable than the photobioreactors (*Abinandan et al., 2015*) although they achieve low biomass productivities and mono-algae culture is not fully secured (*Bilad et al., 2014*).

Closed systems were developed to expand the yield of algae biomass, allow the monoculture under controlled conditions and prevent water evaporation and CO_2 loss (*Ugwu et al., 2008*). Photosynthetic growth requires light (sunlight or artificial UV light), CO_2, water and inorganic salts. Temperature must remain within 20–30°C. Microalgae have a very fast growing rate which can double just in one day (*Rittman B.E., 2008*) and biomass doubling times during exponential growth are commonly as short as 3.5 hours (*Chisti Y., 2007*).

Harvesting and dewatering of microalgae biomass can be considered both as a single operation and as combinations of multiple unit operations in a sequence.

Harvesting is one of the main challenges in biofuel production, due to the high energy input and recovery cost for microscopic microalgae and from diluted microalgal suspension (*Cheah et al., 2016*). Harvesting of microalgae is usually done by sedimentation (one of the simplest techniques), flocculation, flotation and thickening (by centrifugation or filtration) (*Abinandan et al., 2015*). Aiming to reduce the high costs of algae harvesting and streamline the process, other technologies have been tested: ozone-flotation which helps increase the lipid availability (*Nguyen et al., 2013*), coagulation by aluminum and ferric chloride, harvesting using Fe_3O_4 nanoparticles, harvesting using aluminum and magnesium based amino saline clays, harvesting using autoflocculation performed by microalgae due to CO_2 assimilation in cells, bioflocculation (*Abinandan et al., 2015*) and the use of microalgal cells immobilization in suspended media (*Cheah et al., 2016*). Harvesting of microalgae can be done each 12 days, these tiny organisms producing 15 to 300 times more oil for biodiesel production compared to the traditional oily crops on an area basis (*Chisti Y., 2007*).

Dewatering (thickening) processes must be tailored based on the species of microalgae and its growth conditions. Often, for the dewatering of algal biomass are used processes such as membrane filtration, vacuum and pressure filtration, centrifugation, and spiral plate technology, and sometimes dewatering can be followed by a drying step because the water content of harvested algal biomass should be reduced to about 5% (*Fasaei et al., 2018*). Secondary dewatering thickens the biomass to 15–25%, and if it is followed by drying process, it increases the total solid matter to 90–95%.

Extraction of lipids (oils) from microalgal biomass and their conversion to biodiesel are not affected by whether the biomass is produced in raceways or in photobioreactors (*Chisti Y., 2007*). Algae biomass consists of proteins, carbohydrates and natural oil (*Udaiyappan et al., 2017*). The latter is very high in unsaturated fatty acid that can be extracted and converted into biodiesel by esterification/ transesterification, in the presence of acid or alkali as a catalyst.

Algae has higher oil yield per unit area than other oilseed crops. For biofuel production, the lipid content in algae should be at least 20–40% (*Dalrymple et al., 2013*) and it can be adjusted by changing the composition of growth medium. It was reported that *Chlorella* has up to 50% lipids and *Botryococcus braunii* produces the highest oil content of about 80% (*Krishnamoorthy et al., 2022*). Composition of some microalgae strains suitable for biodiesel production is presented in Table 1.

Table 1. Biochemical composition of some algae strains expressed on dry matter basis (*Shalaby E.A., 2011*)

Algae strain	Proteins	Carbohydrates	Lipids	Nucleic acid
Anabaea cylindrica	43 – 56	25 – 30	4 – 7	–
Chlamydomonas rheinhardii	48	17	21	–
Chlorella vulgaris	51 – 58	12 – 17	14 – 22	4-5
Chlorella pyrenoidosa	57	26	2	–
Dundaliella bioculata	49	4	8	–
Dundaliella salina	57	32	6	–
Euglena gracilis	39 – 61	14 – 18	14 – 20	–
Prymnesium parvum	28 – 45	25 – 33	22 – 39	1-2
Porphyridium cruentum	28 – 39	40 – 57	9 – 14	–
Scenedesmus obliquus	50 – 56	10 – 17	12 – 14	3 – 6
Scenedesmus quadricauda	47	–	1.9	–
Scenedesmus dimorphus	8 – 18	21 – 52	16 – 40	–
Spirogyra sp.	6 – 20	22 – 64	11 – 21	–
Spirulina maxima	60 – 71	13 – 16	6 – 7	3 – 4.5
Spirulina platensis	46 – 63	8 – 14	4 – 9	2 – 5
Synechoccus sp.	63	15	11	5
Tetraselmis maculata	52	15	3	–

Other algal strains, including *Phaeodactylum tricornutum* (*Udaiyappan et al., 2017*), *Crypthecodinium cohnii, Dunaliella primolecta*, *Nannochloropsis* sp. (*Medipally et al., 2015*), *Oedogonium* (*Sharif Hossain et al., 2008*), *Arthrospira platensis*, *Nostoc* sp., *Oscillatoria* sp., and *Scenedesmus acuminatus* (*Unpaprom et al., 2015*) contain large quantities of hydrocarbons and lipids and have been employed in biofuels production.

The energy content of algal oils is 35800 $kJ \cdot kg^{-1}$, which is about 80% of the energy contained in petroleum (*Kligerman and Bouwer, 2015*). Nevertheless, not all oils produced by microalgae are considered legitimate biofuels, but suitable oils are common (*Udaiyappan et al., 2017*). Algae can produce 250 times the amount of oil per acre as soybeans and 7 to 31 times higher oil than palm oil (*Sharif Hossain et al., 2008*). Depending on the differences in nutrients concentrations in wastewater and the ability of algal strains to accumulate lipids, 500 billion m^3 of industrial wastewater could produce 37 million tons of algal oil (*Chinnasamy et al., 2010*). Hence, microalgae are a promising feedstock for biodiesel production, with an estimated yield of 58700–136900 $L \cdot ha^{-1} \cdot year^{-1}$ (*Unpaprom et al., 2015*). A realistic estimate of microalgae biomass production lies between 15–25 $t \cdot ha^{-1} \cdot year^{-1}$, while lipid production, with no optimized growth conditions is of 4.5–7.525 $t \cdot ha^{-1} \cdot year^{-1}$ at 30% lipid content in microalgae cells (*Lam and Lee, 2012*). Table 2 presents the oil content of some microalgae species, expressed as % dry wt.

Oil productivity, or the mass of produced oil/ volume of the microalgae broth/day, depends on the algal growth rate and the oil content in the biomass. Microalgae for biomass production have been cultivated under

photoautotrophic, heterotrophic and mixotrophic conditions (*Abinandan et al., 2015*).

Table 2. Oil content of some microalgae *(Chisti Y., 2007)*

Microalgae	Oil content (% dry wt)	Microalgae	Oil content (% dry wt)
Botryococcus braunii	25 – 75	*Nannochloris sp.*	20 – 35
Chlorella sp.	28 – 32	*Nannochloropsis sp.*	31 – 68
Crypthecodinium cohnii	20	*Neochloris oleoabundans*	35 – 54
Cylindrotheca sp.	16 – 37	*Nitzschia sp.*	45 – 47
Dunaliella primolecta	23	*Phaeodactylum tricornutum*	20 – 30
Isochrysis sp.	25 – 33	*Schizochytrium sp.*	50 – 77
Monallaanthus salina	>20	*Tetraselmis sueica*	15 – 23

The simplest method for lipid extraction is the mechanical crushing of microalgae cells using glass beads, screw presses, extruders and pulverization. Other methods of extraction, such as supercritical CO_2, sonication, autoclaving, microwaving, freezing and osmotic shock are less practical for commercial scale biofuel production (*Cheah et al., 2016*).

Table 3. Biomass and lipid productivities of some microalgae in different cultivation methods *(Medipally et al., 2015)*

Cultivation method	Microalgae	Biomass productivity ($g \cdot L^{-1} \cdot d^{-1}$)	Lipid content (% dry wt)	Lipid productivity ($mg \cdot L^{-1} \cdot d^{-1}$)
Phototrophic	*Chlorella vulgaris*	0.02 – 0.2	50 – 58	11.2 – 40
	Chlorella protothecoides	2 – 7.7	14.6 – 57.8	1214
	Chlorella sorokiniana	0.23 – 1.47	19 – 22	44.7
Heterotrophic	*Chlorella vulgaris*	0.15	23	35
	Chlorella protothecoides	3.1 – 3.9	–	2400
	Chlorella sorokiniana	1.48	23.3	–
Mixotrophic	*Chlorella vulgaris*	0.25 – 0.26	20 – 22	52 – 56
	Chlorella protothecoides	23.9	58.4	11800
	Chlorella sorokiniana	0.58	–	29 – 56

Transesterification. Raw microalgal oil (triglycerides) has high viscosity which could ruin the vehicle's engine quickly due to the rapid accumulation of oil sludge, so it requires a chemical conversion (transesterification) into low molecular weight, non-toxic, biodegradable biofuel that offers smooth engine operation. Transesterification uses excess methanol or ethanol in the presence of a catalyst (sodium hydroxide in methanol and sodium methoxide for the former, hydrochloric and sulphuric acid in methanol for the latter) (*Zeng et al., 2011*), to maintain the equilibrium shift towards fatty acid esters production and accelerate the reaction rate (*Cheah et al., 2016*). The transesterification of triglycerides producing fatty acid esters is described by the reaction presented in Figure 5.

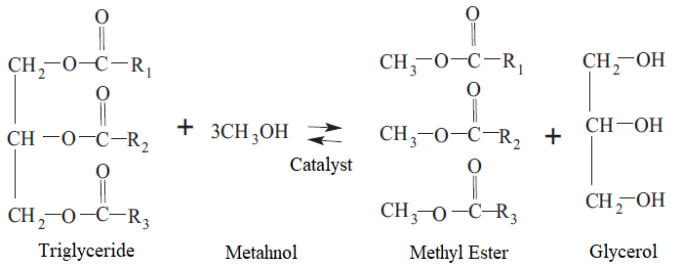

Figure 5 - Transesterification of triglycerides with production of fatty acid esters *(Cheah et al., 2016)*

If triglycerides with short chain alcohol are displaced by alcohol for fatty acid esters and glycerol formation, the process is referred to as alcoholysis. Despite being efficient, transesterification is also energy intensive, while glycerol is difficult to recover, and if the microalgal cell contains wastewater or moisture it could result in variations in pH, saponification, reduced catalytic efficiency and reduced biodiesel yield. Industrial scale transesterification can be improved by using solid catalysts (zeolites, metal oxides and ion-exchange resins), which are selective, active, stable at high temperatures and which can prevent water formation and saponification (*DuPont A., 2013*).

RESULTS

Extensive researches have stated that biodiesel yield depends on the lipid content in algae biomass, which in turn depends on nutrient concentration in the wastewater. At the moment, significant advancements have been obtained mostly at laboratory scale. Improvements in lipid productivity are mandatory for the economic viability of microalgae-based biodiesel at pilot-scale. According to *Rosmahadi et al. (2021)*, *Chlorella vulgaris* is the most utilized microalgae species for biodiesel production, due to its high lipid content (60–70%) and high productivity (7.4 $g \cdot L^{-1}$). *Unpaprom et al. (2015)* coupled wastewater treatment with biodiesel production, by growing *Scenedesmus acuminatus* in continuous stirred photobioreactor, in piggery wastewater effluent.

The batch feeding operation by replacing 10% of algae culture with piggery wastewater effluent every day could provide a stable net biomass productivity of 3.24 $g \cdot L^{-1} \cdot day^{-1}$. Total lipids from 100 mg microalgae were extracted using 2 mL chloroform/ methanol (v/v: 2/1), ultrasonic treatment for 10 min and centrifugation at 4000 rpm for 5 min. The effect of acid hydrolysis of lipids from *Scenedesmus acuminatus* on fatty acid methyl esters production was investigated. Direct transesterification (a one-stage process) of the harvested *Scenedesmus acuminatus* biomass resulted in a higher biodiesel yield content than that in a two-stage process, so it could be feasible to produce biodiesel from wet microalgae biomass directly without drying and lipid extraction.

Guldhe et al. (2017) tested the tungstated zirconia catalyst and obtained a high biodiesel conversion of lipids extracted from microalgae *Scenedesmus obliquus*, namely 94.85% at 100°C, with 15 wt% of catalyst (based on oil weight) and methanol to oil molar ratio of 12:1 in 3 hours. A study by *Hena et al. (2015)* evaluated the production of biodiesel from consortium of native microalgae (*Chlorella, Ankistrodesmus, Chlamydomonas* and *Scenedesmus*) grown in dairy farm treated and untreated wastewater. The microalgae were able to remove more than 98% nutrients and 98% chemical oxygen demand from treated wastewater. To obtain 100 g of algal oil from biomass of consortium grown in treated wastewater, 650 g dry biomass were treated by the dynamic hexane method.

In treated wastewater, the consortium produced 219.8 tons of biomass and algal oil yield of 51.37 thousand $L \cdot ha^{-1} \cdot year^{-1}$, while in untreated wastewater were obtained 137.68 tons of biomass and 33.38 thousand $L \cdot ha^{-1} \cdot year^{-1}$ of algal oil. It was found that 72.7% of algal lipid obtained from consortium could be converted into biodiesel, and loses were mainly due to oil impurities.

Zhu et al. (2013) tested the algae *Chlorella zofingiensis* grown in piggery industry wastewater, which at optimum COD concentration of 1900 $mg \cdot L^{-1}$, showed the highest biomass, lipid, and biodiesel productivities of 296.16 $mg \cdot L^{-1} \cdot day^{-1}$, 110.56 $mg \cdot L^{-1} \cdot day^{-1}$, respectively 30.14 $mg \cdot L^{-1} \cdot day^{-1}$.

Ahmad et al. (2013) showed that 95% of biodiesel yield could be obtained from microalgae *Chlorella vulgaris* by using sodium methoxide, CH_3ONa (base catalyst) at reaction time of 51 minutes and temperature of 160°C. This high yield is due to the alkaline metal oxides (sodium methoxide) which are highly active catalysts even when used in small concentrations. Microalgae *Botryococcus braunii* grown in carpet mill wastewater achieved 34 $mg \cdot L^{-1} \cdot d^{-1}$ of biomass productivity (dry weight) and 4.5 $mg \cdot L^{-1} \cdot d^{-1}$ of lipid productivity (13.2% lipid content), while the same microalgae grown with pig manure showed a biomass productivity of 700 $mg \cdot L^{-1} \cdot d^{-1}$ (dry weight) and lipid productivity of 69 $mg \cdot L^{-1} \cdot d^{-1}$ (9.8 % lipid content) (*Pittman et al., 2011*). In another study, *Chlamydomonas reinhardtii* removed 55.8 $mg \cdot L^{-1} \cdot d^{-1}$ nitrogen and 17.4 $mg \cdot L^{-1} \cdot d^{-1}$ phosphorus from municipal wastewater. The highest biomass productivity was 2 $g \cdot L^{-1} \cdot d^{-1}$ and lipid content of the strain was 25.25% (*Kong et al., 2010*).

Komolafe et al. (2014) tested microalgae *Desmodesmus sp.* and mixed culture of *Oscillatoria* and *Arthrospira*, grown in photobioreactors filled with wastewater, for biodiesel production. Decreases of total nitrogen by 55.4–83.9% and total coliforms by 99.8% were obtained. Ozone-flotation was used for algae harvesting and to reduce the unsaturation of fatty acid methyl esters. *Desmodesmus sp.* grew rapidly; the highest biomass concentration was 0.58 $g \cdot L^{-1}$, while the mixed culture reached 0.45 $g \cdot L^{-1}$. The mixed culture had the highest lipid and fatty acid methyl esters yield.

Shariff Hossain et al. (2008) tested common species *Oedogonium* and *Spirogyra* to compare the amount of biodiesel production. Algae samples were dried for 20 min at 80°C for water removal and then mixed with 20 mL hexane and ether solution to extract the oil. Using 0.25 g NaOH as catalyst and 24 mL methanol, algal oil and biodiesel (methyl ester) production was higher in *Oedogonium* than *Spirogyra* sp., but biomass yield (after oil extraction) was higher in *Spirogyra* than *Oedogonium* sp.

Ihsanulla et al. (2015) extracted oil from *Spirogyra* using a combination of n-hexane and Di-ethyl Ether. The yield of extracted oil was enhanced by smaller algal size, higher algal to solvent ratio and longer contact time. The maximum extracted oil was 0.09 fraction of biomass, by using algal biomass size of 0.4 mm, a blend of both solvents at solvent to biomass ratio of 3.5, and contact time of 24 hours. Transesterification was influenced by oil to methanol ratio, amount of catalyst, reaction time and temperature. The maximum yield > 95% was obtained at 60°C, oil to methanol ratio 8, reaction time 25 minutes and catalyst amount 0.5% of weight of oil.

Jaiswar et al. (2017) reported that the lipid content of freshwater *Neochloris aquatica* grown in artificial pond was 12%, calculated through Nile red fluorescence method and analysis of the fatty acid methyl ester of the tested strain showed saturated, monounsaturated and polyunsaturated fatty acids content of 29.15%, 37.95% and 32.90%.

The results of experimental studies demonstrate that microalgae have the potential to accumulate nutrients present in wastewater and their lipid-rich biomass can be used as a source of biodiesel production.

CONCLUSIONS

Microalgae are useful in wastewater phytoremediation, as they consume high amounts of nutrients, heavy metals and coliform bacteria, and reduce the chemical oxygen demand, biochemical oxygen demand and suspended solids. Depending on their species, wastewater-grown microalgae contain different concentrations of lipids, hydrocarbons and carbohydrates, making them useful products in the conversion into biofuels. To produce biodiesel, transesterification is mandatory after the extraction of lipids, because the extracted (raw) oil has high viscosity which would affect the engines. Although many studies have been developed so far on the production of biodiesel from microalgae biomass, the research is still on-going in order to make this type of biofuel competitive to other fossil fuel reserves. Reducing the production costs for wastewater-grown algae biofuels (especially the costs of microalgae harvesting and pretreatment) is an important goal for this industry.

Acknowledgement

This work was supported by a grant of the Romanian Ministry of Research and Innovation CCDI - UEFISCDI, Project INNOVATIVE TECHNOLOGIES FOR IRRIGATION OF AGRICULTURAL CROPS IN ARID, SEMIARID AND SUBHUMID-DRY CLIMATE, project number PN-III-P1-1.2-PCCDI-2017-0254, Contract no. 27 PCCDI / 2018, within PNCDI III.

Note: This paper was presented at ISB–INMA TEH' 2022 – International Symposium on Technologies and Technical Systems in Agriculture, Food Industry and Environment, organized by University "POLITEHNICA" of Bucuresti, Faculty of Biotechnical Systems Engineering, National Institute for Research–Development of Machines and Installations designed for Agriculture and Food Industry (INMA Bucuresti), National Research & Development Institute for Food Bioresources (IBA Bucuresti), University of Agronomic Sciences and Veterinary Medicine of Bucuresti (UASVMB), Research–Development Institute for Plant Protection – (ICDPP Bucuresti), Research and Development Institute for Processing and Marketing of the Horticultural Products (HORTING), Hydraulics and Pneumatics Research Institute (INOE 2000 IHP) and Romanian Agricultural Mechanical Engineers Society (SIMAR), in Bucuresti, ROMANIA, in 6–7 October, 2022.

References

[1] Abinandan S., Shanthakumar S. (2015). Challenges and opportunities in application of microalgae (Chlorophyta) for wastewater treatment: a review. Renewable and Sustainable Energy Reviews, 52, 123–132

[2] Ahmad F., Khan A.U., Yasar A. (2013). Transesterification of oil extracted from different species of algae for biodiesel production. African Journal of Environmental Science and Technology, 7, 358–364

[3] Bilad M., Discart V., Vandamme D., Foubert I., Muylaert K., Vankelecom I.F. (2014). Coupled cultivation and pre-harvesting of microalgae in a membrane photobioreactor (MPBR). Bioresource Technology, 155, 410–417

[4] Calderon C., Colla M., et al. (2019). Biofuels for transport. Bioenergy Europe Statistical Report.

[5] Chamberlin J.F. (2016). Algal wastewater treatment and biofuel production: an assessment of measurement methods, and impact of nutrient availability and species composition. University of Arkansas, Fayetteville, Theses and Dissertations.

[6] Cheah W.Y., Ling T.C., Show P.L., Juan J.C., Chang J.-S., Lee D.-J. (2016). Cultivation in wastewaters for energy: a microalgae platform. Applied Energy, 179, 609–625.

[7] Chinnasamy S., Bhatnagar A., Hunt R.W., Das K.C. (2010). Microalgae cultivation in wastewater dominated by carpet mill effluents for biofuel applications. Bioresource Technology, 101, 3097–3105

[8] Chisti Y. (2007). Biodiesel from microalgae. Biotechnology Advances, 25, 294–306.

[9] Collotta M., Champagne P., Mabee W., Tomasoni G. (2018). Wastewater and waste CO2 for sustainable biofuels from microalgae. Algal Research, 29, 12–21.

[10] Dalrymple O.K., Hakfhide T., Udom I., Gilles B., Wolan J., Zhang Q., Ergas S. (2013). Wastewater use in algae production for generation of renewable resources: a review and preliminary results. Aquatic Biosystems, 9, 2–11. https://doi.org/10.1186/2046-9063-9-2.

[11] DuPont A. (2013). Best practices for the sustainable production of algae-based biofuel in China. Mitigigation and Adaptation Strategies for Global Change, 18, 97–111. https://doi.org/10.1007/s11027-012-9373-7.

[12] Fasaei F., Bitter J.H., Slegers P.M., van Boxtel A.J.B. (2018). Techno-economic evaluation of microalgae harvesting and dewatering systems. Algal Research, 31, 347–362

[13] Grand View Research. Algae Biofuel Market Size, Share & Trend Analysis By Application (Transportation, Others), By Region (North America, Europe, Asia Pacific, ROW), By Country, And Segment Forecasts, 2020–2025. (https://www.grandviewresearch.com/industry-analysis/algae-biofuel-market).

[14] Guldhe A., Singh P., Ansari F.A., Singh B., Bux F. (2017). Biodiesel synthesis from microalgal lipids using tungstated zirconia as a heterogeneous acid catalyst and its comparison with homogeneous acid and enzyme catalysts. Fuel, 187, 180–188

[15] Guttierez R., Ferrer I., Gonzalez-Molina A., Salvado H., Garcia J., Uggetti E. (2016). Microalgae recycling improves biomass recovery from wastewater treatment high rate algal ponds. Water Research, 106, 539–549

[16] Hannon M., Gimpel J., Tran M., Rasala B., Mayfield S. (2010). Biofuels from algae: challenges and potential. Biofuels, 1(5), 763–784

[17] Hena S., Fatimah S., Tabassum S. (2015). Cultivation of algae consortium in a dairy farm wastewater for biodiesel production. Water Resources and Industry, 10, 1–14

[18] Ihsanulla H., Shah S., Ayaz M., Ahmed I., Ali M., Ahmad N., Ahmad I. (2015). Production of biodiesel from algae. Journal of Pure and Applied Microbiology, 9(1), 79–85.

[19] Jaiswar S., Balar N., Kumar R., Patel M.K., Chauhan P.S. (2017). Morphological and molecular characterization of newly isolated microalgal strain Neochloris aquatic SJ-1 and its high lipid productivity. Biocatalysis and Agricultural Biotechnology, 9, 108–112

[20] Kligerman D.C., Bouwer E.J. (2015). Prospects for biodiesel production from algae-based wastewater treatment in Brazil: a review. Renewable and Sustainable Energy Reviews, 52, 1834–1846

[21] Komolafe O., Velasquez Orta S.B., Monje-Ramirez I., Yanez Noguez I., Harvey A.P., Orta Ledesma M.T. (2014). Biodiesel production from indigenous microalgae grown in wastewater. Bioresource Technology, 154, 297–304

[22] Kong Q.-X., Li L., Martinez B., Chen P., Ruan R. (2010). Culture of microalgae Chlamydomonas reinhardtii in wastewater for biomass feedstock production. Applied Biochemistry and Biotechnology, 160(1), 9–19

[23] Krishnamoorthy A., Rodriguez C., Durrant A. (2022). Sustainable approaches to microalgal pre-treatment techniques for biodiesel production: a review. Sustainability, 14, 9953

[24] Lam M.K., Lee K.T. (2012). Microalgae biofuels: a critical review of issues, problems and the way forward. Biotechnolgy Advances, 30, 673–690

[25] Medipally S.R., Yusoff F.M., Banerjee S., Shariff M. (2015). Microalgae as sustainable renewable energy feedstock for biofuel production. BioMed Research International, 13, 519513

[26] Nguyen T.L., Lee D.J., Chang J.S., Liu J.C. (2013). Effects of ozone and peroxone on algal separation via dispersed air flotation. Colloids and Surfaces B: Biointerfaces, 105, 246–250

[27] Pittman J.K., Dean A.P., Osundeko O. (2011). The potential of sustainable algal biofuel production using wastewater resources. Bioresource Technology, 102(1), 17–25

[28] Qari H., Rehan M., Nizami A.-S. (2017). Key issues in microalgae biofuels: a short review. Energy Procedia, 142, 898–903.

[29] Rittman B.E. (2008). Opportunities for renewable bioenergy using microorganisms. Biotechnology and Bioengineering, 100, 203–212

[30] Rosmahadi N.A., Leong W.-H., Rawindran H., Ho Y.-C., Mohamad M., Ghani N.A., Bashir M.J.K., Usman A., Lam M.-K., Lim J.-W. (2021). Assuaging microalgal harvesting woes via attached growth: a critical review to produce sustainable microalgal feedstock. Sustainability, 13, 11159

[31] Shalaby E.A. (2011). Algal biomass and biodiesel production. Biodiesel - Feedstocks and Processing Technologies, 111–132. InTech.
[32] Sharif Hossain A.B.M., Salleh A., Boyce A.N., Chowdhury P., Naquiuddin. M. (2008). Biodiesel fuel production from algae as renewable energy. American Journal of Biochemistry and Biotechnology, 4(3), 250–254
[33] SundarRajan P.S., Gopinanth K.P., Greetham D., Antonysamy A.J. (2019). A review on cleaner production of biofuel feedstock from integrated CO2 sequestration and wastewater treatment system. Journal of Cleaner Production, 210, 445–458
[34] Udaiyappan A.F.M., Abu Hasan H., Takriff M.S., Abdullah S.R.S. (2017). A review of the potentials, challenges and current status of microalgae biomass applications in industrial wastewater treatment. Journal of Water Process Engineering, 20, 8–21
[35] Ugwu C., Aoyagi H., Uchiyama H. (2008). Photobioreactors for mass cultivation of algae. Bioresource Technology, 99(10), 4021–4028.
[36] Unpaprom Y., Tipnee S., Rameshprabu R. (2015). Biodiesel from green alga Scenedesmus acuminatus. International Journal of Sustainable and Green Energy, 4(1-1), 1–6
[37] Ungureanu N., Vlăduț V., Biriș S.Șt., Zăbavă B.Șt., Popa M. (2019). Microalgal systems for wastewater treatment – review. Proceedings of 6th International Conference „Research People and Actual Tasks on Multidisciplinary Sciences", Lozenec, Bulgaria, pp. 212–217.
[38] Zainal A., Yaakob Z., Takriff M.S., Rajkumar R., Jaharah A.G. (2022). Phycoremediation in anaerobically digested palm oil mill effluent using cyanobacterium, Spirulina platensis. Journal of Biobased Materials and Bioenergy, 6, 1–6
[39] Zeng X., Danquah M.K., Chen X.D., Lu Y. (2011). Microalgae bioengineering: from CO2 fixation to biofuel production. Renewable and Sustainable Energy Reviews, 15, 3252–3260
[40] Zhu L.D., Wang Z.M., Shu Q., Takala J., Hiltunen E., Feng P.Z., Yuan Z.H. (2013). Nutrient removal and biodiesel production by integration of freshwater algae cultivation with piggery wastewater treatment. Water Research, 47, 4294–4302

ISSN: 2067-3809

[1.]Ivan H. IVANOV

DESTRUCTION OF CRANKSHAFTS FROM INTERNAL COMBUSTION ENGINES

[1.] Zangador Research Institute – Varna; University "Asen Zlatarov" – Burgas, BULGARIA

Abstract: The crankshaft, as the main detail in internal combustion engines, is subjected to a variable load caused by the dynamic forces of the combustion process and its rotation. As a result, its surface layers are loaded successively in tension and compression, which causes fatigue of the material. The destruction of crankshafts is a serious problem in the operation of internal combustion engines and creates serious costs for the maintenance of the vehicle fleet. In this research paper are presents the results of a study of damaged crankshafts from internal combustion engines. The failure mechanisms of steel and cast iron crankshafts were established, and penetrant testing was conducted to identify other fatigue cracks. The hardness of the material from which the crankshafts are made was measured, and no significant changes were found. The study was conducted on broken crankshafts from gasoline and diesel engines, and the fracture surface, hardness and local deformations of the main journals and crank pin journals were examined. The crankshafts are made of steel and cast iron, having been dismantled from a car with a mileage of about 300,000 km, a truck with a mileage of about 250,000 km and a forklift with about 8,000 motor hours.

Keywords: Crankshaft, fatigue, cracks

INTRODUCTION

The crankshaft, as the main detail in internal combustion engines, is subjected to a variable load caused by the dynamic forces of the combustion process and its rotation. As a result, its surface layers are loaded successively in tension and compression, which causes fatigue of the material. The destruction of crankshafts is a serious problem in the operation of internal combustion engines and creates serious costs for the maintenance of the vehicle fleet.

The crankshafts are manufactured from steels and high–strength cast irons (nodular cast iron) and are subjected to thermal and chemical–thermal treatment to increase fatigue durability [8,11]. However, in the auto repair industry, numerous cases of their destruction are found, which is a prerequisite for emergency repairs of the engines [10].

Establishing the causes of their destruction, as well as the mechanism and kinetics of the process, is the subject of many studies [1–7, 12–15]. In the present work, the causes, mechanism and kinetics of fatigue failure of cast iron and steel crankshafts are investigated.

The study was conducted on broken crankshafts from gasoline and diesel engines, and the fracture surface, hardness and local deformations of the main journals and crank pin journals were examined. The crankshafts are made of steel and cast iron, having been dismantled from a car with a mileage of about 300,000 km, a truck with a mileage of about 250,000 km and a forklift with about 8,000 motor hours.

RESULTS

When studying the destruction of steel crankshafts, general regularities are established in the mechanism and kinetics of destruction. The primary crack is generated on the surface of the crank pin in the section intended for the exit of the grinding disc during its manufacture. This can be explained by the fact that there is the smallest diameter with a sharp change in the design size – a transition from the main journal to the crank pin journal. This causes a concentration of stresses in the area of the main journal. In the production of crankshafts in these areas, residual compressive stresses on the surface obtained by induction hardening, surface plastic deformation, nitriding, carbonitriding and other technological methods are provided. The failure mechanism can be explained by gradual accumulation of tensile stresses until complete relaxation of compressive stresses, their gradual accumulation in the surface layers, creation of dislocations and microdefects and reaching the failure limit of the material from which the crankshaft is made. The initiation of the crack takes place in the place with the highest concentration of stresses and valley from the roughnesses from the mechanical processing. The crack slowly grows along the cross–section, in a direction perpendicular to the direction of the tensile load in the corresponding half–cycle.

When the "live section" decreases due to the growth of the crack, it cannot withstand the applied external load and a brittle failure occurs, visible from Figure 1 and Figure 2. The advance of the failure front occurs slowly but steadily – with each cycle of the load. On the fracture, the

wavy lines of the crack movement are visible, which have a radial character relative to the initial microcrack and have the appearance of approximate concentric arcs

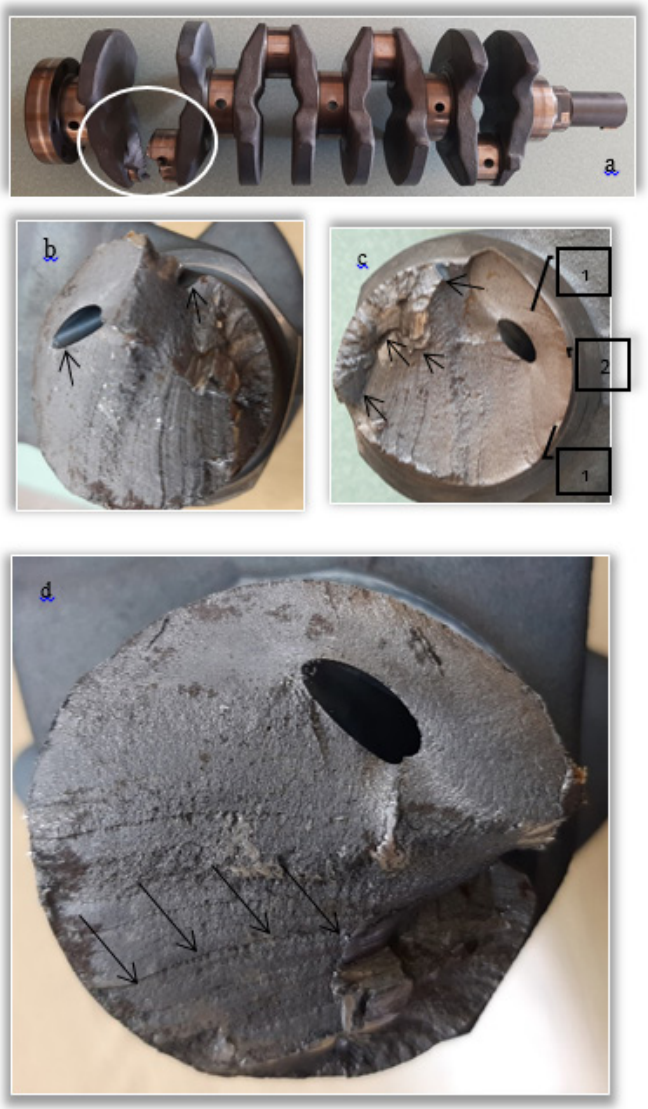

Figure 1. Crankshaft from a car with a mileage of about 300,000 km: a) general appearance and place of destruction; b) failure surface with lubricant hole c) fracture surface – 1) river marks, 2) fracture origin, ⟶) overload fracture; d) beach marks

Secondary cracks located perpendicular to the crack propagation front can be observed in the fracture of the examined crankshaft. Their origin and development can be explained by the special load on the shaft – bending and twisting. While bending stresses promote the development of the primary crack, torsional stresses promote the development of secondary cracks. Secondary cracks can be of "open" and "closed" type. Open cracks start from the surface and develop in depth, while closed cracks start and develop completely surrounded by the material – Figure 2c. The length of open cracks reaches the end of the fatigue crack propagation front and the onset of brittle failure.

Closed cracks are of particular interest Figure 2 and Figure 3. Their appearance can be associated with structural inhomogeneity in the material – presence of non–metallic inclusions, different phases or high–angle grain boundaries, the scale effect. Non–metallic inclusions in steels and graphite in cast iron are stress concentrators. On the other hand, the dimensions of the crankshafts, considered as a scale effect, have a significant influence on the occurrence of secondary closed cracks. It is found that in damaged crankshafts with smaller diameters, secondary cracks do not initiate and develop, and as the dimensions of the crankshafts increase, the secondary cracks propagate perpendicular to the fatigue crack propagation front. This can be explained by the fact that with crankshafts of smaller dimensions, the distance to be traveled is less and there is no possibility for the initiation and development of secondary cracks.

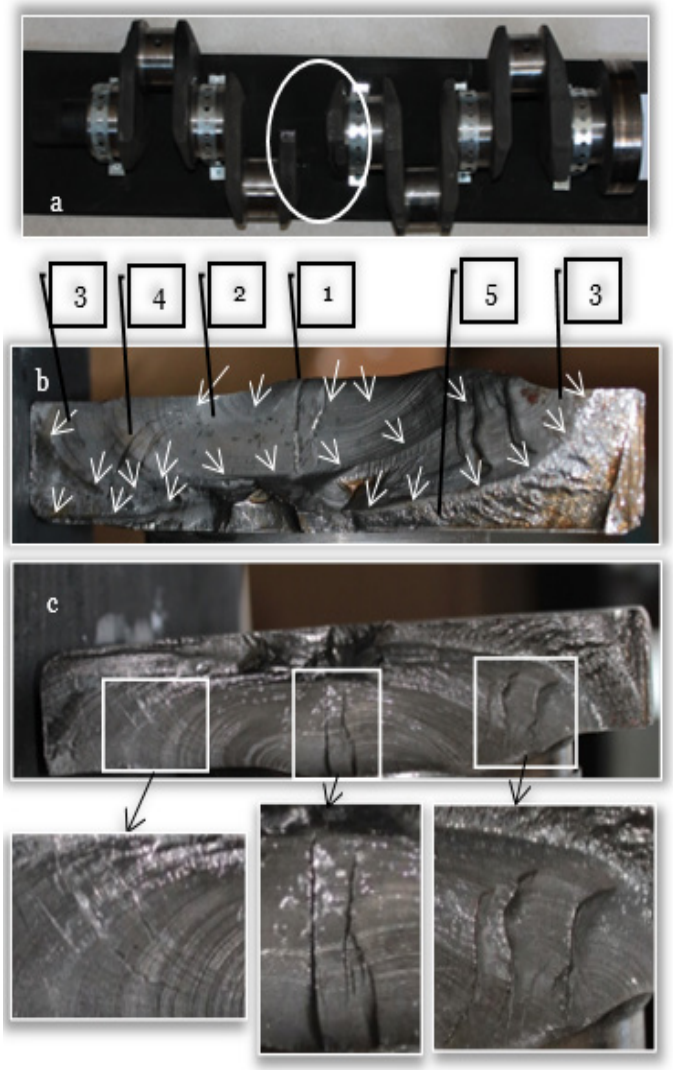

Figure 2. A broken crankshaft from a forklift: a) general appearance and place of destruction b) failure surface:1–crack initiation, 2–primary beach marks, 3–secondary beach marks, 4–river marks, 5–overload fracture c) failure surface from the second part with closed cracks, secondary cracks and beach marks

In addition, as the dimensions of the crankshafts increase, the mechanical properties of castings and forgings deteriorate, because the non–uniformity of the metal increases, the degree of deformation during forging and stamping decreases, it becomes difficult to carry out quality heat treatment in the entire volume of the material.

Regardless of the reasons for the appearance of the secondary cracks, their propagation is facilitated by the sign–changing stresses arising during operation of the crankshaft and their concentration at the sharp edges.

When examining the destroyed cast iron crankshaft, significant deformation was observed in the crank pin journal, which can be explained by the sudden destruction during engine operation and the impact that occurred between the connecting rod and the cylinder block (the cylinder block was also destroyed).

Figure 3. Destroyed cast iron crankshaft from a truck: a) general appearance and place of destruction b) secondary crack "closed type"

Similar deformations in the steel crankshafts were not detected, and the measured diameters fell within the permissible values determined by their manufacturer. Penetrant testing was conducted on all crankshafts, and the occurrence of another fatigue crack was not detected.

The measured hardness in the cross section of the journals is 250HB in the center of the crankshaft to 280HB on the surface – for steel crankshafts and 200HB to 260HB – for cast iron crankshafts.

Figure 4. Destroyed cast iron crankshaft from a truck: a) secondary cracks "open type" b) Rivers marks.

CONCLUSION

Initial research conducted on failed internal combustion engine crankshafts found that in–service material fatigue was a major cause of failure. The occurrence of more than one fatigue crack is not detected. Measurable significant changes in the hardness of the material are not observed.

References

[1] Farrahi G. H. et al., Failure Analysis of a Four Cylinder Diesel Engine Crankshaft Made from Nodular Cast Iron, The Journal of Engine Research (22) 21–28 (2011)
[2] Witek L., Stachowicz F., Zaleski A., Failure investigation of the crankshaft of diesel engine, Procedia Structural Integrity (5) 369–376 (2017)
[3] Yu Z., Xu X., Failure analysis of a diesel engine crankshaft, Engineering Failure Analysis (12) 487–495 (2005)
[4] Keskin A., Aydin K., Crack Analysis of a Gasoline Engine Crankshaft, Gazi University Journal of Science 23 (4) 487–492 (2010)
[5] Fonte M. et al., Failure mode analysis of a diesel motor crankshaft, Engineering Failure Analysis, (82) 681–686 (2017)
[6] Aliakbari K., Safarzadeh N., Mortazavi S. S., The Analysis of Wheel Loader Diesel Engine Crankshaft Failure, International Journal of Engineering 31 (3) 473–479 (2018)
[7] Aliakbari K., Failure analysis of four–cylinder diesel engine crankshaft, Journal of the Brazilian Society of Mechanical Sciences and Engineering 41:30(2019)
[8] Yamagata H., The science and technology of materials in automotive engines, Cambridge, England, WOODHEAD PUBLISHING LIMITED, 2005
[9] Sidashenko A.I., Skoblo T.S. Analysis of premature wearand destruction the machine parts of agricultural machinery, Technical service of agriculture, forestry and transport systems, 1 (1) 105–113 (2014)
[10] Ivanov I., Some aspects of application of not–destructive methods in auto repair production, International Journal "NDT Days" 2 (5) 582–587 (2019)
[11] Ivanov I., Structure of Metals: An Atlas, Varna, Bulgaria, Zangador Research Institute, 2020
[12] Alfares, M., Falah, A., Elkholy, A., Failure analysis of a vehicle engine crankshaft, Journal of Failure Analysis and Prevention, 7 (1) 12–17 (2007)
[13] Iyasu T. J., Goftila G. S., Fitsum T. S., Fatigue Failure Analysis of Crankshafts–A Review IJISET – International Journal of Innovative Science, Engineering & Technology, 7 (5) 93–106 (2020)
[14] Marin N.L., Marin D. E., Study of a crankshaft material destruction mechanism of forced diesels, The Development of the Informational and Resource Providing of Science and Education in the Mining and Metallurgical and the Transportation Sectors 92–99 (2014)
[15] Bai, S. Z., Hu, Y. P., Zhang, H. L., Zhou, S. W., Jia, Y. J., Li, G. X. Failure Analysis of Commercial Vehicle Crankshaft: A Case Study. Applied Mechanics and Materials, (192) 78–82(2012)
[16] Y. Petrov, Modeling of Transients Processies in Linear Electric Circuit Of The Second Order With Generalised Net, Annual of Assen Zlatarov University–Burgas, Bulgaria, (XLVI) 1 (2019)

ISSN: 2067–3809

[1.] Oluranti Adetunji ABIOLA, [2.] Adekola Olayinka OKE, [2.] Dare Aderibigbe ADETAN

THE EFFECT OF FIRING TEMPERATURE ON SOME PHYSICAL PROPERTIES OF OSUN STATE CERAMIC TILES

[1.] Elizade University, Department of Automotive Engineering, Ilara–Mokin, NIGERIA
[2.] Obafemi Awolowo University, Department of Mechanical Engineering, Ile–Ife, NIGERIA

Abstract: The work evaluates the effect of firing temperature on the physical properties of ceramic tiles. This was with the view to determine the optimum processing condition for Osun State ceramic tiles. Ceramic raw materials collected from Osun State were batched using clay–feldspar–silica sand blending ratio of 5:4:1, 5:3:2, 5:2:3, 5:1:4, 6:3:1, 6:2:2, 6:1:3, 7:2:1, 7:1:2 and 8:1:1 by weight; and homogeneously mixed. Three replica samples were molded by dry forming and fired at 1200, 1300 and 1400°C and subjected to water absorption, apparent porosity, apparent relative density and bulk density tests in line with the ISO 10545–3 (1996) standard. The results showed that water absorption, apparent porosity, apparent relative density, and bulk density were within the range 10.43 to 15.02%, 22.77 to 30.20%, 2.26 to 3.09 and 1.34 to 1.45 g/cm3 respectively, while the figures revealed that sample with 60% clay, 30% feldspar and 10% silica sand fired at 1320°C will exhibit the best physical properties. In conclusion, ceramic raw materials collected from Osun State are viable for ceramic tile production.
Keywords: clay feldspar, silica sand, triaxial blend, physical properties, ceramic tiles

INTRODUCTION

Ceramic tiles are tiles made of a triaxial clay–based combination that are frequently used to cover walls and floors in buildings (Irabor *et al.*, 2014; El Nouhy, 2013; Martin–Marquez *et al.*, 2008; Iqbal and Lee, 2000; Abiola *et al.*, 2021). It is essentially a hygienic item with a porous body and a thick layer of white or colorful glaze that is widely used in living rooms, bathrooms, kitchens, hospitals, labs, schools, public restrooms, and shopping centers (El Nouhy, 2013). According to Iyasara *et al.* (2014) The three silicate clay minerals clay, silica sand, and feldspar are combined to create ceramics, which are inorganic compounds that react with one another at the right high temperature. They can survive extremely high temperatures as well as chemical erosion, which many other materials are susceptible to (Carter and Norton, 2007; European Commission, 2007; Jung, 2008).

Ceramic tiles are characterized by low water absorption, usually between 3.3% and 11.1% (Amoros *et al.*, 2007; Griese, 2007; Bryne, 2008; ISO 10545, 1996). Water absorption is commonly referred to as an indicator of porosity for wall and floor tiles (Chukwudi *et al.*, 2012). Amount, size and distribution of porosity are among the important factors which affect the physical and mechanical properties of ceramic tiles. Tiles with the lowest apparent porosity have the lowest water absorption, high bulk density and high compressive strength (Soni *et al.*, 2015). The porosity is connected to the liquid phase during firing and is affected by the transformations that occur during sintering (Ozturk and Ay, 2014).

Meanwhile, the properties of any ceramic body are dependent on the properties of the raw material and firing temperature (Choudhury *et al.*, 2012). Several researchers have reported different triaxial blends as well as diverse optimum firing temperatures for ceramic tiles production. Braganca and Bargmann (2004) reported 1340°C; Amoros *et al.* (2007) and Idowu, (2014), between 1190 and 1220°C; for El–fadaly (2015) it was between 1190 and 1230°C; The American Ceramic Society (2005) stated 1400°C as the maximum firing temperature; while Mathew and Fatile (2014) reported 1218°C as suitable firing temperature.

According to ISO standard 10545 (1996), the physical properties of any ceramic tile (water absorption, apparent porosity, apparent relative density and bulk density) depend mostly on the amount, size and distribution of particles; material composition; and firing temperature (Ozturk and Ay, 2014; Lin and Lan, 2013). Since studies have provided several processing methods for ceramic tiles, it has become imperative to study the effect of material blending ratio and firing temperature on the physical properties of ceramic tiles produced from raw materials collected from Osun State.

MATERIALS AND METHODS

The kaolinite clay utilized in this study was gathered from Ipetumodu, the administrative center of the Ife North Local Government region of Osun State, Nigeria (Oke and

Omidiji, 2016). Silica sand was gathered at the Isasa River in Osun State, Nigeria, which divides the local governments of Ayedaade and Ife North. Feldspar was gotten at Osogbo, the capital of Nigeria's Osun State. The three raw materials collected were beneficiated separately as specified by Abiola *et al.*, (2019).

Preparation of materials

The ceramic raw materials were prepared as described by Abiola *et al.* (2021). Clay, silica sand, and feldspar were thoroughly combined to create a more chemically and physically homogenous substance for producing tiles. Due to many discrepancies regarding the ideal mixing ratio for ceramic materials, the mixing ratios for the raw materials were varied (Braganca and Bargmann, 2004; Amoros *et al.*, 2007; El–Fadaly 2015; Martín–Márquez *et al.*, 2010; Idowu, 2014).

To predict the mixing ratio of ceramic ingredients, Norsker and Danisch's (1993) 10–step tri–axial blending chart was used. Only the ceramic blends with clay–feldspar–silica sand ratios of 5:4:1, 5:3:2, 5:2:3, 5:1:4, 6:3:1, 6:2:2, 6:1:3, 7:2:1, 7:1:2, and 8:1:1 and designated as blends A, B, C, up to J were chosen from the chart's potential sixty–six combinations. Due of the fact that ceramic is referred to as a triaxial blend product, thirty blends that contain fewer than three materials were disregarded (Teo *et al.*, 2016; Idowu, 2014; Irabor *et al.*, 2014; Iyasrara *et al.*, 2014; Soni *et al.*, 2015; El Fadaly, 2015). Since clay is the main component used in the creation of ceramic tiles, 26 additional blends with less than 50% clay percentage were also disregarded (Solanki and Shah, 2016; Soni *et al.*, 2015; Irabor *et al.*, 2014; Adindu *et al.*, 2014; El Ouahabi *et al.*, 2014; El Nouhy, 2013; Misra *et al.*, 2013; Manfredini and Hanuskova, 2012; Murray 1999).

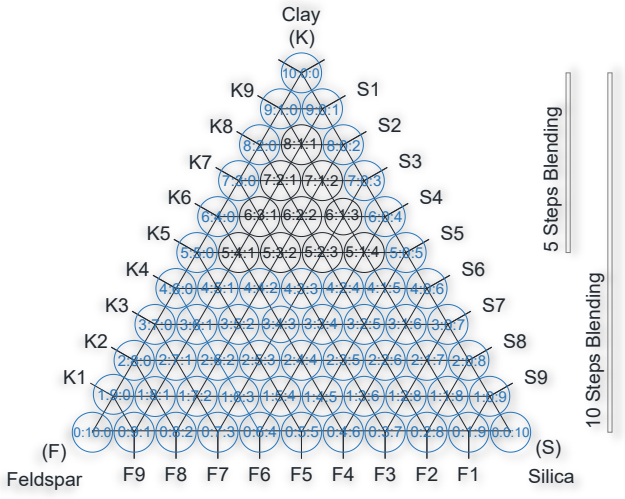

Figure 1: 10 steps triaxial blending chart

Each blend of the ceramic materials, A through J, was compacted to the recommended size for the physical property test sample, 50 x 15 x 15 mm, according to the instructions provided by Bresciani et al. (2004). After forming, the samples were dried by convection in an open laboratory drying oven (model DHG–9101–2A manufactured by Searchtech Instrument) where heated air was circulated around the ceramic samples. Since water should evaporate from a ceramic combination below 100°C, the air around the samples was held at 95°C to remove any water content. The materials were maintained in this condition for 20 hours using the Br.MSME–DI technique (2011). It is anticipated that this drying procedure will stop the final product's eventual differential shrinkage, warping, cracking, and deformation.

According to Br.MSME–DI (2011) recommendation, the ceramic samples were heat–treated in the laboratory drying oven at 300°C before firing in order to provide additional drying, vaporize or decompose organic additives and other impurities, as well as remove leftover, crystalline, and chemically bound water. According to the plan put forth by Br.MSME–DI (2011), the ceramic samples were kept in the kiln for 20 hours at a constant temperature of 300°C. The ceramic samples were removed from the kiln after this time, allowed to naturally cool at room temperature, then fired in a furnace (model XD–1700M manufactured by Zhengzhou Brother Furnace Company, China). The fire temperatures employed for the experiment were 1200, 1300, and 1400°C. These temperatures were used because Martin–Márquez et al. (2008) claimed that firing ceramic tile above the vitrification range will result in a drastic fall in the physical properties due to the forced expulsion of trapped gases, resulting in bloating and blisters and Abiola and Oke (2017) claimed that Ipetumodu clay begins to disintegrate at 1450°C. Additionally, as the American Ceramic Society (2005) states that the highest sintering temperature for the manufacture of ceramic tiles is 1400°C that value was chosen as the maximum firing temperature as well. To assess the behavior of the local tiles made below the recommended maximum firing temperature for ceramic products, lower temperatures (1200°C and 1300°C) were necessary. This was because many researchers had suggested sintering temperatures ranging from 1190 to 1340 °C. (Braganca and Bargmann 2004; Amoros et al., 2007; Idowu, 2014; Mathew and Fatile, 2014; El–fadaly, 2015). To guarantee that the samples' cross–sections were heated to the same temperature, the samples were kept at the appropriate firing temperatures for around an hour (Abeid and Park, 2018; Ashby, 2005). Following that, the samples were held in the kiln for a cycle of at least 18 hours where it was cooled, in line with Br.MSME–DI (2011).

Physical properties test

The ceramic tiles were removed from the kiln after cooling and tested for water absorption, apparent porosity, and apparent relative density in accordance with the recommendations of Abiola et al. (2021) and ISO 10545–3 (1996).

The water absorption was calculated from equation (1):

$$A_w = \frac{m_2 - m_1}{m_1} \text{ x } 100\% \quad (1)$$

where $\mathbf{A_w}$ is water absorption (%); $\mathbf{m_1}$ is the average mass of the dry samples in gram (g); and $\mathbf{m_2}$ is the average mass of the wet samples in gram (g) (ISO 10545–3, 1996).
Apparent porosity was calculated from equation (2) as:

$$P_a = \frac{m_2 - m_1}{m_2 - m_3} \text{ x } 100\% \quad (2)$$

where $\mathbf{P_a}$ is the apparent porosity (%); $\mathbf{m_1}$ is the average mass of the dry samples in gram (g); $\mathbf{m_2}$ is the average mass of the wet samples in gram (g); and $\mathbf{m_3}$ is the average mass of the suspended samples impregnated by boiling water in gram (g) (ISO 10545–3, 1996).
Meanwhile, apparent relative density was calculated using equation (3) (ISO 10545–3, 1996) as:

$$RD_a = \frac{m_1}{m_1 - m_3} \quad (3)$$

where $\mathbf{RD_a}$ is the apparent relative density; $\mathbf{m_1}$ and $\mathbf{m_3}$ are the same as in equation (2) (ISO 10545–3, 1996).
Bulk density was determined using equation (4) as:

$$BD = \frac{m_1}{V} \quad (4)$$

where BD is the bulk density, in g/cm^3; $\mathbf{m_1}$ is the average mass of the dry samples in gram (g); and *V* is the exterior volume of the sample, in cm^3 (ISO 10545–3, 1996).

Experimental design

The experiment was created using Design Expert 6.0.8 Portable using the surface response approach. In order to determine the impact of firing temperatures (1200 oC, 1300 oC, and 1400 oC) and triaxial blend ratios (5:4:1, 5:3:2, 6:2:2, 6:1:3, 7:2:1, 7:1:2, and 8:1:1) on the physical properties (water absorption, apparent porosity, apparent relative density, and bulk density) of ceramic tiles, a two–factor design matrix linear model was used. Design matrix of sixty (60) experiments design for two factors were used on each combination of firing temperature and blending ratio for physical properties.

RESULTS AND DISCUSSION

Water absorption

The results of the physical properties tests are as seen in Figure 2. Water absorption decreased with increased temperature and later reduced with continued increase in temperature. The reduced water absorption with increased temperature could be due to the liquid phase formation at high temperature and densification as the sample cools to room temperature (Alves *et al.*, 2015; Kimambo *et al.*, 2014). The liquid phase that is formed fills the pores and decreased the porosity (Viruthagiri *et al.*, 2009). Thus, increased temperature reduces or eliminates pores within the ceramic article, thereby, reducing the article's porosity and its tendency to absorb water. (Soni *et al.*, 2015).

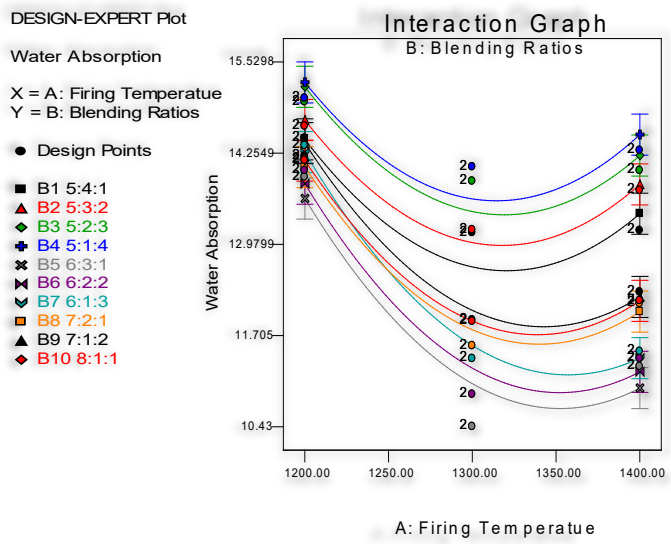

Figure 2: Water absorption of the ceramic tile samples fired at different temperatures

The general increase in water absorption for all samples as firing temperature rises from 1300°C to 1400°C may be due to bloating which takes place as a result of the expansion of gases enclosed in the pores; this causes the increase in porosity (Kimambo *et al.*, 2014; Hettiarachchil *et al.*, 2014). In addition, the high firing temperature can cause mullite crystals to become coarse and decrease densification and hence increase water absorption (Kimambo *et al.*, 2014).
Ceramic tiles, characterized by low water absorption between 3.3% and 11.1% is the most important physical property for ceramic tiles mostly used as floor tiles (Amoros *et al.*, 2007; Bryne, 2008; ISO 10545, 1996). According to technical standards, the tiles with water absorption higher than 10% can be used as wall tiles and the majority of standard wall tiles have glazed porous bodies with water absorption between 10% and 20% (Kimambo *et al.*, 2014). Thus, the tiles produced in this study (with water absorption in the range 15.02–10.43%) are suitable wall tiles.
Figure 2 shows that only the ceramic samples "E" and "F" fired at temperature 1300°C have water absorption 10.43% and 10.88% respectively which falls within the ISO standard and 15.02% been the maximum recorded for sample D fired at 1200°C. Meanwhile Idowu (2014) recorded a much higher water absorption of 20% with ceramic tiles produced from clay, silica sand and feldspar collected from Ifon, Igbokoda and Ijero respectively while Mathew and Fatile (2014) recorded a much better water absorption of between 0.2% to 0.38% with material collected from Ijero, Ajaokuta and Okpella. Ogundare *et al.*, (2015) alighted a similar result (water absorption: 0.9%– 3.9%) with porcelain tiles produced materials collected form Ijero and Okpella. The water absorption of 5.61% to 17.12% was recorded in the study of Chukwudi *et*

al., (2012) while Soni et al., (2015) recorded 0.9% to 5.9% in its study. El–Nouhy (2013) collected 14 different ceramic tile samples produced in Egypt and found all the samples to have water absorption ranging from 8.5% to 16.0%.

Apparent porosity

The results in Figure 3 show that the behaviour of apparent porosity is similar to water absorption (Soni *et al.*, 2015) as they both generally decreased with increased temperature and later increased with continued increase in temperature. The reduced apparent porosity with increased temperature could also be due to the liquid phase formation at high temperature and densification as the sample cools to room temperature (Alves *et al.*, 2015; Kimambo *et al.*, 2014) as explained for water absorption.

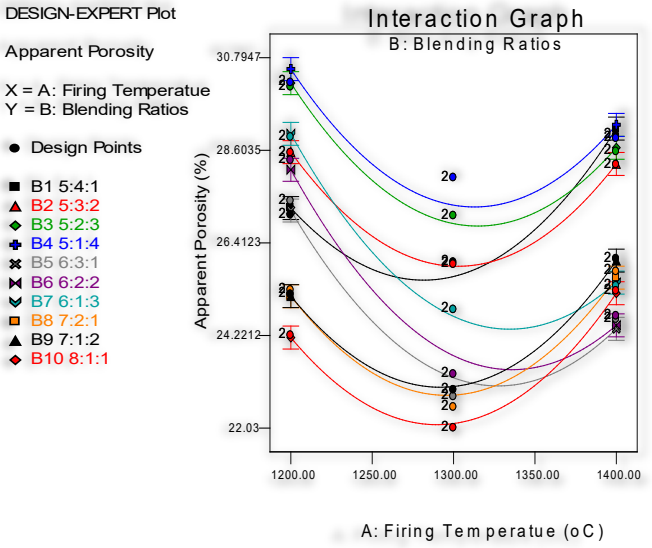

Figure 3: Apparent porosity of the ceramic tile samples fired at different temperatures

Figure 3 shows the minimum and maximum apparent porosity recorded as 22.77% for sample E fired at 1300°C and 30.20% for sample D fired at 1200°C respectively. The result is similar to the findings of Chukwudi *et al.*, (2012); Ogundare *et al.*, (2015); and Soni *et al.*, (2015) which recording apparent porosity of 11.29% to 31.32%; 11% to 16%; and 5% to 26% for samples fired at 1200°C; 1250°C; and 1350°C respectively. The apparent porosity established by El–Nouhy (2013) in his study ranged from 17.5% to 27.5%.

The values of the apparent porosity of all the ceramic samples were found to decrease with an increase in firing temperature and later increase with further increase in temperature as shown in Figure 3. The increase in apparent porosity at higher firing temperature is believed to be caused by bloating which takes place as gas is expelled from the matrixes, thereby resulting in increased apparent porosity (Kimambo *et al.*, 2014; Matin–Marquez *et al.*, 2008). The increase in the apparent porosity with further increase in firing temperature from 1300°C to 1400°C may be due to increase in fluxing oxides, Na_2O and K_2O and feldspar content in the tiles (Kimambo *et al.*, 2014; El Nouhy, 2013; Matin–Marquez *et al.*, 2008).

Apparent relative density

The apparent relative density for samples A, E, G, H, I and J shown in Figure 4 increased as firing temperature increases. This is similar to the submission of Choudhury *et al.*, (2012) and Zabotto *et al.*, (2012). It could be seen with the samples that feldspar has a direct relationship with the apparent relative density as increased feldspar result in increased apparent relative density. This is in line with the result of Chao *et al.*, (2010) and could be due to bloating in the matrixes. The increase in the apparent relative density of the ceramic samples with increased firing temperature could also be an indication that cation concentration is increased as increased cation within the matrix will cause increase apparent relative density (Zabotto *et al.*, 2012).

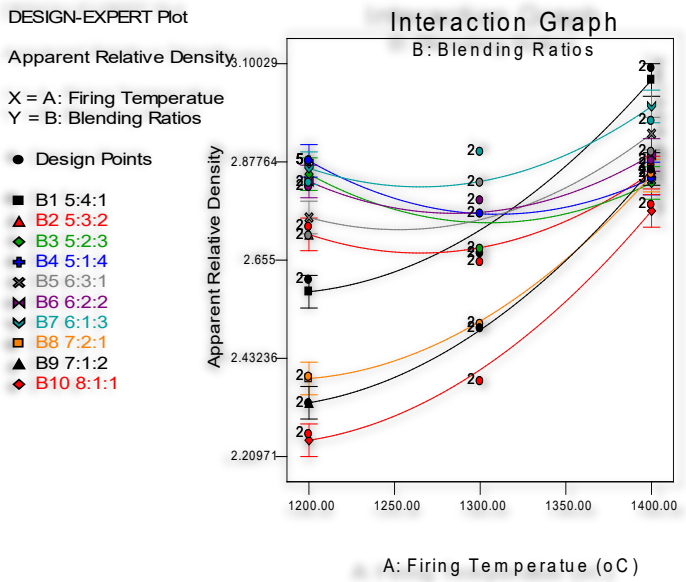

Figure 4: Apparent relative density of the ceramic tile samples fired at different temperatures

Bulk density

The bulk density of ceramic samples reduced with increased firing temperature as shown in Figure 5. The lower bulk density at higher firing temperature may be attributed to bloating which takes place as gasses are expelled from the matrices to cause the increase in porosity (Kimambo *et al.*, 2014). Sample D fired at 1400°C has the least bulk density when compared to the rest of the samples. This is because the bulk density of any ceramic article decreases with a decrease in the feldspar content. The feldspar which is a fluxing oxide helps in the production of liquid phases which fill the pores and increase the bulk density of the ceramic body (El Nouhy, 2013). The bulk density of the ceramic body attains its maximum level when the available liquid phase is enough to block the open pores (Kimambo *et al.*, 2014).

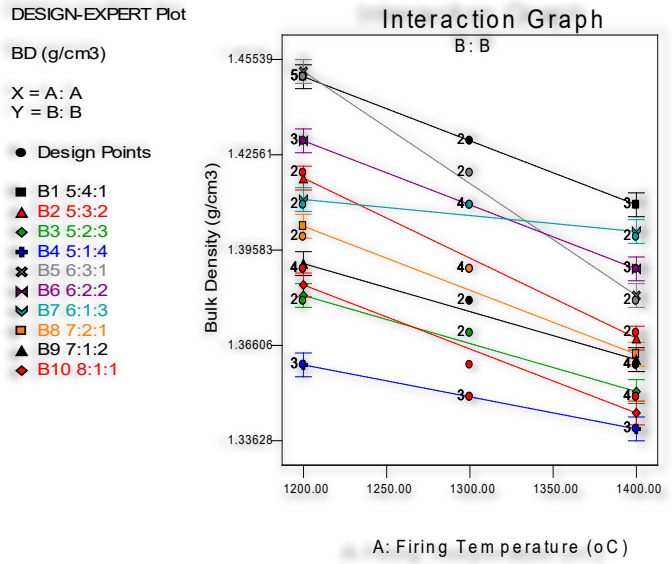

Figure 5: Bulk density of the ceramic tile samples fired at different temperatures

CONCLUSION

There is appreciation in the physical properties of ceramic tiles as firing temperature increases from 1200°C to just above 1300°C and these properties deteriorate with a further increase in temperature. Therefore, the ceramic sample will attain the best physical properties at about 1320°C (as can be deduced from the Figures).

The ceramic sample produced from Osun State raw materials in this study will be suitable for wall tiles since the water absorption is between 10% and 15%.

References

[1] Abeid, S. and Park, S.E.: Suitability of vermiculite and rice husk ash as raw materials for production of ceramic tiles. International Journal of Materials Science and Applications, 7 (2), 39–48, 2018.

[2] Abiola, O.A. and Oke, A.O.: Carbonised palm kernel shell effect on the physico–chemical properties of clay–sand mixture. Journal of Applied Science, Engineering and Technology, 17 (1), 17–23, 2017.

[3] Abiola, O.A.; Oke, A.O.; Omidiji, B.V. and Adetan, D.A.: The effect of beneficiation on some properties of Osun State ceramic raw materials. Journal of Casting & Materials Engineering, 3 (3), 62–66, 2019.

[4] Abiola, O.A.; Oke, A.O.; Omidiji, B.V. and Adetan, D.A.: The effect of raw materials on some properties of Osun State ceramic tiles. Journal of Engineering studies and Research, 27 (1), 7–12, 2019.

[5] Adindu, C.I.; Moses, J.; Thaddeus, C.A. and Tse, D.T.: Exploring ceramic raw materials in Nigeria and their contribution to nation's development. American Journal of Engineering Research, 3 (9), 127–134, 2014.

[7] Alves, H.J.; Melchiades, F.G. and Boschi, A.O.: Effect of feldspar particle size on the porous microstructure and stain resistance of polished porcelain tiles. Journal of the European Ceramic Society, 32, 2095–2102, 2012.

[8] Amoros, J.L.; Orts, M.J.; Garcıa–Ten, J.; Gozalbo, A. and Sanchez, E.: Effect of the green porous texture on porcelain tile properties. Journal of the European Ceramic Society, 27, 2295–2301, 2007.

[9] Ashby, M.F.: Materials selection in mechanical design, Third Edition, Pergamon Press, Butterworth–Heinemann Linacre House, Jordan Hill, Oxford, 2005.

[10] Braganca, S.R. and Bergmann, C.P.: Traditional and glass powder porcelain: Technical and microstructure analysis. Journal European Ceramic Society, 24 (8), 2383–2388, 2004.

[11] Bresciani, A.; Ricci, C. and Imola S.: Innovative process for ceramic tile manufacturing by double pressing with continuous precompaction. Castlelon, p. 49–60, 2004.

[12] Br.MSME–DI: Ceramic glazed wall tiles, small scale production enterprise. W.B.S.I.D.C Industrial Estate, J.P. Avenue, Durgapur–12, p. 1–18, 2011.

[13] Bryne, M. F.: Properties of Ceramic Tile, 2008. http://www.thetileryatp.com/assets/files/press/A6_Tile_Properties.pdf. (Accessed July 10, 2018).

[14] Carter, C.B. and Norton, M.G.: Ceramic materials: Science and engineering. First Edition, Springer–Verlag, New York. p. 3 – 4, 2007.

[15] Chao, S.; Petrovsky, V. and Dogan, F.: Effects of sintering temperature on the microstructure and dielectric properties of titanium dioxide ceramics. Material Science, 45, 6685–6693, 2010.

[16] Choudhury, S.; Bhuiyan, M.A and Hoque, S.M.: Effect of sintering temperature on apparent density and transport properties of NiFe2O4: Synthesized from nano size powder of NiO and Fe2O3. Int. Nano Lett. 1 (2), 111–116, 2012.

[17] Chukwudi, B.C.; Ademusuru, P.O. and Okorie, B.A.: Characterization of sintered ceramic tiles produced from steel slag. Journal of Minerals and Materials Characterization and Engineering, 11, 863–868, 2012.

[18] El–Fadaly, E.: Characterization of porcelain stoneware tiles based on solid ceramic wastes. International Journal of Science and Research, 4 (1), 602–608, 2015.

[19] El Nouhy, H.A.: Assessment of some locally produced Egyptian ceramic wall tiles. Housing and Building National Research Center Journal, 9, 201–209, 2013.

[20] El Ouahabi1, M.; Daoudi, L.; De Vleeschouwer, F.; Bindler, R. and Fagel, N.: Potentiality of clay raw materials from northern Morocco in ceramic industry: Tetouan and Meknes areas. Journal of Minerals and Materials Characterization and Engineering, 2 (3), 145–159, 2014.

[21] European Commission: Reference document on best available techniques in the ceramic manufacturing industry, 2007. http://eippcb.jrc.es. (Accessed September 9, 2016).

[22] Griese, B.: Porcelain in the ceramic tile industry. Tilt Council of North America's Product Performance Testing Laboratory, p. 70–73, 2007. https://www.tcnatile.com/images/pdfs/ Porcelain%20in%20the%20Ceramic%20Tile% 20Industry.pdf. (Accessed October 16, 2016).

[23] Hettiarachchi1, P.; Wickramasinghearachchi, R.C. and Pitawala H.M.T.G.A.: A comparison of fluxing effects of granite and feldspar on red clay body composition. Journal of Geological Society of Sri Lanka, 16, 101–108, 2014.

[24] Idowu, I.O.: Production of vitrified porcelain tiles using local raw materials from southwestern Nigeria. Journal of Emerging Trends in Engineering and Applied Sciences, 5 (6), 421– 428, 2014.

[25] Iqbal, Y. and Lee, W.E.: Microstructural evolution in triaxial porcelain. Journal of American Ceramic Society, 83 (12), 3121–3127, 2000.

[26] Irabor, P.S.A.; Jimoh, S.O, and Omowumi, O.J.: Ceramic raw materials development in Nigeria. International Journal of Scientific and Technological Research, 3 (9), 275–287, 2014.

[27] ISO 10545: EN ISO norms for ceramic tiles – Testing methods, 1996. www.norfloor.no/media/ wysiwyg/DIY/ISO_10545–2.pdf. (Accessed September 25, 2016).

[28] Iyasara, A.C.; Joseph, M. and Azubuike, T.C.: The use of local ceramic materials for the production of dental porcelain. American Journal of Engineering Research, 3 (9), 135–139, 2014.

[29] Jung, P.: Quality Control: Preparation of Samples for XRF Analysis. The article was written for Retsch Inc., Newtown, PA. p. 23–27, 2008.

[30] Kimambo, V.; Philip, J.Y.N. and Lugwisha, E.H.: Suitability of Tanzanian kaolin, quartz and feldspar as raw materials for the production of porcelain tiles. International Journal of Science Technology and Society, 2 (6), 201–209, 2014.
[31] Lin, K.L. and Lan, J.Y.: Water retention characteristics of porous ceramics produced from waste diatomite and coal fly ash. Journal of Clean Energy Technologies, 1 (3), 211–215, 2013.
[32] Manfredini, T. and Hanuskova, M.: Natural raw materials in "traditional" ceramic manufacturing. Journal of the University of Chemical Technology and Metallurgy, 47 (4): 465–470, 2012.
[33] Martín–Márquez, J.; Rincón, J. Ma. and Romero, M.: Effect of firing temperature on sintering of porcelain stoneware tiles. Ceramics International, 34, 1867–1873, 2008.
[34] Martín–Márquez, J.; Rincon, J. Ma. and Romero, M.: Mullite development on firing in porcelain stoneware bodies. Journal of the European Ceramic Society, 30 (7), 1599–1607, 2010.
[35] Mathew, G.O. and Fatile, B.O.: Characterization of vitrified porcelain tiles using feldspar from three selected deposits in Nigeria. Research Journal of Recent Sciences, 3 (9), 67–72, 2014.
[36] Misra, S.N.; Machhoya, B.B. and Savsani, R.M.: Thermo physical characteristics of vitrified tile polishing waste for use in traditional ceramics–an initiative of CGCRI, Naroda centre. International Conference on Ceramics, Bikaner, India. International Journal of Modern Physics: Conference Series, 22, 118–133, 2013.
[37] Murray, H.H.: Applied clay mineralogy today and tomorrow. Clay Minerals, 34, 39 – 49, 1999.
[38] Norsker and Danisch: Glazed for the self–reliant potter. Publication of the Deutsches Zentrum für Entwicklungstechnologien, Germany, 1993.
[39] Ogundare, T.; Fatile, O. and Ajayi, O.: Development and characterization of parian bodies using feldspar from two selected deposits. Leonardo Electronic Journal of Practices and Technologies, 27, 147–156, 2015.
[40] Oke, A.O and Omidiji, B.V.: Investigation of same moulding properties of a Nigeria clay–bonded sand. Archives of Foundry Engineering, 16 (3), 71–76, 2016.
[41] Ozturk, Z.B. and Ay, N.: Investigation of porosity of ceramic tiles by means of image analysis method. Journal of Ceramic Processing Research, 15 (6), 393–397, 2014.
[42] Solanki, K.M. and Shah, S.R.: Analysis of drying process in ceramic tiles industries. International Journal of Advance Research and Innovative Ideas in Education, 2 (3), 409–418, 2016.
[43] Soni, A.; Mathur, R. and Kumar, K.: Study on particle size distribution and its effects on shrinkage, porosity and bulk density of tri–axial porcelain tiles. Indian Journal of Research, 4 (5), 58–60, 2015.
[44] Teo, P.T.; Seman, A.A.; Basu P. and Sharif N.M.: Characterization of EAF steel slag waste: the potential green resource for ceramic tile production. 5th International Conference on Recent Advances in Materials, Minerals and Environment (RAMM) & 2nd International Postgraduate Conference on Materials, Mineral and Polymer (MAMIP), 4–6 August 2015. Elsevier, Procedia Chemistry, 19, 842 – 846, 2016.
[45] The American Ceramic Society: Kiln firing chart: Pottery making illustration, 2005. http://www.ceramicartdaily.net/PMI/KilnFiringChart.pdf. (Accessed September 13, 2016).
[46] Viruthagiri, G.; Gobi, R. and Rajamannan, B.: Mechanical properties related to the use of Glass waste as a raw material in porcelain stoneware tile mixtures. Recent Research in Science and Technology, 1 (2), 52–57, 2009.
[47] Zabotto, F.L.; Gualdi, A.J. and Eiras, J.A.: Influence of the sintering temperature on the magnetic and electric properties of $NiFe_2O_4$ ferrites. Materials Research, 15(3), 428–433, 2012.

ISSN: 2067-3809

[1.]Florentina Cristina MĂNĂILĂ, [2.]Filip ILIE, [3.]Evelin–Anda LAZA

SOME NOTES REGARDING THE CONSTRUCTION AND OPERATION OF A STRAWBERRY PICKING ROBOT

[1.]Department of Biotechnical Systems Engineering, University POLITEHNICA of Bucharest, ROMANIA
[2.]Department of Machine Elements and Tribology, University POLITEHNICA of Bucharest, ROMANIA
[3.]INMA Bucharest, ROMANIA

Abstract: Mechanized, automated and robotic agriculture starts from seeding the field and spraying fertilizer, to irrigating the land and controlling weeds, then moves on to harvesting, sorting and packaging. The main area of application of robots in agriculture today is at the harvesting stage. When harvesting and picking fruits or vegetables, the progress is most obvious these days. Technology allows them to have sophisticated mechanisms, the possibility of visualizing the space in which they are going to carry out their activity. Undoubtedly, robots have a positive effect on the labor market and worldwide, and the trend is sure to continue. This paper presents notions about an agricultural robot, how can be made, and the activity it can carry out. It is the case of a robot for picking strawberries with purpose to ease people's work and to apply advanced technology in agriculture. The robot moves and is programmed to pick a certain amount of fruit with the help of a robotic arm, improving work productivity. Also, with the help of the automatic localization and navigation system, the human no longer intervenes while the robot is working. However, continuous robotization and automation solutions are needed for improvement and to continue the evolution.

Keywords: strawberries, picking robot, digital agriculture, robotic arm

INTRODUCTION

The evolution of technology has allowed mechanized, automated and robotic equipment to be obtained, which can ease or even replace human work in many fields of activity. With the evolution of technology, various automatic systems have been adopted to improve the performance of some activities and to contribute to the improvement of the quality of life. This also had a major impact on the development of technologies in the agricultural field that is how robots appeared that replace, through work, man.

Mechanized, automated and robotic agriculture starts from seeding the field and spraying fertilizer, to irrigating the land and controlling weeds, then moves on to harvesting, sorting and packaging.

The main area of application of robots in agriculture today is at the harvesting stage. When harvesting and picking fruits or vegetables, the progress is most obvious these days. Technology allows them to have sophisticated mechanisms, the possibility of visualizing the space in which they are going to carry out their activity. Undoubtedly, robots have a positive effect on the labor market and worldwide, and the trend is sure to continue. The form of automation could be doubled by artificial intelligence, making no job safe, according to an analysis by the International Data Corporation, cited by Gizmodo (*International Data Corporation, 2017*). For this, robotization and automation solutions are needed to succeed in evolving in this field (*https://revistadinlemn.ro/2019*).

Fruit production that requires selective harvesting is heavily dependent on humans as labor. This applies to harvesting fruits, such as strawberries and raspberries, or vegetables, such as peppers, tomatoes, cucumbers, etc. Some fruits, such as strawberries and tomatoes, tend to grow upright. These are difficult to pick up without causing them to be hit. It is one of the primary challenges for fruit harvesting systems.

Fruits, leaves, stems and other surrounding obstacles are difficult to separate from the target, both within detection and handling. In the field of agricultural robotics, many researchers are trying to avoid obstacles in both vision and manipulation.

Thus, a robot capable of distinguishing the quality of fruits and sorting them without damaging them is the Rubion robot, made by a Belgian company in 2014 (*Bonirob, Aranvid et al., 2017*), which not only moves through the strawberry fields, it finds the ripe fruits, he picks them without damaging them and sorts them immediately, choosing those that are ready for the final packaging (Figure 1).

Also, this company intends to launch robotic assemblers for other crops in the future [5]. A strawberry harvesting gripper that can open its fingers to capture a target from below is presented in ref. [6]. In the field of robotic manipulation, most studies focus on obstacle avoidance.

However, there are some studies that separate obstacles for simple situations. For a picking application, in the 2D environment, two linear directions were proposed to separate rigid obstacles during the picking path, to reach the targeted fruit [7]. All objects were placed on the 2D surface without stacking, which is simple compared to naturally growing plants.

Figure 1 – Rubion robot

Therefore, this work brings a consistent contribution to the knowledge, analysis, and use of robots in agriculture, with the aim of making human life easier and highlighting the evolution of technology. The main purpose of this work is to exemplify and present some mobile, automated robots that have the ability to ease people's work, as well as to improve the quality of techniques and services used in agriculture. The robots for picking strawberries are based on the same operating principle.

MATERIALS & METHODS

The essential problem in selecting the target fruits to be picked with the help of robots is avoiding obstacles. Fruits, leaves, stems and other surrounding obstacles are difficult to separate from the target, both within detection and handling.

Without moving obstacles in the way, which prevent the robotic arm from grabbing the target and also being able to be lowered with the target if they are located close to it. Similar problems arise when we approach fruit from other angles.

To solve this problem, it was proposed to use a single operation of linear displacement of the obstacles below the target based on their detection, from a 3D camera.

Without stacking, the vision system can easily track the target and obstacles, which are easy to control, closed–loop vision.

Unfortunately, in the agricultural environment, for strawberry plants for example, the fruits are located in 3D in diverse and unlimited environments. Selective picking of a ripe fruit in clusters requires 3D motion planning to separate the target from obstacles if using obstacle separation methods. Occlusions make it difficult for the vision system to track object changes. Also, flexible peduncles, deformable fruits, and many other crop variations make separation operations extremely difficult, and the dynamics of these objects are difficult to calculate and predict.

To avoid occlusions in fruit picking, a "3D–move–to–see" method has been proposed to find the best view with fewer occlusions (Xiong & Ge, 2020).

If an obstacle is located above the target, such as the cases shown in Figure 2(a), the handle may swallow or damage the obstacles when moving up to capture the target strawberry. Furthermore, obstacles can stop the fingers from closing, thus resulting in a failure. To solve this problem, manual operation is proposed, which opposes the move operation used in other layers.

The pulling operation allows the grabber to select the target fruit without catching unwanted obstacles. The operation comprises a pull–up step to move the target to an area containing fewer obstacles (Figure 7(b)) and a backward move that lifts upside obstacles (Figure 7(c)), before closing the grippers (Figure 7(d)). The handle moves higher to a cutting position. The pulling operation is performed only when there are obstacles in the center block.

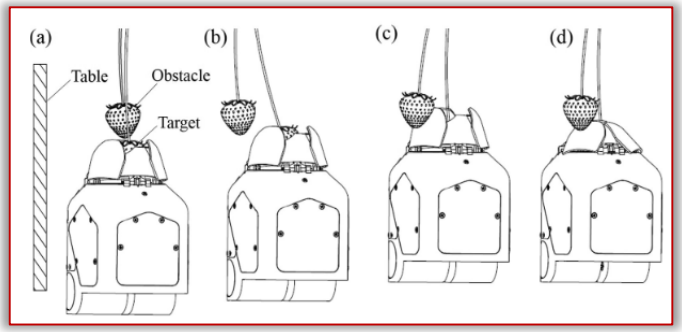

Figure 2 – Operation to avoid obstacle capture: an upward thrust moves the target to an area containing fewer obstacles (a) and (b); an upward step moves the upper obstacles one side (c) the position before closing the grippers (d)

Object detection using deep learning operation and point cloud to display both target position and obstacle information is one of the main objectives, Figure 3.

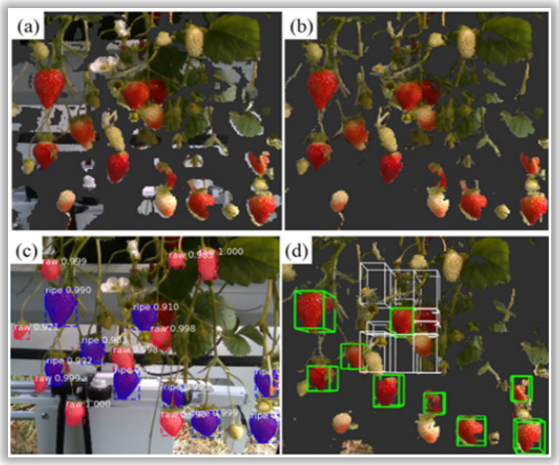

Figure 3 – Selecting the target plant and avoiding obstacles: (a) – the entire visual field; (b) –separating ripe strawberries from raw ones; (c) – using deep learning to detect ripe strawberries in an RGB image: (d) – localizing ripe fruit

The workflow for fruit detection and obstacle determination is to visualize the entire field (see Figure 3(a)), separate ripe from unripe strawberries (see Figure 3(b)), use deep learning to detect ripe strawberries in an RGB image (see Figure 3(c)) and the location of ripe fruits (see Figure 3(d)).

An old robot used Cartesian arms, Figure 4(a), and the new, low–cost type no longer uses Cartesian arms, Figure 4(b). The new arm is lighter and moves faster than the old Cartesian arms.

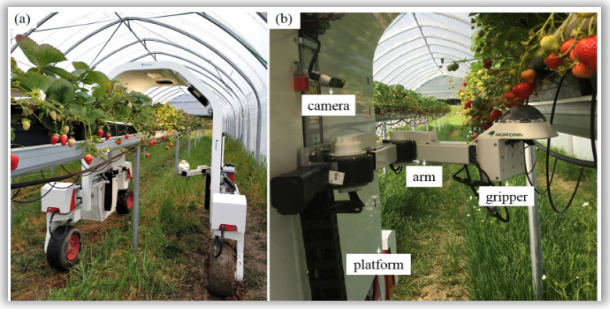

Figure 4 – The low–cost robot model, mounted inside in the shape of a "U" (a), the picking system with camera, manipulators and LED panels (b)

The picking system (Figure 4(b)), including the camera, manipulators and LED panels, was mounted inside in a "U" shape. The robot passes through the mass of strawberries, covering all the plants, with the possibility of using several manipulators that pick on each side of the tablet (see Figure 2(a)), following the detection of ripe strawberries, their location and detachment.

RESULTS

The robot, like any machine, must be assigned a series of tasks. This operation, generally called programming the robot, is of great importance, competing alongside the practical construction, for the success of the realization. Programming difficulty increases with:

- increasing the degree of autonomy of the robot – to be autonomous, the robot must "know" what it has to do in all possible situations, and even more, it must have a strategy for the unforeseen;
- increasing the number of operations performed – each additional operation brings with it the subprogram/ subprograms necessary to perform it, as well as the conditions under which it is launched;
- increasing the complexity of the robot structure – more actuation elements and/or more sensors lead to additional command lines;
- the possibility of evolution in unknown spaces – situations of ignorance require more complex approaches, compared to the situation of a completely known evolution space;
- possibly other constraints imposed, specific to a certain application.

There are numerous concerns in the field, starting from the optimization of trajectories or operations, in the case of knowledge of the evolution space, or the development of algorithms in order to "learn" and adapt the robot to changes in the evolution space.

Depending on the required performance, the level of autonomy, the sensors it has, and its mode of locomotion, an optimal possible trajectory can be determined for a robot.

Determining the optimal trajectory for a mobile robot is an important concern in the study of mobile robots. On the world level, the establishment of new methods of optimizing trajectories is being sought. For example, researchers from Japan proposed to determine a method for establishing the optimal trajectory of a mobile robot located in a known closed enclosure. The proposed method is based on genetic algorithms (GA), which represent a computational model of biological evolution. GAS is useful both for solving given problems and for modeling evolutionary systems.

The robot has a map of the premises, a map divided into identical units, one unit being equal to the size of the robot. Each unit has been associated with a code; with the help of GA the robot chooses the optimal trajectory. Thus, an example of some experimental results is shown in Figure 5.

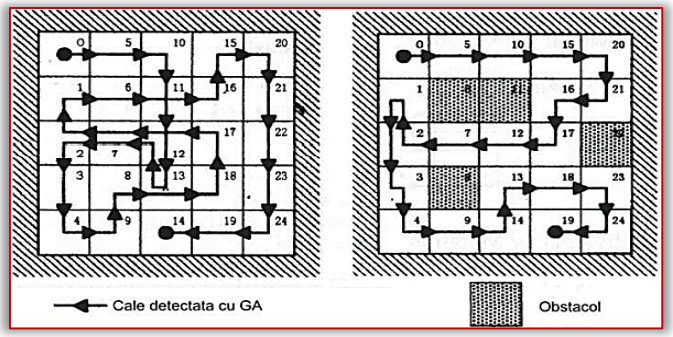

Figure 5 – GAS experimental results: workspace without obstacles (a); workspace with 4 obstacles (b)

They consist in determining a path for the robot to move in the chosen workspace. To begin with, an optimal trajectory was determined in the absence of any obstacles. The same problem was solved in the case of the appearance of four obstacles (see Figure 5(b)).

There are concerns of developing new control methods for mobile robots with evolution in unknown environments, also in Japan. There is the problem of adapting the robot to the space of evolution, to its eventual modification. The aim is to establish some learning techniques. For this, the Classifier System (CS), the machine learning method, is applied.

Experimental results are also obtained with GA. In general, CS consists of 2 important parts: the conditions part and the action part.

It receives signals from the environment and searches until they match an existing condition. After finding it, the decision of an action is taken.

A new stage in increasing the degree of autonomy of robots is represented by self–calibration methods. Studies in this sense are carried out at the Department of Aeronautics and Space Engineering of Tohoku University in Japan [8]. As is known, there are differences between the theoretical design and the practical implementation, as a result of working assumptions, dimensional tolerances, errors from sensors, etc.

An optimal solution is the creation of a device capable of self–calibration, allowing the identification of the real kinematics of the robot.

Also, communication with the robot on mission is also a problem of command and programming. A completely autonomous mobile robot, it no longer responds to external commands, until the completion of the cycle of operations for which it was programmed.

The operation of programming such a robot is very difficult, involving the anticipation of all unforeseen events that may occur.

That is why most of the time a compromise is accepted between autonomy and remote control, i.e., the introduction of a human operator on the control loop capable of making decisions in unforeseen situations, or of taking over the management completely in certain cases.

In this case, the need for fast communication between the robot and the operator becomes obvious, and the amount of information needed to be transmitted or received is very large. The success of the mission may depend on the quality of the transmission.

The field of communications is a field in full swing. Radio communication lines, by electric cable, by optical fiber, optical transmissions, etc. were made. Wireless communications are in continuous development.

Communication protocols have also emerged as a necessity, being logical structures that normalize the flow of communicated data, identify errors and request retransmission, possibly replacing certain data lost during transmission. There are two main types of protocols:

- asynchronous links – taking as examples the RS232 links in electric cable communication;
- synchronous – with example RS422;

Coding – in certain fields, the data transmitted from and to the robot must be protected, to avoid their interception. Thus, the need for codification is imposed, as numerous methods have been developed to achieve this (*Steffen, 2020*).

CONCLUSIONS

The paper highlights some notions in the knowledge, analysis, and use of robots in agriculture, with the aim of making human life easier and highlighting the evolution of technology. At the same time, it highlights certain procedures for the analysis and use of robots in agriculture. The primary field of application of robots in agriculture today is at the harvesting stage.

To exemplify and present some mobile, automated robots, which have the ability to ease people's work, as well as to improve the quality of the techniques and services used in agriculture, there are also the analyzed robots for picking strawberries.

They represent a way to capitalize on the method of picking strawberries, to manage to ease people's work, and to apply advanced technology in agriculture.

The robotics and automation solutions presented come with obvious and demonstrable improvements in precision, efficiency, yield, flexibility and last but not least, significant cost reductions.

A well–planned and integrated automation system can improve labor productivity by more than 50%. However, continuous robotization and automation solutions are also needed in this field in order to succeed in evolving.

Note: This paper was presented at ISB–INMA TEH' 2022 – International Symposium on Technologies and Technical Systems in Agriculture, Food Industry and Environment, organized by University "POLITEHNICA" of Bucuresti, Faculty of Biotechnical Systems Engineering, National Institute for Research–Development of Machines and Installations designed for Agriculture and Food Industry (INMA Bucuresti), National Research & Development Institute for Food Bioresources (IBA Bucuresti), University of Agronomic Sciences and Veterinary Medicine of Bucuresti (UASVMB), Research–Development Institute for Plant Protection – (ICDPP Bucuresti), Research and Development Institute for Processing and Marketing of the Horticultural Products (HORTING), Hydraulics and Pneumatics Research Institute (INOE 2000 IHP) and Romanian Agricultural Mechanical Engineers Society (SIMAR), in Bucuresti, ROMANIA, in 6–7 October, 2022.

References

[1] International Data Corporation, cited by Gizmodo, https://www.zf.ro › business–international › A devastating future for employees: The introduction of robots on the labor market will lead to a decrease in wages and the replacement of people. A revolution that will change everything, March 29. 2017 (zf.ro).
[2] https://revistadinlemn.ro/2019/06/20/robotizare–automatizare–productie–mobilier/.
[3] Bonirob with a soil penetrometer/Download Scientific Diagram (researchgate.net), Available online.
[4] Aranvid K.R, Raja P., Pérez–Ruiz M. Task–based agricultural mobile robots in arable farming: A review, Spanish Journal of Agricultural Research 2017, 15(1)
[5] https://agroverde.ro/blog/a–fost–nevoie–de–cinci–ani–pentru–a–crea–un–robot–de–capsuni.
[6] Xiong Y.,Ge Y., From P. J. An obstacle separation method for robotic picking of fruits in clusters, Computers and Electronics in Agriculture 2020, 175, 105397
[7] Danielczuk M., Mahler J., Correa C., Goldberg K. Linear push policies to increase grasp access for robot bin picking 2018, IEEE 14th international conference on automation science and engineering (CASE), 20–24 August, Munich, Germany
[8] Steffen L. Meet Odd.Bot – The Weed–Pulling Robot That Uses No Chemicals (intelligentliving.co) 2020, March 2, Available online.
[9] Gramescu B. Mobile robots 2018, CD–ROM electronic edition, Bucharest

ISSN: 2067-3809

[1.]Elena Mihaela NAGY, [1.]Teodor Gabriel FODOREAN, [1.]Nicolae CIOICA, [2.]Lucian FECHETE–TUTUNARU

INFLUENCE OF MINERAL ADDITIVES IN THE COMPOSITION OF GRANULAR ORGANO–MINERAL FERTILIZERS BASED ON BIOSOLIDS ON THEIR PROPERTIES

[1.]INMA Bucharest, ROMANIA
[2.]Technical University of Cluj Napoca, Faculty of Automotive, Mechatronics and Mechanical Engineering, ROMANIA

Abstract: The use of sludge in agriculture can contribute to reducing environmental pollution due to the disposal of waste sludge from wastewater treatment plants, thus avoiding incineration or other polluting and costly processes. Biosolids for agriculture are obtained from raw sewage sludge by digestion and stabilisation processes. These processes ensure the reduction of toxic chemicals and pathogen concentrations in sludge so that its use in agriculture does not harm soil, plants, groundwater and not least the health of consumers of agricultural plant and animal products. Biosolids can be used as a source of organic matter for some organic or organo–mineral fertilizers. In order to obtain a valuable organo–mineral fertilizer in terms of nutrient composition, it is necessary to enrich the biosolid by adding minerals/ingredients to the recipe. The characteristics of the resulting fertilizers must meet the requirements of the organo–mineral fertilizer category. The paper presents research on the influence of mineral fertilizer additions on some physico–chemical properties of granular biosolid fertilizers, such as: grain moisture, grain size fraction, compressive strength and bulk density.
Keywords: mineral**,** biosolids, fertilizer, properties

INTRODUCTION

In order to reduce the negative effects of the use of chemical fertilisers on the environment, research in recent years has focused on finding new sources of fertilisers with a higher organic content. In order to benefit from similar advantages as mineral fertilizers, ways of processing organic fertilizers are currently being sought that allow for the easiest possible application, ensure the necessary concentration and stability during plant growing seasons (*Aguilera, J., et al., 2012*).

An important source of organic matter and nutrients that can be used in agriculture as a fertilizer is sludge from sewage treatment plants. The use of sludge in agriculture can contribute to reducing environmental pollution due to the disposal of waste sludge from wastewater treatment plants, thus avoiding incineration or other polluting and costly processes (*Adugna, 2016; Bowszys et al., 2015;*).

Biosolids for agriculture are obtained from raw sewage sludge by digestion and stabilisation processes. These processes ensure the reduction of toxic chemicals and pathogen concentrations in sludge so that its use in agriculture does not harm soil, plants, groundwater and not least the health of consumers of agricultural plant and animal products (*Kominko et al., 2018; Kumar et al., 2017; Pöykiö et al., 2019*).

Organo–mineral fertilizers, according to the European Parliament Regulation on CE–marked fertilizer products, are obtained by mixing organic material with mineral fertilizers and nutrients of biological origin (*EC No. 1069/2009 and EC No. 1107/2009, Annex 1, 2016*). Organo–mineral fertilizers obtained by mixing organic material (e.g. biosolids) and minerals in well–established proportions offer various advantages (*Blaga, Gh. et al, 2008; Parent et al. 2003; Lee & Bartlett, 1976; Tishkovitch et al., 1983*).

Generally organo–mineral fertilizers are made in granular form, a form that allows precise application with chemical fertilizer application equipment, reduction of storage space and pollution due to dust arising during handling (*Deeks et al., 2013*).

In this paper some properties of biosolids–based fertilizer granules obtained after a technology developed by INMA Bucharest (*Siminiceanu, I., 1980; Nagy, M. E., et al. 2018*), were studied to highlight the influence of some mineral additions in the recipe on their properties.

MATERIAL AND METHOD

To obtain organo–mineral granular fertilizers, a mixture of organic (biosolid, milasses and protein hydrolyzate based on wool) and mineral (N,P,K) components was processed by reactive extrusion and granulation. The main organic component used in the formula was the biosolid obtained from raw sewage sludge from Mioveni wastewater treatment plant. The main quality indicators of the biosolid used are presented in table 1.

The manufacturing formula was prepared in two variants whose composition is presented in table 2. The saples subjected to experients are presented in figure 2. In addition to organic and mineral components, starch has been added to the formula to provide the matrix required for reactive extrusion processing. The experiments aimed

to determine the influence of the addition of minerals in the granular fertilizer formula on its properties. The properties studied were particle size fractions, the water content of the granules, bulk density of the granules and compressive strength.

Table 1. Biosolid quality indicators *(Raport de încercări INCDPM)*

No.	Quality Indicators	U. M.	Determined values
1	Dry matter	%	67.86
2	Volatile substance	%	35.34
3	pH measured at 20,6 ^{0}C	pH units	7.09
4	Nitrogen	% D.M	1.52
5	Organic carbon	% D.M	21.5
6	P_2O_5	% D.M.	1.38
7	K_2O	% D.M	0.675
8	CaO	% D.M	0.35
9	Cadmium	mg/kg D.M	1.04
10	Chromium	mg/kg D.M	44.8
11	Copper	mg/kg D.M	74.3
12	Nickel	mg/kg D.M	26.5

(a)

(b)

Figure 1 – Granular fertilizer material based on biosolids
a) –variant V1, b)–variant V2

Table 2. Composition of formulas used to manufacture granular fertilizer material based on biosolids

Nr crt.	Substance used	Percentages, %	
		Variant 1	Variant 2
1	Dry compost, humidity 20%	30,00	30,00
2	Monoamoniufosfat (MAP)	24,50	0,00
3	Mineral fertilizer NP 20:20	0,00	24,00
4	Potassium nitrate, KNO3	22,20	23,10
5	Urea	5,30	6,30
6	Protein hydrolyzate solution,11 %	4,00	4,00
7	Starch	7,98	7,47
8	Magnesium sulphate, $MgSO_4$	3,30	2,82
9	Zinc sulphate, Zn SO_4	0,08	0,07
10	Copper sulphate, $CuSO_4$	0,05	0,04
11	Iron sulphate, $FeSO_4$	0,11	0,09
12	Manganese sulphate, $MnSO_4$	0,22	0,19
13	Cobalt sulphate, $CoSO_4$	0,03	0,03
14	Molasses of sugar beat	2,23	1,89

In order to determine the particle size fractions, samples of 50 g of each variant were sieved through diferent sieves with an eye size of 4; 2; 1; 0.5 and 0.25 mm.

To determine the water content of the granules we used samples of about 5 g of granules, which were dried at 80 °C, with a thermobalance type AXIS–100 with a weighing accuracy of 0.01%, fig.2. At every 20 seconds the masses were recorded until at least 3 consecutive equal values were obtained. The difference between the initial and final mass of the samples gives us the moisture content.

Figure 2 – Determination of moisture content with thermobalance AXIS –100

In order to determine the bulk density of the organo–mineral fertilizer we used a calibrated vessel of volume V = 0.03 dm^3 with mass m = 27.55 g. For measurements we poured the granules into the vessel from a height of 5 cm, than the vessel was buffered 50 times by a wooden table and weighed again, to obtain the mass m_1. Compact bulk density was calculated using the formula:

$$\rho = (m_1 - m) / V \quad (1)$$

The compression tests, figure 3, were performed with a manual press equipped with a 5 kN force transducer, a mechanical dial indicator, the data being taken over and processed by means of a Spider 8 data acquisition plate. One granule was used for the measurements, the measurements being repeated by 5 times to determine the average value of the compressive strength for each variant.

Figure 3 – Compression test

RESULTS

In table 3 are presented the results obtained from the granulometric analysis of the granular organo–mineral fertilizer based on biosolids.

From the analysis of the data obtained we observe that the granules in both variants falls within the technical requirements established by EC Regulation no. 2003/2003 regarding the granulometric structure of fertilizers, namely: min. 90% between 1 and 4 mm and max. 10% less than 1 mm or more than 4 mm. Also, the addition of NP 20–20 (variant 2) leads to an increase in the percentage of granules between 1 and 2 mm due to a lower phosphorus content compared to variant 1 to which MAP with a P_2O_5 content of 61%has been added. The data obtained from the determination of water content and bulk density are presented in Table 4.

Table 3. Granulometric composition

Granulometric fraction	Granule mass, g / percentage parts,%			
	Variant 1		Variant 2	
between 2 and 4 mm	43,10	85,6%	34,73	68,9%
between 1and 2 mm	6,46	12,8%	15,09	29,9%
between 0,5 and 1 mm	0,52	1%	0,21	0,4%
between 0,25 and 0,5 mm	0,21	0,4%	0,29	0,6%
< 0,25	0,09	0,2%	0,11	0,2%
Total	50,38	100%	50,43	100%

Table 4. Results obtained from experiments

No.	Characteristics	U.M.	Fertilizer material based on biosolids	
			Variant I	Variant II
1	Water content	%	1,33%	3,74%
2	Bulk density	kg/m^3	855,1	854,7

Analysing the data obtained, we note that the water content falls within normal limits, the higher value being registered for Variant 2–with less phosphorus. The bulk density is not influenced by mineral additions (phosphorus content), and has relatively low values due to the biosolid component which is characterized by low specific weight.

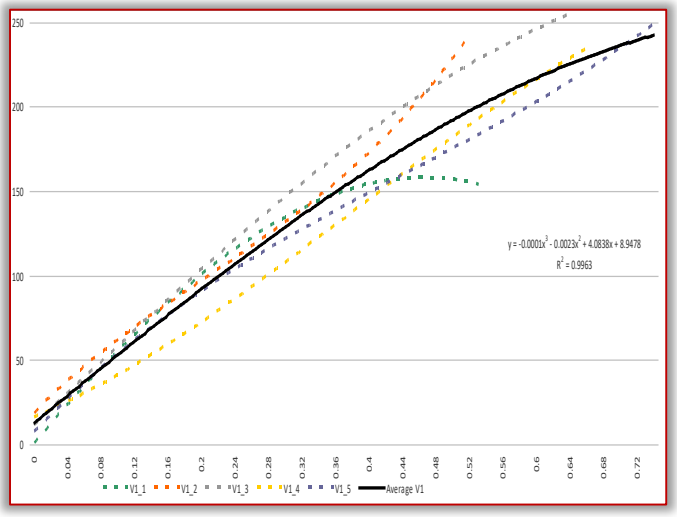

Figure 4 – Diagrams of compressive strength for Variant 1– with Monoammoniumphosphate (MAP)

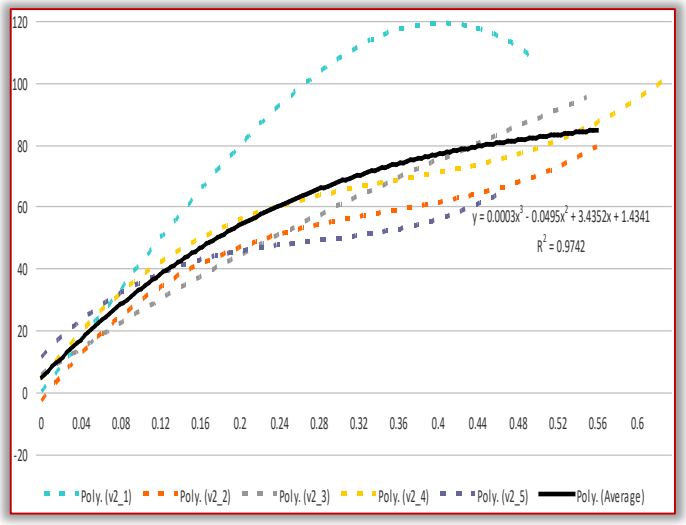

Figure 5 – Diagrams of compressive strength for Variant 2 – with NP 20–20

From the graphs shown in figure 4 and figure 5 it can be seen that for both variants the polynomial equation obtained shows an almost linear behaviour of the granule deformation in relation to the applied compressive force. For Variant 1 the predominantly linear character is observed up to a stress of 150 N and an average deformation of about 0.36 mm, while in the case of Variant 2 – with a lower phosphorus content, the value up to which the predominantly linear character is observed is less than 60 N at a deformation of about 0.24 mm.

Above these values, polynomial character is observed for both samples, in the case of variant 1 up to a maximum value of 250 N with a deformation of about 0.68 mm, and for variant 2 up to a maximum value of 85 N at which the deformation reached the value of 0.56 mm.

Above these values of compressive strength, the granules do not deform anymore during mechanical stress.

CONCLUSIONS

From the research carried out, it was observed that the manufacturing recipes used allow obtaining a granular fertilizer material based on biosolids that meets the requirements for organo–mineral fertilizers.

The analysis of the obtained results shows the influence of the phosphorus content on the properties of the granules, respectively the samples of the variant 2 with a lower phosphorus content have a lower compressive strength (60–85 N) which leads to a higher fraction of granules with diameters between 1–2 mm (12.8%).

Also the lower phosphorus content means that the granules in variant 2 have a higher water content (3.74%) than those in variant 1 (1.33%).

A good understanding of the characteristics of granular organo–mineral fertilizers based on biosolids allows the identification of the mineral additions needed to optimize formulations according to requirements.

Acknowledgement

This research work was carried out with the support of Ministry of Research, Innovation and Digitalization through Program 1 – Development of the national

research–development system, Subprogram 1.2 – Institutional performance – Projects for financing excellence in RDI, Contract no. 1PFE/30.12.2021 and with the support of Ministry of Agriculture and Rural Development through the Sectorial Plan – "Agriculture and Rural Development – ADER 2022", contract no. 7.3.10.

Note: This paper was presented at ISB–INMA TEH' 2022 – International Symposium on Technologies and Technical Systems in Agriculture, Food Industry and Environment, organized by University "POLITEHNICA" of Bucuresti, Faculty of Biotechnical Systems Engineering, National Institute for Research–Development of Machines and Installations designed for Agriculture and Food Industry (INMA Bucuresti), National Research & Development Institute for Food Bioresources (IBA Bucuresti), University of Agronomic Sciences and Veterinary Medicine of Bucuresti (UASVMB), Research–Development Institute for Plant Protection – (ICDPP Bucuresti), Research and Development Institute for Processing and Marketing of the Horticultural Products (HORTING), Hydraulics and Pneumatics Research Institute (INOE 2000 IHP) and Romanian Agricultural Mechanical Engineers Society (SIMAR), in Bucuresti, ROMANIA, in 6–7 October, 2022.

References

[1] Adugna G., (2016) A review on impact of compost on soil properties, water use and crop productivity, Academic Research Journal of Agricultural Science and Research, vol. 4, no. 3:93–104

[2] Aguilera J., Motavalli P. P., Gonzales M. A., Valdivia C., (2012), Initial and residual effects of organic and inorganic amendments on soil properties in a potato–based cropping system, American Journal of Experimental Agriculture, Vol.2, pp. 641–666.

[3] Blaga Gh., et al. (2008). Pedologie, Ed. Mega, Cluj–Napoca.

[4] Bowszys, T., Wierzbowska, J., Sternik, P. & Busse, M.K., (2015). Effect of the application of sewage sludge compost on the content and leaching of zinc and copper from soils under agricultural use, Journal of Ecological Engineering, vol. 16, no. 1: 1–7.

[5] Deeks, L. K., Chaney, K.C., Murray, C. & Sakrabani, R., (2013) A new sludge–derived organo–mineral fertilizer gives similar crop yields as conventional fertilizers, Agronomy for Sustainable Development, vol. 33, pp. 539–549.

[6] Kominko, H., Gorazda, K., Wzorek, Z., & Wojtas, K., (2018), Sustainable Management of Sewage Sludge for the Production of Organo–Mineral Fertilizers, Waste Biomass Valorization, vol. 9, pp. 1817–1826.

[7] Kumar, V., Chopra, A.K., & Kumar, A., (2017), A review on sewage sludge (Biosolids) a resource for sustainable agriculture, Archives of Agriculture and Environmental Science, vol. 2, no.4, pp. 340–347;

[8] Lee, Y.S. and R.J. Bartlett.(1976). Stimulation of plant growth by humic substances. Soil Science Society of America Journal 40: pp. 479–576

[9] Nagy M. E., et al. (2018). Research on the development of a technology for obtaining peat–based granular organo–mineral fertilizers, ISB INMATEH 2018– Proceedings, pp. 73–79.

[10] Parent L.–E.,Khiari L., Pellerin A., .(2003) The P fertilization of potato: Increasing agronomic efficiency and decreasing environmental risk. Acta Horticulturae, Vol. 627, pp.35–41.

[11] Pöykiö R. et al., (2019), Characterisation of municipal sewage sludge as a soil improver and a fertilizer product, Ecological Chemistry and Engineering S, vol. 26, no. 3, pp.547–557.

[12] Siminiceanu I., (1980). Tehnologia ingrasamintelor compuse: granulare, conditionare, testare, Institutul Politehnic Iasi, Facultatea de Chimie Industriala.

[13] Tishkovitch, A.V., A.S. Meyerovsky, G.P. Viryassov, G.A. Oussyouke´Vitch and E.V. Barranikova.(1983).Peat as a fertilizer [in Russian]. Ed Nauka i tekhnika, Minsk, Belarus.

[14] *** Regulament al Parlamentului European și al Consiliului de stabilire a normelor privind punerea la dispoziție pe piață a produselor fertilizante cu marcaj CE și de modificare a Regulamentelor (CE) nr.1069/2009 și (CE) nr. 1107/2009, Anexa 1, 2016.

ISSN: 2067-3809

[1.]Carmen BĂLȚATU, [2.]Sorin–Stefan BIRIȘ, [1.]Eugen MARIN, [1.]Marinela MATEESCU, [1.]Gabriel GHEORGHE, [1.]Dragos MANEA, [3.]Gabriela MATACHE,[4.]Robert BILA, [4.]Oana–Diana MANOLELI–PREDA, [4.]Adrian PANDELE

DESIGN AND STRESS ANALYSIS OF THE SCREW OF THE MECHANICAL PRESS TO OBTAIN GRAPE SEED OIL

[1.]INMA Bucharest, ROMANIA
[2.]Politechnica University of Bucharest, Faculty of Biotechnical Systems Engineering, ROMANIA
[3.]INOE 2000–IHP Bucharest, ROMANIA
[4.]ROLIX IMPEX SERIES SRL, ROMANIA

Abstract: The extraction of oil from oilseed material by mechanical pressing is carried out in special machines called mechanical presses. The press's primary component sections are the transmission, press bearings, feed area, press chamber, screw, and barrel output. The screw plays a crucial role in a press's operation. A rotating helical body (screw) inside a cylinder–shaped enclosed space produces the pressing force (pressing chamber) in mechanical presses. In this article, we have designed the screw of an oil press to obtain oil from grape seeds. To make the 3D model, we used SolidWorks software, after which we also simulated the model under stress conditions. In the first phase, the behavior of the 3D model will be simulated for the screw with which a small press is equipped, a model most often used in farms for obtaining oil. Later we also simulated a screw model with a larger pitch to observe the differences in behavior between them. In this paper, we show whether the different pitch of the screw press models influences their degree of erosion and fatigue.

Keywords: grape seeds, Solidworks, screw press, simulation

INTRODUCTION

The extraction of oil from oilseed material by mechanical pressing is carried out in special machines called mechanical presses. These machines fall into two main categories: hydraulic presses and auger presses.

Hydraulic presses, so called because they are operated by liquid pressure, were first made in England and patented by Joseph Bromah in 1795. The working pressure, in these presses, is applied to a stationary mass by means of levers, jacks or hydraulic cylinders, and the oil removed from the compressed oily material is collected by rings at the bottom, (*Bargale, 1997*).

V. D. Anderson created the first screw press in the United States in 1900. In contrast to hydraulic presses, this press allowed operations to be carried out continuously, processing higher capacity with less equipment and less work, (*P. Evon et. al, 2009; C.N. Okoye et. al, 2008*). Thus, screw presses have gradually replaced hydraulic presses in oil extraction units, (*R.P. Hutchins et. Al, 1949*).

Mechanical presses are grouped into the following categories based on the degree of oil separation (more specifically, the amount of oil still in the broken), (*Milea D., et. al, 2018*):

- pre– or ante–press presses that guarantee the separation of 75–85% of the oil; these presses are made for moderate pre–press (with 18–22% oil in the broken) or advanced ante–press (with 12–14% oil in the broken); the latter kind may process 50% more seed while operating in moderate pressing mode;
- presses used for final pressing, which eject shattered objects with 3–5% oil;
- double action presses combine two pressing chambers in one machine to perform the final pressing and the pre–pressing.

The press's primary component sections are the transmission, press bearings, feed area, press chamber, screw, and barrel output. The press drive's main function is to transfer power from the press auger to the electric drive motor. Because it needs to be situated in the coolest, cleanest, and most effective region feasible for the best performance, the transmission is placed before the press feed area, where the pressure is the lowest, (*Choi, Y. et. al, 2009*).

The feed area is compounded from the food connection, horizontal feed zone, and vertical feed zone. A conveyor auger is located between the two zones, and the horizontal zone's screw speed variation allows the press's material feed rate to change, (*M.O. Faborode et. al, 1993*).

The pressing chamber for industrial press models is of the slotted drum type (Figure1). This type of pressing chamber consists of metal bars arranged side by side and separated by spacers to create oil discharge slots. The perforated cylinder press chamber (Figure 1), a different type of press chamber, consists of a cylinder with oil

discharge ports in the form of milling holes placed in a certain location of the cylinder. As one gets closer to the discharge end, the compressive forces generated in the press chamber increase. Oil is driven through the perforations in the cylinder and discharged from the seed close to them. The oil is released from the press as pellets through the discharge end, which is made of replaceable nozzles. To prevent clogging of the barrel at the outflow, the nozzles are typically heated, (*M.O. Faborode et. al, 1993*).

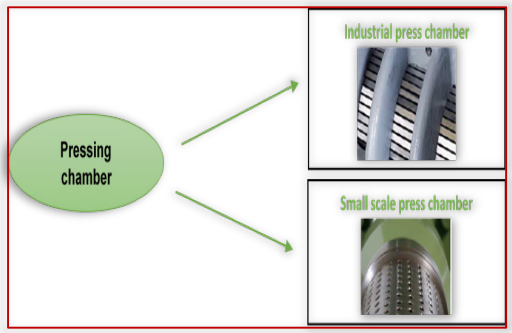

Figure 1 – Tow models of pressing champers (E. Ferchau, 2000, J.B. Xiao et. al,2007)

The screw plays a crucial role in a press's operation. A rotating helical body (screw) inside a cylinder–shaped enclosed space produces the pressing force (pressing chamber) in mechanical presses. The helical coil can be produced separately and welded to a tubular shaft or a solid shaft, or the screw can be created by spinning a cylindrical bar (the material matching the helical groove is removed). The design of the screw assembly is crucial for a successful press since it must consider how to produce high–quality oil and barrels with the least amount of energy. Different screw configurations are possible; some fundamental auger configurations are listed here, Figure 2. The screw variations with a diameter of and perhaps with variable pitch are thought to be inexpensive, (*V.V. Jinescu, 2007*), as variable diameter design variants are pricey.

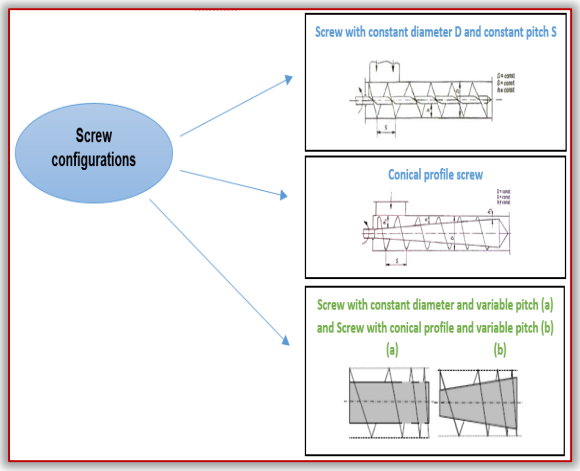

Figure 2 – Multiple models of the screw (*V.V. Jinescu, 2007, P. Sari, 2006*)

For this paper, we used the screw from a small press with a continuous pitch and a conical profile as a model. The screw has been 3d modeled and subjected to a simulation. The screw press's design has a significant impact on the amount and calibre of oil produced, (*Yaolin, 1981*). The pressing screw is a component of an assembly, and it is the most crucial component. It functions under the influence of friction forces from oil–based materials and various types of resistance forces, with surface wear and screw tooth fracture serving as the primary failure modes, (*Xuege Zhang et al. 2012; Yanan Pi et. al, 1996*).

MATERIALS AND METHOD

The oil press used as a model in these papers is presented in Figure3. Is a press whit a small working capacity, suitable for farms that want to obtain cold–pressed oil from various oilseeds.

Figure 3 – Small screw press

For this screw press, we have two screws with different pitches, Figure4, which have been 3D designed in the SolidWorks program.

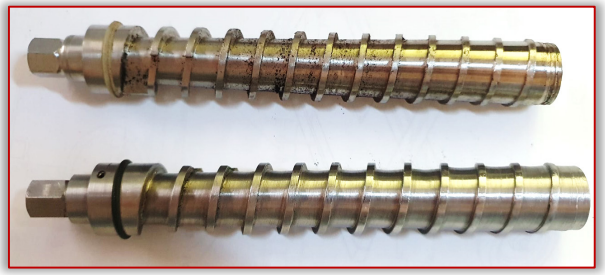

Figure 4 – Two screws with different pitches

After the 3D design of the two screw models, we prepared the part for its torsion simulation. We selected the material from which the screw is made, namely AISI 316 – Stainless Steel. This is steel that can be used for equipment in the food industry and has the properties shown in Figure 5.

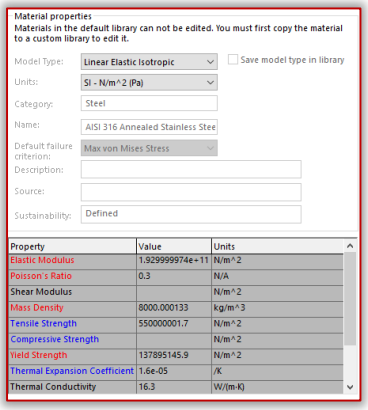

Figure 5a – Material properties AISI 316 – Stainless Steel

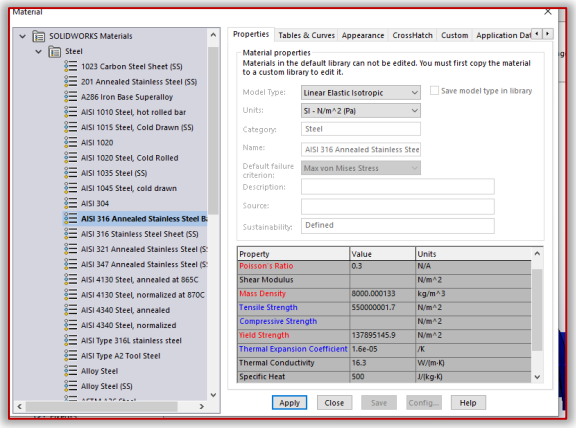

Figure 5b – Material properties AISI 316 – Stainless Steel

The next step was to fix the screw and apply 5Nm torque on all its surface, like in Figure 6.

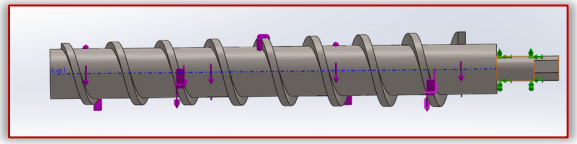

Figure 6 – 3D model of screw

A very important stage of design analysis is meshing. The software's automatic mesher creates a mesh based on the specifications for the global element size, tolerance, and local mesh control.

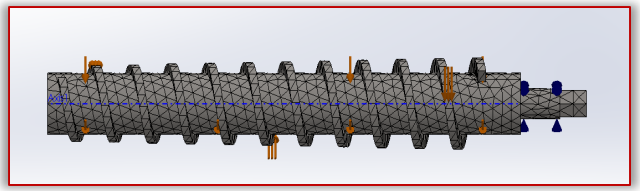

Figure 7 – Mesh of screw

RESULTS

The six components of stress are used to calculate von Mises stresses using the von Mises stress plot. The von Mises stress results are traditionally calculated using only the positive values of the stress components since the results of linear dynamic harmonic studies are generated for the greatest steady–state oscillation amplitude. When one stress component is positive and another is negative, there may be "stress phase offsets." According to the von Mises equation, the square of the difference between the values of a positive and negative stress component may be greater than the difference between the values of a positive and negative stress component.

Given that the screw is embedded in the thinnest end, the toque motion makes the screw have the most constricted area in the screw fixing area. According to the von Mises diagram, in the case of the larger pitch screw, the values shown are higher than for the 10mm pitch screw. The difference can also be seen in Figure 9, in which samples are taken along the screw and the maximum point of the screw is shown.

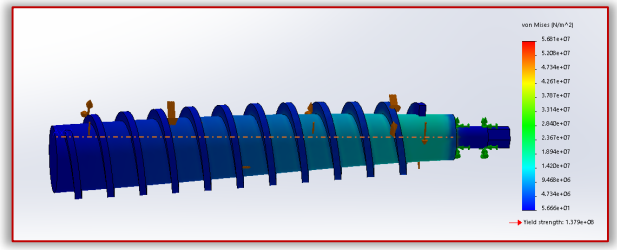

(a)

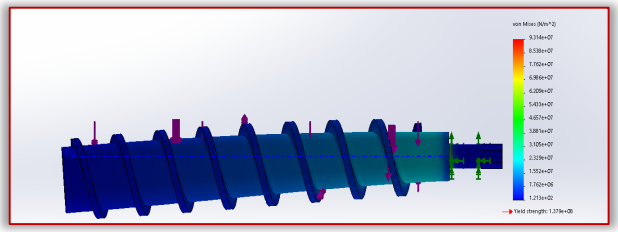

(b)

Figure 8 – von Mises stresses of screw: a) 10 mm pitch; b) 18 mm pitch.

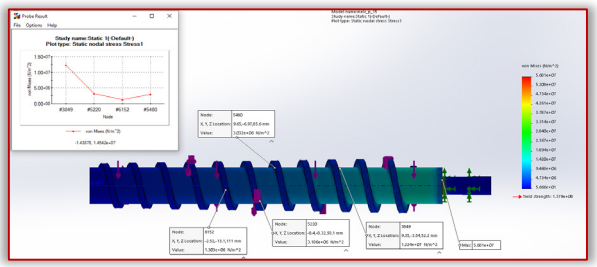

(a)

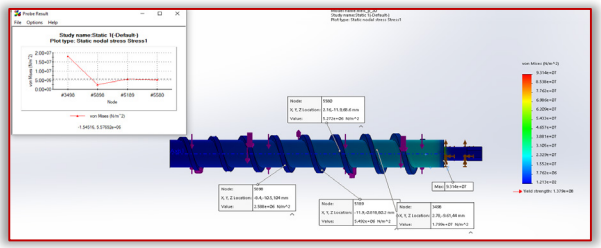

(b)

Figure 9 – Samples along the screw: a) 10 mm pitch; b) 18 mm pitch

It is clear that the stress is primarily concentrated at the side and root of the screw flight, increases spirally, and peaks at the root position close to the screw end. This pattern closely resembles the results of the strength check calculation and corresponds to the real loading conditions.

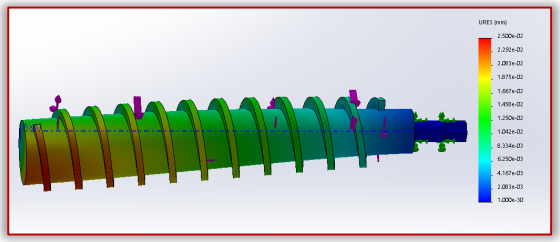

(a)

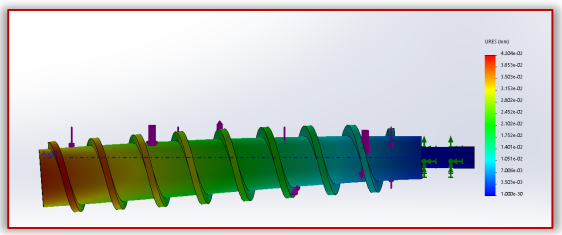

(b)

Figure 10. Displacement along the screw: a) 10 mm pitch; b) 18 mm pitch

CONCLUSIONS

Taking a typical screw press as an example, a simplified three–dimensional model of its pressing screw was established, and then a static calculation was done for this model using the finite element method to obtain its continuous deformation and stress distribution. This was done in consideration of the complexity and drawbacks of the traditional analysis and check method for the pressing screw.

According to this study, the pressing screw's stress mostly develops at the side and root of its screw flight, rises with the spiral, and peaks close to the root end. The interaction of the axial force and circumferential force results in this stress concentration state. It can be efficiently resolved by changing the design of the structure, selecting different materials, upgrading the processing procedures, or employing different heat treatment methods, hence increasing the security and dependability of the entire system.

Using the finite element method can save a significant amount of processing time and allow for direct observation of the object's deformation and stress distribution in comparison to the traditional design, analysis, and check procedure. It significantly increases design efficiency and dependability and serves as a crucial point of reference for structural design.

Acknowledgement

This paper was financed with the support of National Agency for Scientific Research and Innovation, NUCLEU Programme, no. 5N / 07.02.2019, project PN 19/10/01/03 – "Fundamentarea tehnologiei de recoltare şi prelucrare primară a tulpinilor de cânepă în verde".

Note: This paper was presented at ISB–INMA TEH' 2022 – International Symposium on Technologies and Technical Systems in Agriculture, Food Industry and Environment, organized by University "POLITEHNICA" of Bucuresti, Faculty of Biotechnical Systems Engineering, National Institute for Research–Development of Machines and Installations designed for Agriculture and Food Industry (INMA Bucuresti), National Research & Development Institute for Food Bioresources (IBA Bucuresti), University of Agronomic Sciences and Veterinary Medicine of Bucuresti (UASVMB), Research–Development Institute for Plant Protection – (ICDPP Bucuresti), Research and Development Institute for Processing and Marketing of the Horticultural Products (HORTING), Hydraulics and Pneumatics Research Institute (INOE 2000 IHP) and Romanian Agricultural Mechanical Engineers Society (SIMAR), in Bucuresti, ROMANIA, in 6–7 October, 2022.

References

[1] Choi, Y., & Lee, J. (2009). Antioxidant and antiproliferative properties of a tocotrienol–rich fraction from grape seeds. Food Chemistry, 114(4),1386–1390

[2] C.N. Okoye, J. Jiang, L.Y. Hui, „Design and development of secondary controlled industrial palm kernel nut vegetable oil expeller plant for energy saving and recuperation", J Food Eng, 2008; 87:578–90.

[3] E. Ferchau, „Equipment of Decentralized Cold Pressing of Oil Seeds", Webpage of Folkecenter For Renewable Energy, 2000, www.folkecenter.dk.

[4] J.B. Xiao, J.W. Chen, M. Xu, „Supercritical fluid CO2 extraction of essential oil from Marchantia convoluta: global yields and extract chemical composition", Electronic Journal of Biotechnology, vol. 10, no. 1, 2007

[5] Milea D., Vişan A.L., Păun A., Bogdanof C.G., Stroescu Gh. (2018) Performant equipments designed for grape marc seeds separation and calibration for supperior capitalization in food and phytopharmaceutical industry, 853–862, http://isbinmateh.inma.ro/archive.html

[6] Milea D., Vişan A–L., Păun A., Bogdanof C–G., Ciupercă R., Paraschiv G. (2018) Technological and ecological aspects of some wine waste recycling and their capitalization in food industry, Annals of the University of Craiova – Agriculture, Montanology, Cadastre Series, Vol. 48, pg. 320–327, http://anale.agro–craiova.ro/index.php/aamc/article/view/838

[7] M.O. Faborode, J.F. Favier, „Identification and Significance of the Oil–point in Seed–oil Expression", Journal of Agricultural Engineering Research, v. 65, p. 335–345, 1996.

[8] P.C. Bargale, „Mechanical oil expression from selected oilseeds under uniaxial compression", Ph.D. Thesis, University of Saskatchewan, Canada, 1997.

[9] P. Evon, V. Vandenbossche, P.Y. Pontalier, L. Rigal, „Aqueous extraction of residual oil from sunflower press cake using a twin–screw extruder: feasibility study", Ind Crop Prod, 2009; 29:455–65.

[10] P. Sari, „Preliminary design and construction of a prototype canola seed oil extraction machine", Ph.D. Thesis, Middle East Technical University, Ankara, Turkey, 2006.

[11] R.P. Hutchins, „Processing of oilseeds and nuts by hydraulic and mechanical screw press method", Journal of the American Oil Chemists' Society, 26:559–563, 1949.

[12] V.V. Jinescu, 2007, „Maşini cu elemente elicoidale", vol. I, Editura AGIR, Bucureşti.

[13] Yaolin Tan. Oils and fats technology, Vol. 6 (1981), p. 287

[14] Yanan Pi, Xingming Wang, Lili Dai, etc. China oils and fats, Vol. 21 (1996), p. 49

[15] Xuege Zhang, Yi Wu, Jinglan Ruan. Packaging and food machinery, Vol. 30 (2012), p. 47

ISSN: 2067-3809

[1.] Peter Olabisi OLUSEYI, [1.] E.A. OJO

OPTIMUM PROTECTION STRATEGY OF PV SYSTEMS AGAINST LIGHTNING INDUCED FAULTS

[1.] Department of Electrical and Electronics Engineering, University of Lagos, Lagos, NIGERIA

Abstract: The incidence of lightning discharges and efficient protection of photovoltaic electrical networks against induced faults has been a crucial problem. A common method for solving this problem is to install surge protection devices in the photovoltaic electrical network. However, for a large PV electrical system, a great challenge is to find critical points in the network where surge protection devices can be installed to adequately protect the total photovoltaic electrical network while keeping the total number of installed surge protection devices at a minimum. To solve this challenge, this paper presents a method for the optimization of photovoltaic network protection using the genetic algorithm optimization method to find specific points for the installation of a minimum number of surge protection devices while maximizing the number of protected equipment in the network. The photovoltaic system is modeled and simulated using mathematical laboratory/Simulink (i.e. MATLAB/Simulink). The results obtained showed that at lightning strike, the voltage levels in the photovoltaic network were kept within acceptable limits while minimizing the number of surge protection devices used. Thus, it can be concluded that the genetic algorithm (GA) protection optimization method is effective for a large photovoltaic network.
Keywords: Genetic algorithm; Surge protective device; Lightning discharge; Photovoltaic system

INTRODUCTION

This paper presents a method for the optimum protection strategy of photovoltaic systems against lightning induced faults. The objectives of this research are to establish the effects of lightning discharge on photovoltaic network, model the case study photovoltaic network and develop a method for the strategic placement of surge protective devices in a given photovoltaic network. Lightning discharge is a transient current pulse. It is a short-lived phenomenon and it is observed that a single strike is consisting of several small strikes of different properties. Lightning is capable of injecting overvoltage transients into DC networks resulting into undesirable effects on direct current (DC) equipment including photovoltaic (PV) cells (Shahniaand, F. et al, 2006).

In the 1980s, photovoltaics became a popular power source for consumer electronic devices, including calculators, watches, radios, lanterns and other small battery-charging applications. Following the energy crises of the 1970s, significant efforts also began to develop PV power systems for residential and commercial uses, both for stand-alone, remote power as well as for utility-connected applications. During the same period, international applications for PV systems to power rural health clinics, refrigeration, water pumping, telecommunications, and off-grid households increased dramatically, and remain a major portion of the present world market for PV products. (Florida Solar Energy Center, 2007).

Photovoltaic (PV) systems are susceptible to failures from atmospheric discharges that could interrupt the normal operation of converting solar energy to electrical power energy. Atmospheric discharges are able to cause failures on PV systems mainly due to expanded surface areas, installation in wide-open areas and elevated heights. PV systems can experience large discharge of energy from a lightning strike and electromagnetic interference due to the coupling elements of the PV systems which include cables, solar module metallic frame, earthing system, etc (Fallah et al, 2013).

In many parts of the world where PV systems are installed, most designers and installers ignore the likelihood of lightning discharge in the area which could induce faults in the systems, thus the PV systems are not adequately protected against lightning induced faults (Ittarat, S. 2013). Lack of adequate protection on the systems can induce faults on systems thereby incurring an avoidable cost of repair. Accumulated cost of repair is eventually higher than the cost of providing an adequate protection on the systems. Inadequate or lack of protection can also increase the time of the return of investment on the PV systems (Ehrhardt, A. et al, 2014). Therefore, it is necessary to incorporate an appropriate lightning protection system (LPS). However, the avoidance of lightning is not adequate as lightning current passing through an LPS may induce faults in the PV system due to inductive coupling. Thus, PV systems should be strategically placed and the insulation of conducting components wherever possible should be done (Kern, A. et al, 2004 , Fallah et al, 2013 & Spooner, E. 2001).

Various methods of lightning protection have been investigated, developed and applied. The earliest described method of lightning protection was the Franklin rod system proposed by Lichtenberg, G.C in 1778. This system consists of 3 main parts: Air terminal, Down conductor and Ground terminal. In 1876, James Clerk Maxwell suggested the Faraday Cage approach of protection in which case the lightning current is constrained to the exterior of the cage and it is not necessarily grounded (Vladimir, A.R 2017).

COMMON PV PROTECTION PRACTICES

Empirical methods based on statistics and experiments were employed in evaluating the need for protection and protection levels of PV installations against lightning induced faults over varying potential situations. In a method, two levels of lightning protection measures have been defined for optimum protection of PV systems for various PV installation situations. These are Protection Level A for common lightning risk and Protection Level B for high lightning risk. For protection level A. all exposed conductive parts are interconnected and then properly connected to the ground; individual components are not to be independently connected to the ground. The external protection by varistors on DC and alternating current (AC) circuits is then implemented. Specific protection is provided on other external lines such as telephone lines with no direct link to the PV system. Protection level B, the ground conductors of individual components are interconnected, thereafter properly connected to the ground. External protection by varistors is also provided on DC connections of the installation while appropriate protection is staged on AC aerial grid if present. The shielding of sensitive cables is also done to provide a comprehensive Level B protection for high lightning risk (Lea, P. 2003).

Similarly, a template for the optimum protection of structures adopting the external protection system only was developed. In practical terms, the external lighting protection system consists of an air termination, down conductors and ground electrodes. However, the basic installation of the protection system may not adequately provide protection for the structures when the attractive radius of the structure to lightning extends beyond that of the protection mast. Therefore, the researcher adopted the rolling sphere principle in optimizing the external protection system allocation. In the rolling sphere principle, a sphere is rolled over the protecting structure and areas which the sphere cannot touch are within the protection zone. The radius of the sphere varies between 20 and 60 m depending on the degree of protection required. The researcher however, established a standard radius of 45m wherein an increased degree of protection can be obtained by the reduction of the radius. (Fallah et al, 2013).

The use of Surge Protective Device (SPD) is also a common choice for the protection of PV installations. SPDs installation in a method, is performed as close to the terminals of the equipment. In order to achieve optimum internal protection, three classes of SPDs and respective installation application are defined: SPDs type I, which provide primary protection against 10/350µs lightning current and are installed mainly at the entry point of the installation at the borders between lightning protection zone 0 to 1 (LPZ 0–LPZ 1), representing zones outside the structure and zone in the structure respectively. SPDs type II provide protection against 8/20µs surge currents and are installed at main node points of the installation at the borders between LPZ 1–LPZ 2, with LPZ2 representing the inverter unit. SPDs type III provide fine protection against 8/20µs surge currents and 1.2/50µs surge overvoltages and they protect sensitive electronic devices from impact by lightning striking far away. Type III SPDs should always be installed at least after type II SPDs. (Tong, C. et al, 2014 & Pons, E. et al, 2013).

MODELING AND ANALYSIS

The solar PV system was modeled in the MATLAB Simulink environment. The components of the PV system model include the PV cell array, buck converter, charge controller, battery and inverter. The nodes to be analyzed for voltage surge are identified as points between each component in the PV network. A line diagram showing connected components and nodes is shown in Figure 1.

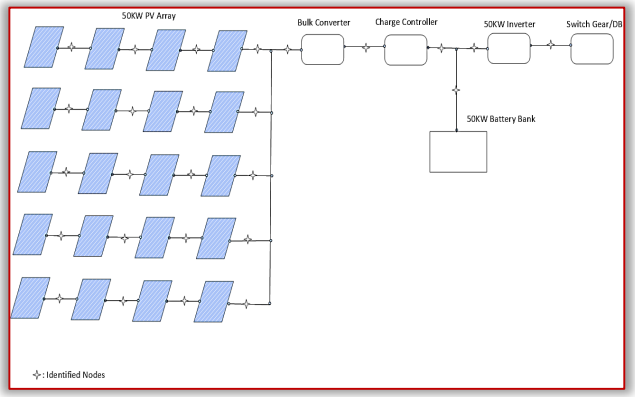

Figure 1. PV Model Under Case Study Showing Identified Nodes

The predefined PV model block available in the Simulink library is used with an irradiance value of 1000 and temperature value of 25 degrees Celsius.

The buck converter as shown in Figure 2 acts as a regulator to convert the DC input from the array of PVs to either a higher amount of DC or a lower amount of DC as required by the system for the charging of the battery system or the conversion of the DC power to AC power by the inverter system (Esram, T. et al, 2007). The buck system is built up of a high-power inductor coupled with a small value resistor, a insulated-gate bipolar transistor

(IGBT) switching component, snubber diode and a coupled resistor-capacitor component for the input and output terminals of the buck converter. The IGBT duty cycle is controlled by an input signal, s_boost from the pulse width modulation (PWM) generator.

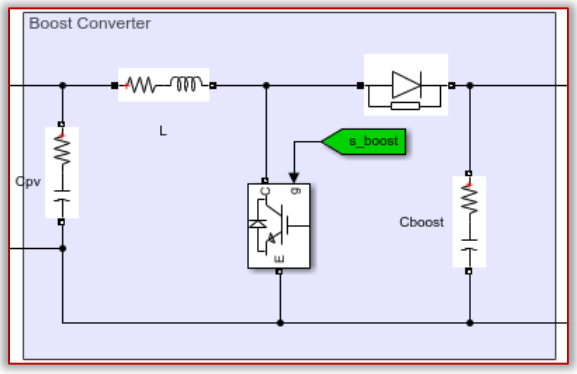

Figure 2. Buck Converter

The current (I) and voltage (V) characteristics of a PV cell is non-linear under certain irradiance and temperature. Therefore, it is necessary to automatically find an optimum I and V point at which maximum power can be achieved from the PV cell in a process called Maximum Power Point Tracking (MPPT) (Esram, T. et al, 2007). This thesis has adopted the perturb and observe (P&O) maximum power point tracking (MPPT), which is effective in tracking and ease of implementation. The P&O MPPT Simulink circuit implementation is shown in Figure 3.

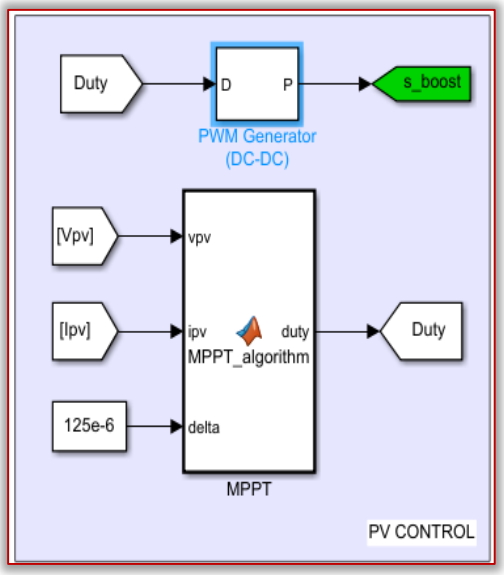

Figure 3. Perturb and Observe MPPT

The MPPT algorithm is scripted to implement a trial-and-error process in finding the maximum power point. The algorithm monitors for changes in power and perturbs operating voltage of the solar PV panel by changing the duty cycle to the switching device of the inverter and the buck converter in a repeated process until maximum power point is reached.

The battery charge controller as shown in Figure 4 monitors the battery current and voltage parameters to determine the duty cycle of the charge controller. The battery control device compares the battery voltage level against a voltage reference. If the voltage level of the battery is less than the reference voltage, the proportional integral (PI) controller outputs an error signal which is taken as the battery current reference. The current reference is then compared with the battery current via the second PI controller. This error signal obtained is fed into the input of the PWM generator as the duty cycle. The duty cycle is used to determine the percentage of the pulse period that the output is on. A branch is taken from the PWM output and inverted to yield two outputs [s_P] and [s_N] of opposing signals at a given time, thereby delivering charging current to the battery as required.

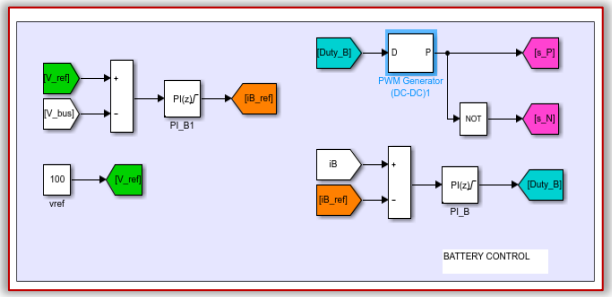

(a)

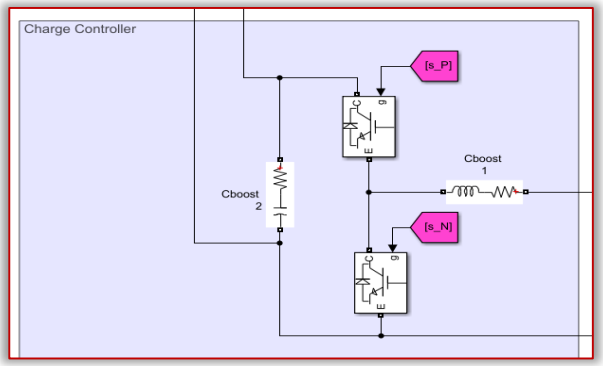

(b)

Figure 4 (a) Battery charger Controller (b) Charge Controller

The inverter model used in this thesis is a single-phase, full bridge, sine wave inverter. It is modeled using 4 metal-oxide-semiconductor field-effect transistor (MOSFETs), 3 capacitors and 2 inductors connected as shown in Figure 5 (a). Each MOSFET has internal diode resistance of 0.01 Ohms, the capacitors value is 0.006F each and inductors value of 0.003H. The switching circuit that controls the MOSFETs is as shown in Figure 5 (b). It consists of a sawtooth generator block, sine wave generator block, a relay block and a NOT logical operator block.

The lightning simulator circuit is built with a network of components as shown in Figure 6. The circuit consists of a DC source, resistors, capacitor, pulse generator, and a gate-controlled switch. The DC voltage is set to 100kV, capacitor value set to 10e-6 F, resistors have values of 240k, 1.2k and 0.24k Ohms.

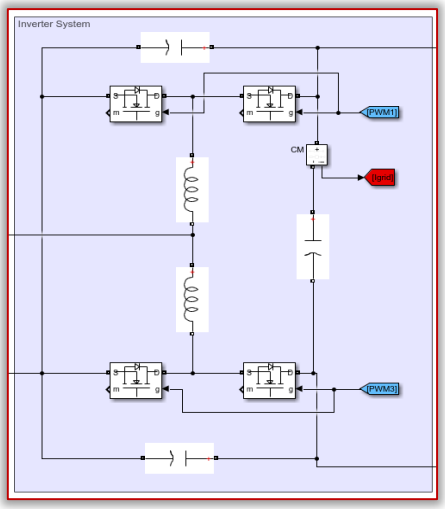

(a)

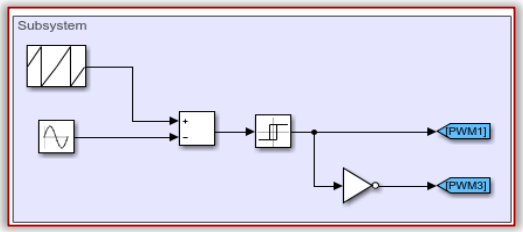

(b)

Figure 5 (a) Single Phase Full Bridge Inverter (b) MOSFETs Switching Circuit

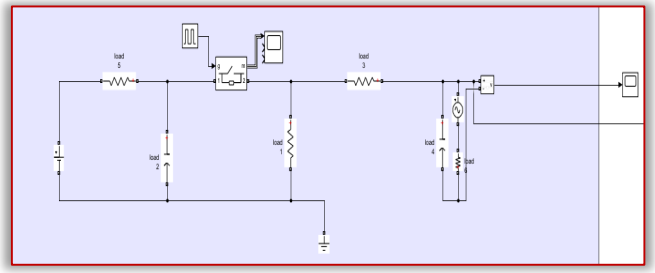

Figure 6. Lightning Simulator Circuit

GENETIC ALGORITHM

The Genetic Algorithm flowchart for the optimum allocation of SPDs is presented, as shown in Figure 7.

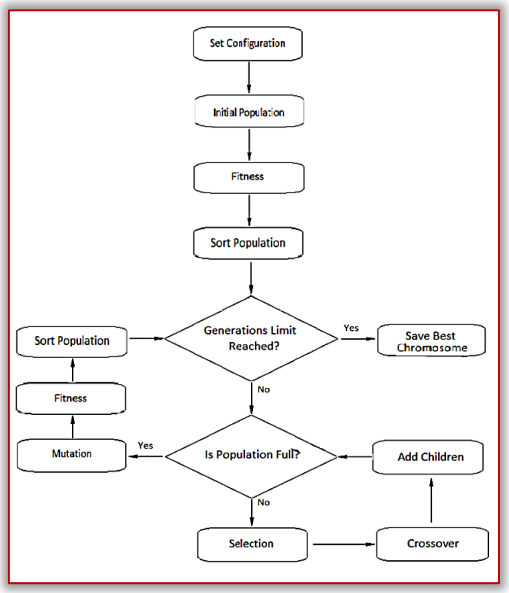

Figure 7. Genetic algorithm flowchart.

The program starts with the desired configuration such as the size of the population, generation limit, mutation and fitness, all of which determine the run time of the program to reach a desired solution.

Chromosome represents a solution to be tested as a probable optimal solution to the problem of optimization. Each gene represents a network node that is candidate to receive a surge protection device. The number of chromosome genes is equal to the total number of electric nodes in this case study. In order to run the genetic algorithm successfully, the genes are encoded from real values to discrete values which are in this case, binary values of 0s and 1s. The population is a set of chromosomes that form a set of genetic algorithm generation, which will undergo changes via mutation and crossover in the course of the program. The population size for this study is set to 4 as shown in Figure 8. The genes of the chromosomes have been stochastically generated while ensuring that no chromosome is set to extreme maximum (i.e. all genes set to 1) and extreme minimum (i.e. all genes set to 0). Setting chromosomes to extreme maximum and minimum can considerably increase convergence time which is undesirable and also prove counter intuitive since the aim of optimization is to use the least possible number of surge protection devices to protect the maximum number of equipment possible in the PV system. An example of the chromosomes is as shown in Figure 8.

1	1	0	0	1	1	0	0	1	1	0
1	0	1	0	1	0	1	0	1	0	1
1	1	1	0	1	1	1	0	1	1	1
1	0	0	0	1	0	0	0	1	0	0

Figure 8. A population set showing chromosomes

The fitness of the genetic algorithm, in which the created initial chromosomes are tested, is then critically determined. Since the aim of protection is to prevent induced faults due to lightning induced overvoltage and overcurrent, it means that the system will maintain a certain voltage limit beyond which it is considered unsafe for the system. For this study, the voltage beyond which a fault can occur is termed **Vlimit** and is set to 260V. When the chromosomes are tested with lightning induced voltages, and the system voltage remains within the **Vlimit** of 260V, the chromosomes are considered fit. Thus, this is considered the first test for fitness which is tested by running the simulation via MATLAB Simulink. The first fitness equation is given in Equation 1.

$$\mathbf{Vlimit} \leq 260\mathbf{V} \quad (1)$$

The second fitness equation is composed of the sum of two terms. The first term E consists of evaluating the

percentage of equipment that has been protected according to Equation 2. Protected equipment is one whose electrical node has electric voltage level within the **Vlimit**.

$$E = \frac{E_{total} - E_{over}}{E_{total}} \times 100 \quad (2)$$

Where E_{total} is the total number of equipment in the PV network, E_{over} is the total number of equipment that is connected at electric nodes that have exceeded the **Vlimit**.

The second term S evaluates the number of surge arresters that were required to perform the optimal allocation as shown in Equation 3.

$$S = \frac{S_{desired} - S_{allocated}}{S_{max} - S_{desired}} \times 100 \quad (3)$$

Where S_{max} is the maximum number of surge protection devices that can be allocated in the electrical PV system. $S_{desired}$ is the user-defined number of arresters to be allocated and $S_{allocated}$ is the amount of allocated surge arresters by the genetic algorithm procedure.

The final fitness equation is defined by Equation 4, as the weighted sum of the terms E and S. It is possible that the weighted sum in Equation 4 generates a negative value, and in this case the fitness value will be set to zero.

$$Fitness = \max(E + S) \quad (4)$$

Further to the chromosomes evaluation by the fitness function, two best chromosomes are selected using the proportionate selection method in which chromosomes with the highest fitness scores are selected as parent to generate a new pair of chromosomes in a process called the Crossover. The single point crossover solution is used where half the genes of the parents' chromosomes is taken to create a child chromosome. The crossover method is illustrated in Figure 9.

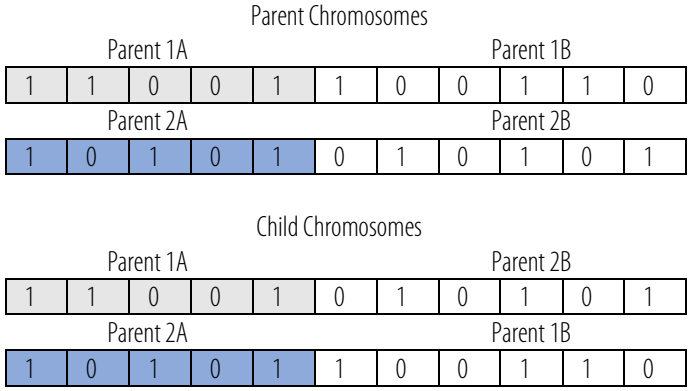

Figure 9. Parent to Child chromosome Illustration

Thereafter are the child chromosomes mutated using the point mutation in which only one random bit or gene is changed. This is as illustrated in Figure 10.

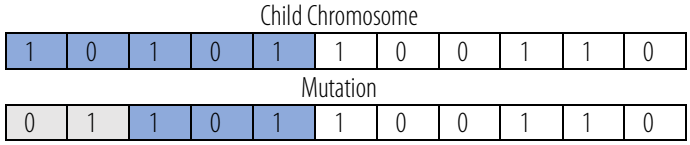

Figure 10. Child Chromosome Mutation Illustrated

ANALYSIS

The final chromosome generated by the genetic algorithm program is given as [0 0 1 0 1 0 1 1 0 0 1]. By comparison to the nodes on the PV network [a b c d e f g h I j k], the solution presented by the genetic algorithm suggested that 5 SPDs be installed on nodes C, E, G, H and K.

From the result obtained, it could be deduced that all equipment was adequately protected, therefore, the percentage of equipment protected according to Equation (2) is evaluated as:

$$E = \frac{E_{total} - E_{over}}{E_{total}} \times 100$$

$$E = \frac{24 - 0}{24} \times 100$$

$$E = 100$$

The percentage of SPDs used according to Equation (3) is evaluated as:

$$S = \frac{S_{desired} - S_{allocated}}{S_{max} - S_{desired}} \times 100$$

$$S = \frac{7 - 5}{10 - 7} \times 100$$

$$S = 66.7$$

The genetic algorithm program run made a maximum fitness score of 166.7.

DISCUSSION OF RESULTS

At normal operations, it is observed that the PV output levels are relatively stable and averaging 100V. All nodes of the PV system connected in parallel have the same output levels as expected. The steady voltage is maintained across the charge controller, battery, nodes G,H,I,J and Inverter input ports. The sine-wave output from the inverter maintains 240V.

At lightning strike condition on a critical node J, an unwanted surge in voltage was propagated through the photovoltaic network. The results shown in Figure 11 (a) & (b) indicated a surge exceeding 300v that lasted for about 0.005sec on the PV array nodes. Afterwards the voltage was at zero level and at about time 0.014 sec of the simulation, a second surge of about 250v was recorded. The recorded high voltages are dangerous for the solar panel arrays which 100v average output is expected. At nodes G, H and I beyond the buck converter, the resulting surge was as high as 1.5kV for a period of 0.005 sec as shown in Figure 11(b). Node I which connects to the battery recorded an unusual waveform as seen in Figure 11(c). The DC voltage was forced into a sinusoidal waveform for a short duration. Node K, at the inverter output recorded the highest surge in excess of 15kV, settled in less than 0.002 sec which was then followed by a second sinusoidal surge of about a thousand volts which lasted for about 0.02 sec as shown in Figure 11(d).

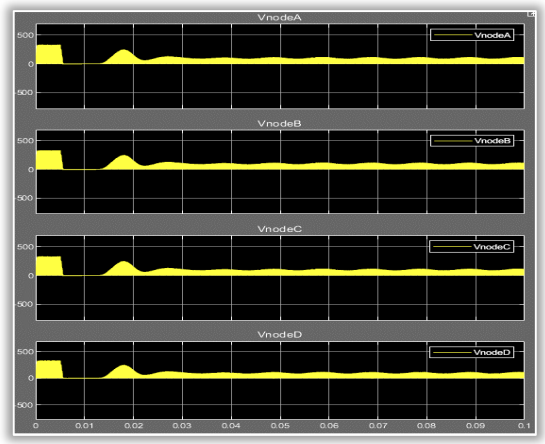

(a)

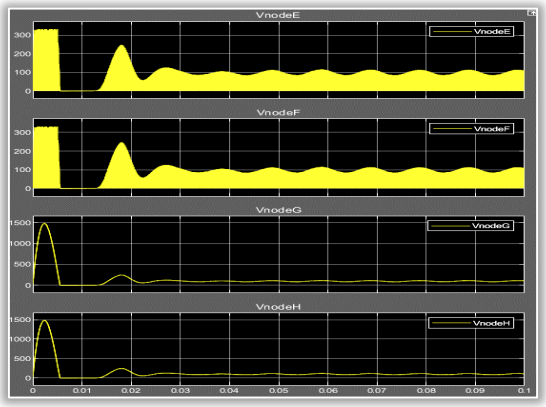

(b)

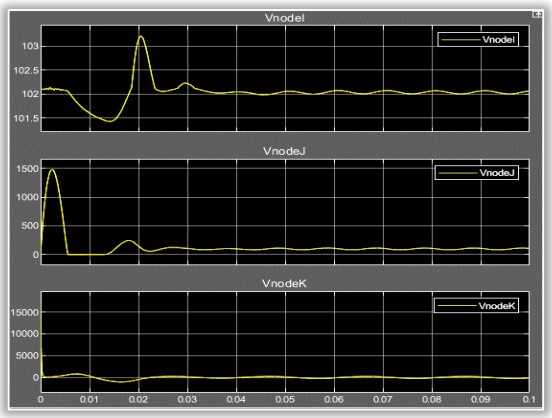

(c)

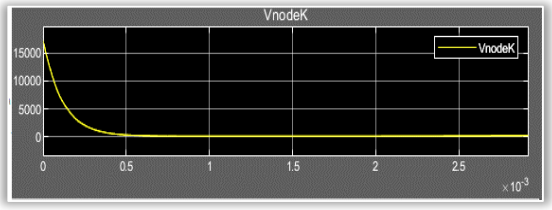

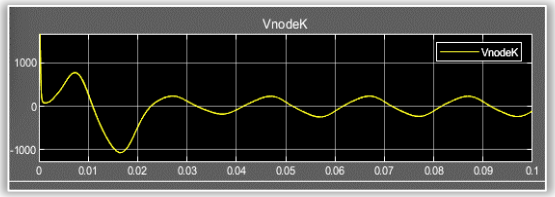

(d)

Figure 11. Graph showing levels with lightning discharge (a) at nodes A-D (b) at nodes E-H (c) at nodes I-K (d) at node K scaled to show portions of peak levels

With Genetic Algorithm applied, the results obtained at lightning strike are as shown in Figure 12.

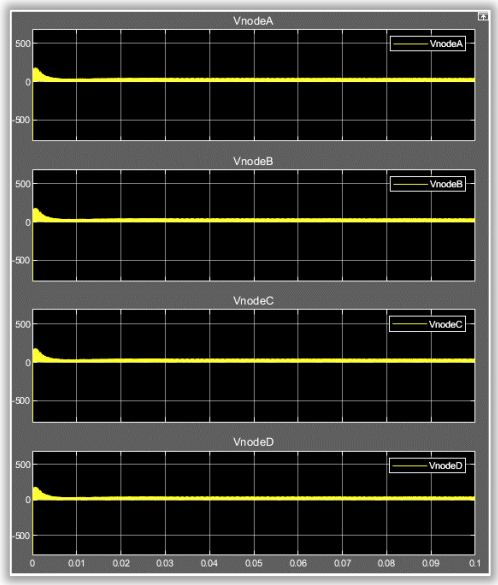

(a)

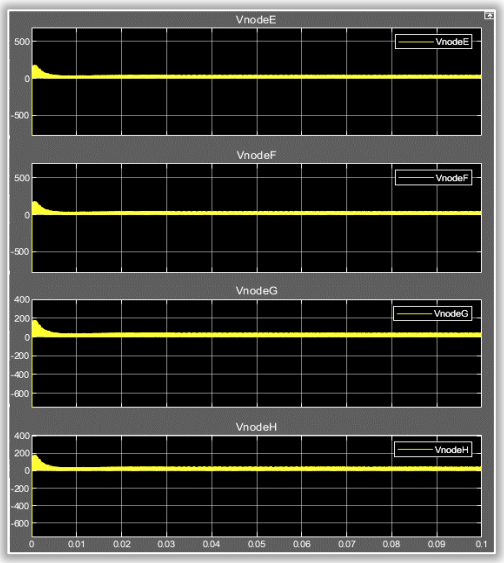

(b)

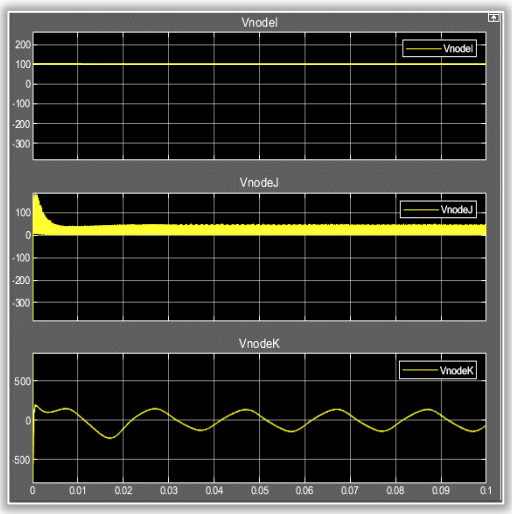

(c)

Figure 12. Graph showing levels (a) at nodes A-D (b) at nodes E-H (c) at nodes I-K with lightning discharge and genetic algorithm optimum solution

It could be observed that the genetic algorithm optimally allocated SPDs that successfully reduced the lightning induced overvoltages, thus keeping the network protected. The voltage levels across all nodes were kept at an acceptable limit of 200v for the DC side and 250v for the AC side of the inverter. At the end of the program run, the genetic algorithm allocated 5 SPDs out of a set limit of 7 SPDs.

CONCLUSION

A method combining the use of genetic algorithm optimization method for the optimum protection strategy of photovoltaic systems against lightning induced faults, by the strategic allocation of SPDs and the consideration of lightning discharge incidence on identifiable critical nodes is presented. The genetic algorithm optimization, applied in the strategic allocation of surge protective devices proved effective, obtaining very good results with respect to reducing overvoltages at all nodes of the network, ultimately protecting the network from lightning induced faults.

This method allows the effective planning of the protection of PV systems to be met while keeping the financial investments at minimum in surge protection devices for the network. The results indicated that the proposed method is applicable in real world protection applications that cut across large and dynamic PV systems, serving as a guide in surge protection devices allocation and planning.

References

[1] Ehrhardt, A. & Beier, S.: Spark gaps for DC applications. Proceedings of The 27th international conference on electrical contacts, Dresden, Germany. 2014.
[2] Esram, T. & Chapman, P.L.: Comparison of Photovoltaic Array Maximum Power Point Tracking techniques. IEEE Transaction on Energy Conversion 22: 434-449, 2007.
[3] Fallah, Gomes, N., Zainal, C., Ab Kadir, M., Nourirad, A., Baojahmadi, G. and Ahmed, M: Lightning protection techniques for roof-top pv systems. 7th International Power Engineering and Optimization Conference. Langkawi, Malaysia.
[4] Florida Solar Energy Center: History of Photovoltaics. The Florida Solar Energy Center (FSEC) is a research institute, University of Central Florida, 2007.
[5] Gabriel V. S. R: Surge Arrester Allocation in Electrical Distributed Systems. Energies 12: 4110, 2019
[6] Ittarat, S., Hiranvarodom, S., & Plangklang, B.: A computer program for evaluating the risk of lightning impact and for designing the installation of lightning rod protection for photovoltaic system. 10th Eco-energy and Materials Science and Engineering Symposium. 2019.
[7] Kern, A. & Krichel, F.: Considerations about the lightning protection system of mains independent renewable energy hybrid-systems–practical experiences. J. Electrostat 60: 257–263, 2004.
[8] Lea, P.: Task 3: Common Practices for Protection Against the Effects of Lightning on
[9] Stand-Alone Photovoltaic systems. International Energy Agency 2003
[10] Pons, E. & Tommasini, R.: Lightning protection of PV systems. 4th International Youth Conference on Energy (IYCE), 6–8, 2013.
[11] Shahniaand, F. & Gharehpetian, G.B.: Lightning and Switching Transient Overvoltages in Power Distribution Systems Feeding DC Electrified Railways. 3-rd International Conference on Technical and Physical Problems in Power Engineering. Ankara, Turkey. 2006.
[12] Spooner, E. & Harbidge, G.: Review of international standards for grid connected photovoltaic systems. Renewable Energy 22: 235–239, 2001.
[13] Tong, C., Wang, Q., Gao, Y. & Tong, M.: Dynamic lightning protection of smart grid distribution system. Electrical Power System 113: 228–236, 2014.
[14] Vladimir, A. R.: Lightning protection: history and modern approaches. 86th AMS Annual Meeting; 2nd Conference on Meteorological Applications of Lightning, Atlanta, GEORGIA, 2017.

ISSN: 2067-3809

Fascicule 3

[July – September]

tome [2023] XVI

ACTA Technica CORVINIENSIS
BULLETIN OF ENGINEERING

ISSN: 2067-3809

[1.]S. OZDEMIR, [2.]B. AYHAN, [3.]H.H. OZTURK, [3.]Z. BEREKET BARUT

DETERMINATION OF ENERGY CONSUMPTION AND CARBON DIOXIDE EMISSIONS RELATED TO FUEL CONSUMPTION FOR AGRICULTURAL MECHANIZATION APPLICATIONS

[1,3.] University of Cukurova Faculty of Agriculture Dept. of Machinery and Technologies Engineering, Balcalı, Sarıcam, Adana, TÜRKIYE
[2.]Adana Agricultural Extension and Training Center, TÜRKIYE

Abstract: Energy efficiency is the goal of efforts to reduce the amount of energy required to provide products and services. In agricultural production, not only solar energy is used efficiently in the photosynthesis process, but also energy is used directly as fuel or electricity and indirectly due to energy consumption in the production processes of agricultural machinery, fertilizers or pesticides. The energy consumption per unit production area by the tractor and irrigation pump engines used during agricultural production processes is calculated regarding the diesel fuel and engine oil consumptions. During the operation of tractors and other engine–powered equipment, carbon (C) in the fuel is converted into carbon dioxide (CO_2) released in the engine exhaust. The fuel–based CO_2 emission calculation method is the preferred approach, as data on fuel consumed is generally more reliable. In this study, the methods used to determine energy consumption and CO_2 emissions related to fuel consumption in agricultural mechanization applications are discussed.

Keywords: agriculture, mechanization, fuel, consumption, energy, consumption, emissions

INTRODUCTION

Agriculture plays an important role in the economy of all countries in the world. In agricultural policies, it is aimed not only agricultural production in sufficient quantity and quality, but also the protection of the environment and the economic development of rural areas. Agricultural production is closely related to the economy, environment and energy consumption. Therefore, it interacts with all policies in these areas. The need for energy as an input in agricultural production can determine the profitability of production, which greatly influences the producer's investment in advanced agricultural systems.

Therefore, economically cost–effective energy measures are needed and at the same time commitments to reduce carbon emissions are made. Globally, energy use is projected to increase significantly in the coming years, with a widespread impact on the economy, including in the agricultural sector. This topic reveals the importance of research and development studies to develop more energy efficient technologies in agricultural production. Energy efficiency is the goal of efforts to reduce the amount of energy required to provide products and services. In agricultural production, not only solar energy is used efficiently in the photosynthesis process, but also energy is used directly as fuel or electricity and indirectly due to energy consumption in the production processes of agricultural machinery, fertilizers or pesticides.

While assessments of energy use in agriculture generally focus on direct energy use, it should be accepted that 50% and more of total energy use is related to nitrogen fertilizer production and other indirect energy uses (Woods et al. 2010; Pelletier et al., 2011). The energy use and energy saving potentials of different production systems in different environments are also drastically different.

MATERIALS AND METHODS

Fuel Consumption In Agricultural Production

About 1/3 of the total energy consumption in agriculture is spent on fuel. Production method and area are very important factors for fuel consumption. Fuel consumption varies between 500–15,900 liters/year. Diesel consumption for different products varies in the range of 60–120 liters/ha, depending on the processing intensity. The number of transactions is very important. (Handler and Nadlinger, 2012).

Amount of Fuel Consumed

Fuel consumption in agricultural production processes, consumed by tractor and irrigation pump engines in the use of tools and machinery;

- Diesel fuel consumption,
- Lubricant oil consumption and
- Total fuel (Diesel fuel + lubricant oil) consumption.

Diesel fuel and lubricant oil values consumed per unit production area (ha) by the tractor engine used during agricultural production processes are evaluated as the total fuel consumption.

$$m_t = m_D + m_l \ [L/ha] \quad (1)$$

where:
m_t – total fuel consumption (L/ha),
m_D – Diesel fuel consumption (L/ha) and
m_l – lubricanting oil consumption (L/ha).

Fuel Consumption

Fuel consumption is determined for each application in the production process, based on the size of the equipment used and the power required to perform the operation. Diesel engines, gasoline engines or electric motors can provide power for agricultural applications. The type of engine used is specified as a machine variable. Fuel consumption (liter/hour, L/h) in gasoline and Diesel engines is determined as follows, depending on the power of the tractor or other engine used and the load value of the engine (ASAE, 2000):

$$m_D = (YTH) \times (NMG) \times (YKV) \times (TMY) \times (YKI) \ [L/h] \quad (2)$$

where:
m_D – hourly fuel consumption of tractor engine (L/h),
YTH – Fuel consumption rate (L/kW–h),
NMG – Maximum usable or rated motor power (kW),
YKV – Fuel usage efficiency (decimal),
TMY – tractor or engine load (0–1) and
YKI – Fuel usage index (decimal).

Fuel usage efficiency (YKV) is a fuel usage reducing factor that takes into account the time consumed for turning and some minor adjustments where the engine is running at less than operating speed. As an average value for fuel use efficiency (YKV), the value determined by adding 1.0 to the area efficiency can be considered. Thus, when the area efficiency specified for an application decreases, the fuel usage efficiency decreases as well.

In the fuel use index (YKI), the time spent outside the actual operation is taken into account for transporting tools or machines to the agricultural production area and for some arrangements. It is normally taken into account as 1.10 in the fuel usage index (YKI). The motor load (TMY) for any given operation is determined by dividing the average power required to perform the operation by the maximum available power.

Fuel Consumption Rate

Fuel consumption rate (YTH) for diesel engines depends on engine load and throttle setting (ASABE, 2011):

$$YTH = GA\,(0.22 + 0.096 / TMY)\ [L/kW–h] \quad (3)$$

where:
GA – partial throttle setting factor and is determined as follows:

$$GA = 1 – (T – 1)\,(0.45\ TMY – 0.877) \quad (4)$$

where:
T – throttle setting and its value ranges from 0.0 to 1.0.

For simplicity, the throttle setting can be considered 50% greater than the engine load at 1.0 maximum. Therefore, for engine loads greater than 0.66, the throttle is assumed to be at maximum. For gasoline engines, this relationship is defined as follows:

$$YTH = GA\,(2{,}74\,(TMY) + 3{,}15 – 0{,}203 \sqrt{(697\,(TMY)))}\ [L/kW–h] \quad (5)$$

Lubricant Oil Consumption

The hourly lubricant oil consumption of the tractor engine used for agricultural production operations is determined based on the rated power of the tractor. For estimating the hourly lubricant oil consumption in Diesel tractor engines, the following linear equation based on engine rated power (P_e) and specified in ASABE Standard D497.7 Section 3.4 (2011) is used as the reference model.

$$m_l = 0.00059 \times P_e + 0.02169\ [L/h] \quad (6)$$

By Cancante et al., (2017), using MINITAB 17.0™ data processing software, linear regression (LRA) and analysis of variance (ANOVA) and the coefficients specified in equation (6) were determined as follows.

$$m_l = 0.000239 \times P_e + 0.00989\ [L/h] \quad (7)$$

where:
m_l – hourly lubricant oil consumption of the tractor engine (L/h) and
P_e – the rated power of the tractor (kW).

The Pearson correlation coefficient for the variables in equation (7) was r=0.90 ($p<0.05$). The standard errors of the constant term and linear coefficient in the developed model are 1.50 10–3 L/h and 9.0 10–6 L/h kW, respectively.

Fuel Energy Consumption

The total fuel energy consumption in the agricultural production processes is consumed by the tractor and irrigation pump motors in the use of tools and machinery;

- Energy consumption related to Diesel fuel consumption,
- Energy consumption related to lubricant oil consumption and
- Considered as the total energy consumption for Diesel fuel+ lubricant oil consumption.

The fuel energy consumption (EC_f, MJ/ha) of diesel fuel and lubricant oil consumed per unit production area (ha) by the tractor and irrigation pump engines used during agricultural production processes is determined as follows.

$$EC_f = EC_D + EC_l\ [MJ/ha] \quad (8)$$

where:
EC_f – total fuel energy consumption (MJ/ha),
EC_D – Diesel fuel energy consumption (MJ/ha) and
EC_l – lubricant oil energy con sumption (MJ/ha).

Diesel fuel energy consumption (EC_D, MJ/ha) per unit production area (ha) by the tractor and irrigation pump engines used during production operations is determined as follows.

$$EC_D = m_D + LHV_D \ [MJ/ha] \quad (9)$$

where:
EC_D – Diesel fuel energy consumption (MJ/ha),
m_D – Diesel fuel consumption (L/ha) and
LHV_D – the lower heating value of Diesel fuel (MJ/L).
The lower calorific value of Diesel fuel consumed during production operations in the field with agricultural tools and machinery is taken into account as LHVD = 37.1 MJ/L (IPCC, 1996).
Lubricant oil energy (ECl, MJ/ha) per unit production area (ha) of lubricant oil consumption by tractor and irrigation pump engines used during production operations is determined as follows.

$$EC_I = m_I + LHV_I \ [MJ/ha] \quad (10)$$

where:
EC_I – lubricant oil energy consumption (MJ/ha),
m_I – lubricant oil consumption (L/ha) and
LHV_I – the lower heating value of lubricant oil (MJ/L).
The lower calorific value of lubricant oil consumed during production operations in the field with agricultural tools and machinery is taken into account as LHV_I = 38.2 MJ/L (IPCC, 1996).

Carbon Dioxide Emissions from Fuel Consumption

During the operation of tractors and other engine–powered equipment, carbon (C) in the fuel is converted into carbon dioxide (CO_2) released in the engine exhaust. The amount of CO_2 released is proportional to the amount of fuel consumed. The conversion factor used is 2.637 kg CO_2–equivalent per liter of Diesel fuel consumed. Fuel consumption is determined during the execution of each application. By summing up the amount of fuel consumed in all applications, the annual total amount of fuel used in the business is determined. This total value is then multiplied by the emission factor to determine the CO2 emissions from the combustion of the fuel.
In the process of agricultural production processes, carbon dioxide (CO_2) emissions are consumed during the use of tools and machinery;

- CO_2 emissions related to Diesel fuel consumption,
- CO_2 emissions related to lubricant oil consumption and
- The total CO_2 emissions related to the total fuel (Diesel fuel + lubricant oil) consumption.

Taking into account the lubricant oil consumption value of the tractor engine, CO_2 emissions related to lubricant oil consumption can also be calculated.
The fuel–based CO_2 emission calculation method recommended by the Intergovernmental Panel on Climate Change is taken into account in the calculations to determine the CO_2 emissions related to the use of fuel as a result of agricultural production (IPCC, 1996). The proposed approach for calculating CO_2 emissions based on fuel consumption is summarized in equations (12) and (13).
The total CO_2 emission ($kgCO_2$/ha) related to the unit production area (ha) fuel consumption by the tools and machines used during agricultural production processes is determined as follows.

$$CO_{2,t} = CO_{2,D} + CO_{2,I} \ [kgCO_2/ha] \quad (11)$$

where:
$CO_{2,t}$ – total CO_2 emissions related to fuel consumption ($kgCO_2$/ha),
$CO_{2,D}$ – CO_2 emissions related to Diesel fuel consumption ($kgCO_2$/ha) and
$CO_{2,I}$ – CO_2 emissions related to lubricant oil consumption ($kgCO_2$/ha).
The CO2 emission (CO2, D, kgCO2/ha) related to Diesel fuel consumption per unit production area (ha) by agricultural tools and machinery used during production processes is determined as follows.

$$CO_{2,D} = m_D \times LHV_D \times EF_D \ [kgCO_2/ha] \quad (12)$$

where:
$CO_{2,D}$ – emissions related to Diesel fuel consumption ($kgCO_2$/ha),
m_D – Diesel consumption (L/ha),
LHV_D – the lower calorific value of Diesel fuel (37.1 MJ/L) and
EF_D – CO_2 emission factor for Diesel fuel (0.07401 $kgCO_2$/MJ).
The CO_2 emission ($CO_{2,I}$, $kgCO_2$/ha) related to the lubricant oil consumption per unit production area (ha) by the agricultural tools and machinery used during production processes is determined as follows.

$$CO_{2,I} = m_I \times LHV_I \times EF_I \ [kgCO_2/ha] \quad (13)$$

where:
$CO_{2,I}$ – emissions related to lubricant oil consumption ($kgCO_2$/ha),
m_I – lubricant oil consumption (L/ha),
LHV_I – the lower calorific value of lubricant oil (38.2 MJ/L) and
EF_I – CO_2 emission factor for lubricant oil (0.07328 $kgCO_2$/MJ).

CONCLUSIONS

Diesel and gasoline engines are the most important power sources used in agricultural applications. Fuel consumption is determined for each application in the production process, based on the size of the equipment used and the power required to perform the operation. Fuel consumption in gasoline and Diesel engines is determined depending on the power of the tractor or other engine used and the load value of the engine. The hourly oil consumption of the tractor engine used for agricultural production operations is determined based on the rated power of the tractor.

Note: This paper was presented at ISB–INMA TEH' 2022 – International Symposium on Technologies and Technical Systems in Agriculture, Food Industry and

Environment, organized by University "POLITEHNICA" of Bucuresti, Faculty of Biotechnical Systems Engineering, National Institute for Research–Development of Machines and Installations designed for Agriculture and Food Industry (INMA Bucuresti), National Research & Development Institute for Food Bioresources (IBA Bucuresti), University of Agronomic Sciences and Veterinary Medicine of Bucuresti (UASVMB), Research–Development Institute for Plant Protection – (ICDPP Bucuresti), Research and Development Institute for Processing and Marketing of the Horticultural Products (HORTING), Hydraulics and Pneumatics Research Institute (INOE 2000 IHP) and Romanian Agricultural Mechanical Engineers Society (SIMAR), in Bucuresti, ROMANIA, in 6–7 October, 2022.

References

[1] ASAE. (2000). ASAE Standards, 47th Ed. 2000. D497.4. and EP496.2. Agricultural Machinery Management. ASAE, St. Joseph, MI. ASABE Standards, 57th Ed. 2010. D384.2, Manure production and characteristics. ASABE, St. Joseph, MI.

[2] ASABE Standards. (2011). D497.7: Agricultural machinery management data. St. Joseph, MI: ASABE.

[3] Calcante, A., Brambilla, M., Oberti, R., & Bisaglia, C., 2017. Proposal to Estimate the Engine Oil Consumption in Agricultural Tractors. Appl. Eng. Agric., 33(2), 191–194.

[4] Handler, F., & Nadlinger, M. (2012), D 3.8 Strategies for saving fuel with tractors Trainer handbook Version 12/2012. Efficient 20. IEE/09/764/SI2.558250.

[5] IPCC, (1996), Climate Change, 1995: The Science of Climate Change. Contribution of Working Group I to the Second Assessment Report of the Intergovernmental Panel on Climate Change [Houghton, J.T., et al. (eds.)]. Cambridge University Press, Cambridge, NY, USA, 572 pp.

[6] IPCC, (2007), Climate Change 2007: Synthesis Report. Contribution of Working Groups I, II and III to the Fourth Assessment Report of the Intergovernmental Panel on Climate Change [Core Writing Team, Pachauri, R.K and Reisinger, A. (eds.)]. IPCC, Geneva, Switzerland, 104 pp.

[7] Pelletier, N. (2008). Environmental performance in the US broiler poultry sector: Life cycle energy use and greenhouse gas, ozone depleting, acidifying and eutrophying emissions. Agric. Systems 98(2): 67–73.

[8] Woods, J., Williams, A., Hughes, J.K., Black, M., & Murphy, R., (2010), Energy and the food system. Philosophical Transactions of the Royal Society B: Biological Sciences 365 (1554):2991–3006.

ISSN: 2067-3809

[1.]Mihaela NIȚU, [1.]Augustina PRUTEANU, [1.]Iuliana GĂGEANU, [2.]Oana–Diana MANOLELI–PREDA, [2.]Robert BILA

NATURAL DECARBONISATION IN CONTROLLED MICROCLIMATES IN THE CONCEPT OF NEUTRAL AGRICULTURE – REVIEW

[1.]National Institute of Research – Development for Machines and Installations Designed for Agriculture and Food Industry – INMA Bucharest, ROMANIA
[2.]Rolix Impex Series SRL, ROMANIA

Abstract: In terms of emission absorption, agriculture, unlike other sectors, has the ability to fix the carbon in the atmosphere through the process of photosynthesis and sequester it in soil and biomass. In the context of climate change, outdoor agricultural production is usually subjected to uncertainty, obtaining random quantities from year to year, which leads to an increased demand for growing crops under controlled conditions. Due to the increased need for safe and deterministic food, the greenhouse is a protected space for food production that has its own microclimate. One of the most important objectives of a greenhouse is to maximize productivity by obtaining a competitive advantage, and an effective way to increase productivity is to fertilize plants with CO_2. In this paper will be presented various studies on the interest in enriching crops with CO_2 and its effect on crops.

Keywords: carbon dioxide, natural decarbonisation, controlled microclimates, neutral agriculture

INTRODUCTION

According to the 2015 Paris Agreement, the limit of 450 ppm of CO_2 in the atmosphere is approached as a protection limit (in a certain probability of validity) that must not be exceeded in order to avoid situations capable of causing irreversible problems. The current value of the CO_2 concentration is close to 417 ppm, and the upward trend is not in line with such a tight and strict limit. To keep the limit of the 450 ppm CO_2 limit could be achieved by sequestering CO_2 in the atmosphere *(Luan, H., Gao, W., et al, 2019 Wang, Y., Hu, N., et al, 2017; Xu, P., Zhu, J., et al, 2021)*.

Climate change is one of the biggest challenges facing humanity today, with the global economy as its main objective to increase the level of decarbonization. Agricultural activity is a source of greenhouse gases (GHGs), but also a sink, especially by storing carbon dioxide in soil organic matter and biomass. In terms of emission absorption, agriculture, unlike other sectors, has the ability to fix the carbon in the atmosphere through the process of photosynthesis and sequester it in soil and biomass. Also, biomass produced in agriculture and used for energy (energy from renewable sources) or as a raw material (biomaterials, plant chemistry) is another way to increase carbon biosequestration. Biochemists have shown that fertilizing the air with carbon dioxide is a great way to get high yields from different crops, plant growth can be stimulated by increasing CO_2. Thus, the interest in enriching crops with CO_2 is increasingly present in agriculture, in response to plant enrichment with CO_2, in different climatic conditions *(Runion, G. B., Finegan, H. M., et al, 2011 Liu, H., Zhang, J., et al, 2018; Liu K., Huang, J., et al, 2019)*.

Because horticultural plants are generally grown in containers without resource limitations (i.e., water and nutrients), increased root growth or mycorrhizal colonization may not become critical for survival and growth until after outplanting into the landscape. However, as a result of limited rooting space, growth in containers has been shown to dampen the response to CO2 enrichment. For plants to use a higher level of atmospheric CO2, they must have a means of storing the additional carbohydrates produced. Plants with a tuberous or woody root system tend to respond to CO2 enrichment to a greater degree than plants with smaller or more fibrous root systems *(Xu, X., Schaeffer, S. et al, 2020; Kallenbach, CM, et al, 2010)*.

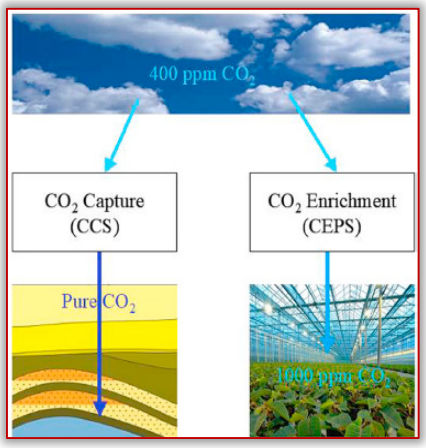

Figure 1 – Illustration of (a) CCS (Carbon Capture and Storage) and (b) CEPS (Carbon Enrichment for Plant Stimulation) processes (Baoa, J. et al., 2018)

Carbon dioxide links the atmosphere to the biosphere and is an essential substrate for photosynthesis. Elevated CO_2 stimulates photosynthesis leading to increased carbon (C) uptake and assimilation, thereby increasing plant growth. However, as a result of differences in CO_2 use during photosynthesis, plants with a C_3 photosynthetic pathway often exhibit greater growth response relative to those with a C_4 pathway *(Qiu, QY, Wu, LF, et al, 2016; Raheem, A, Zhang, J, et al, 2019)*.

In addition to the aforementioned effects of CO2 on photosynthesis and C allocation, increased CO2 can impact growth by improving plant water relations. Water is also a crucial resource in many horticultural production units, and its conservation is becoming an increasingly important issue. The fact that increased CO2 can increase plant WUE may indicate that plants can be watered less frequently as CO2 levels continue to rise. However, since these plants are generally grown with optimal nutrients, increased CO2 may increase the size of the plant to a point where watering frequency will need to be maintained at current levels or even increased. This interaction between high CO2 and resource availability is also extremely important for horticultural species after planting in the landscape, where periodic droughts can be relatively frequent (*Qaswar, M, Jing, H, et al, 2020*).

MATERIALS AND METHODS

In the paper *(Prior, S. A.. et al., 2011)* a study was conducted on plant growth by CO2 stimulation. In this study, it was shown that applying more CO2 can increase the water use efficiency of the plant and lead to less water use.

The study *(Luan, H. et al., 2021)* aimed to appraise the changes of organic C stability within soil aggregates after eight years of fertilization (chemical *vs.* organic fertilization) in a greenhouse vegetable field in Tianjin, China. Changes in the stability of organic C in soil aggregates were evaluated by four methods, i.e., the modified Walkley–Black method (chemical method), 13C NMR spectroscopy (spectroscopic method), extracellular enzyme assay (biological method), and thermogravimetric analysis (thermogravimetric method). The aggregates were isolated and separated by a wet–sieving method into four fractions: large macroaggregates (>2 mm), small macroaggregates (0.25–2 mm), microaggregates (0.053–0.25 mm), and silt/clay fractions (<0.053 mm).

In the study *(Lin, S, et al., 2021)*, soil CO2 and CH4 fluxes under various fertilization treatments in tea soil were investigated during a 50–day period.The experiment consisted of five treatments: no fertilizer (CK), single nitrogen (urea, N), single oilseed rape cake fertilizer (R), nitrogen þ cake fertilizer (2:1, NR1), and nitrogen þ cake fertilizer (1:2, NR2).The fertilization proportion of NR1 and NR2 was determined by the nitrogen content of nitrogen fertilizer and cake fertilizer.

To hold global temperature rise below 2°C by 2050, global greenhouse gas emissions must be reduced by more than 80%. In this sense, in the study *(Baoa, J. et al., 2018)* was proposed develop a modern urban vertical farming system, i.e. greenhouses equipped with a Carbon Enrichment Plant Stimulation System (CEPS) to improve land use efficiency and thus increases food productivity and, at the same time, to sequester CO2 from the ambient air. The the implementation of such a CEPS system will have the potential to remove more than 500 million tons of CO2 from the air annually and increases the current food productivity more than 15 times than the open field operation.

In the paper *(Wanga, T.. et al., 2014)*, an integrated system combined direct air capture (DAC) (Figure 2) and greenhouse agriculture is proposed, in which moisture swing adsorption technology is used to concentrate CO2 from the atmosphere and then feed CO2 to the greenhouse. Allso, absorption isotherm study and desorption kinetic study have been achieved in the paper.

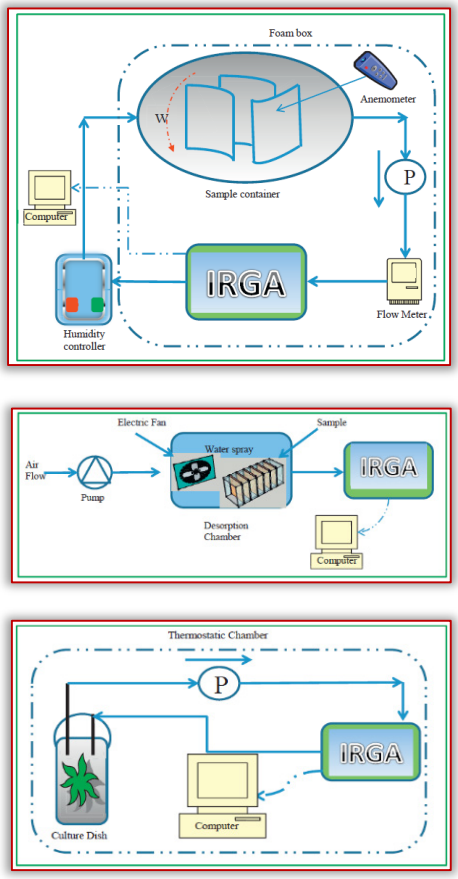

Figure 2 – Schematic of experimental system for absorption equilibrium study (Wanga, T.. et al., 2014)

(Stanghellini, C., et al., 2010) applied a simple model for estimating potential production loss, using data obtained in commercial greenhouses in Almería, Spain, and Sicily, Italy. They analysed the cost, potential benefits and consequences of bringing more CO2 into the greenhouse: either through increased ventilation, at the cost of lowering temperature, or through artificial supply. They

found that while the reduction in production caused by depletion is comparable to the reduction resulting from lower temperatures caused by ventilation to avoid depletion, compensating the effect of depletion is much cheaper than making up the loss by heating.

RESULTS

In the paper (*Prior, S.A.. et al., 2011*), after reviewing the available literature on CO2, a number of priority objectives for future research were provided regarding the need to breed or screen horticultural plant cultivars and species for increased drought tolerance; determination of the amount of carbon sequestered in soil by horticultural production practices to improve soil water holding capacity and help mitigate projected global climate change; determining the contribution of the horticultural industry to these projected changes by the flux of CO2 and other trace gases (ie nitrous oxide from fertilizer application and methane under anaerobic conditions) into the atmosphere; and determining how CO2–induced changes in plant growth and water relations will occur influences complex interactions with pests (weeds, insects and diseases).

Such data is necessary to develop best management strategies for the agriculture industry to adapt to future environmental conditions.

In the paper *(Luan, H. et al., 2021)*, the results showed that organic amendments increased the organic C content and reduced the chemical, spectroscopic, thermogravimetric, and biological stability of organic C within soil aggregates relative to chemical fertilization alone. Within soil aggregates, the content of organic C was the highest in microaggregates and decreased in the order microaggregates > macroaggregates > silt / clay fractions. Meanwhile, organic C spectroscopic, thermogravimetric, and biological stability were the highest in silt/clay fractions, followed by macroaggregates and microaggregates. Moreover, the modified Walkley–Black method was not suitable for interpreting organic C stability at the aggregate scale due to the weak correlation between organic C chemical properties and other stability characteristics within the soil aggregates. This study showed that eight years of organic amendments improved the soil structure in a GVP system by inceasing the proportions of large macroaggregates and enhancing soil aggregate stability (MWD).

The results of paper *(Wanga, T.. et al., 2014)* show that the behaviour of membrane conforms to Langmuir model and its capacity reaches to 0.83 mol of CO2 per kilogram of sorbent. When the output CO2 concentration of the desorber is around 1000 ppm, desorption efficiency increases from 71.3% to 79.6% when the temperature is changed from 25°C to 40°C. Besides, based on the experiment of the uptake kinetics of plants under different light and different light intensity, energy consumption and techno–economic analysis of the system have been carried out.

In the study *(Lin, S, et al., 2021)*, the results (Figure 3) revealed that the single application of nitrogen had no significant effect on soil CO2 flux. However, the addition of cake fertilizer significantly increased CO2 emissions through enhanced soil microbial biomass carbon (MBC). Additionally, CO2 emissions were directly proportional to the amount of carbon (C) in the fertilizer. All treatments were minor sinks for CH4 except for the treatment NR1. Specifically, the cumulative CH4 fluxes of NR1 and NR2 were significantly higher than rest of the three treatments, which implies that application of urea and oilseed rape cake reduced the capability of CH4 oxidation in tea soil. Structural equation models (Figure 4) indicated that soil CO2 flux is significantly and positively correlated with soil dissolved organic carbon, MBC and soil pH, while mineral nitrogen content was the main factor affecting CH4 flux. Overall, the application of oilseed rape cake increased the oxidation of CH4 and promoted soil C sequestration but inevitably increased the soil CO2 emissions.

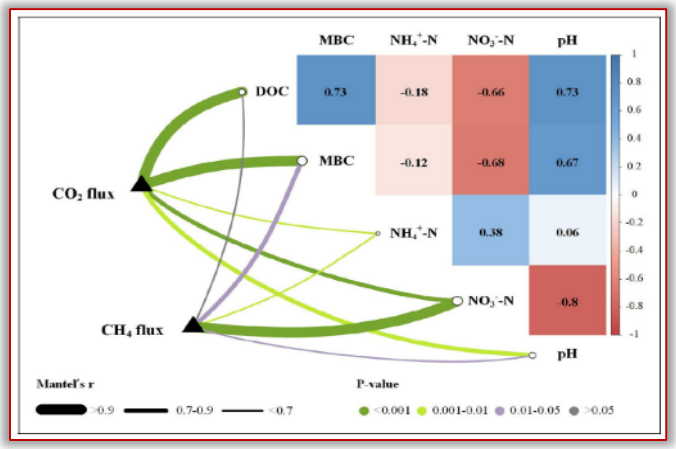

Figure 3 – Environmental drivers of CO2 and CH4 fluxes *(Lin, S, et al., 2021)*

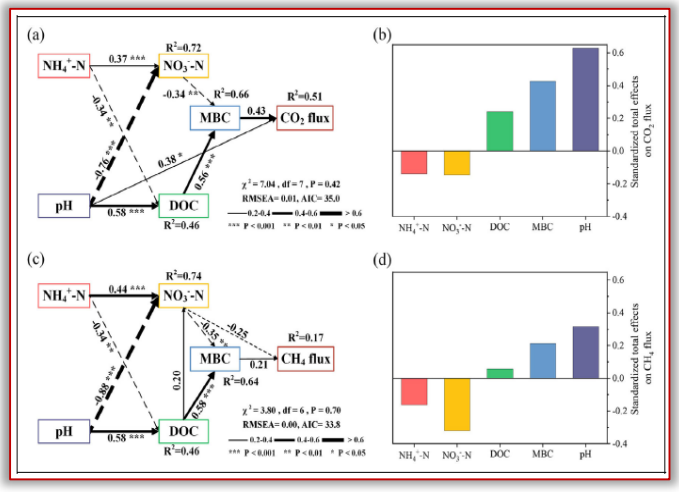

Figure 4 – The structural equation model (SEM) showing the effects of NH4 þ–N, NO3 –N, microbial biomass C (MBC), dissolved organic C (DOC), and pH on CO2 (A) and CH4 (C) fluxes (Lin, S, et al., 2021)

Pairwise comparisons of physicochemical property are shown, with a color gradient denoting Spearman's correlation coefficients. CO2 flux and CH4 flux were related to each environmental factor by partial (geographic distance–corrected) Mantel tests. Edge width corresponds to the Mantel's statistic for the corresponding distance correlations, and edge color denotes the statistical significance based on 9,999 permutations *(Lin, S, et al., 2021)*.

Standardized total effects of soil NH4 þ–N, NO3––N, MBC, DOC, and pH on CO2 (B) and CH4 (D) fluxes as revealed by SEM. The width of the arrows indicates the strength of the standardized path coefficient. Solid lines represent positive path coefficients and dashed lines represent negative path coefficients. R2 values represent the proportion of the variance explained for each endogenous variable *(Lin, S, et al., 2021)*.

In the papier *(Baoa, J. et al., 2018)* the greenhouse gas emission reduction potential of CEPS technology for urban greenhouse industry consisted of two components: net CO2 sequestered from the air by plants through photosynthesis and CO2 displaced from the natural gas combustion source (Figure 5). For every ton of CO2 captured from the air, one CO2 from the natural gas combustion source will be displaced. A fraction of this ton of CO2 injected into the greenhouse will also be fixed by the plants, depending on the plant growth rate and the residence time of the air in the greenhouse. In general, more than one ton of net CO2 reduction will be achieved for each CO2 captured by the adsorption column. In order to quantify the net CO2 reduction, a full life cycle analysis will be carried out in the future.

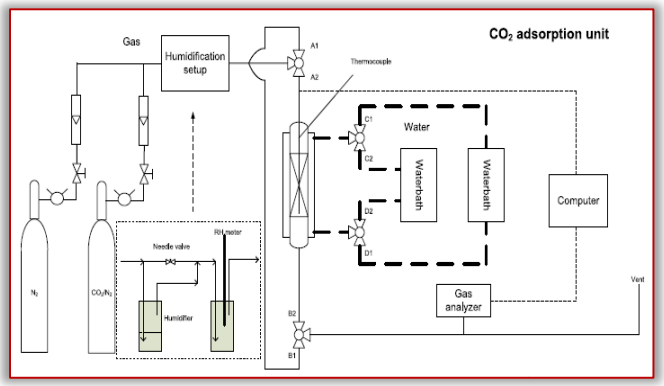

Figure 5 – Process diagram of CO2 adsorption and desorption unit with humidification unit (Baoa, J. et al., 2018)

In the papier *(Stanghellini, C., et al., 2010)*, they found that the optimal CO2 enrichment depends on the margin between crop growth value and cost of CO2 supply. Trying to determine the optimum concentration by experiment is not feasible because the economic value of enrichment is not constant but varies with solar radiation through photosynthesis rate and with the ventilation rate in the greenhouse through the loss of CO2. The optimal CO2 reference value depends on several influences: the effect of CO2 on photosynthetic assimilation rate, fruiting and to the vegetative structure, the distribution of photosynthate in subsequent harvests, and the price of fruit at those harvests, in addition to the amount of CO2 used, greenhouse ventilation rate and CO2 price.

CONCLUSIONS

In general, increased CO2 increases plant growth growth (both above and below ground) and improves plant water relations (reduces transpiration and increases WUE). Agricultural practices such as fertilization considerably influence soil greenhouse gas fluxes. Basic research on the response of various horticultural species to future levels of atmospheric CO2 may become crucial to breeding or screening horticultural plant cultivars and species for increased drought tolerance as a result of predicted changes in precipitation role models.

How CO2–induced changes in plant growth and water relations will affect complex interactions with pests (weeds, insects, and diseases) is an area of scarce research not only for horticulture, but for plants in general.

Moisture swing adsorption technology is used to capture CO2 from the atmosphere and provide it to the greenhouse. In the absence of artificial supplies of carbon dioxide in the greenhouse environment, the CO2 absorbed during photosynthesis must ultimately come from the external environment through the ventilation openings.

The concentration of CO2 within the greenhouse must be lower than that outside in order to obtain inward flow. Since potential assimilation is heavily dependent on carbon dioxide concentration, assimilation is reduced, whatever the light level or crop status.

The ventilation of the greenhouse implies a trade–off between ensuring inflow of CO2 and maintaining an adequate temperature within the greenhouse, particularly during sunny days.

All this information is necessary to develop at its best management strategies for the agricultural industry to successfully adapt to future environmental changes.

Note: This paper was presented at ISB–INMA TEH' 2022 – International Symposium on Technologies and Technical Systems in Agriculture, Food Industry and Environment, organized by University "POLITEHNICA" of Bucuresti, Faculty of Biotechnical Systems Engineering, National Institute for Research–Development of Machines and Installations designed for Agriculture and Food Industry (INMA Bucuresti), National Research & Development Institute for Food Bioresources (IBA Bucuresti), University of Agronomic Sciences and Veterinary Medicine of Bucuresti (UASVMB), Research–Development Institute for Plant Protection – (ICDPP Bucuresti), Research and Development Institute for Processing and Marketing of the Horticultural Products (HORTING), Hydraulics and Pneumatics Research Institute (INOE 2000 IHP) and Romanian Agricultural Mechanical Engineers Society (SIMAR), in Bucuresti, ROMANIA, in 6–7 October, 2022.

Acknowledgement

This research was supported by the Romanian Ministry of Research Innovation and Digitalization, through Program 1 – Development of the National Research–Development System, Subprogram 1.2 – Institutional performance – Projects for financing excellence in RDI, Contract no. 1PFE/30.12.2021.

References

[1] Baoa, J., Wei–Hua Lub, Jigang Zhaob,c, Xiaotao T. Bia (2018). Greenhouses for CO2 sequestration from atmosphere. KeAi Communications Co. Ltd, Carbon Resources Conversion 1, 183–190

[2] Kallenbach, CM, Rolston, DE, Horwath, WR. (2010). Cover cropping affects soil N2O and CO2 emissions differently depending on type of irrigation. Agriculture Ecosystems & Environment 137(3–4): 251–260

[3] Liu, H., Zhang, J., Ai, Z., Wu, Y., Xu, H., Li, Q., Xue, S., Liu, G., (2018). Year fertilization changes the dynamics of soil oxidizable organic carbon fractions and the stability of soil organic carbon in soybean–corn agroecosystem. Agriculture Ecosystems and Environment, 265, 320–330.

[4] Liu K., Huang, J., Li, D., Yu, X., Ye, H., Hu, H., Hu, Z., Huang, Q., Zhang, H., (2019). Comparison of carbon sequestration efficiency in soil aggregates between upland and paddy soils in a red soil region of China. Journal of Integrative Agriculture, 18, 1348–1359.

[5] Lin, S, Zhang, S., Shen, G., Shaaban M., Ju, W., Cui, Y., Duan, C., Fang, L., (2021). Effects of inorganic and organic fertilizers on CO2 and CH4 fluxes from tea plantation soil. Elementa Science of the Anthropocene, 9: 1, 1–13

[6] Luan H., Yuan, S., Gao, W., Tang, J.–W., Li, R., Zhang, H., Huang S., (2021). Changes in organic C stability within soil aggregates under different fertilization patterns in a greenhouse vegetable field. Journal of Integrative Agriculture, 20(10): 2758–2771, 2758 – 2771

[7] Luan, H., Gao, W., Huang S., Tang, J., Li, M., Zhang, H., Chen, X., (2019). Partial substitution of chemical fertilizer with organic amendments affects soil organic carbon composition and stability in a greenhouse vegetable production system. Soil and Tillage Research, 191, 185–196.

[8] Prior, S. A., Runion, B. Christopher Marble, G.S., Rogers H. H, Gilliam, C. H., Torbert ,H. A. (2011). A Review of Elevated Atmospheric CO_2 Effects on Plant Growth and Water Relations: Implications for Horticulture. American Society for Horticultural Science Journals, Volume 46: Issue 2, 158 – 162

[9] Qaswar, M, Jing, H, Ahmed,W, Li, D, Liu, S, Lu, Z, Cai, A, Lisheng, L, Yongmei, X, Jusheng, G, Huimin, Z. (2020). Yield sustainability, soil organic carbon sequestration and nutrients balance under longterm combined application of manure and inorganic fertilizers in acidic paddy soil. Soil & Tillage Research 198, 104569, 42 – 51

[10] Qiu, QY, Wu, LF, Ouyang, Z, Li, BB, Xu, YY, Wu, SS, Gregorich, EG. (2016). Effects of plant–derived dissolved organic matter (DOM) on soil CO2 and N2O emissions and soil carbon and nitrogen sequestrations. Applied Soil Ecology 96, 122–130.

[11] Raheem, A, Zhang, J, Huang, J, Jiane, Y, Siddik, MA, Deng, A, Gao, J, Zhang, W. (2019). Greenhouse gas emissions from a rice–rice–green manure cropping system in South China. Geoderma 353, 331–339

[12] Runion, G. B., Finegan, H. M., Prior, S. A., Rogers, H. H., Gjerstad, D. H., (2011) Effects of Elevated Atmospheric CO_2 on Non–native Plants: Comparison of Two Important Southeastern Ornamentals. Environmental Control in Biology, Volume 49; Issue 3, 107 – 117

[13] Stanghellini, C., Incrocci, L., Gázquez, J.C. & Dimauro, B. (2008). Carbon dioxide concentration in Mediterranean greenhouses: How much lost production? Acta Hort., 801, 1541–1550

[14] [14] Wang, Y., Hu, N., Ge, T., Kuzyakov, Y., Wang, Z., Li, Z., Tang, Z., Chen, Y., Wu, C., Lou, Y., (2017). Soil aggregation regulates distributions of carbon, microbial community and enzyme activities after 23–year manure amendment. Applied Soil Ecology, 111, 65–72.

[15] Wanga, T., Huanga, J., Hea, X., Wua, J., Fanga, M., Chenga, J., (2014). CO2 fertilization system integrated with a low–cost direct air capture technology. ScienceDirect – Energy Procedia 63, 6842 – 6851

[16] [Xu, P., Zhu, J., Wang, H., Shi, L., Zhuang, Y., Fu, Q., Chen, J., Hu, H., Huang, Q., (2021). Regulation of soil aggregate size under different fertilizations on dissolved organic matter, cellobiose hydrolyzing microbial community and their roles in organic matter mineralization. Science of the Total Environment, 755, 142595, 269–276.

[17] Xu, X., Schaeffer, S., Sun, Z., Zhang, J., An, T., Wang, J., (2020). Carbon stabilization in aggregate fractions responds to straw input levels under varied soil fertility levels. Soil and Tillage Research, 199, 104593, 165–172.

ISSN: 2067-3809

Fascicule 3

[July – September]

tome [2023] XVI

ACTA Technica CORVINIENSIS
BULLETIN OF ENGINEERING

ISSN: 2067-3809

MANUSCRIPT PREPARATION – GENERAL GUIDELINES

Manuscripts submitted for consideration to **ACTA TECHNICA CORVINIENSIS – Bulletin of Engineering** must conform to the following requirements that will facilitate preparation of the article for publication. These instructions are written in a form that satisfies all of the formatting requirements for the author manuscript. Please use them as a template in preparing your manuscript. Authors must take special care to follow these instructions concerning margins.

INVITATION

We are looking forward to a fruitful collaboration and we welcome you to publish in our ACTA TECHNICA CORVINIENSIS – Bulletin of Engineering. You are invited to contribute review or research papers as well as opinion in the fields of science and technology including engineering. We accept contributions (full papers) in the fields of applied sciences and technology including all branches of engineering and management.

ACTA TECHNICA CORVINIENSIS – Bulletin of Engineering publishes invited review papers covering the full spectrum of engineering and management. The reviews, both experimental and theoretical, provide general background information as well as a critical assessment on topics in a state of flux. We are primarily interested in those contributions which bring new insights, and papers will be selected on the basis of the importance of the new knowledge they provide.

Submission of a paper implies that the work described has not been published previously (except in the form of an abstract or as part of a published lecture or academic thesis) that it is not under consideration for publication elsewhere. It is not accepted to submit materials which in any way violate copyrights of third persons or law rights. An author is fully responsible ethically and legally for breaking given conditions or misleading the Editor or the Publisher.

ACTA TECHNICA CORVINIENSIS – Bulletin of Engineering is an international and interdisciplinary journal which reports on scientific and technical contributions. Every year, in four online issues (fascicules 1–4), ACTA TECHNICA CORVINIENSIS – Bulletin of Engineering [e-ISSN: 2067-3809] publishes a series of reviews covering the most exciting and developing areas of engineering. Each issue contains papers reviewed by international researchers who are experts in their fields. The result is a journal that gives the scientists and engineers the opportunity to keep informed of all the current developments in their own, and related, areas of research, ensuring the new ideas across an increasingly the interdisciplinary field. Topical reviews in materials science and engineering, each including:

- surveys of work accomplished to date
- current trends in research and applications
- future prospects.

As an open-access journal ACTA TECHNICA CORVINIENSIS – Bulletin of Engineering will serve the whole engineering research community, offering a stimulating combination of the following:

- Research Papers – concise, high impact original research articles,
- Scientific Papers – concise, high impact original theoretical articles,
- Perspectives – commissioned commentaries highlighting the impact and wider implications of research appearing in the journal.

ACTA TECHNICA CORVINIENSIS – Bulletin of Engineering encourages the submission of comments on papers published particularly in our journal. The journal publishes articles focused on topics of current interest within the scope of the journal and coordinated by invited guest editors. Interested authors are invited to contact one of the Editors for further details.

BASIC MANUSCRIPT REQUIREMENTS

The basic instructions and manuscript requirements are simple:

- Manuscript shall be formatted for an A4 size page.
- The all margins of page (top, bottom, left, and right) shall be 20 mm.
- The text shall have both the left and right margins justified.
- Single-spaced text, tables, and references, written with 11 or 12-point Georgia or Times New Roman typeface.
- No Line numbering on any pages and no page numbers.
- Manuscript length must not exceed 15 pages (including text and references).
- Number of the figures and tables combined must not exceed 20.
- Manuscripts that exceed these guidelines will be subject to reductions in length.

The original of the technical paper will be sent through e-mail as attached document (*.doc, Windows 95 or higher). Manuscripts should be submitted to e-mail: redactie@fih.upt.ro, with mention "for ACTA TECHNICA CORVINIENSIS".

STRUCTURE

The manuscript should be organized in the following order: Title of the paper, Authors' names and affiliation, Abstract, Key Words, Introduction, Body of the paper (in sequential headings), Discussion & Results, Conclusion or Concluding

Remarks, Acknowledgements (where applicable), References, and Appendices (where applicable).

THE TITLE

The title is centered on the page and is CAPITALIZED AND SET IN BOLDFACE (font size 14 pt). It should adequately describe the content of the paper. An abbreviated title of less than 60 characters (including spaces) should also be suggested. Maximum length of title: 20 words.

AUTHOR'S NAME AND AFFILIATION

The author's name(s) follows the title and is also centered on the page (font size 11 pt). A blank line is required between the title and the author's name(s). Last names should be spelled out in full and succeeded by author's initials. The author's affiliation (in font size 11 pt) is provided below. Phone and fax numbers do not appear.

ABSTRACT

State the paper's purpose, methods or procedures presentation, new results, and conclusions are presented. A nonmathematical abstract, not exceeding 200 words, is required for all papers. It should be an abbreviated, accurate presentation of the contents of the paper. It should contain sufficient information to enable readers to decide whether they should obtain and read the entire paper. Do not cite references in the abstract.

KEY WORDS

The author should provide a list of three to five key words that clearly describe the subject matter of the paper.

TEXT LAYOUT

The manuscript must be typed single spacing. Use extra line spacing between equations, illustrations, figures and tables. The body of the text should be prepared using Georgia or Times New Roman. The font size used for preparation of the manuscript must be 11 or 12 points. The first paragraph following a heading should not be indented. The following paragraphs must be indented 10 mm. Note that there is no line spacing between paragraphs unless a subheading is used. Symbols for physical quantities in the text should be written in italics. Conclude the text with a summary or conclusion section. Spell out all initials, acronyms, or abbreviations (not units of measure) at first use. Put the initials or abbreviation in parentheses after the spelled-out version. The manuscript must be writing in the third person ("the author concludes... ").

FIGURES AND TABLES

Figures (diagrams and photographs) should be numbered consecutively using Arabic numbers. They should be placed in the text soon after the point where they are referenced. Figures should be centered in a column and should have a figure caption placed underneath. Captions should be centered in the column, in the format "Figure 1" and are in upper and lower case letters.

When referring to a figure in the body of the text, the abbreviation "Figure" is used illustrations must be submitted in digital format, with a good resolution. Table captions appear centered above the table in upper and lower case letters.

When referring to a table in the text, "Table" with the proper number is used. Captions should be centered in the column, in the format "Table 1" and are in upper and lower case letters. Tables are numbered consecutively and independently of any figures. All figures and tables must be incorporated into the text.

EQUATIONS & MATHEMATICAL EXPRESSIONS

Place equations on separate lines, centered, and numbered in parentheses at the right margin. Equation numbers should appear in parentheses and be numbered consecutively. All equation numbers must appear on the right-hand side of the equation and should be referred to within the text.

CONCLUSIONS

A conclusion section must be included and should indicate clearly the advantages, limitations and possible applications of the paper. Discuss about future work.

Acknowledgements

An acknowledgement section may be presented after the conclusion, if desired. Individuals or units other than authors who were of direct help in the work could be acknowledged by a brief statement following the text. The acknowledgment should give essential credits, but its length should be kept to a minimum; word count should be <100 words.

References

References should be listed together at the end of the paper in alphabetical order by author's surname. List of references indent 10 mm from the second line of each references. Personal communications and unpublished data are not acceptable references.

- *Journal Papers:* Surname 1, Initials; Surname 2, Initials and Surname 3, Initials: Title, Journal Name, volume (number), pages, year.
- *Books:* Surname 1, Initials and Surname 2, Initials: Title, Edition (if existent), Place of publication, Publisher, year.
- *Proceedings Papers:* Surname 1, Initials; Surname 2, Initials and Surname 3, Initials: Paper title, Proceedings title, pages, year.

ISSN: 2067-3809

INDEXES & DATABASES

We are very pleased to inform that our international scientific journal ACTA TECHNICA CORVINIENSIS – Bulletin of Engineering completed its 15 years of publication successfully [2008–2022, Tome I–XV].
In a very short period the ACTA TECHNICA CORVINIENSIS – Bulletin of Engineering has acquired global presence and scholars from all over the world have taken it with great enthusiasm.
We are extremely grateful and heartily acknowledge the kind of support and encouragement from all contributors and all collaborators!

ACTA TECHNICA CORVINIENSIS – Bulletin of Engineering is accredited and ranked in the "B+" CATEGORY Journal by CNCSIS – The National University Research Council's Classification of Romanian Journals, position no. 940 (http://cncsis.gov.ro/).
ACTA TECHNICA CORVINIENSIS – Bulletin of Engineering is a part of the ROAD, the Directory of Open Access scholarly Resources (http://road.issn.org/).

ACTA TECHNICA CORVINIENSIS – Bulletin of Engineering is also indexed in the digital libraries of the following world's universities and research centers:

WorldCat – the world's largest library catalog
https://www.worldcat.org/
National Lybrary of Australia
http://trove.nla.gov.au/
University Library of Regensburg – GIGA German Institute of Global and Area Studies
http://opac.giga-hamburg.de/ezb/
Simon Fraser University – Electronic Journals Library
http://cufts2.lib.sfu.ca/
University of Wisconsin – Madison Libraries
http://library.wisc.edu/
University of Toronto Libraries
http://search.library.utoronto.ca/
The University of Queensland
https://www.library.uq.edu.au/
The New York Public Library
http://nypl.bibliocommons.com/
State Library of New South Wales
http://library.sl.nsw.gov.au/
University of Alberta Libraries – University of Alberta
http://www.library.ualberta.ca/
The University of Hong Kong Libraries
http://sunzi.lib.hku.hk/
The University Library – The University of California
http://harvest.lib.ucdavis.edu/

ACTA TECHNICA CORVINIENSIS – Bulletin of Engineering is indexed, abstracted and covered in the world–known bibliographical databases and directories including:

INDEX COPERNICUS – JOURNAL MASTER LIST
http://journals.indexcopernicus.com/
GENAMICSJOURNALSEEK Database
http://journalseek.net/
DOAJ – Directory of Open Access Journals
http://www.doaj.org/
EVISA Database
http://www.speciation.net/
CHEMICAL ABSTRACTS SERVICE (CAS)
http://www.cas.org/
EBSCO Publishing
http://www.ebscohost.com/
GOOGLE SCHOLAR
http://scholar.google.com
SCIRUS – Elsevier
http://www.scirus.com/
ULRICHSweb – Global serials directory
http://ulrichsweb.serialssolutions.com
getCITED
http://www.getcited.org
BASE – Bielefeld Academic Search Engine
http://www.base-search.net
Electronic Journals Library
http://rzblx1.uni-regensburg.de
Open J–Gate
http://www.openj-gate.com
ProQUEST Research Library
http://www.proquest.com
Directory of Research Journals Indexing
http://www.drji.org/
Directory Indexing of International Research Journals
http://www.citefactor.org/

ISSN: 2067-3809